

Design, Synthesis, Metal Complexation and Self Assembly of Peptide Nucleic Acids with Modified and Unnatural Nucleobases

A thesis

Submitted in partial fulfillment of the requirements

Of the degree of

Doctor of Philosophy

By

Vijay N. Kadam

ID: 20093034

Thesis Supervisor: Prof. Krishna N. Ganesh



INDIAN INSTITUTE OF SCIENCE EDUCATION AND RESEARCH, PUNE

MAY 2016

This Thesis is dedicated to...

My parents, wife and teachers





भारतीय विज्ञान शिक्षा एवं अनुसंधान संस्थान, पुणे

INDIAN INSTITUTE OF SCIENCE EDUCATION AND RESEARCH (IISER), PUNE

(An Autonomous Institution, Ministry of Human Resource Development, Govt. of India)

Dr. Homi Bhabha Road, Pune 411008

Prof. Krishna N. Ganesh

Professor and Coordinator, Chemistry

Director, IISER Pune

J. C. Bose Fellow (DST), IISER Pune

CERTIFICATE

Certified that the work incorporated in the thesis entitled “*Design, Synthesis, Metal Complexation and Self Assembly of Peptide Nucleic Acids with Modified and Unnatural Nucleobases*” submitted by **Mr. Vijay N. Kadam** was carried out by the candidate, under my supervision. The work presented here or any part of it has not been included in any other thesis submitted previously for the award of any degree or diploma from any other university or institution.

Date: 2nd May, 2016 Pune

Prof. Krishna N. Ganesh

(Research Supervisor)

DECLARATION

I declare that, this written submission represents my ideas in my own words and where others' ideas have been included; I have adequately cited and referenced the original sources. I also declare that I have adhered to all principles of academic honesty and integrity and have not misrepresented or fabricated or falsified any idea / data / fact/ source in my submission. I understand that violation of the above will be cause for disciplinary action by the Institute and can also evoke penal action from the sources which have thus not been properly cited or from whom proper permission has not been taken when needed.

Date: 2nd May 2016

Mr. Vijay N. Kadam

ID: 20093034

Acknowledgements

It gives me genuine pleasure to express my deep sense of thanks and gratitude towards my research supervisor Prof. Krishna N. Ganesh for his constant support, guidance and motivation throughout my doctoral research. His overwhelming inspiration has made me easy to complete my doctoral research in the area of nucleic acid analogs. Additionally his lessons on independent thinking, writing skills, presentation skills and many more things has helped in shaping a researcher in me. I am also thankful to him on his constant support on personal difficulties.

I am very grateful to Director, IISER Pune for providing a very well infrastructure and facilities to pursue my doctoral research. I also thank CSIR, India for financial assistance and graduate research fellowship. I would also like to thank Directors of NCL, Dr. Sivaram and Dr. Sourav Pal for allowing me to work in NCL lab in early research period.

I am very grateful to my research advisory committee members Dr. Raghavendra Kikkeri and Dr. H. V. Thulasiram for their fruitful suggestions, comments and encouragement through various RAC meetings. I would like to specially thank Dr. Raghavendra Kikeri for his help and discussion regarding various ideas or aspects of research. I sincerely thank Dr. S. G. Srivatsan for his encouragement and kind help.

I acknowledge my seniors Dr. Mahesh, Dr. Roopa, Dr. Shridhar, Dr. Ashwani, Dr. Gitali, Dr. Amit, Dr. Manaswini, Dr. Tanpreet and Pradnya for their help in initial years of research in NCL. I am very thankful to my colleagues Dr. Deepak, Dr. Nitin, Dr. Satheesh, Madhan, Dr. Dhruvjiyoti Datta and juniors cum colleagues Prabhakar, Shahaji Pramod (Topi), Manoj, Pramod B. Eranna, Bhuvana and Esha for always keeping cheerful atmosphere around and giving the relaxation needed in tough times of research. My special thanks to Dr. Satheesh for helping me in research and scientific discussion.

Whenever I needed some serious relaxation to kickback power to move forward afresh, my friends were around me. Life was cheerful, enjoyable and pleasant with friends Maroti, Sharad, Shekhar, Amar, Sachin, Prakash, Sandip, Susheel, Gopal (GK), Anupam, Satish, Pramod S., Santosh, Ganesh, Kiran Reddy, Bapu, Smita, Ashok, Sanjog, Dnyaneshwar, Balu, Nagesh, Ganesh Murhade, Tukaram, Alok and many countless friends; and the members of Lab 101 who helped me to release the sort of tension in difficult times of research. I cannot forget the time spent in Dilraj Park and Jitendra Society with Sharad(Samratbhau) , Santosh (Santy), Dnyaneshwar (Mauli),

Pundlik (Patil), Balya, Kiran (Mickey), Gajanan (Durkya), Amit, Venu, Sagar, Dinesh, Harshal, Mahesh, Ranjeet, Avinash, Chinu, Somesh, Vaibhav, Sonaji, Sachin P., Sachin(Raje), Deepak and Dr. Balaji.

I am grateful to technical staff, Pooja (NMR), Swati (MALDI), Nayana (HRMS), Yatheesh and Anil (SEM) and Mayuresh for their help. I am grateful to the purchase section especially, Vrushali, Zunjarrao, Nitin and Mahesh for their immediate response to purchase indent. Finally, I would like to thank those who helped me directly and indirectly during my research.

I shall always remain indebted to my parents and my entire family, for their unconditional love, blessings, sacrifices, patience and support. The values and virtues they have instilled in me have made me achieve whatever I have achieved so far. I would like to thank a very very special person my lovely wife, Bhagyashri for her continuous support and faith. I would also like to thank to my brother-in-law Satish. Finally, I would like to thank my cute nephew Soham for letting me to forget all the tension & frustration coming from the research and also thankful to nieces Aishwarya, Vedika and nephews Nil and Adwait for keeping me joyful and happy. I hope with my hard work and dedication, I would be able to translate their dreams into reality.

Vijay K.

Table of contents

Abbreviations	iv
Abstract of thesis	viii

Chapter 1: Design, Synthesis and Metal Complexation Studies of *aeg*-PNA with Metal Binding Ligand Replacing Base Pairing

1.1	Introduction	1
1.2	Base Pairing in nucleic acids	2
1.3	Metal mediated base pairing	5
1.4	Metallo-PNAs	8
1.5	Synthetic methods for the preparation of PNA oligomers	11
1.6	Present work: Rationale and Objective	15
1.7	Results and discussions	16
1.8.1	Molar extinction coefficient of ethyl <i>N</i> -Boc-aminoethyl-3-hydroxy-2-methyl-4-pyridone glycine (MHP-PNA) monomer	19
1.8.2	UV-Vis spectroscopic titrations of the ethyl <i>N</i> -Boc-aminoethyl-3-hydroxy-2-methyl-4-pyridone glycinate 9 with metal salts	20
1.8.3	Photoluminescence studies of ethyl <i>N</i> -Boc-aminoethyl-3-hydroxy-2-methyl-4-pyridone (MHP) glycinate 9	24
1.8.4	Solid state photoluminescence of ethyl <i>N</i> -Boc-aminoethyl-3-hydroxy-2-methyl-4-pyridone (MHP) glycinate 9 with Europium nitrate	26
1.9	Stoichiometry of complex formation of MHP with Metal salts	26
1.10	Determination of binding constant by UV spectroscopy	28
1.11	MALDI-TOF Studies of ethyl- <i>N</i> -Boc-aminoethyl-2-methyl-3-hydroxy-4-pyridone (MHP) glycinate 9 with metal salts	30
1.12	Biophysical studies of PNA oligomers	33
1.13	Comparison of thermal stability of PNA:PNA duplexes	41
1.14	Co-ordination chemistry of metal complexes	42
1.15	Binding models	43

1.16	Conclusion	44
1.17	Experimental procedures	45
1.18	UV titration	47
1.19	Fluorescence titration	47
1.20	UV- T_m measurement	47
1.21	Procedures and spectral data	48
1.22	References	53
1.23	Appendix I	57

Chapter 2: Polarity Sensing by Fluorescent PNA: Micro-environmental changes in the Major Groove of PNA:DNA/RNA/PNA Hybrids

2.1	Introduction	75
2.2	Molecular recognition of nucleic acid	78
2.3	DNA-Drug interactions in minor groove	79
2.4	Major groove binders	81
2.5	Intercalation	84
2.6	Fluorescence spectroscopy	87
2.7	Solvent polarity and local environment effects	88
2.8	Solvent polarity scale	89
2.9	Characterization of polarity in grooves	90
2.10	Present work: Rationale and objective	93
2.11	Results and discussion	95
2.12	Solvent dependent fluorescence study	100
2.13	Biophysical studies	102
2.13.2a	Circular dichroism (CD) of PNA:DNA/RNA duplexes	107
2.13.2b	Circular dichroism (CD) of PNA:PNA duplexes	109
2.14	Determination of dielectric constant as a measure of polarity	110
2.15	Determination of dielectric constants of PNA:DNA/RNA/PNA duplexes	112
2.16	Comparison between dielectric constants of PNA:DNA, PNA:RNA,	117

2.17	Summary	118
2.18	Experimental methods	119
2.19	Biophysical studies	120
2.20	Procedures and spectral data	122
2.21	References	127
2.22	Appendix-II	130

Chapter 3: Biophysical Studies of Tetraplex Formation of Base Modified aeg-PNA hexamers

3A. Biophysical studies of tetraplexes of 5-aminouracil linked aeg-PNA

3.A.1	Introduction	151
3A.2	Characterization of G-tetrad formation in DNA	153
3A.3	Thermal denaturation by UV and CD spectroscopy	155
3A.4	Polymorphism in DNA G-quartet	156
3A.5	Other quadruplex forming sequences	158
3A.6	Applications of G-quadruplexes	159
3A.7	Rationale and objective of present work	160
3A.8	Result and discussion	162
3A.8.3a	CD spectroscopy	163
3A.8.3b	Salt dependent CD spectroscopy	164
3A.8.3c	pH dependent CD study of PNA-2 (U^{NH_2})	165
3A.8.3d	Concentration dependent CD of PNA-2 (U^{NH_2})	166
3A.9	Modulating the self-assembly of tetraplex formation by fatty acid conjugation to PNA oligomers	166
3A.10	Synthesis and characterization of fatty acid chain conjugated PNA hexamers	167
3A.11	CD spectroscopy of fatty acid chain conjugated PNA hexamers	168
3A.12	Characterization of self assembled structure by FESEM	169
3A.13	Summary	172

3B. Host-guest complexation of adamantyl-G₄ PNA quadruplex with sugar capped β -cyclodextrin to study carbohydrate-protein interaction

3B.1	Introduction	174
3B.2	Rationale and objective of present work	176
3B.3	Results and discussion	177
3B.3.1	Synthesis of adamantyl tetraethylene glycol-U- <i>aeg</i> -PNA monomer (U [#])	177
3B.3.2	Synthesis and characterization of PNA oligomers	177
3B.4	UV-Vis spectroscopy	178
3B.5	CD spectroscopic measurements	178
3B.6	Study of host-guest interaction by CD spectroscopy	179
3B.7	Summary	180
3.2	Experimental procedures	181
3.2.1	Synthesis, Cleavage and purification PNA oligomers	181
3.2.2	Circular dichroism	181
3.2.3	Sample preparation for FESEM	181
3.2.4	Procedures and spectral data	182
3.3	References	184
3.4	Appendix II	188

Abbreviations

A	Adenine
ACN	Acetonitrile
<i>aeg</i>	Aminoethylglycine
aq.	Aqueous
Å	Angstrom
(Boc) ₂ O	Boc anhydride
Bn	Benzyl
C	Cytosine

Calcd	Calculated
Cbz	Benzyloxycarbonyl
CD	Circular Dichroism
CHCA	α -cyano-4-hydroxycinnamic acid
Cu (NO ₃) ₂	Copper nitrate
Co (NO ₃) ₂	Cobalt nitrate
DCM	Dichloromethane
DHB	2,5-dihydroxybenzoic acid
ϵ	Dielectric constant
DIPEA	N,N-Diisopropylethylamine
DMF	N,N-dimethylformamide
DNA	2'-deoxyribonucleic acid
DNS	5-(dimethylamino)naphthalene-2-sulfonamide
EDTA	Ethylene diamine tetraacetic acid
ESI	Electrospray ionization
Et	Ethyl
EtOAc	Ethyl acetate
Eu(NO ₃) ₃	Europium nitrate
<i>ex</i>	Excitation
<i>em</i>	Emission
Fe	Iron
Fmoc	9-Fluorenylmethoxycarbonyl
g	gram
G	Guanine
h	Hour
HBTU	2-(1H-Benzotriazole-1-yl)-1,1,3,3 tetramethyl-uronum-hexafluoro-phosphate
HOBt	N-Hydroxybenzotriazole
HPLC	High Performance Liquid Chromatography
Ho(NO ₃) ₃	Holmium nitrate
HTH	Helix-turn-helix
I	Inosine
<i>in situ</i>	In the reaction mixture
K ₂ CO ₃	Potassium carbonate

λ	Lambda
La(NO ₃) ₃	Lanthanum nitrate
LiOH	Lithium hydroxide
Lys	Lysine
MALDI-TOF	Matrix Assisted Laser Desorption Ionisation- Time of Flight
MBHA	4-Methyl benzhydryl amine
mg	milligram
MHz	Megahertz
MHP	3-Hydroxy-2-methyl-4-pyridone
Min	Minute
MS	Mass spectrometry
μ L	Microliter
μ M	Micromolar
mL	milliliter
mM	millimolar
mmol	millimoles
MS	Mass spectrometry
MW	Microwave oven
mRNA	Messenger RNA
NaHCO ₃	Sodium bicarbonate
NaOH	Sodium hydroxide
Ni (NO ₃) ₂	Nickel nitrate
nm	Nanometer
NMR	Nuclear Magnetic Resonance
<i>f</i>	Orientation polarity
Obsvd	Observed
PAGE	Polyacrylamide Gel Electrophoresis
Pd/C	Palladium on charcoal
ppm	Parts per million
PNA	Peptide Nucleic Acid
n	Refractive index
RNA	Ribonucleic Acid
RP	Reverse Phase (-HPLC)

RT	Room temperature
SPPS	Solid Phase Peptide Synthesis
<i>ss</i>	Single strand/single stranded
T	Thymine
Tb(NO ₃) ₃	Terbium nitrate
TEA	Triethylamine
TFA	Trifluoroacetic acid
TFMSA	Trifluoromethane sulfonic acid
TLC	Thin layer chromatography
tRNA	Transfer RNA
<i>T_m</i>	Melting temperature
Ni(NO ₃) ₂	Nickel nitrate
U	Uracil
UV-Vis	Ultraviolet-Visible
Zn(NO ₃) ₂	Zinc nitrate

Abstract of Thesis

The thesis entitled “**Design, Synthesis, Metal Complexation and Self Assembly of Peptide Nucleic Acids with Modified and Unnatural Nucleobases**” is comprised of studies towards metal complexation and self assembly of peptide nucleic acids carrying the modified and unnatural nucleobases. The modified and unnatural nucleobases linked to PNA backbone are 3-hydroxy-2-methyl-4-pyridone; 5-aminouracil, 5-amidodansyluracil and adamantyl tetra ethylene glycol conjugated uracil. The PNA oligomers obtained by solid phase peptide synthesis were investigated for metal stabilized PNA:PNA duplexes, determination of major groove polarity of PNA:DNA/RNA/PNA duplexes and tetraplex formation by various biophysical techniques.

The thesis is presented as three chapters:

Chapter 1 describes the design, synthesis and metal complexation studies of base modified *aeg-PNA*.

Chapter 2 deals with the determination of dielectric constant of PNA:DNA/RNA/PNA duplexes by incorporating fluorescent U-dansyl base into PNA oligomers having different chemical environment.

Chapter 3 reports on biophysical studies of tetraplex formation of 5-aminouracil modified *aeg-PNA* and designing of tetraplex for host-guest interaction.

A.1 Chapter 1: Design, Synthesis and Metal Complexation Studies of *aeg-PNA* With Metal Binding Ligand Replacing Base Pairing

This chapter describes the studies on metal mediated base pairing in peptide nucleic acids. The present work deal with the design of PNA:PNA duplexes stabilized by metal coordinated H-bonding by replacing natural base pairing. The self assembly and molecular recognition properties of PNA provides the best platform to design PNA based biosensors and nanostructures owing to the neutral character of PNA.

In view of this, our laboratory has involved in the use of catechol on PNA backbone as metal binding ligand. However, it exhibited poor binding affinity to

Cu^{2+} and Ni^{2+} . Hence in the present work, 3-hydroxy-2-methyl-4-pyridone was chosen because of its better metal binding properties.

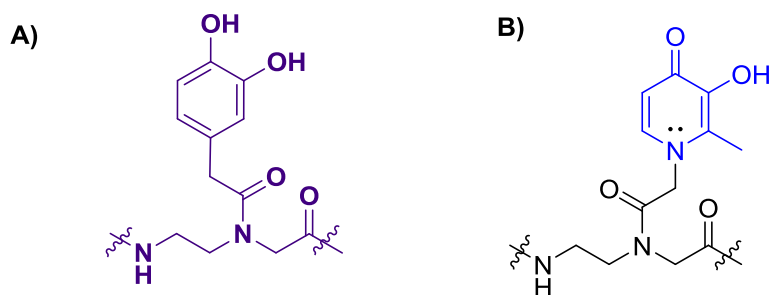


Figure 1. Structures of A) Catechol PNA and B) 3-hydroxy-2-methyl-4-pyridone PNA.

The 3-hydroxy-2-methyl-4-pyridone was linked to *aeg*-PNA backbone owing to its high stabilization property of DNA duplexes in the presence of Cu^{2+} . Our studies also showed that 3-hydroxy-2-methyl-4-pyridone strongly binds to rare earth metals which could have application in developing luminescent materials for organic light emitting diodes.

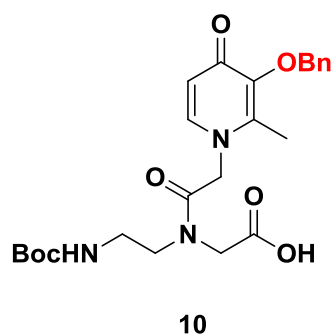
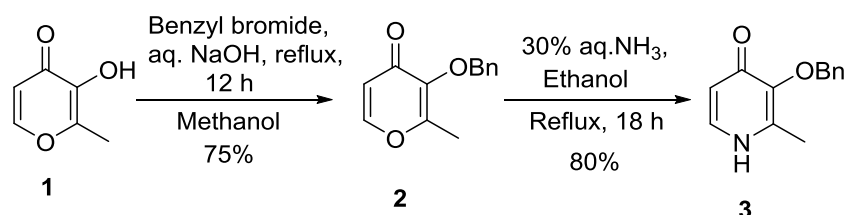


Figure 2. Structure of 3-benzyloxy-2-methyl-4-pyridone linked *aeg*-PNA monomer.

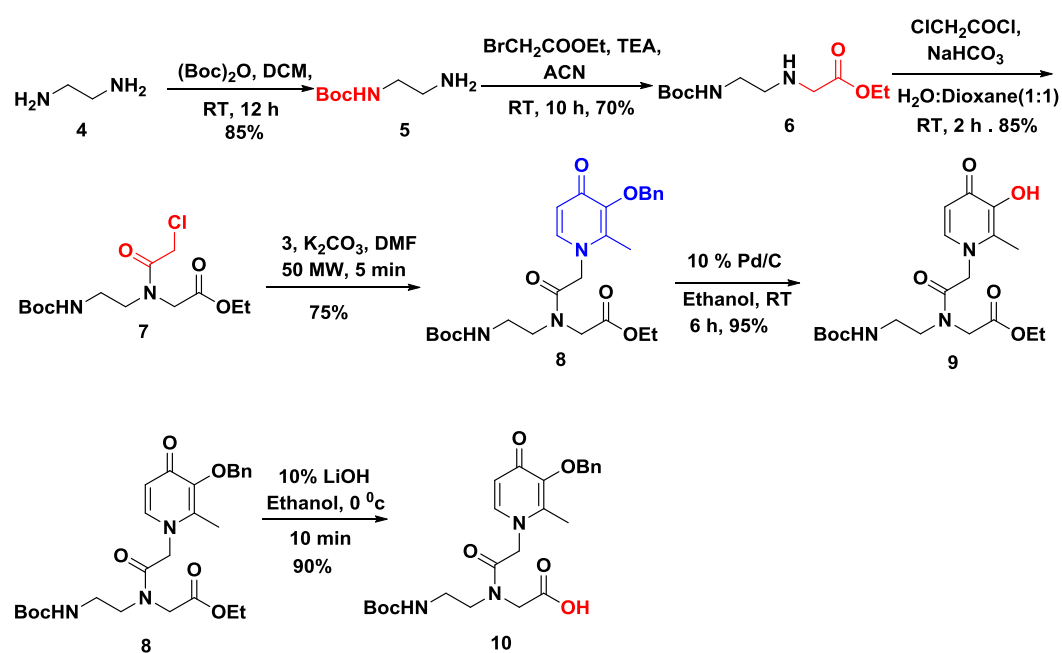
A.1.1 Synthesis of *N*-Boc-aminoethyl-(3-benzyloxy-2-methyl-4-oxopyridonyl-*N*-actamido) glycine monomer

In an attempt towards the synthesis of *N*-Boc (3-hydroxy-2-methyl-4-oxopyridonyl *N*-actamido) aminoethyl glycine monomer, the commercially available 3-hydroxy-2-methyl pyrone **1** was O-benzylated with benzyl bromide in methanol to obtain **2** which was subsequently treated with aqueous ammonia in ethanol to give crystalline 2-methyl 3-benzyloxy 4-pyridone **3**. This was used in Scheme 2 for linking to *aeg*-PNA backbone.

Scheme 1: Synthesis of 3-benzyloxy-2-methyl-4-pyridone



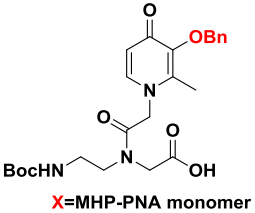
The commercially available ethylenediamine was treated with Boc-anhydride (0.1 eq) to get *N*-Boc ethylenediamine (**5**) which was *N*-alkylated by reaction with ethyl bromoacetate compound **6**. This was *N*-acylated by treating with chloroacetyl chloride to obtain compound **7** which was reacted with 3-benzyloxy 2-methyl 4-pyridone **3** to yield **8**. This upon hydrogenation with 10% Pd/C in ethanol gave the compound **9**. The hydrolysis of ester **8** with 10% lithium hydroxide leads to target monomer acid **10**.

Scheme 2: Synthesis of ethyl *N*-Boc-aminoethyl-3-benzyloxy-2-methyl-4-pyridone glycine

The compound ethyl *N*-Boc-aminoethyl-3-hydroxy-2-methyl-4-pyridone glycinate (MHP) **9** was used for metal complexation, studied by UV-Vis titration, binding constant determination, Job's plot by UV-Vis spectroscopy, fluorescence titration and MALDI-TOF mass spectrometric techniques.

The PNA oligomers were synthesized by employing standard solid phase peptide synthesis protocol using *Boc* strategy. The PNA sequences bearing 3-hydroxy-2-methyl-4-pyridone linked *aeg*-PNA monomer (X) were synthesized to find the effect of metal coordination on the stability of PNA:PNA duplexes (Table 1). The PNA sequences with unmodified (A/G/C/T) monomeric units were also synthesized for comparative studies.

Table 1. PNA oligomers with modified/unmodified *aeg*-PNA monomers.

Entry	Sequence code	PNA sequence	Monomers Used
1	PNA-1	H-GCGATCGC LysNH ₂	A/G/C/T = <i>aeg</i> PNA
2	PNA-2	H- GCGA $\color{red}{\text{X}}$ TTCGC LysNH ₂	
3	PNA-3	H-ATAGA $\color{red}{\text{X}}$ CATC LysNH ₂	
4	PNA-4	H-GATG $\color{red}{\text{X}}$ TCTAT LysNH ₂	
5	PNA-5	H-TATCT $\color{red}{\text{X}}$ GTAG LysNH ₂	
6	PNA-6	H-ATAGATCATC LysNH ₂	
7	PNA-7	H-GATGATCTAT LysNH ₂	A/G/C/T = <i>aeg</i> PNA
8	PNA-8	H-TATCTAGTAG LysNH ₂	

All the PNA oligomers were purified by RP-HPLC and characterized by MALDI-TOF mass spectroscopy. These purified PNA oligomers were used for metal complexation studies by UV spectroscopy, fluorescence spectroscopy and temperature dependent UV spectroscopy.

A.1.2 Complexation studies of the ethyl *N*-Boc-aminoethyl-3-hydroxy-2-methyl -4-pyridone glycinate (MHP) **9** with metal salts

The complexation studies of ethyl *N*-Boc-aminoethyl-3-hydroxy-2-methyl-4-pyridone glycinate (MHP) **9** with different metal ions were carried out using copper nitrate, nickel nitrate, cobalt nitrate, zinc nitrate, lanthanum nitrate, europium nitrate, terbium nitrate and holmium nitrate by UV-Vis and fluorescence spectroscopy. From results, it was observed that ethyl *N*-Boc-aminoethyl-3-hydroxy-2-methyl-4-pyridone glycinate (MHP) **9** exhibits strong binding with rare earth metal salts showing saturation at one equivalent of metal ion per MHP **9** in methanol. In addition to metal salts, MHP **9** exhibited binding with copper nitrate as well.

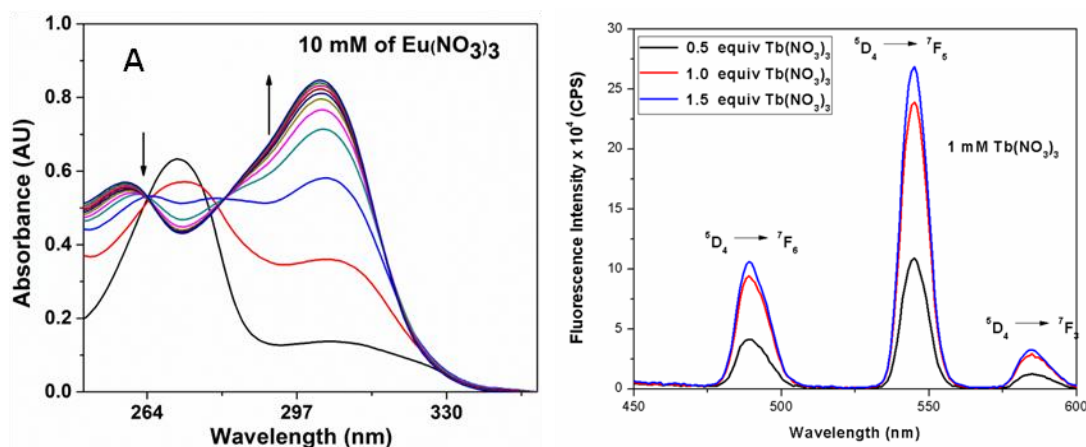


Figure 2. A) Change in the absorption spectra of the ethyl *N*-Boc-aminoethyl-2-methyl-3-hydroxy-4-pyridone glycinate (MHP) **9** (100 μ M) in methanol and B) Photoluminescence spectrum of ethyl *N*-Boc-aminoethyl-3-hydroxy-2-methyl-4-pyridone glycinate (MHP) **9** (10 μ M) upon addition of $\text{Tb}(\text{NO}_3)_3$ (1mM) in methanol.

The binding stoichiometry between metal salts and ethyl *N*-Boc-aminoethyl-3-hydroxy-2-methyl-4-pyridone glycinate (MHP) **9** was determined by Job's plot and MALDI-TOF mass spectroscopy. Job's plot suggested that the stoichiometry of complex formation of MHP **9** with rare earth metal salts was 1:1 and MALDI-TOF mass analysis exhibited 2:1 and 1:1 binding stoichiometry.

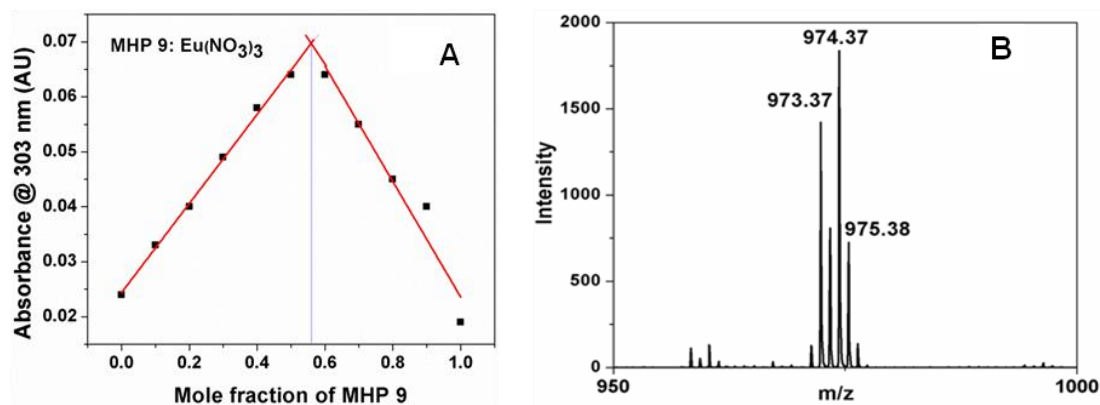


Figure 4. A) Job's plot of ethyl *N*-Boc-aminoethyl-3-hydroxy-2-methyl-4-pyridone glycinate (MHP) **9** with europium nitrate and B) MALDI-TOF mass spectrum of ethyl *N*-Boc-aminoethyl-3-hydroxy-2-methyl-4-pyridone glycinate (MHP) **9** with europium nitrate.

The binding constant (K) of complex formation was determined from a Benesi–Hildebrand plots by UV-Vis spectroscopy. The binding constants for complexation of MHP **9** with different metal salts were found to be in the range 10^4 M^{-1} as summarized in Table 2.

Table 2. Binding constant values of complexation of MHP 9 with different metal salts.

Sr. No.	Metal salt	Binding constant K ($\times 10^4 \text{ M}^{-1}$)
1	Europium Nitrate	6.17
2	Terbium Nitrate	5.28
3	Holmium Nitrate	6.5
4	Lanthanum Nitrate	1.04

After establishing the formation of complex by MHP 9 monomer with different rare earths, the complex formation with MHP incorporated PNA oligomers forming stable PNA:PNA duplexes were studied by UV-Vis spectroscopy, fluorescence spectroscopy and temperature dependent UV spectroscopy.

A.1.3 Biophysical studies of PNA oligomers

The extent of stability of MHP incorporated PNA:PNA duplexes by metal mediated base pairing was determined by temperature dependent UV spectroscopy (Figure 5).

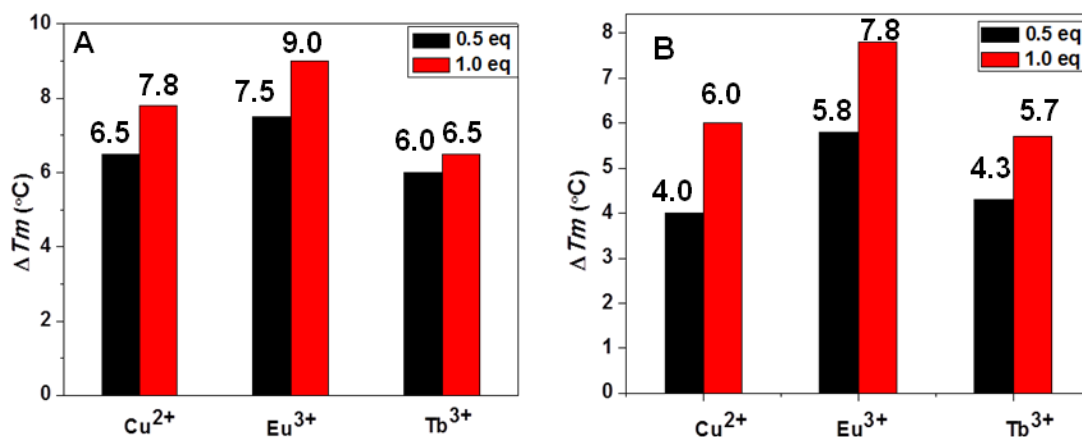


Figure 5. Comparison of ΔT_m (°C) of MHP incorporated PNA:PNA duplexes A) antiparallel and B) parallel orientation.

Overall results suggested that incorporation of 3-hydroxy-2-methyl-4-pyridone *aeg*-PNA monomer into PNA oligomers leads to stabilization of PNA:PNA duplexes indicating the positive impact of metal coordination on the stability of PNA:PNA duplexes.

A.2 Chapter 2: Polarity Sensing by Fluorescent PNA: Micro-environmental changes in the Major Groove of PNA:DNA/RNA/PNA Hybrids

In view of growing interest in biological and material applications of DNA duplexes with RNA/PNA/XNA and modified nucleic acids, it is relevant to study how the polarity of grooves changes with the structural diversity of complementary DNA analogues. PNA is a promising analog of DNA, which has potential for nucleic acid based therapeutics. In this context, it is important to study characterization of the major groove of its duplex with complementary DNA/RNA/PNA.

As the polyamide backbone of PNA is more hydrophobic as compared to the sugar-phosphate backbone of DNA/RNA, it will affect the major groove polarity being structurally different than DNA/RNA. In this context, the characterization of polarity of PNA:DNA/RNA/PNA duplexes by fluorescence strategy is demonstrated in this chapter.

This chapter deals with the synthesis of hydrophilic (5-aminouracil), neutral (uracil) and fluorescent 5-amidodansyluracil *aeg*-PNA monomers which were incorporated in PNA oligomers in such a way that 5-amidodansyluracil is flanked by hydrophobic (T), hydrophilic (U^{NH_2}) or neutral (U) bases. The change in major groove polarity of PNA:DNA/RNA/PNA duplexes was determined by measuring the Stokes shift.

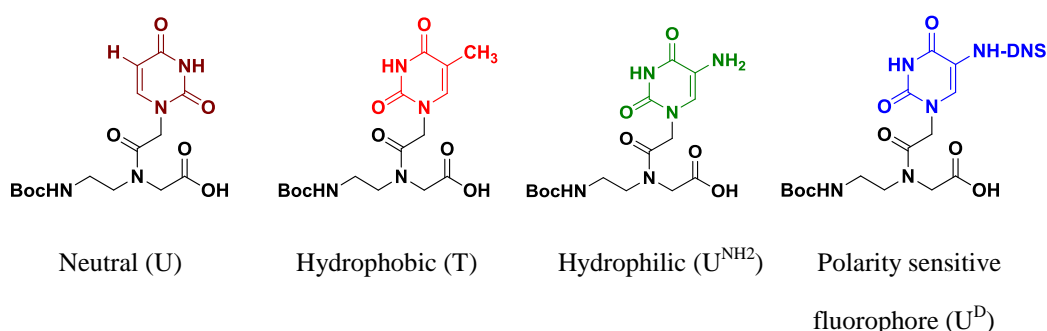
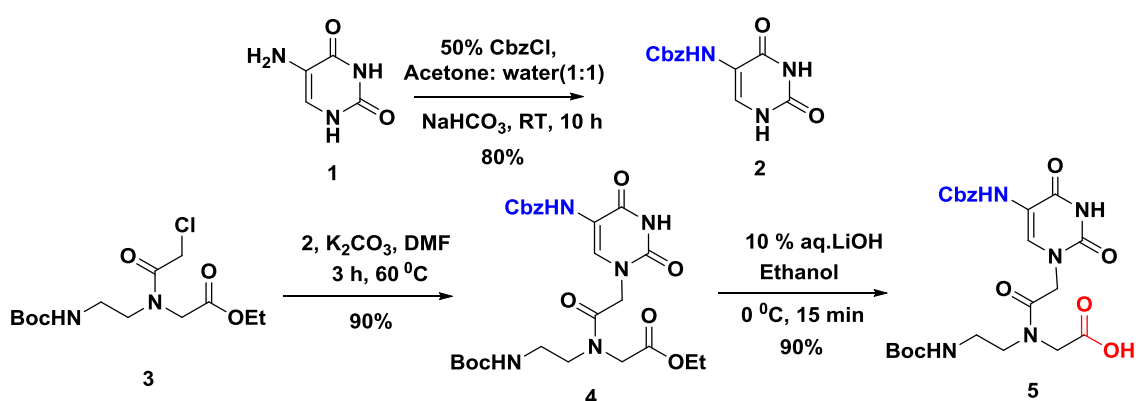


Figure 6. Structures of desired PNA monomers.

A.2.1 Synthesis and characterization of (5NHCbzU-aeg, 5NHDNSU-aeg, U-aeg) PNA monomers

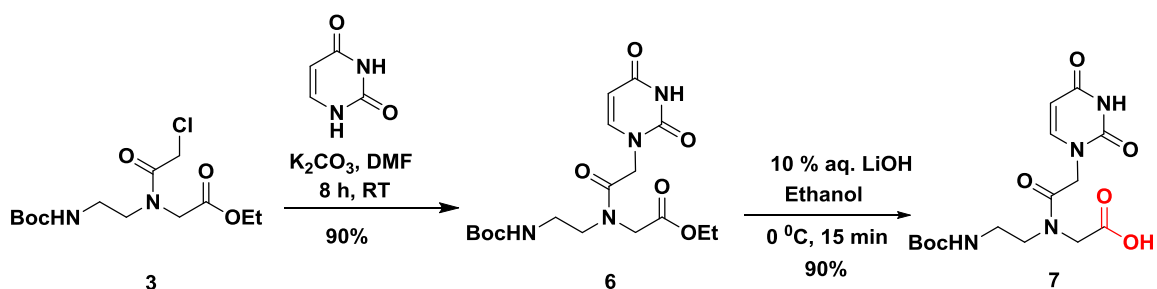
The commercially available 5-aminouracil was treated with 50% benzyl chloroformate in toluene to obtain Cbz protected 5-aminouracil (**2**) (Scheme 1). This compound was reacted with the N/C-protected aminoethyl glycyl chloroacetamide compound (**3**) to give the protected PNA monomer (**4**). This ester upon hydrolysis with 10% aq. LiOH gave the desired 5NHCbzU-aeg monomer **5**.

Scheme 3: Synthesis of 5NHCbzU-aeg PNA monomer

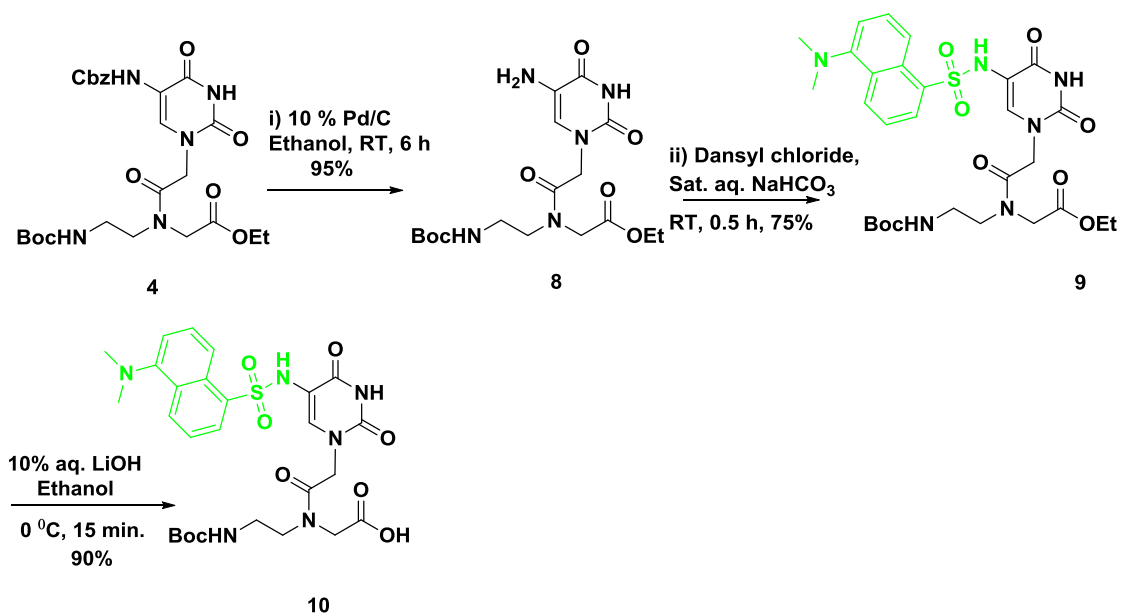


Compound **3** was reacted with commercially available uracil base (Scheme 2) to give compound **6**, which was hydrolyzed with 10% aq. LiOH to obtain the desired *U*-aeg PNA monomer **7**.

Scheme 4: Synthesis of *U*-aeg PNA monomer



Compound **4** was hydrogenated with 10% Pd/C in ethanol to obtain Cbz deprotected 5-amino-uracil **8** (Scheme 3), which on subsequent reaction with dansyl chloride gave the ester **9**. This upon hydrolysis with 10% aq. LiOH yielded the desired 5NHDNSU-aeg PNA monomer acid **10**.

Scheme 5: Synthesis of 5NHDNSU-*aeg* PNA monomer

The synthesized PNA monomers were incorporated into the desired *aeg*-PNA oligomers by employing standard solid phase peptide synthesis protocol using *Boc* strategy. The PNA oligomers were designed in such a way that the dansyl fluorophore (U^D) is flanked by hydrophobic (T), neutral (U) or hydrophilic environment (U^{NH_2}) of adjacent bases.

Table 3: Synthesis of PNA oligomers

Entry	Sequence code	PNA sequence	Monomers used
1	PNA 1	H-CGAC TTT CAG LysNH ₂	A/G/C/T/U = <i>aeg</i> PNA
2	PNA 2	H-CGAC TU^DT CAG LysNH ₂	
3	PNA 3	H-CGAC UU^DT CAG LysNH ₂	
4	PNA 4	H-CGAC UU^DU CAG LysNH ₂	
5	PNA 5	H-CGAC U^{NH2}U^DU^{NH2} CAG LysNH ₂	
6	PNA 6	H-CGAC U^{NH2}U^DT CAG LysNH ₂	
7	PNA 7	H-CTG AAA GTCG LysNH ₂	

The thermal stability of synthesized PNA oligomers with complementary DNA/RNA/PNA duplexes was examined by temperature dependent UV-spectroscopy. From comparison of data, it was observed that PNA:PNA duplexes are more stable as

compared to PNA:DNA and PNA:RNA duplexes except for PNA-5:PNA and PNA-6:PNA duplex having U^{NH₂} substitution.

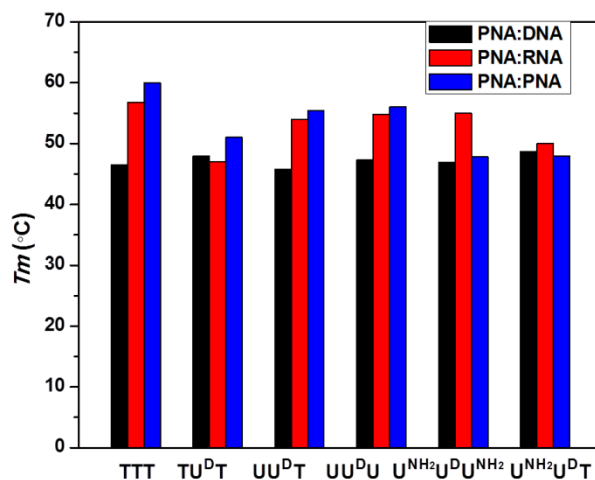
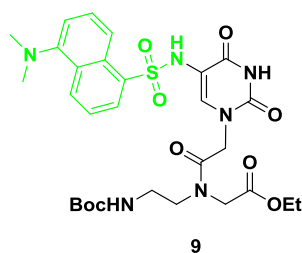


Figure 7. Comparative T_m of PNA:DNA, PNA:RNA and PNA:PNA duplexes.

The polarity of PNA:DNA/RNA/PNA duplexes was characterized by estimating the dielectric constant of PNA:DNA/RNA/PNA duplexes. Using U-dansyl as fluorescent probe, the fluorescence parameters (λ_{ex} and λ_{em}) of the compound **9** were measured in media of different dielectric constants generated by varying ratios of dioxane:water. The Stokes shift plotted against orientation polarity (f), exhibiting linear relationship suggested that the general solvent effects have dominant influence on the observed fluorescence properties of compound **9**.



Assuming that such a correlation of orientation polarity and dielectric constant for dansyl fluorophore in the monomer is valid for incorporated dansyl in PNA decamers, the observed Stokes shift of duplexes of these PNA with complementary DNA/RNA/PNA in buffer were used to estimate the major groove polarity by using Lippert equation.

$$f = \frac{\varepsilon - 1}{2\varepsilon + 1} - \frac{n^2 - 1}{2n^2 + 1}$$

The fluorescence spectra of different oligomers and their corresponding duplexes with complementary DNA, RNA and PNA were recorded in both single strand and duplex form. The data showed considerable variations in fluorescence parameters (λ_{ex} and λ_{em}) dependent on solvent. The Stoke's shift derived from this data was used to calculate local dielectric constant through the orientation polarity employing Lippert equation for each of the PNA/DNA, PNA/RNA and PNA/PNA duplexes.

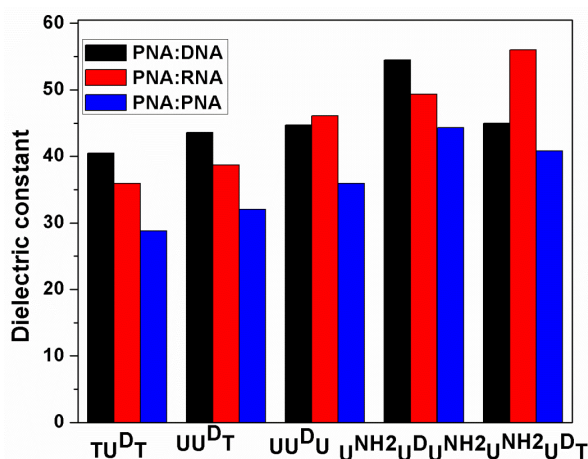


Figure 8. Comparison of dielectric constants of PNA:DNA/RNA/PNA duplexes.

Results showed that the PNA:PNA duplexes are more nonpolar as compared to PNA:DNA/RNA duplexes which may be due to the hydrophobic backbone of PNA as compare to DNA and RNA.

A.3 Chapter 3: Biophysical Studies of Tetraplex Formation of Base Modified aeg-PNA Hexamers

This chapter deals with the use of 5-aminouracil base for the formation of tetraplex and utilization of base modified PNA tetraplexes for host-guest interaction to study carbohydrate-protein interaction.

The supramolecular architecture of G-quartets has led to the development of interesting and functional non-covalent assemblies such as G-wire, ion-channels and self assembled ionophores. In recent years considerable efforts have been directed towards the synthesis and investigation of new DNA analogs with improved binding properties with nucleic acids other than the natural canonical counterparts. Search for

more stable quadruplexes from modified analogs of DNA may also help in understanding the formation of quadruplex.

Since, PNA was developed to mimic the Watson-Crick and Hoogsteen base pairing; they can participate in the formation of G quadruplex in two ways: (1) G-rich PNAs forming quadruplexes alone or in presence of DNA templates and (2) self assembly of G-rich sequences of PNA-DNA chimeras.

A.3.1 Biophysical Studies of Tetraplexes of 5-Aminouracil Linked *aeg*-PNA

In present work, 5-aminouracil linked *aeg*-PNA monomer is incorporated into PNA oligomers to utilize the 5-aminouracil for tetraplex structure formation which mimics guanine..

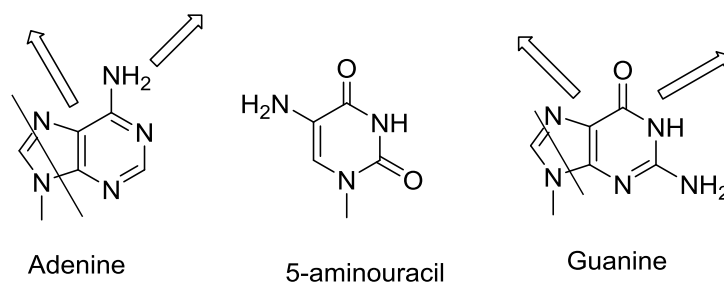


Figure 9. Structural similarity between purines and 5-aminouracil.

In this context, 5-aminouracil modified *aeg*-PNA monomer was synthesized and incorporated into PNA oligomers ($TU^{NH_2}U^{NH_2}U^{NH_2}U^{NH_2}TLysNH_2$, where, U^{NH_2} is 5-aminouracil). The fatty acid chain was conjugated to PNA oligomers at N-terminus to induce aggregation that may form from the self assembly. The quartet formation was studied by biophysical techniques (CD) and the self assembled structures were examined by FESEM.

The *N*-Boc protected monomers were incorporated into PNA oligomers through established solid phase peptide synthesis protocol. The synthesized oligomers were purified by RP-HPLC and characterized by MALDI-TOF mass spectroscopy (Table 4).

Table 4: MALDI-TOF of PNA hexamers.

Sequence code	PNA sequence	Mol. formula	Calcd mass	Obsvd mass
PNA-1	H-TGGGGT LysCONH ₂	C ₇₂ H ₉₇ N ₃₉ O ₂₁	1842.7643	1842.9417
PNA-2	H-T(U ^{NH₂}) ₄ T LysCONH ₂	C ₆₈ H ₉₆ N ₃₁ O ₂₅	1746.7194	1746.9674
PNA-3	H-TUUUUT LysCONH ₂	C ₆₈ H ₉₃ N ₂₇ O ₂₅	1686.6758	1686.6104

G = *aeg*-guanine ; U^{NH₂} = *aeg*-5-aminouracil; U = *aeg*-uracil.

The tetraplex formation of synthesized oligomers was studied by CD spectroscopy. From CD spectroscopic measurements it was observed that PNA-2 (U^{NH₂}) can form tetraplex structure like guanine while PNA-3 (U) did not show any characteristic CD signature for tetraplex formation.

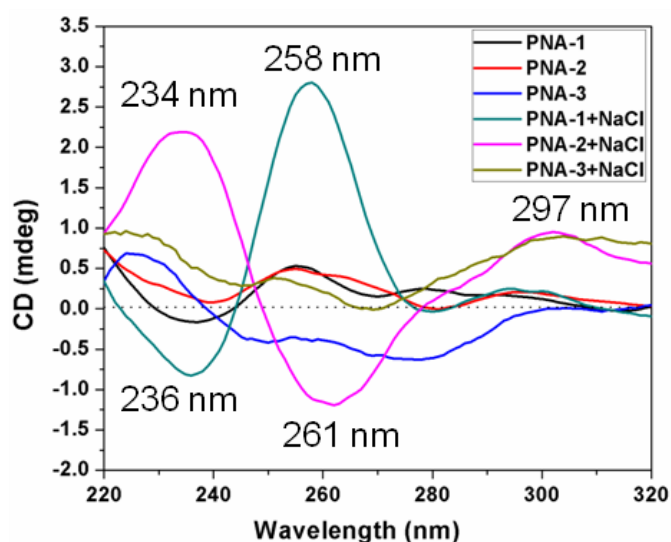


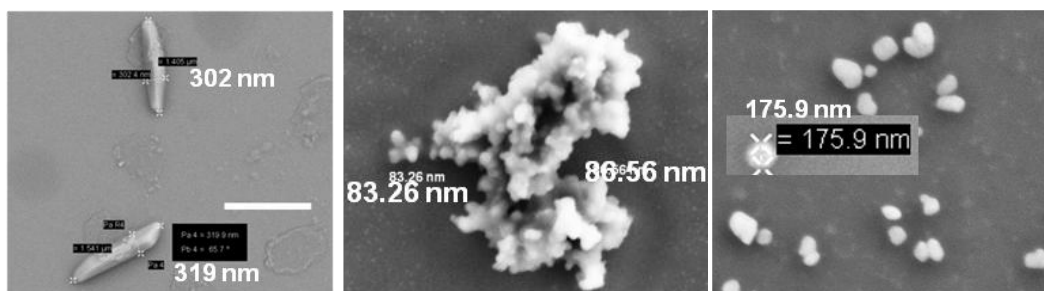
Figure 10. CD profile of PNAs 1-3 in the absence and presence of NaCl in phosphate buffer.

The concentration and pH dependent CD was recorded to examine the concentration and pH at which tetraplex formation takes place by 5-aminouracil. The results showed that 5-aminouracil forms tetraplex structure at 25 μ M concentration at physiological pH. As tetraplex structures are self-assembled molecules, the fatty acid chain was conjugated to enhance the self-assembly of tetraplex structure. Table 5 shows the MALDI-TOF mass of synthesized PNA oligomers.

Table 5: MALDI-TOF mass of fatty acid chain conjugated PNA hexamers.

PNA	PNA sequence	Mol formula	Calcd mass	Obsvd mass
PNA-4	CF ₃ -(CF ₂) ₇ -(CH ₂) ₂ -CONHTG ₄ TKNH ₂	C ₈₃ H ₉₉ F ₁₇ N ₃₉ O ₂₂	2316.7555	2316.639
PNA-5	CH ₃ -(CH ₂) ₉ -CONHTG ₄ T KNH ₂	C ₈₃ H ₁₁₆ N ₃₉ O ₂₂	2010.9157	2010.890
PNA-6	CF ₃ -(CF ₂) ₇ -(CH ₂) ₂ -CONH T(U ^{NH₂}) ₄ T KNH ₂	C ₇₉ H ₉₉ F ₁₇ N ₃₁ O ₂₆	2220.71	2220.821
PNA-7	CH ₃ -(CH ₂) ₉ -CONHT(U ^{NH₂}) ₄ T KNH ₂	C ₇₉ H ₁₁₆ N ₃₁ O ₂₆	1914.8708	1914.972
PNA-8	CF ₃ -(CF ₂) ₇ -(CH ₂) ₂ -CONHTU ₄ T KNH ₂	C ₇₉ H ₉₅ F ₁₇ N ₂₇ O ₂₆	2160.6670	2160.595
PNA-9	CH ₃ -(CH ₂) ₉ -CONHTU ₄ T KNH ₂	C ₇₉ H ₁₁₂ N ₂₇ O ₂₆	1854.8272	1854.953

Field emission scanning electron microscopy (FESEM) was employed to observe the self assembled structures formed by synthesized PNA oligomers. The results indicated that self assembly of PNA oligomers can be enhanced by the conjugation of hydrocarbon chain and fluoroalkyl chain effects are relatively more for U^{NH₂}-PNAs that can form tetraplex. It showed that 5-aminouracil induces more ordered nanoparticle formation.

**Figure 11. FESEM images of PNA-2, PNA-6 and PNA-7.**

A.3.2 Host-Guest Complexation of Adamantyl-G₄ PNA Quadruplex With Sugar capped β -Cyclodextrin to Study Carbohydrate-Protein Interaction

There is growing interest on developing multivalent systems for studying carbohydrate-protein interactions. Multivalent systems can be generated from the self assembled structures. G-quadruplexes are the self assembled structures formed by the self association of guanine. Since PNAs form stable G-quadruplexeslike DNA, PNA based quadruplexes can be used to develop multivalent system to study the

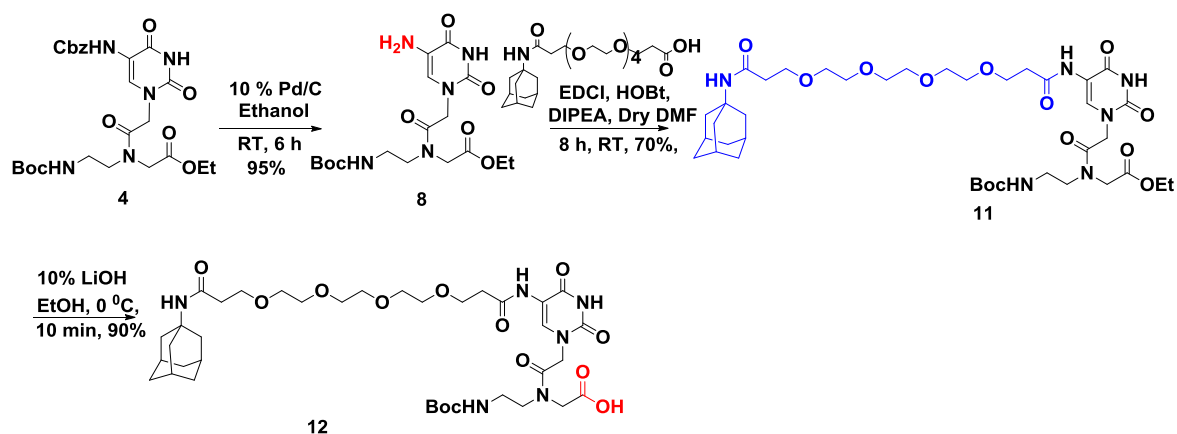
carbohydrate –protein interactions. In this context, the present work involves the synthesis of adamantyl linked PNA quadruplexes to study the carbohydrate-protein interactions.

In view of this the main idea behind present work is to develop PNA based multivalent system as PNA is stable to nucleases.

A.3.2a Synthesis of adamantyl tetraethylene glycol-U-*aeg*-PNA monomer (U[#])

Compound **4** on hydrogenation with 10% Pd/C yielded the compound **8**, which was subsequently coupled with adamantyl tetraethylene glycol acid by using EDCI, HOBt and DIPEA in DMF to obtain compound **11**. This compound upon hydrolysis with 10% aq. LiOH gave the desired *aeg*-PNA-adamantyl tetraethylene glycol-U-acid monomer **12** (U[#]).

Scheme 6: Synthesis of adamantyl tetraethylene glycol-U-*aeg*-PNA monomer (U[#])



The *N*-Boc protected monomer was incorporated into PNA oligomers through established solid phase peptide synthesis protocol. The synthesized oligomers were purified by RP-HPLC and characterized by MALDI-TOF mass spectroscopy. CD spectroscopic measurements of the synthesized PNA oligomers were recorded in the presence and absence of 100 mM NaCl followed by host-guest interaction of PNA tetraplex. Results suggested that both PNAs form tetraplex in the presence of sodium chloride and interacts with β -cyclodextrin.

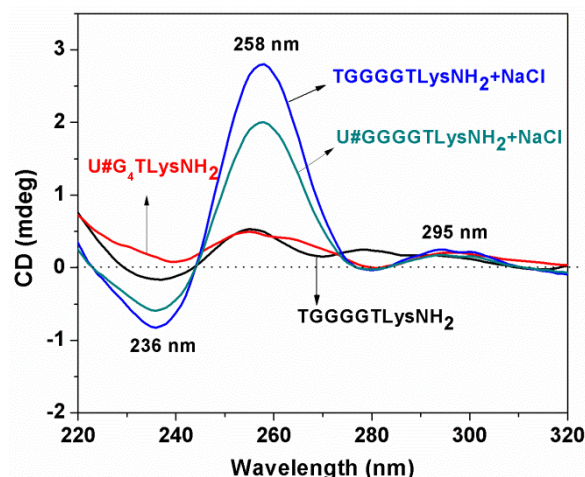


Figure 12. CD profile of PNA oligomers.

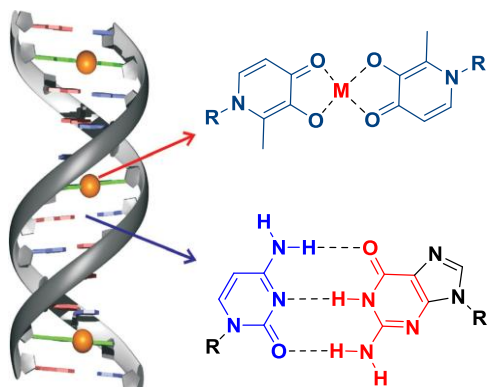
Summary of thesis

- Rationally designed PNA monomers were synthesized and were incorporated into *aeg* PNA sequence at desired positions by solid phase peptide synthesis protocol using *Boc* strategy. The synthesized PNA oligomers were purified by RP-HPLC and characterized by MALDI-TOF spectrometry.
- Modified 3-hydroxy-2-methyl-4-pyridone PNA monomer (MHP) and MHP incorporated PNA oligomers were utilized for metal complexation studies by employing UV-Vis, fluorescence, MALDI-TOF and temperature dependent UV spectroscopic studies.
- Results showed that 3-hydroxy-2-methyl-4-pyridone PNA monomer (MHP) binds strongly with rare earth metal salts.
- Thermal melting studies showed that metal coordination highly stabilizes the MHP incorporated PNA duplexes.
- Polarity of the major groove of PNA:DNA/RNA/PNA duplexes was determined by fluorescence spectroscopy measuring Stokes shift .
- It was found that the PNA:DNA/RNA duplexes are more polar as compared to PNA:PNA duplexes.
- These results were compared with dielectric constant of DNA:DNA duplexes and observed that DNA:DNA duplexes are more hydrated as compared to PNA:DNA/RNA/PNA duplexes suggesting that hydrophobic backbone of PNA play an important role in polarity of the major groove of duplexes.

- The 5-aminouracil linked PNA hexamers were studied for tetraplex formation by CD spectroscopy. It was found that 5-aminouracil can lead to form the tetraplex structure as that of guanine.
- FESEM results suggested that the enhancement of self-assembled structure of 5-aminouracil PNA can be enhanced by conjugation of fatty acid chain.
- Host-guest interaction of base modified PNA tetraplexes was studied with β -cyclodextrin by CD spectroscopy. Results showed that it changes the orientation of tetraplex structure.

Chapter 1

Design, Synthesis and Metal Complexation Studies of *aeg*-PNA with Metal Binding Ligand Replacing Base Pairing



This chapter deals with the synthesis of metal complexing ligand 3-hydroxy-2-methyl-4-pyridone linked to *aeg*-PNA backbone and its subsequent incorporation into PNA oligomers by SPPS. Metal complexation property of the ligand was investigated at monomer and oligomer level by employing various techniques.

1.1 Introduction

DNA is the basic hereditary material present in almost all living organisms and contains all information necessary to make proteins.¹ It has been 62 years since Watson and Crick elucidated the double-helical structure of DNA (Figure 1). DNA is a polymer made up of repeating units of nucleotides. Each nucleotide unit consists of a nitrogenous base, a deoxyribose sugar, and a phosphate backbone.² The main chemical constituents of DNA are the (i) sugar-phosphate unit present on the outer side of the helix which constitutes the backbone of each strand and (ii) the nitrogenous bases adenine (A), thymine (T), guanine (G) and cytosine (C) which are pointed towards the center of the helix. Each base is connected to a sugar via a β -glycosyl linkage. Hydrogen bonds between complementary base pairs (A:T; G:C) holds the two strands together (Figure 1). The molecular architecture of DNA consists of a double stranded helix of uniform diameter, with right handed twist. RNA contains ribose rather than deoxyribose sugar with the base composition adenine (A), uracil (U), guanine (G) and cytosine (C).

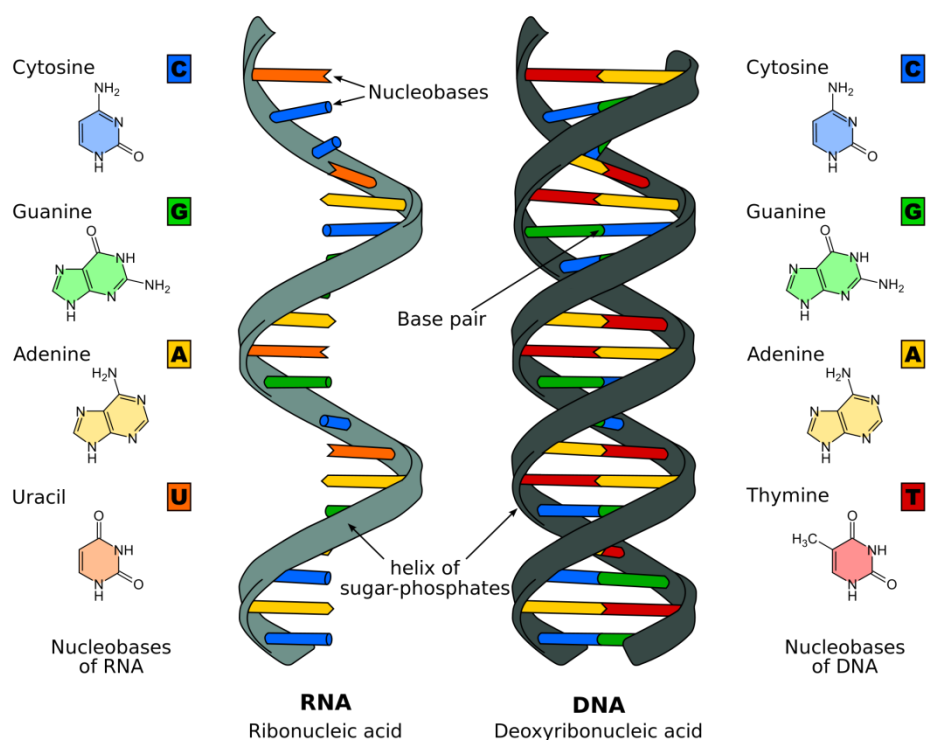


Figure 1. Structure of nucleic acids.

Figure obtained from website,

https://upload.wikimedia.org/wikipedia/commons/3/37/Difference_DNA_RNA-EN.svg

The DNA double helix is nature's simple and elegant solution to the problem of storing, retrieving, and communicating the genetic information of living organism.³ The specificity and the reversibility of the hydrogen bond formation between the complementary nucleobases is one of the most important characteristic features of DNA double helix. It allows the strands of the double helix to unwind and rewind in exactly the same configuration. Chemists are fascinated by DNA after the elucidation of its double helix and remarkable properties, governed by its structure. Tremendous efforts have been made to understand its structure, function and applications in biology as well as physicochemical and material science.⁴ The construction of DNA and design of its analogues for use in the recognition of specific DNA and RNA sequences has emerged as intellectual and practical assignment for synthetic and structural organic chemists. The recognition of DNA and RNA sequences by complementary oligonucleotides is a central feature of biotechnology and is vital for hybridization based biological applications. The study of such complementary recognition is possible with widely used experimental techniques and diagnostic protocols.

1.2 Base pairing in nucleic acids

The nucleobases are the key components that converse chemical variability to DNA/RNA. Watson and Crick recognized the complementarities in hydrogen-bonding capability of A:T and G:C base pairs during DNA model-building studies in 1952. The nucleobases have complementary hydrogen bond donors and acceptors that generate specific associations between bases. Association via base pairing is normally seen between purines (Guanine, Adenine) and pyrimidine bases (Thymine, Cytosine, and Uracil), utilizing the basic Watson–Crick base pairing motif.² The G:C base pairing, with its three hydrogen bonds is more stable than the A:T/A:U base pairing with only two hydrogen bonds. The mutual recognition of A by T and of C by G using hydrogen bonds establishes the fidelity of DNA transcription and translation. The N-H groups of the bases are potent hydrogen donors (D), while the sp^2 -hybridized electron pairs on the oxygen of the base C=O groups and on the ring nitrogen are much better hydrogen bonding acceptors (A) than the oxygen of either the phosphate or the pentose. The acceptors: donors (A: D) hydrogen bonds so formed more partial ionic in character.

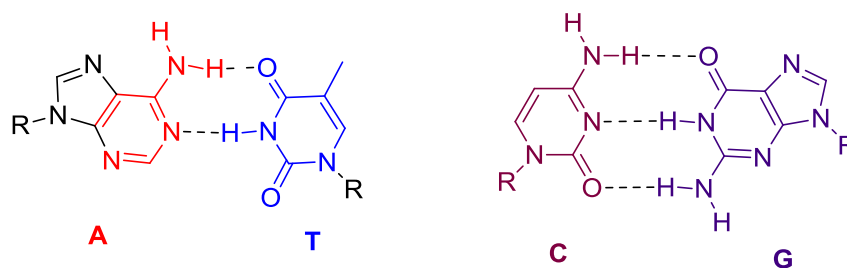


Figure 2. Watson Crick hydrogen bonding.

While Watson–Crick base pairing is found to be the dominant pattern, other base pairings also have been suggested of which the most significant to be identified are Hoogsteen base pairs⁵ and Crick ‘wobble’ base pairs.⁶ Hoogsteen base pairing allows binding of pyrimidine third strand in the major groove of purine: pyrimidine duplexes to form triple helical structures in 1:2 stoichiometry of [poly(dA):2poly(dT)] and [poly(rG):2poly(rC)]. The triplexes do occur in DNA and RNA in polypurine: polypyrimidine structures.

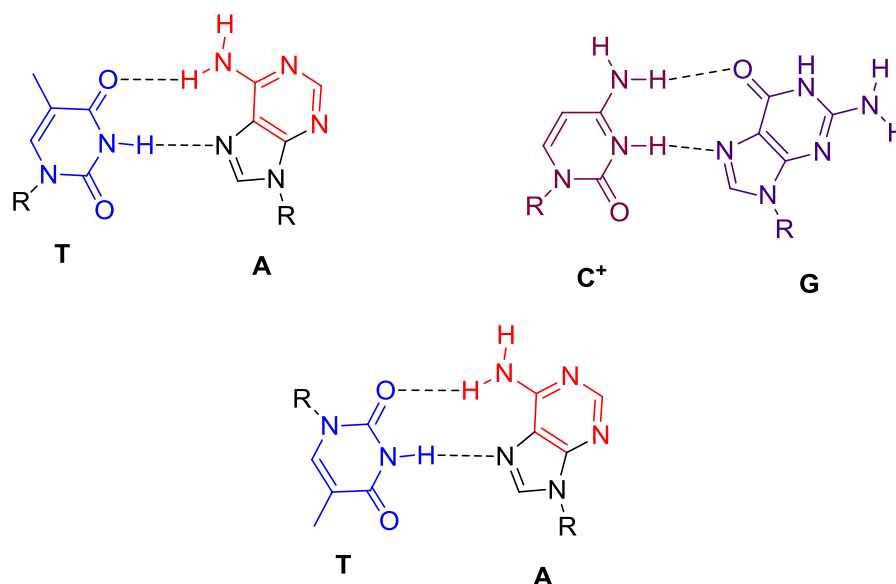


Figure 3. Reverse Watson-Crick hydrogen bonding.

Francis Crick proposed the hypothesis for the existence of ‘wobble’ base pairings to explain the degeneracy of the genetic code.⁶ This hypothesis explains that, only the first two bases of the codon of tRNA have a precise pairing with the bases of the anticodon of mRNA, whereas the pairing between the third bases of codon and anticodon may Wobble (non-specific). In Wobble base pairing (Figure 4), a single purine base is able to recognize different pyrimidines (e.g. I:U and I:A where I =

inosine, U = uracil, A = adenine). This has importance in the interaction of messenger RNA (*m*-RNA) with transfer RNA (*t*-RNA) on the ribosome during protein synthesis (codon-anticodon interactions). Several mismatched base pairs and anomalous hydrogen bonding patterns have been seen in X-ray studies of synthetic oligodeoxynucleotides.⁷

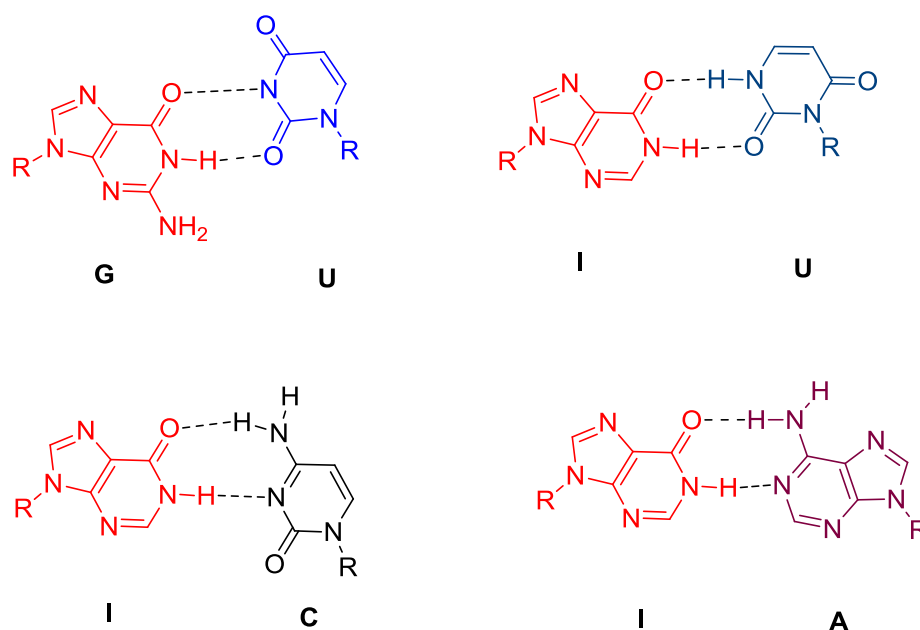


Figure 4. Wobble base pairing.

In addition to biological functions, nucleic acids' ability to function as the carrier for storage and transfer of information has been extensively utilized recently for the creation of nanostructures and molecular electronics.⁸ In this context, nucleic acids and particularly DNA provides a promising tool for bottom-up fabrication of inorganic and bioorganic molecular devices. The DNA sequences can be designed to self assemble into different types of architectures such as duplexes, triplexes, quadruplexes and nanostructures. Several attempts have been made to exploit and extend these properties of DNA by modifying backbone and nucleobases for various applications in both biological and nanomaterials chemistry. Keeping the fundamental design of the DNA double helix intact, several groups⁹ have studied replacement of the natural base pairs of DNA molecule with ligands that show pronounced affinity to bind to metal ions.

1.3 Metal mediated base pairing

It is well known that hydrogen bonding contributes significantly to folding and assembly of biomolecules through the intra- and intermolecular recognition. Metal coordination also plays vital role in maintaining and stabilizing biologically relevant structures in terms of molecular recognition. In this context, it has been of interest to see if natural base pairing can be replaced by metal mediated base pairing, which may provide valuable insights into the origin of chemical evolution that might involve both inorganic and organic compounds.¹⁰

Metal mediated base pairs have an advantage in comparison with unnatural since metal ions can be incorporated based on their unique physical and chemical properties, altered hydrogen bonding pattern and shape complementarity.¹¹ Accordingly, rational selection of metal ions would enable appropriate adjustment of the coordination properties of metallo-base pairs, such as their selectivity and structures as well as thermodynamic stability.

Simplest idea behind metal coordinate base pairing was to replace hydrogen atom within hydrogen bonded base pairs by a metal ion since it can accept lone pair of electrons on heteroatom (Figure 5). Lee et al.¹² in 1993 found that Zn^{2+} ion stabilizes the DNA duplexes at elevated pH at which hydrogen atoms involved in hydrogen bonding were released and metal ions were bound to the nucleobases. Another idea was to convert natural mismatched pair into a metal-coordinated base pair. It is well known that T-T mismatch is converted to a stable metallo-base pair in the presence of Hg^{2+} ions as originally proposed by Katz¹³ and further studied by Marzilli et al.¹⁴ Such metal mediated base pairing is being used for metal responsive functional DNA molecules including allosteric DNAzymes¹⁵ and logic gates.¹⁶

Although the idea of replacing the hydrogen atom of H-bond by metal ions is simple, it would inconveniently disorder the complementarity rule of natural base pairing. Thus, such metal coordinated base pairs could not become orthogonal to natural base pairs. This drawback tempted researchers to develop a novel metal mediated base pairing system by using synthetic ligand type nucleobases. The artificial metal coordinated base pairing is designed to match the structural requirement like size and shape of the canonical base pairs. Most important thing for ideal metallo-base

pairing is that the central metal ion should be chosen in such a way that not to disturb the duplex structure to great extent.¹⁷

A strategy for metal ion incorporation into nucleic acid duplexes first proposed by Tanaka and Shionoya¹⁸ involves the replacement of the natural nucleobases by ligands that have a higher affinity for metal ions than the natural nucleobases. The metal complexes of ligand-modified nucleic acids can mimic as alternative base pairs. If the ligands are aromatic and the geometry of the metal complex is planar, the complexes can participate in π -stacking interactions with adjacent nucleobase pairs. Sequences can be designed in a way to assemble into different types of induced architectures such as duplexes, triplexes, and a variety of branched nanostructures.¹⁹ In the past decade, numerous ligands have been introduced into DNA oligomers.¹⁷

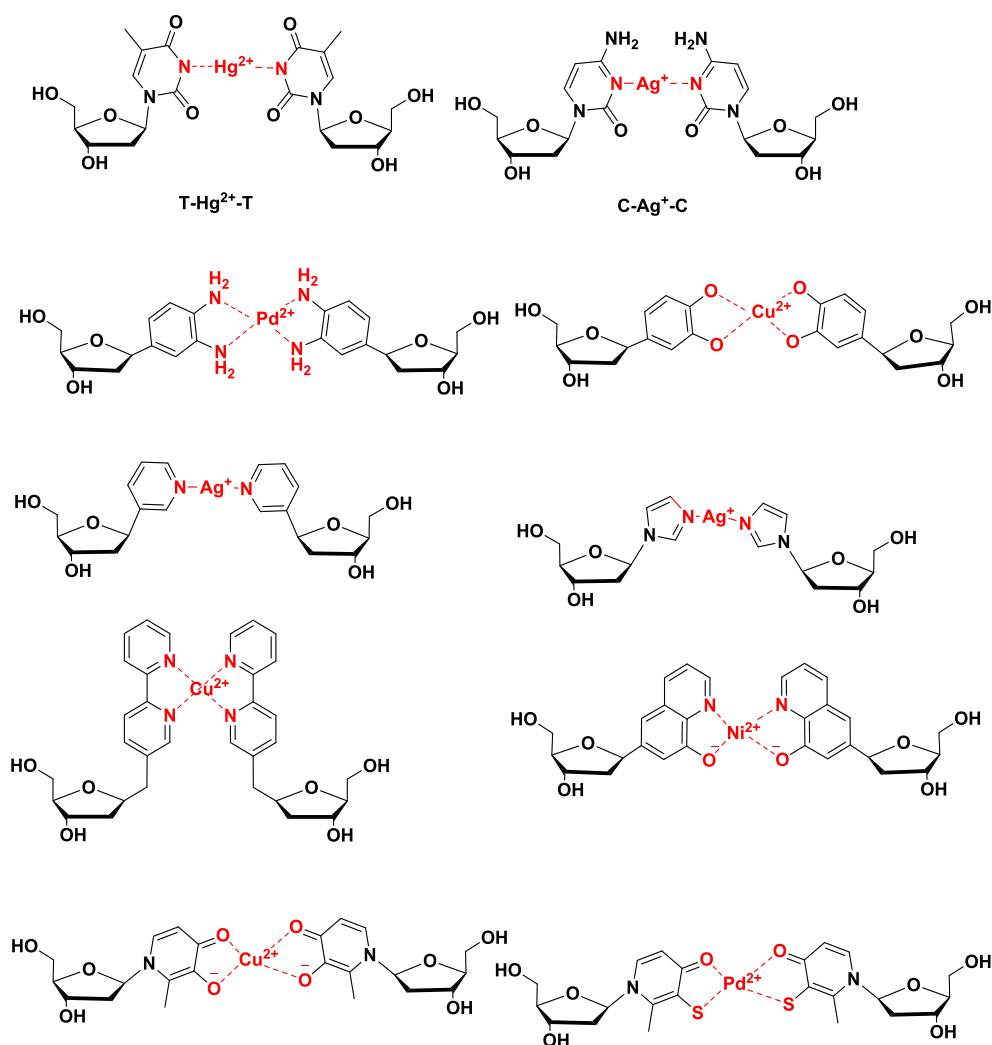


Figure 5. Alternative metal-mediated base pairs.¹⁷

The metal mediated base pairing also can be studied for peptide nucleic acids (PNA), an artificial analog of DNA, introduced by Nielsen et al.²⁰ The structure of PNA is remarkably simple consisting of repeating N-(1-aminoethyl)-glycine units linked by amide bonds (Figure 6). The purine (A, G) and pyrimidine (C, T) bases are attached to the backbone through methylene carbonyl linkages and hence PNA is a molecular hybrid of peptides and nucleic acids in a rare structural combination. PNAs are devoid of any sugar moieties or phosphate groups and therefore, it was a surprise that it mimicked the behavior of DNA in many respects and demonstrated superior properties in some applications.²¹ For two decades peptide nucleic acids (PNA) have emerged as one of the most potential but underutilized oligonucleotides analogs for the recognition of nucleic acids (DNA/RNA, Figure 6).²²

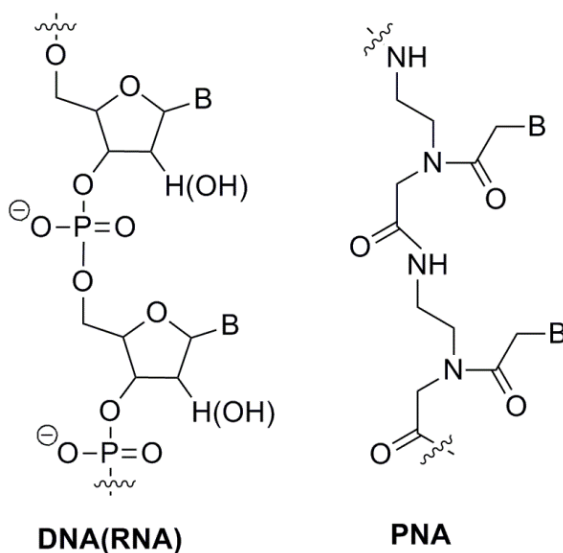


Figure 6. Structures of DNA and PNA.

The self-assembly and molecular recognition properties of nucleic acids and their artificial analogues, such as peptide nucleic acids (PNAs), facilitate the design of new functional supramolecular structures. These supramolecular structures find promising applications as sensors for small molecules or nanomachines for molecular computing or drug delivery.¹⁰ The interesting spectroscopic, redox, and magnetic properties of metal ions can be used to expand the genetic code by storing and reading information into a sequence of metal complexes.

1.4 Metallo-PNAs

The chelation abilities of DNA are relatively weak for binding to metal ions, leading to the disordered, uncontrollable stoichiometries and geometries. PNA, an artificial analogue of DNA allows the incorporation of distinct, high affinity metal binding sites that can solve these problems. The neutral character of PNA makes it peculiar when metal complexes are incorporated into PNA as alternate base pairs, because the overall charge of the inorganic-PNA co-ordination complex totally depend on inorganic component of the complex. Therefore PNA is an ideal choice for making nanostructures.

1.4.1 Metallo-PNA as biosensors

Wang et al.²³ developed DNA biosensors with PNA recognition layers as PNA have remarkable hybridization properties (higher thermal duplex stability) and mismatch discrimination. PNA-derived biosensors have capability of distinguishing closely related sequences as compared to DNA under less restrictive reaction conditions.^{24,25} Introducing redox property into the PNA recognition layer facilitates the electrochemical DNA detection. The PNA recognition layer was used as free-diffusing redox mediators,²⁶ redox-active intercalators or minor-groove binders²⁷⁻³⁰ or as covalently bound redox labels.³¹⁻³⁴ Label-free PNA-based biosensors were utilized with the help of electrochemical impedance spectroscopy,^{35,36} scanning electrochemical microscope (SECM),³⁷ reflection absorption infrared spectroscopy (RAIRS) or X-ray photoelectron spectroscopy (XPS) techniques.³⁸

Kramer et al.³⁹ inserted ter-pyridyl (tpy) moieties into the PNA backbone and showed that the cellular uptake of PNA is enhanced by Zn²⁺ ion (Figure 7). Researchers have developed ferrocenyl click derivatives, chromium tricarbonyl, Fischer type carbene complexes of tungsten and redox active ruthenium complexes in order to evaluate the electrochemical behaviour of organometallic moieties within the PNA sequence.⁴⁰⁻⁴² this has found great applications in spectroscopic analysis and bio-imaging agents. Figure 7 shows the various types of metal binding ligands attached to *aeg*-PNA.⁴³⁻⁴⁷

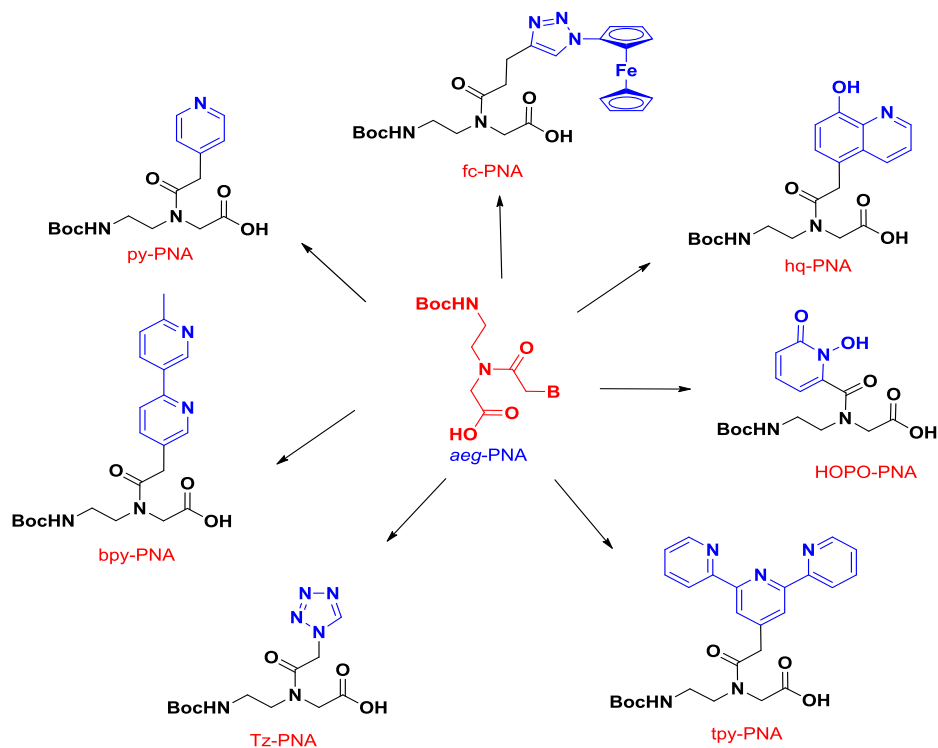


Figure 7. Metal binding ligands attached to aeg PNA.⁴³⁻⁴⁷

Mokhir et al.⁴⁸ designed various PNA oligomers that bind specifically to Zn^{2+} ions which is found at higher concentrations in various organs and some cancerous cells (Figure 8). Keeping this in mind, bi and tri-dentate ligand conjugated PNAs were prepared and found to increase the thermal stability PNA:DNA/RNA duplexes.

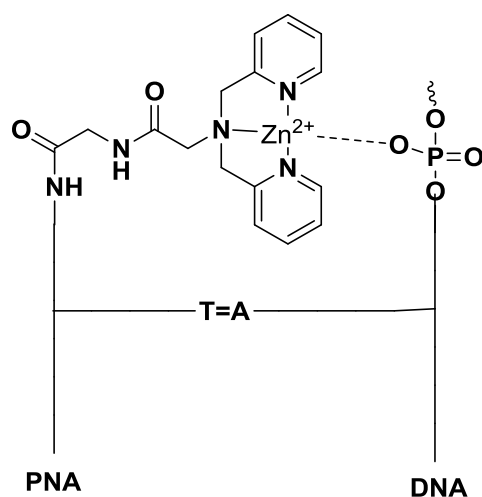


Figure 8. PNA/DNA duplexes stabilized by Zn^{2+} ion.

1.4.2 Metallo-PNA as artificial nuclease

The development of artificial restriction endonucleases or ribonucleases is a very promising field. Sequence specific cleavage of DNA/RNA by synthetic analogues would be a versatile technique in molecular biology. In contrast to restriction endonucleases which cleave short sequences only, artificial nucleases could cleave any DNA/RNA sequence. PNAs are nuclease resistant and are suitable candidates to serve as artificial nucleases. Stromberg et al.⁵⁰ recently described the PNA based artificial nucleases. Nielsen et al.⁵¹ used the metallo-PNA for oxidative cleavage of double stranded DNA, by preparing catalytic manganese porphyrin-PNA conjugate.

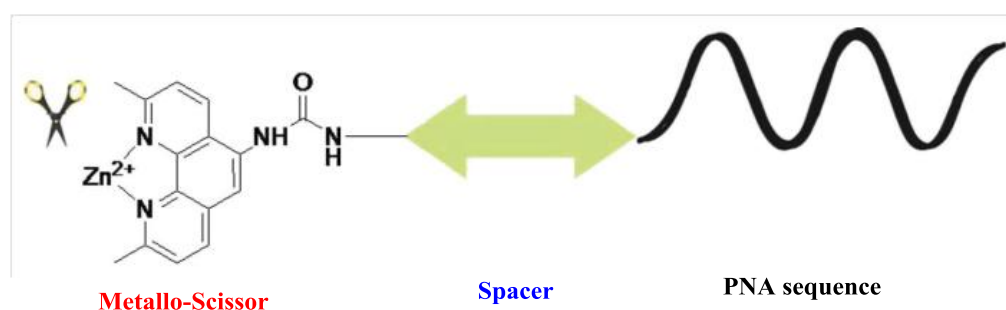


Figure 9. Artificial nucleases containing PNA sequence.

1.4.3 Improvement of cellular uptake of PNA using metal complexes

One of the major drawbacks of PNA in the development of antisense therapeutics is its poor cellular uptake. For proper distribution at intracellular level, one has to cross several barriers. Delivery methods that are well established for DNA/RNA may not be suitable for uncharged neutral PNA.

Usually the PNAs were conjugated with cell penetrating peptide (CPP) for better intracellular entry. Such conjugation efficiently improved the cellular uptake of PNA which got trapped in endosomes and therefore unable to distribute equally in the cytoplasm or transport into the nucleus.⁵²⁻⁵⁵ Metal complexes were therefore introduced not only to enhance cellular uptake and endosomal escape but also to compete or even replace fluorescent markers for better results. The modified PNA oligomers with terpyridine (tpy) improved cellular and nuclear uptake which were further enhanced by Zn(II) conjugation.⁵¹

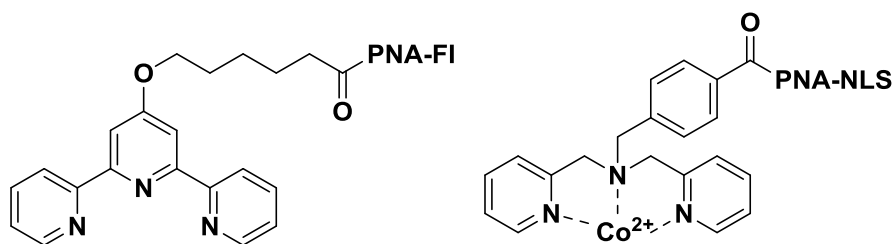


Figure 10. Terpyridyl PNA conjugate with fluorophore and PNA-NLS conjugate with cobalt.

1.5 Synthetic methods for the preparation of PNA oligomers

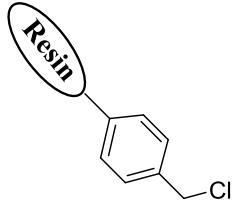
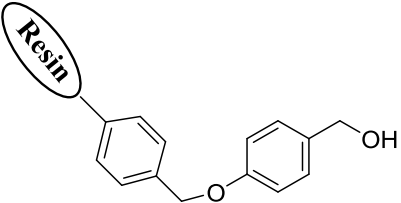
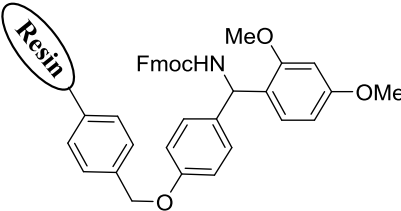
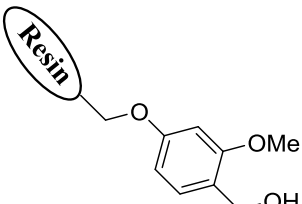
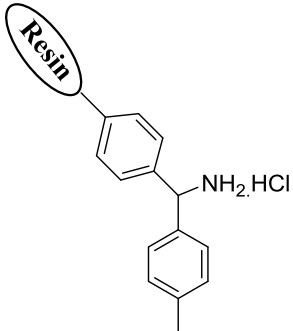
There are various methods to synthesize PNA oligomers. Solution phase synthesis of PNA oligomers is restricted due to its tedious and time consuming process. Solid phase synthesis is the obvious choice due to its ease of handling and scale up capability. The difference between solution and solid phase synthesis is given in the Table 1.

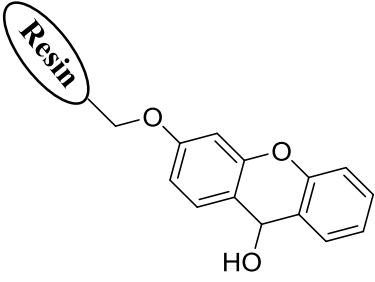
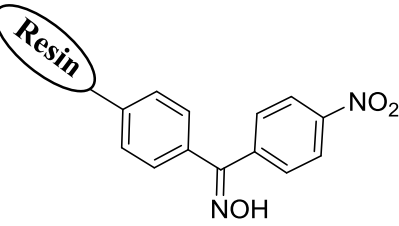
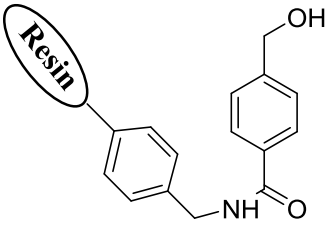
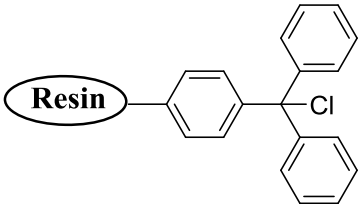
Table 1: Difference between solid phase and solution phase peptide synthesis.

Solid phase peptide synthesis	Solution phase peptide synthesis
Practically feasible for small and lengthy sequences.	Practically very difficult as purification of polar intermediate peptides is infeasible.
Isolation and purification of intermediates is not needed.	Isolation and purification is needed for each step.
Excess of coupling reagents and monomers is needed.	Excess use of coupling reagents and monomers is not needed.
Recemization is not observed.	Recemization is observed.
Time saving process	Time consuming process

Peptides with different functionalities at termini can be synthesized by proper choice of resin. A brief discussion about resins used in solid phase peptide synthesis is given below.

Table 2: Structure of resins.

Resin structure	Protecting group used	Resin cleavage conditions	Final product
 <p>Merrifield resin</p>	Boc	HF/TFA HBr/TFMSA	Peptide acids
 <p>Wang resin</p>	Fmoc	TFA	Peptide acids
 <p>Rink amide resin</p>	Fmoc	20% TFA/DCM	Peptide carboxamides
 <p>SASRIN resin</p>	Fmoc	1% TFA/DCM	Peptide acids
 <p>MBHA resin</p>	Boc	TFA/TFMSA	Peptide carboxamides

 Sieber resin	Fmoc	1% TFA/DCM	Peptide acids
 Oxime resin	Boc	NaOH, N ₂ H ₄ NH ₃ , RNH ₂	Peptide acids
 PAM resin	Boc	TFA/TFMSA	Peptide acids
 Trityl resin	Fmoc	1-5 % TFA/DCM	Peptide acids

Generally, in solid phase peptide synthesis *Boc* strategy or *Fmoc* strategy is used. The *Boc* and *Fmoc* groups are the protecting groups used for *N*-protection and are acid⁵⁶ and base labile⁵⁷ respectively. The *C*-terminus of amino acids is attached directly to the resin or through linker. Other functional groups on the side chains are protected orthogonally with *Boc* and *Fmoc* groups. *Fmoc* chemistry is known to give peptides of higher purity and better yield compared to *Boc* chemistry.

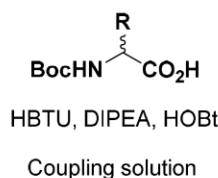
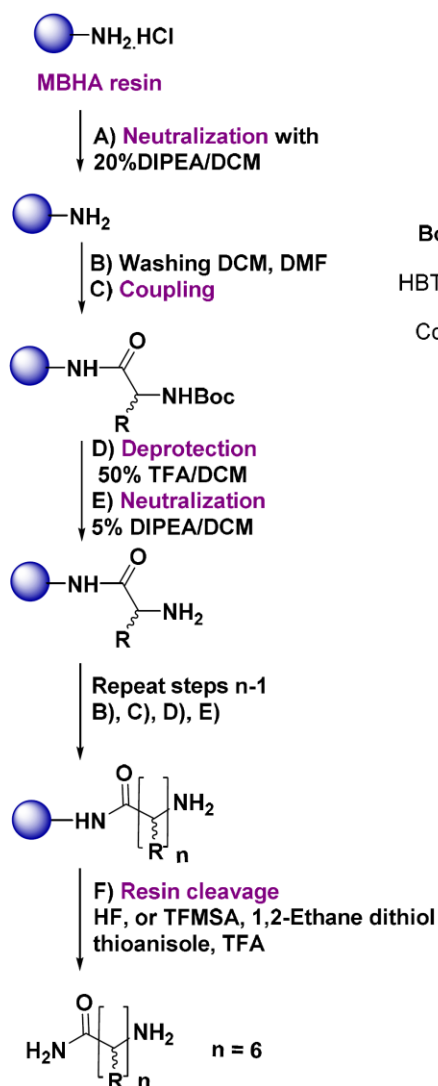
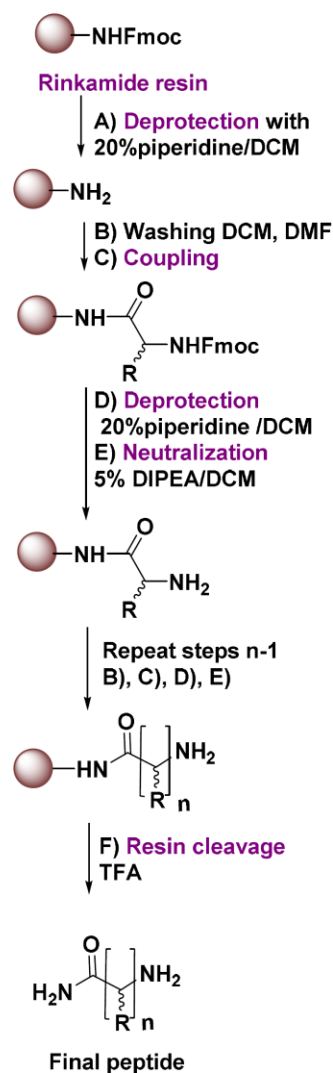
Boc-chemistry**Fmoc-chemistry**

Figure 11. General protocols for the synthesis of peptides by *Boc* and *Fmoc* strategy.

The cleavage of *Boc* and *Fmoc* groups is carried out by using trifluoroacetic acid (TFA) and 20% piperidine in DMF respectively. Once the peptide is synthesized up to desired length, it is cleaved from solid support, employing different deprotection conditions. The final cleavage of resin is achieved using strong acid such as hydrogen fluoride and trifluoromethanesulphonic acid (TFMSA) in case of *Boc* protection and 20% TFA in DCM for *Fmoc* protection.

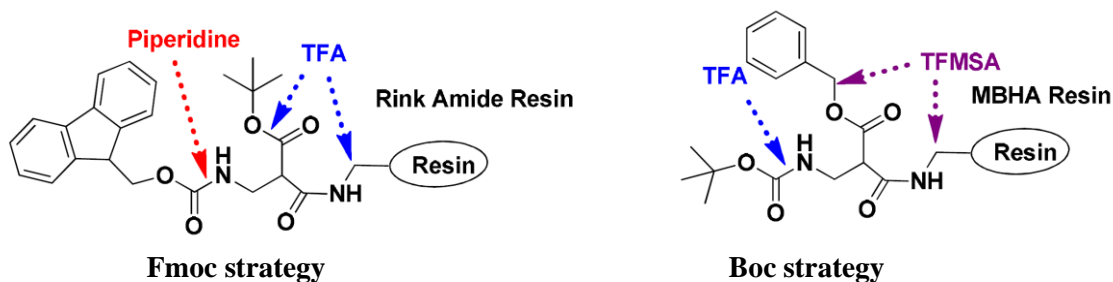


Figure 12. Cleavage of resins by *Boc* and *Fmoc* strategy.

1.6 Present work: Rationale and objective

The rationale behind synthesis of *aeg*-PNA possessing ligands that have affinity towards metal is to generate molecular assembly or molecular wires based on metal-ligand and metal-metal interactions. The properties of metal complexes can be tuned by changing metal ions that control

1. Thermodynamics and kinetics of complexation and decomplexation.
2. Changes in co-ordination numbers and geometries.
3. Physicochemical properties such as redox, magnetic, optical and lewis acidity
4. The assembly of oligomers.

Previous work from the laboratory involved the use of catechol on PNA backbone as metal binding ligand. However, it exhibited poor binding affinity to Cu^{2+} and Ni^{2+} . Hence in present work, 3-hydroxy-2-methyl-4-pyridone which is better for metal binding was chosen.

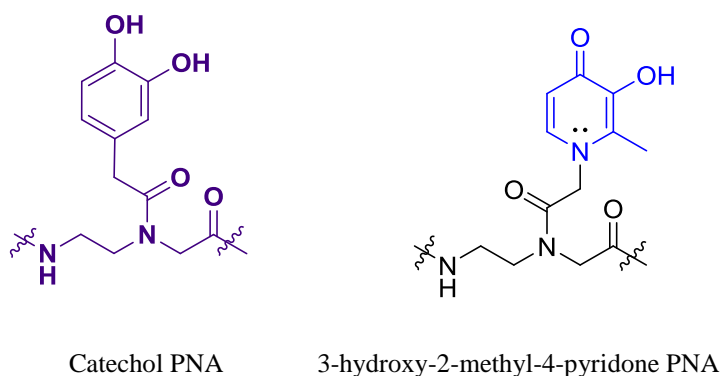


Figure 13. Structures of catechol PNA and 3-hydroxy-2-methyl-4-pyridone PNA.

This ligand has been earlier incorporated into DNA oligomers, leading to high stabilization of the duplexes in presence of Cu^{2+} ion¹⁸. Intentions to incorporate 3-hydroxy 2-methyl 4-pyridone into the PNA was,

- To make Cu^{2+} stabilized PNA duplexes that can be useful as PNA based biosensors, in view of the biological relevance of Cu^{2+} .
- In addition to Cu^{2+} , the ligand also complex with the lanthanides.
- As lanthanides possess luminescence properties, complexation of ligand modified PNA with lanthanides can be used for making luminescent materials which may have application in organic light emitting diodes.

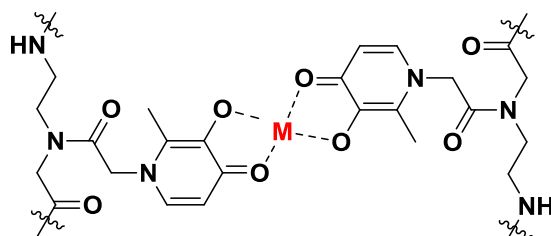


Figure 14. Metal mediated base pairing in 3-hydroxy-2-methyl-4-pyridone.

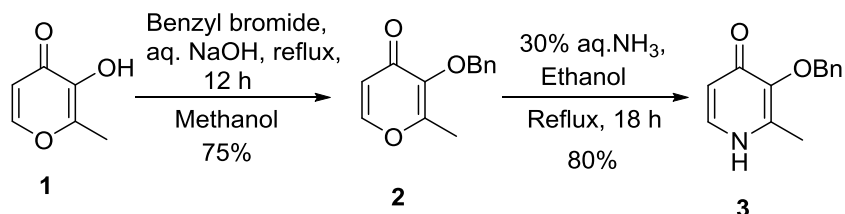
1.7 Results and Discussion

The 3-hydroxy 2-methyl-4-pyridone *aeg*-PNA monomer was synthesized and incorporated into PNA oligomers. The metal complexation of *aeg*-PNA monomer and PNA oligomers were studied by UV-Vis, fluorescence, and temperature dependent UV spectroscopic techniques.

1.7.1 Synthesis of *N*-Boc-aminoethyl-(3-benzyloxy-2-methyl-4-oxopyridonyl-*N*-actamido) glycine monomer

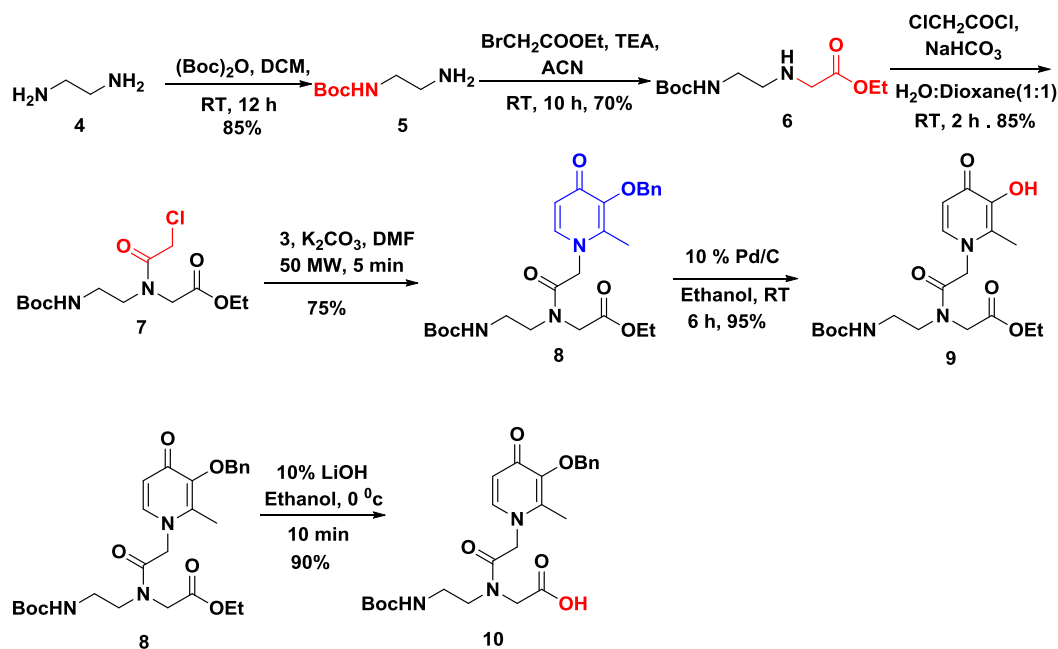
Commercially available 3-hydroxy-2-methyl-4-pyridone **1** was O-benzylated with benzyl bromide in methanol to obtain **2** which was subsequently treated with aqueous ammonia in ethanol to give crystalline 3-benzyloxy-2-methyl-4-pyridone **3**.

Scheme 1:



The commercially available ethylenediamine was treated with Boc-anhydride (0.1 eq) to get *N*-Boc ethylenediamine (**5**) which was *N*-alkylated by reaction with ethyl bromoacetate compound **6**. This was *N*-acylated by treating with chloroacetyl chloride to obtain compound **7** which was reacted with 3-benzyloxy 2-methyl 4-pyridone **3** to yield **8**. This upon hydrogenation with 10% Pd/C in ethanol gave the compound **9**. The hydrolysis of ester **8** with 10% lithium hydroxide leads to target monomer **10**.

Scheme 2:



1.7.2 Design and Synthesis of PNA oligomers

The desired PNA oligomers were synthesized manually on solid phase by *t*-Boc strategy on MBHA resin under microwave condition from *C*-terminus to *N*-terminus. The modified PNA monomer **10** was incorporated at desired position in the unmodified *aeg*-PNA sequence. The Fmoc strategy was avoided because the terminal free amine generated has tendency to attack on the tertiary amide leading to acyl migration.⁵⁹

MBHA resin (4-methyl-benzhydryl amine resin) was chosen as the solid support on which the oligomers were synthesized and the monomers were coupled by *in situ* activation with HBTU / HOBt. In the synthesis of all oligomers, orthogonally protected (Boc/Ci-Cbz) L-lysine was selected as the C-terminal spacer-amino acid and it is linked to the resin through amide bond. The amine content on the resin was suitably lowered from 0.67 mmol/g to 0.35 mmol/g by partial acylation of amine using calculated amount of acetic anhydride.⁵⁹ The free amine groups on the resin available for coupling was confirmed before starting synthesis by Kaiser's test.

The deprotection of the *t*-Boc and the completion of coupling reaction were monitored by Kaiser's test.⁶⁰ The *t*-Boc deprotection leads to a positive Kaiser's test, where the resin beads show blue color (Ruhemann's purple). On the other hand, resin beads were colorless after completion of coupling reaction which means a negative Kaiser's test. It is the most employed qualitative test for the detection of free amino group (deprotection/coupling). Eight PNA oligomers (PNA 1-PNA 8) were synthesized using SPPS protocol (Table 3). The first two are self complementary sequences (PNA-1 and PNA-2) and pairs of (PNA 3:PNA 4), (PNA 3:PNA 5), (PNA 6:PNA 7) and are (PNA 6:PNA 8) are complementary sequences for duplex formation (Table 3).

Table 3: PNA oligomers with modified/unmodified *aeg*-PNA monomers.

Entry	Sequence code	PNA sequence	Monomers Used
1	PNA-1	H-GCGATCGC LysNH ₂	A/G/C/T = <i>aeg</i> PNA
2	PNA-2	H- GCGA X TTCGC LysNH ₂	<p>X=MHP-PNA monomer</p>
3	PNA-3	H-ATAGA X CATC LysNH ₂	
4	PNA-4	H-GATG X TCTAT LysNH ₂	
5	PNA-5	H-TATCT X GTAG LysNH ₂	
6	PNA-6	H-ATAGATCATC LysNH ₂	
7	PNA-7	H-GATGATCTAT LysNH ₂	A/G/C/T = <i>aeg</i> PNA
8	PNA-8	H-TATCTAGTAG LysNH ₂	

1.7.3 Cleavage of the PNA oligomers from solid support

The PNA oligomers were cleaved from the solid support (MBHA resin), using trifluoromethanesulphonic acid (TFMSA) in the presence of trifluoroacetic acid to give

aeg-PNA oligomers, having amide group at C terminus. After cleavage, the polyamide oligomers obtained in solution were precipitated by addition of cold diethyl ether.

1.7.4 Purification and characterization of the PNA oligomers

The synthesized PNA oligomers were purified by RP-HPLC. The purified PNA oligomers were characterized by MALDI-TOF mass spectrometry using 2,5-dihydroxybenzoic acid (DHB) as matrix. The calculated and observed molecular weights for all PNAs with their molecular formula are shown in Table 4. The HPLC and MALDI-TOF spectra of the PNA oligomers are shown in Appendix-I.

Table 4: MALDI-TOF of PNA oligomers.

Entry	Sequence code	Mol. formula	Calcd. mass	Observed mass
1	PNA 1	C ₉₁ H ₁₂₁ N ₅₀ O ₂₅	2313.9734	2314.0159
2	PNA 2	C ₁₀₃ H ₁₃₇ N ₅₃ O ₂₉	2579.0797	2579.9371
3	PNA 3	C ₁₁₅ H ₁₅₁ N ₅₉ O ₃₀	2838.2104	2838.3505
4	PNA 4	C ₁₁₆ H ₁₅₁ N ₅₅ O ₃₄	2858.1777	2858.3537
5	PNA 5	C ₁₁₆ H ₁₅₁ N ₅₅ O ₃₄	2858.1777	2858.191
6	PNA 6	C ₁₁₄ H ₁₄₉ N ₆₀ O ₃₀	2838.1978	2838.8647
7	PNA 7	C ₁₁₅ H ₁₄₉ N ₅₉ O ₃₂	2869.1924	2869.4029
8	PNA 8	C ₁₁₅ H ₁₅₀ N ₅₉ O ₃₂	2869.1924	2869.7876

1.8.1 Molar extinction coefficient of ethyl *N*-Boc-aminoethyl-3-hydroxy-2-methyl-4-pyridone glycinate **9** (MHP)

Molar extinction coefficient of ethyl *N*-Boc-aminoethyl-3-hydroxy-2-methyl-4-pyridone glycinate (MHP) **9** was determined by UV spectrophotometric method. According to Lambert Beer's law, if the absorbing species has molar concentration c , and path length l , the absorbance A is given by,

$$A = \epsilon cl$$

where, ϵ is molar extinction coefficient.

In order to calculate the molar extinction coefficient, known concentration of compound **9** in spectroscopic grade methanol was prepared and the absorbance spectra of ethyl *N*-Boc-aminoethyl-3-hydroxy-2-methyl-4-pyridone glycinate (MHP) **9** solutions at different concentrations were recorded on UV-Vis spectrophotometer. The concentration was plotted against absorbance and the slope obtained from linear fitting is used for obtaining molar extinction coefficient (ϵ) of the monomeric solution. The ϵ

value of ethyl *N*-Boc-aminoethyl-3-hydroxy-2-methyl-4-pyridone glycinate **9** was $4 \text{ mM}^{-1}\text{cm}^{-1}$.

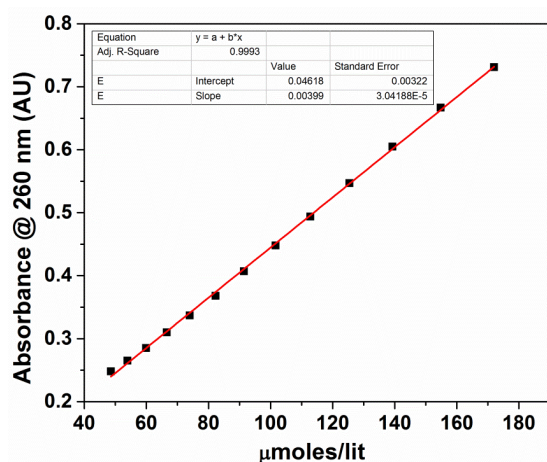


Figure 15. Plot of concentration vs absorbance for calculating molar extinction coefficient (ϵ) of ethyl *N*-Boc-aminoethyl-3-hydroxy-2-methyl-4-pyridone glycinate **9** (MHP)

1.8.2 UV-Vis spectroscopic titrations of the ethyl *N*-Boc-aminoethyl-3-hydroxy-2-methyl-4-pyridone glycinate (MHP) **9** with metal salts

The complexation studies of ethyl *N*-Boc-aminoethyl-3-hydroxy-2-methyl-4-pyridone glycinate (MHP) **9** with different metal ions were carried out using copper nitrate, nickel nitrate, cobalt nitrate, zinc nitrate, lanthanum nitrate, europium nitrate, terbium nitrate and holmium nitrate. A change in the ultraviolet (UV) absorption upon complexation with individual metal ions was used to quantify the strength of complex formation. The titration with solutions of different metal salts with 3-hydroxy-2-methyl-4-pyridone linked *aeg*-PNA monomer was followed by changes in their UV-Vis spectra.

1.8.2a Titration with $\text{Ln}(\text{NO}_3)_3$

Upon addition of aliquots of $\text{Ln}(\text{NO}_3)_3$ to the ethyl *N*-Boc-aminoethyl-3-hydroxy-2-methyl-4-pyridone glycinate (MHP) **9** in methanol, UV spectra of **9** exhibited reduction in intensity of absorption band at 278 nm with appearance of a new absorption band at 303 nm. This feature along with observation of two isosbestic points at 265 nm and 282 nm indicates the formation of complex by ethyl *N*-Boc-aminoethyl-3-hydroxy 2-methyl 4-pyridone glycinate (MHP) **9** with Ln^{3+} metal ion (Figure 16).

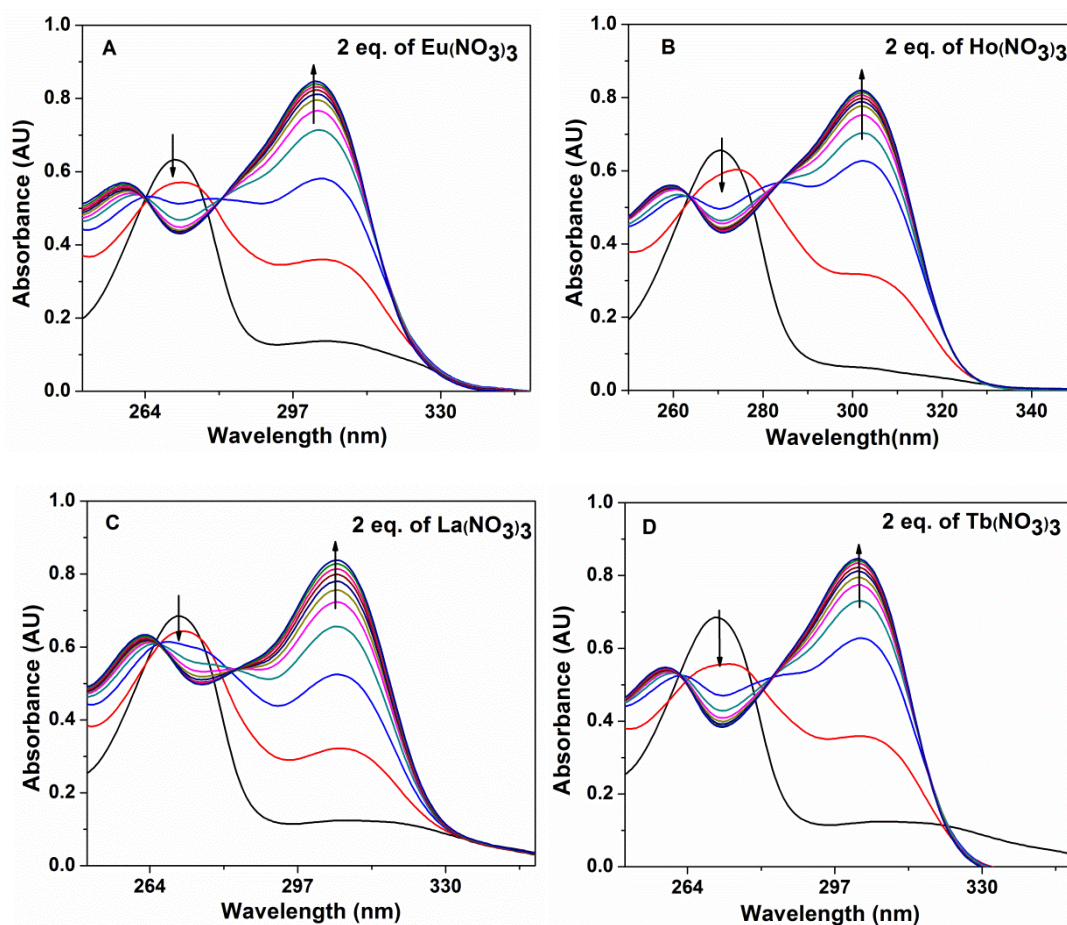


Figure 16. Change in the absorption spectra of the ethyl *N*-Boc-aminoethyl-2-methyl-3-hydroxy-4-pyridone glycinate (MHP) **9** (100 μ M) in methanol upon the addition of solutions of A) $\text{Eu}(\text{NO}_3)_3$, B) $\text{Ho}(\text{NO}_3)_3$, C) $\text{La}(\text{NO}_3)_3$ and D) $\text{Tb}(\text{NO}_3)_3$ (10 mM) in methanol.

The titration curves for Eu^{3+} , La^{3+} , Ho^{3+} and Tb^{3+} plotted as the change in absorbance as a function of concentration MHP **9**, are shown in Figure 17. The plot of molar absorptivity at 303 nm vs equivalents of Ln^{3+} shows saturation at one equivalent of metal ion per compound **9** in methanol.

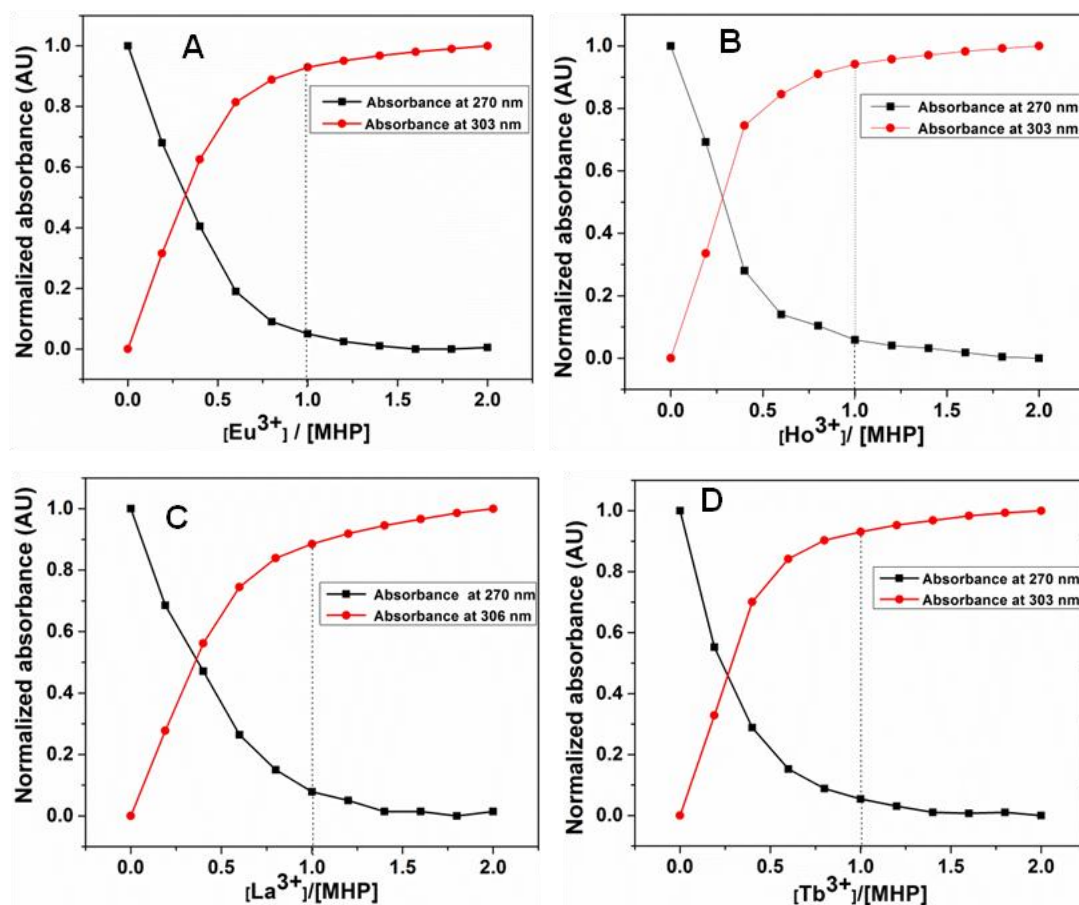


Figure 17. A) Plot of change in absorbance as a function of concentration of ethyl *N*-Boc-aminoethyl-3-hydroxy-2-methyl-4-pyridone glycinate (MHP) **9** solution B) with A) $\text{Eu}(\text{NO}_3)_3$, B) $\text{Ho}(\text{NO}_3)_3$, C) $\text{La}(\text{NO}_3)_3$ and D) $\text{Tb}(\text{NO}_3)_3$ (10 mM) in methanol.

1.8.2b $\text{Cu}(\text{NO}_3)_2$

Copper nitrate was titrated with aliquots of ethyl *N*-Boc-aminoethyl-3-hydroxy-2-methyl-4-pyridone glycinate (MHP) **9** solution in methanol. Bathochromic shift was observed with increase in the intensity of absorption band, but without formation of any new absorption band (Figure 18A). To make sure of complex formation of copper nitrate with ethyl *N*-Boc-aminoethyl-3-hydroxy-2-methyl-4-pyridone glycinate (MHP) **9**, $\text{Cu}(\text{NO}_3)_2$ was reverse titrated with MHP **9** solution. In the reverse titration, no isosbestic point was observed and indicated no formation of complex (Figure 18B). Then 0.5 M NaOH (10 μL) was added to the cuvette containing 100 μM MHP **9** (2 mL) in order to deprotonate the enolic proton of MHP ligand for coordination with Cu^{2+} ion.

The addition of 10 μL NaOH resulted in bathochromic shift with new absorption band at 303 nm. When aliquots of copper nitrate (10 mM) were added,

continuous shifting of bands was observed with isosbestic points at 286 nm and 300 nm. This suggested formation of complex between ethyl *N*-Boc-aminoethyl-3-hydroxy-2-methyl-4-pyridone glycinate (MHP) **9** and copper nitrate (Figure 18C).

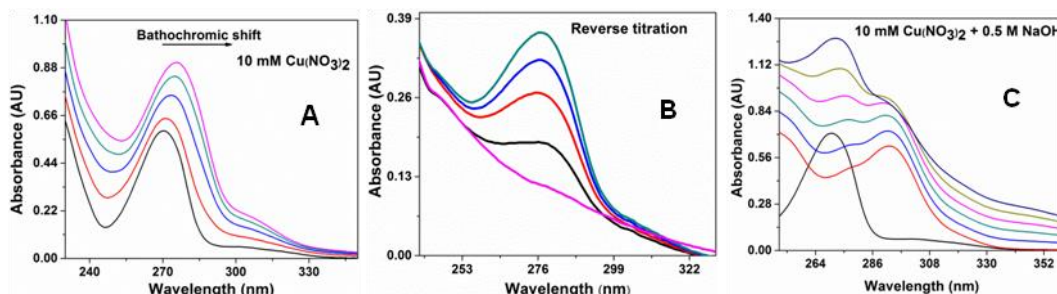


Figure 18. A) Change in the absorption spectra of the ethyl *N*-Boc-aminoethyl-3-hydroxy-2-methyl-4-pyridone glycinate (MHP) **9** (100 μ M) in methanol upon the addition of metal salt $\text{Cu}(\text{NO}_3)_2$ (10 mM), B) Reverse titration and C) UV absorption spectra after addition of 0.5 M NaOH (10 μ L).

$\text{Co}(\text{NO}_3)_2$, $\text{Ni}(\text{NO}_3)_2$ and $\text{Zn}(\text{NO}_3)_2$: Individual titration of metal salts copper nitrate, zinc nitrate and nickel nitrate with the ethyl-*N*-Boc-aminoethyl-3-hydroxy-2-methyl-4-pyridone glycinate (MHP) **9** solution in methanol revealed absence of any new absorption band (Figure 19A, B, C) or changes in spectra. This indicated that MHP **9** does not form complexes with these metal salts. NaOH was not added further to these salts because they exhibited no bathochromic shift upon addition of cobalt nitrate, zinc nitrate and nickel nitrate to MHP **9** solution. UV-Vis titration results have been summarized in Table 5.

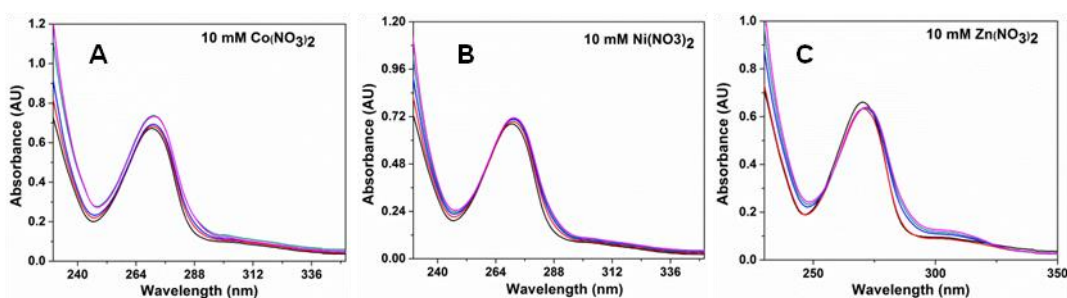


Figure 19. UV absorption spectra of the ethyl *N*-Boc-aminoethyl-3-hydroxy-2-methyl-4-pyridone glycinate (MHP) **9** (100 μ M) in methanol upon the addition of metal salt A) $\text{Co}(\text{NO}_3)_2$ (10 mM), B) $\text{Ni}(\text{NO}_3)_2$ and C) $\text{Zn}(\text{NO}_3)_2$.

Table 5: Summary of UV-Vis titrations for ethyl *N*-Boc-aminoethyl-3-hydroxy-2-methyl-4-pyridone glycinate (MHP) **9 (100 μ M in methanol).**

Sr. No.	Metal salts(10 mM)	Observation	Inflection points	Isosbestic points
1	Lanthanum nitrate	Binding	270 nm and 306 nm	265 nm and 282 nm
2	Europium nitrate	Binding	270 nm and 303 nm	264 nm and 280 nm
3	Terbium nitrate	Binding	270 nm and 303 nm	262 nm and 280 nm
4	Holmium nitrate	Binding	270 nm and 303 nm	263 nm and 281 nm
5	Copper nitrate	Binding		286 nm and 300 nm
6	Co (NO ₃) ₂ , Ni (NO ₃) ₂ and Zn (NO ₃) ₂	No binding		

In summary rare earth metals La³⁺, Eu³⁺, Tb³⁺ and Ho³⁺ and the transition metal ion Cu²⁺ formed complexes with MHP **9** while other transition metal ions Co²⁺, Ni²⁺ and Zn²⁺ did not form any complexes. Since rare earth metals exhibit interesting photoluminescence properties, which are studied in next section.

1.8.3 Photoluminescence studies of ethyl *N*-Boc-aminoethyl-3-hydroxy-2-methyl-4-pyridone glycinate (MHP) **9**

Due to wide variety of applications in the chemical biology, the chemistry of lanthanide compounds having inherent luminescence property is the subject of increasing interest in the last few years,^{61,62} Europium (III) and terbium (III) ions have suitable energy gap between the emissive excited state and the ground state. This leads to a large Stokes shift of emission, with unlikely overlap of the emission bands with the absorption bands.^{63,64} Photoluminescence studies were carried out for the complexation of ethyl *N*-Boc-aminoethyl-3-hydroxy-2-methyl-4-pyridone glycinate (MHP) **9** with europium nitrate and terbium nitrate.

Tb(NO₃)₃: Upon addition of terbium nitrate to a solution of ethyl *N*-Boc-aminoethyl-3-hydroxy-2-methyl-4-pyridone glycinate (MHP) **9** in methanol, a large fluorescence emission from 450 nm to 600 nm was observed (Figure 20). The emission maxima seen from 489-584 nm is characteristic to ⁵D₄ → ⁷F_J (J= 3 to 6) transitions of Tb³⁺ ion. The most intensive band lies at 545 nm and may be attributed to the ⁵D₄ → ⁷F₅ transition, while the medium emission band with maximum at 489 nm and the low intensity band at 584 nm arise from ⁵D₄ → ⁷F₆ and ⁵D₄ → ⁷F₃ transitions, respectively. This strongly suggested the photosensitization of ethyl *N*-Boc-aminoethyl-3-hydroxy-2-methyl-4-

pyridone glycinate (MHP) **9** by Tb^{3+} ion strongly suggested formation of $\text{MHP}:\text{Tb}^{3+}$ complex (Figure 20).

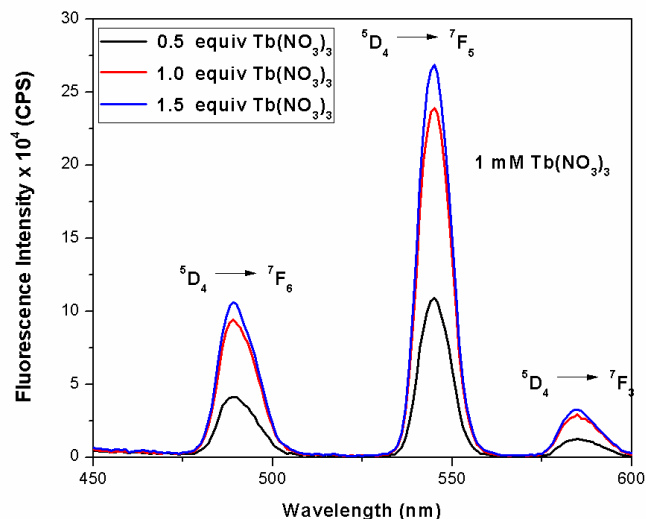


Figure 20. Photoluminescence spectrum of ethyl *N*-Boc-aminoethyl-3-hydroxy-2-methyl-4-pyridone glycinate (MHP) **9** (10 μM) upon addition of $\text{Tb}(\text{NO}_3)_3$ (1mM) in methanol.

$\text{Eu}(\text{NO}_3)_3$: Europium nitrate upon addition of a solution of ethyl *N*-Boc-aminoethyl-3-hydroxy-2-methyl-4-pyridone glycinate (MHP) **9** gave a characteristic sharp emission band at 609 nm. This may be attributed to ${}^5\text{D}_0 \rightarrow {}^7\text{F}_2$ transition. Thus the photosensitization of ethyl *N*-Boc-aminoethyl-3-hydroxy-2-methyl-4-pyridone glycinate (MHP) **9** by Eu^{3+} ion also indicated the formation of $\text{MHP}:\text{Eu}^{3+}$ complex (Figure 21).

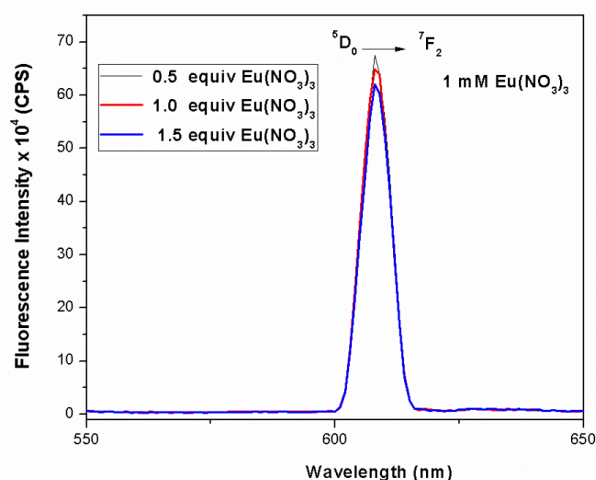


Figure 21. Photoluminescence spectrum of ethyl *N*-Boc-aminoethyl-3-hydroxy-2-methyl-4-pyridone glycinate (MHP) **9** (10 μM) upon addition of $\text{Eu}(\text{NO}_3)_3$ (1mM) in methanol.

1.8.4 Solid state photoluminescence of ethyl *N*-Boc-aminoethyl-3-hydroxy-2-methyl-4-pyridone glycinate (MHP) **9** with Europium nitrate

As we excited MHP **9** with europium nitrate at 303 nm, the observed band in photoluminescence spectrum (Figure 21) might be arise from lamp (overtone band). This is because the band was observed at 609 nm which is double to excitation wavelength. From the observed emission band at 609 nm in solution state, it was unable to conclude that europium nitrate sensitizes MHP **9**. Hence to confirm the sensitization of MHP **9** by complexation with europium, photoluminescence was also recorded in solid state. Two intensive emission bands were observed at 609 nm and 615 nm (Figure 22) and the emission band at 615 nm confirmed the formation of MHP:Eu³⁺ complex.

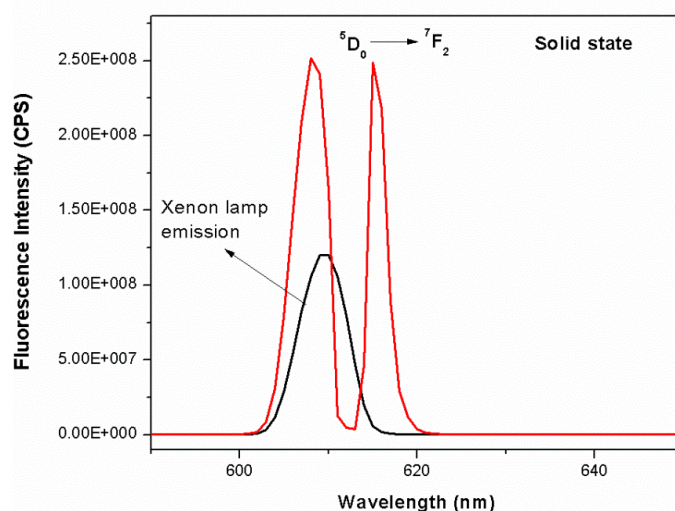
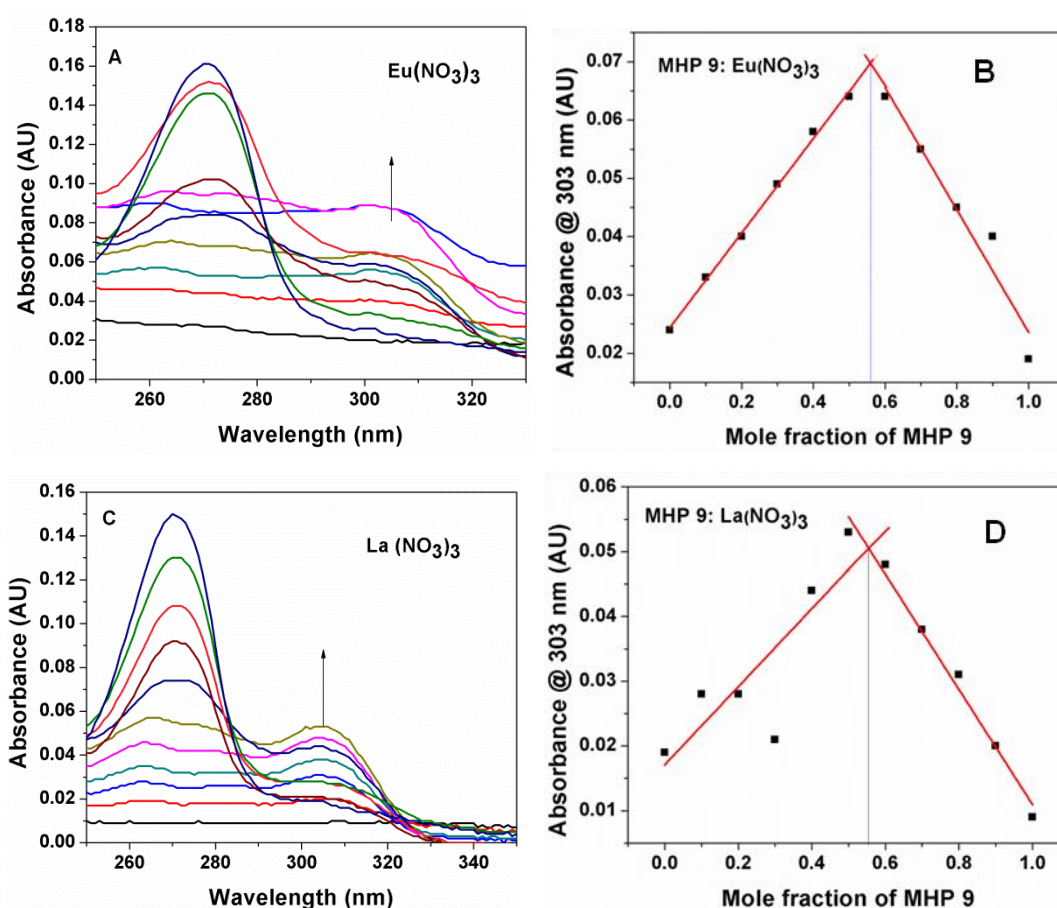


Figure 22. Photoluminescence spectrum of co-ordination complex of ethyl *N*-Boc-aminoethyl-3-hydroxy-2-methyl-4-pyridone glycinate (MHP) **9** with Eu(NO₃)₃ in solid state.

1.9 Stoichiometry of complex formation of MHP **9** with metal salts

The continuous variation Job's method was used to determine the binding stoichiometry between metal and ethyl *N*-Boc-aminoethyl-3-hydroxy-2-methyl-4-pyridone glycinate (MHP) **9** (Figure 23). In this method, the relative concentration of individual components was varied keeping the overall concentration constant and the absorbance is plotted against the mole fraction of metal salts.

Various stoichiometric mixtures of ethyl *N*-Boc-aminoethyl-3-hydroxy-2-methyl-4-pyridone glycinate (MHP) **9** and metal salts in varying molar ratios (1:0, 0.9:0.1, 0.8:0.2, 0.7:0.3, 0.6:0.4, 0.5:0.5, 0.4:0.6, 0.3:0.7, 0.2:0.8, 0.1:0.9 and 0:1) were prepared in methanol keeping the total concentration of ethyl *N*-Boc-aminoethyl-3-hydroxy-2-methyl-4-pyridone glycinate (MHP) **9** as 200 μ M. The absorbance spectra were recorded (Figure 22) and the absorbance at 303 nm was plotted against the relative molar ratio (Figure 22). The intersection point in the Job's plot was found to be at 0.50, which indicates binding stoichiometry 1:1 for the complexes of ethyl *N*-Boc-aminoethyl-3-hydroxy-2-methyl-4-pyridone glycinate (MHP) **9** with lanthanides (Figure 23).



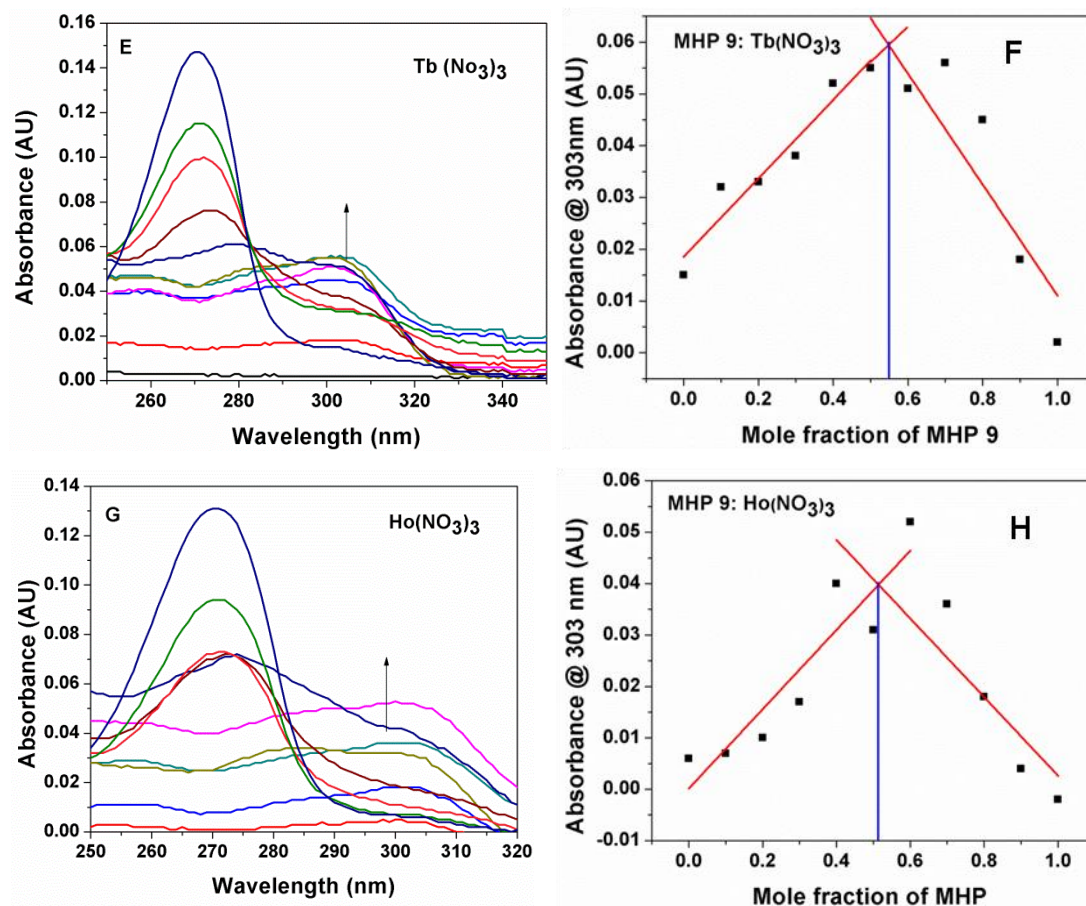


Figure 23. UV-Vis absorption spectra of ethyl *N*-Boc-aminoethyl-3-hydroxy-2-methyl-4-Pyridone glycinate (MHP) **9** with metal salts in molar ratios of (a) 0:1.0 (b) 0.1:0.9 (c) 0.2:0.8 (d) 0.3:0.7 (e) 0.4:0.6 (f) 0.5:0.5 (g) 0.6:0.4 (h) 0.7:0.3 (i) 0.8:0.2 (j) 0.9:0.1 (k) 200:0; (A) UV spectra and (B) Job's plot with $\text{Eu}(\text{NO}_3)_3$, (C) UV spectra and (D) Job's plot with $\text{La}(\text{NO}_3)_3$, (E) UV Spectra and (F) Job's plot with $\text{Tb}(\text{NO}_3)_3$, (G) UV Spectra and (H) Job's plot with $\text{Ho}(\text{NO}_3)_3$.

Thus the Job's plots showed a binding stoichiometry of 1:1 for ethyl *N*-Boc-aminoethyl-3-hydroxy-2-methyl-4-pyridone (MHP) glycinate **9** with the lanthanide metal ions Eu^{3+} , Tb^{3+} , La^{3+} and Ho^{3+} .

1.10 Determination of binding constant by UV spectroscopy

The strength of interactions between the two species is represented by the binding constants. The intrinsic binding constant, K , of the metal complex to monomer/polyamide oligomers can be determined from a Benesi-Hildebrand plot which is generated by plotting an observable property of complex e.g. ΔA_{max} with the concentration of variable component e.g. metal ion. The Benesi-Hildebrand equation is,

$$\frac{1}{\Delta A} = \frac{1}{\Delta A_{\text{max}}} + \left[\frac{1}{K[L]} \times \frac{1}{\Delta A_{\text{max}}} \right]$$

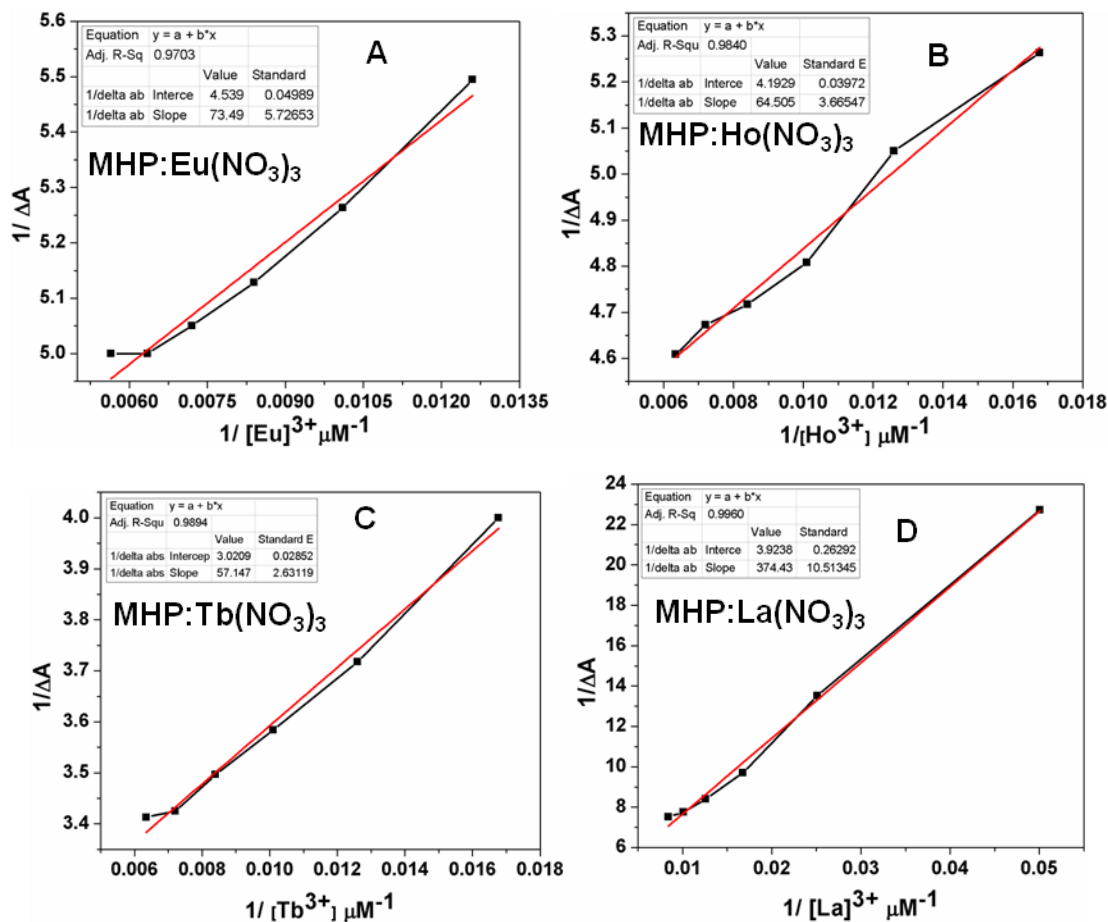


Figure 24. Benesi Hildebrand's plots for complex of MHP 9 with A) Eu(NO₃)₃, B) Ho(NO₃)₃, C) Tb(NO₃)₃ and D) La(NO₃)₃ (10 mM) in methanol.

The absorbance spectra of MHP 9 with increasing concentrations of metal salts were recorded and the absorbance values were plotted against the metal concentration (Figure 24) as inverse plot (ΔA^{-1} vs $[M]^{-1}$). The binding constant (K) was determined from the intercept to slope ratio in the Benesi–Hildebrand plots. The binding constants for complexation of MHP 9 with different metal salts were found to be in the range 10^4 M^{-1} as summarized in Table 6.

Table 6: Binding constant values of complexation of MHP 9 with different metal salts.

Sr. No.	Metal salt	Binding constant K ($\times 10^4 \text{M}^{-1}$)
1	Europium Nitrate	6.17
2	Terbium Nitrate	5.28
3	Holmium Nitrate	6.5
4	Lanthanum Nitrate	1.04

Values are accurate to $\pm 0.1 \times 10^4 \text{M}^{-1}$

The order of binding constant value is $\text{Ho} \approx \text{Eu} > \text{Tb} > \text{La}$, with Ho^{3+} binding six times stronger than La^{3+} ion. Since all metal salts were used as nitrates, there is no effect of counter anion on the relative binding strength.

1.11 MALDI-TOF Studies of ethyl-*N*-Boc-aminoethyl-3-hydroxy-2-methyl-4-pyridone (MHP) glycinate **9** with metal salts

The stoichiometry of binding of ethyl-*N*-Boc-aminoethyl-3-hydroxy-2-methyl-4-pyridone (MHP) glycinate **9** with metal salts can also be evaluated from mass of the complex. The MALDI-TOF spectra of complexes of MHP **9** with individual metal salts were recorded.

1.11.1 MHP **9**: Eu^{3+} complex

Ethyl-*N*-Boc-aminoethyl-3-hydroxy-2-methyl-4-pyridone (MHP) glycinate **9** was treated with europium nitrate pentahydrate salt in methanol and stirred at room temperature for overnight, followed by concentration to obtain solid. The MALDI-TOF mass spectrum was recorded by applying the methanolic solution on 2,3 dihydroxybenzoic acid (DHB) matrix. The mass spectrum showed presence of two types of molecular stoichiometry (Figure 26) i.e. molecular ion peaks at m/z 973.37 (Calculated: 973.31 for 2:1) and 626.11 (Calculated: 626.11 for 1:1). The probable structures of trivalent (1:1) and tetravalent (1:2) metal:ligand complexes are given below.

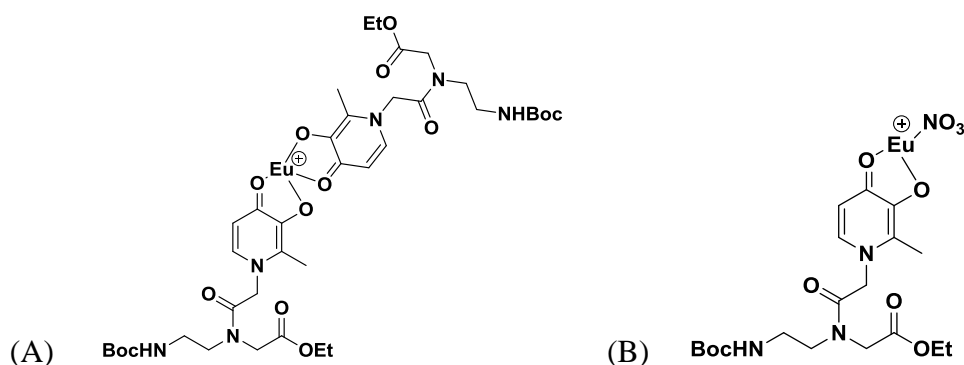


Figure 25. A) Probable structure of 2:1 complex and B) 1:1 complex of ethyl-*N*-Boc-aminoethyl-3-hydroxy-2-methyl-4-pyridone glycinate (MHP) **9** with Europium nitrate.

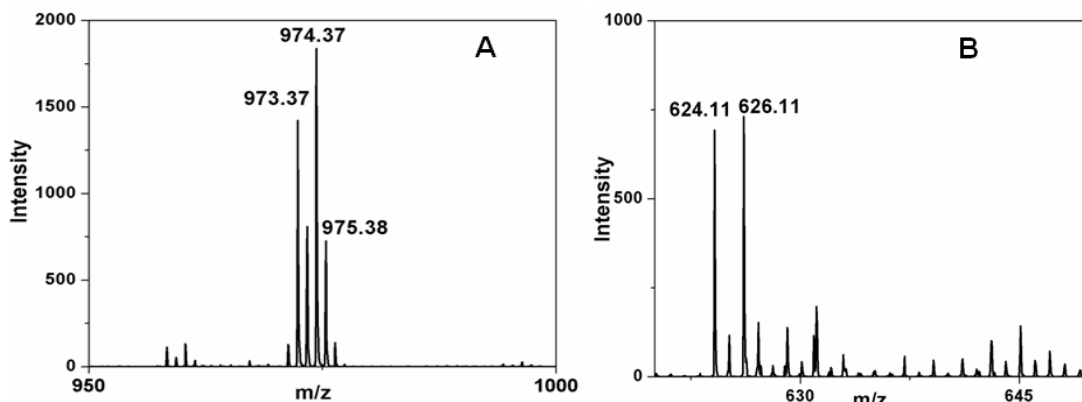


Figure 26. MALDI-TOF of A) 2:1 complex and B) 1:1 complex of MHP:Eu³⁺.

1.11.2 MHP 9:Cu²⁺ complex

Ethyl-*N*-Boc-aminoethyl-3-hydroxy-2-methyl-4-pyridone (MHP) glycinate **9** was treated with copper nitrate salt in methanol and stirred at 50 °C for 3 h followed by concentration to obtain green solid. The MALDI-TOF mass spectrum was recorded by applying methanolic solution on 2,3-dihydroxybenzoic acid matrix. The mass spectrum showed presence of two types of molecular stoichiometry (Figure 28) i.e. molecular ion peaks at *m/z* 885.46 (Calculated: 885.33 for 2:1) and 599.24 (Calculated: 599.11 for 1:1). The probable structures of trivalent (1:1) and tetravalent (1:2) metal:ligand complexes are given below.

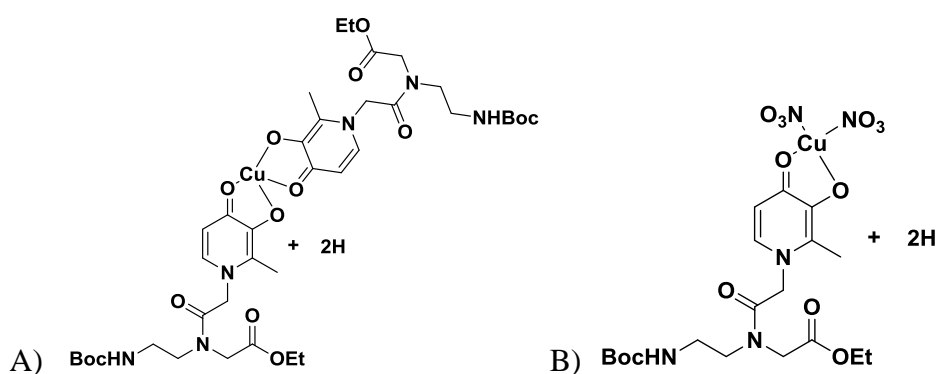


Figure 27. A) Probable structure of 2:1 complex and B) 1:1 complex of ethyl-*N*-Boc-aminoethyl-3-hydroxy-2-methyl-4-pyridone glycinate (MHP) **9** with copper nitrate.

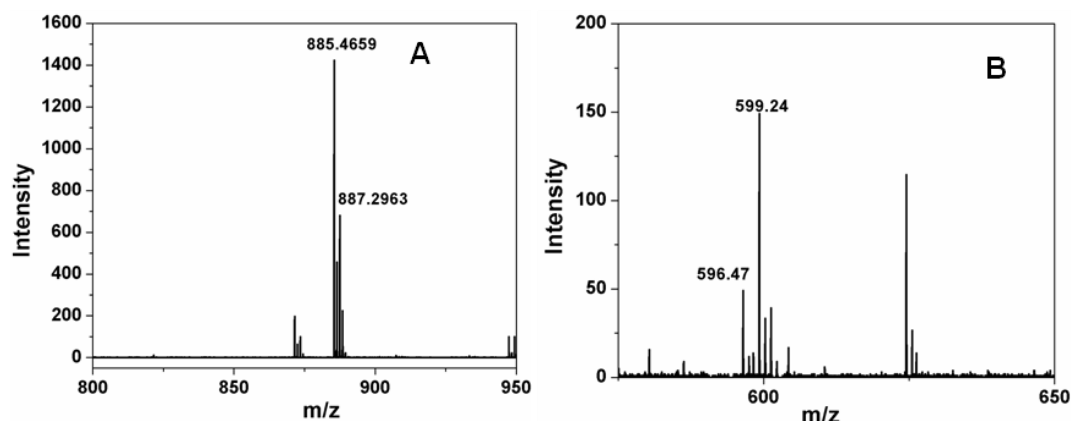


Figure 28. MALDI-TOF of a) 2:1 complex and b) 1:1 complex of MHP:Cu²⁺.

1.11.3 MHP 9: Tb³⁺ complex

Ethyl-*N*-Boc-aminoethyl-3-hydroxy-2-methyl-4-pyridone glycinate (MHP) **9** was treated with terbium nitrate salt in methanol and stirred at room temperature for overnight, followed by concentration to obtain solid. The MALDI-TOF mass spectrum was recorded by applying methanolic solution on 2,3-dihydroxybenzoic acid matrix. The mass spectrum showed molecular ion peak at *m/z* 975.0875 which is 4 units less than expected *m/z* 979.3108. Though the observed molecular ion peak did not match with expected molecular ion peak, it suggested the formation some type of complex which may be attributed to 2:1 MHP:Tb³⁺ complex (Figure 30). Another peak at *m/z* 988.9976 was observed which did not match with any probable structure. The probable structure of tetravalent (1:2) metal:ligand complex as below.

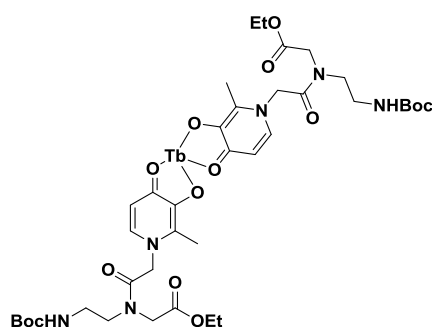


Figure 29. Probable structure of 2:1 complex of ethyl-*N*-Boc-aminoethyl-3-hydroxy-2-methyl-4-pyridone glycinate (MHP) **9** with terbium nitrate.

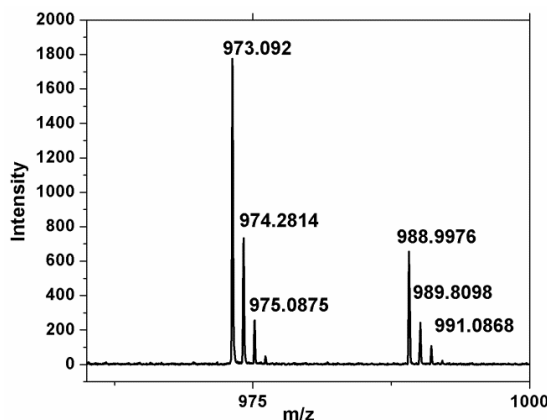


Figure 30. MALDI-TOF spectrum of 2:1 MHP:Tb³⁺ complex.

After establishing the formation of complex by MHP **9** monomer with different rare earth metals, the complex formation with MHP incorporated PNA oligomers were studied.

1.12 Biophysical studies of PNA oligomers

This section describes the biophysical studies of MHP incorporated PNA:PNA duplexes by UV-Vis, fluorescence and temperature dependent spectroscopic techniques.

1.12.1 UV titration of PNA-2 with metal salts

The self complementary modified PNA sequence PNA-2 (H-GCGA~~X~~TCGC LysNH₂) was titrated with different metal salts. From changes in the UV spectrophotometric profiles, it was found that modified PNA sequence PNA-2 binds with the metal salts to form stable PNA:PNA duplex.

The aliquots of metal nitrate salts Eu(NO₃)₃, Tb(NO₃)₃ and Cu(NO₃)₂ in aqueous solution were individually added to the PNA-2 in 10 mM HEPES buffer. The changes in the UV spectrum of self complementary sequence PNA-2 (H-GCGA~~X~~TCGC LysNH₂) in the presence of increasing concentration of individual Eu³⁺, Tb³⁺ and Cu²⁺ ions are shown in Figure 30a, 30c and 30e respectively. With the increase in concentration of these individual metal salts, the spectra exhibited reduction in absorbance intensity at 260 nm with appearance of new absorption band at 303 nm. These spectral changes suggested the coordination of 3-hydroxy-2-methyl-4-pyridone unit of PNA oligomer with the metal salts. Thus, the changes in UV spectrum indicated

the formation of duplex of modified PNA-2 with individual metal salts Cu^{2+} , Eu^{3+} and Tb^{3+} (Figure 31).

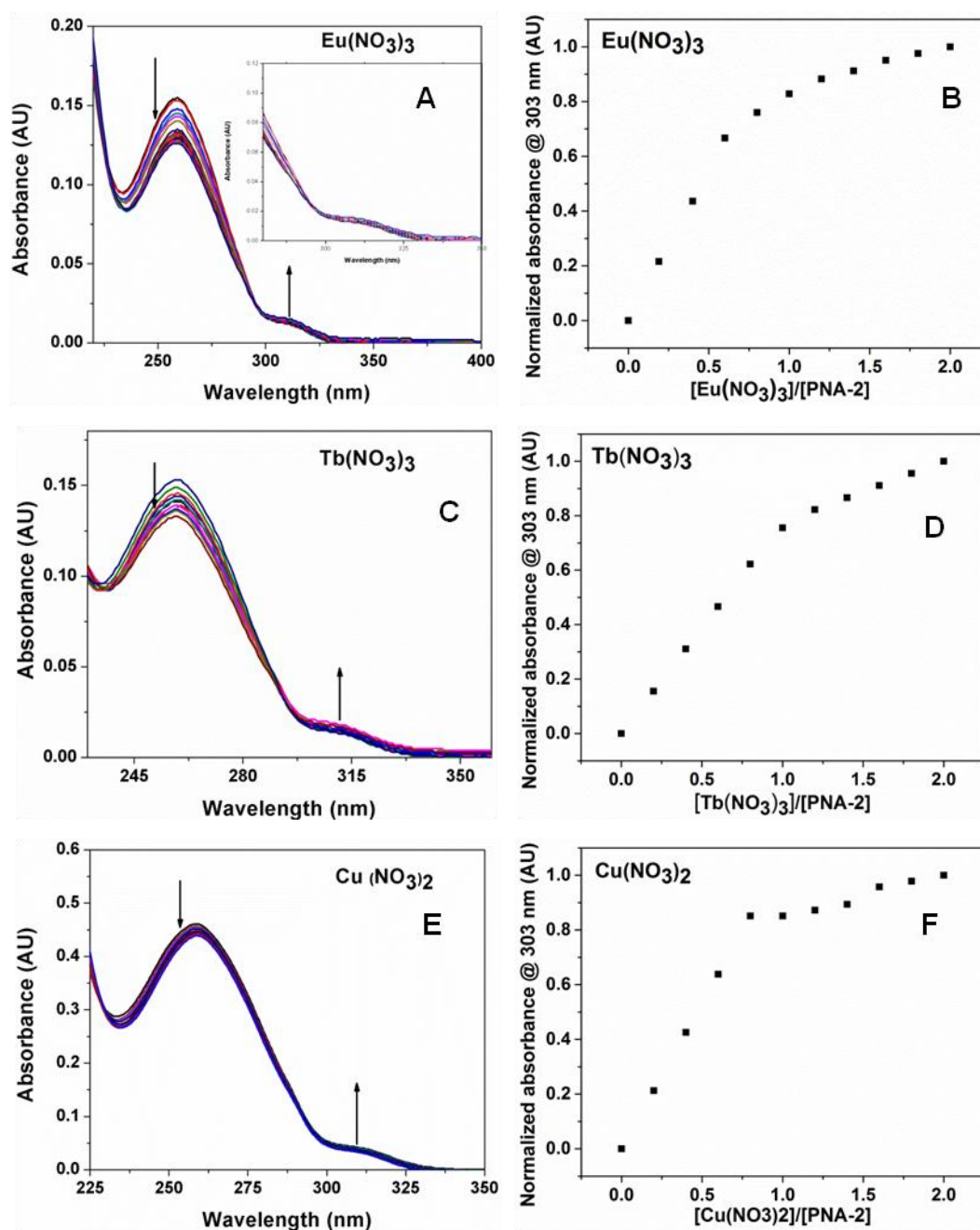


Figure 31. Change in the absorption spectra of PNA-2 upon the addition of metal salts A) $\text{Eu}(\text{NO}_3)_3$, C) $\text{Tb}(\text{NO}_3)_3$ and E) $\text{Cu}(\text{NO}_3)_2$ (200 μM) and plot of change in absorbance against function of concentration of PNA-2 with B) $\text{Eu}(\text{NO}_3)_3$, D) $\text{Tb}(\text{NO}_3)_3$ and F) $\text{Cu}(\text{NO}_3)_2$.

1.12.2 Fluorescence Titration of PNA-2 with Terbium nitrate

PNA-2 was dissolved with terbium nitrate in 10 mM HEPES buffer and the fluorescence spectrum of the solution was recorded. Two emission bands at 490 nm and 547 nm were observed (Figure 32). The emission band at 547 nm was most intensive band as compared to emission band at 490 nm. These bands are characteristics of Tb^{3+} ion complexation with MHP in PNA. The most intensive band at 547 nm may be attributed to the $^5D_4 \rightarrow ^7F_5$ transition whereas emission band at 490 nm is attributed to $^5D_4 \rightarrow ^7F_6$ transition. The observation of characteristic emission bands suggested the formation of MHP-PNA duplex in presence of Tb^{3+} . The band at 570 nm was not observed probably because of its weak nature which may be impossible at oligomer level.

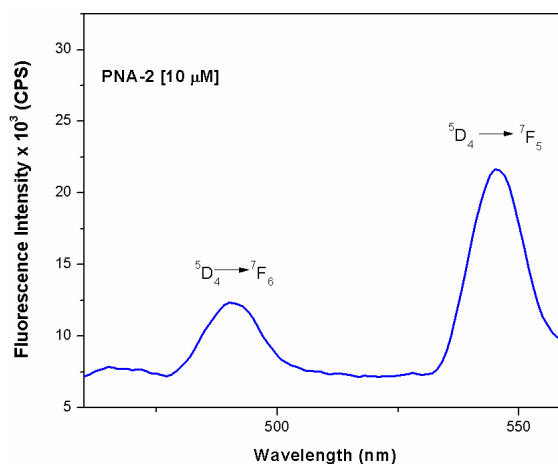


Figure 32. Photoluminescence spectrum of PNA-2 upon addition of $Tb(NO_3)_3$ (1mM).

However, the fluorescence bands may also arise from complex of metal salt with ss-PNA. To confirm the formation of PNA:PNA duplex, thermal melting studies were carried out.

1.12.3 Thermal melting studies

In order to investigate the effect of MHP-PNA on the PNA:PNA duplexes, the thermal stability of PNA:PNA duplexes was examined by temperature dependent UV spectroscopy in the absence and presence of metal salts. The PNA:PNA duplexes were obtained by annealing corresponding PNA oligomers in 10 mM phosphate buffer (pH 7.2) containing 10 mM NaCl in the absence and presence of metal salts. NaCl was added to decrease the electrostatic repulsion between two strands.

The thermal stability (T_m) of the PNA:PNA duplexes was evaluated from melting curves monitored at 260 nm. The temperature-absorbance curves were sigmoidal which suggested the formation of 1:1 PNA:PNA duplexes. The T_m derived from midpoint of first derivative plots.

1.12.3a PNA:PNA duplexes derived from the self complementary PNA sequences

The melting temperatures (T_m) of PNA:PNA duplexes derived from self complementary sequences PNA-1 (H-GCGATCGC-LysNH₂ without MHP) and PNA-2 (H-GCGA~~X~~TCGC-LysNH₂, X=MHP) suggested the stabilization of MHP containing PNA:PNA duplex (PNA-2) in the presence of metal salts (Figure 33). Table 7 shows the melting temperatures for PNA duplexes that have natural base pairs (PNA-1) or 3-hydroxy-2-methyl-4-pyridone moiety situated in the same sequence context (PNA-2), in the absence and presence of Eu³⁺, Tb³⁺ and Cu²⁺. From Table 7, it was observed that T_m of PNA-1 did not vary with increasing concentration of Cu²⁺. Addition of Tb³⁺ and Eu³⁺ ion also did not show any enhancement in the T_m of PNA-1 (Figure 32A). However, addition of Cu²⁺, Eu³⁺ and Tb³⁺ effectively enhanced the thermal stability of MHP-PNA duplex from PNA-2 as seen by T_m values.

With 0.5 eq. of Cu²⁺, T_m was increased by 7.1 °C and with 1 eq. of Cu²⁺ the T_m increased by 8.4 °C, suggesting the formation and stabilization of PNA-2:PNA-2 duplex. Upon addition of 0.5 eq. of Eu³⁺, the melting temperature was enhanced by 4.6 °C and at 1.0 eq. the T_m significantly increased by 9.4 °C. When Tb³⁺ was added in 0.5 eq. the T_m was increased by 5.2 °C, while with 1 eq. of Tb³⁺, the T_m of duplex increased by 7.2 °C. The enhancement of T_m of PNA-2 duplex by addition of metal ions suggested stabilization of the PNA duplex (Figure 33). Among the three metals used, Eu³⁺ stabilized the PNA duplex to maximum extent.

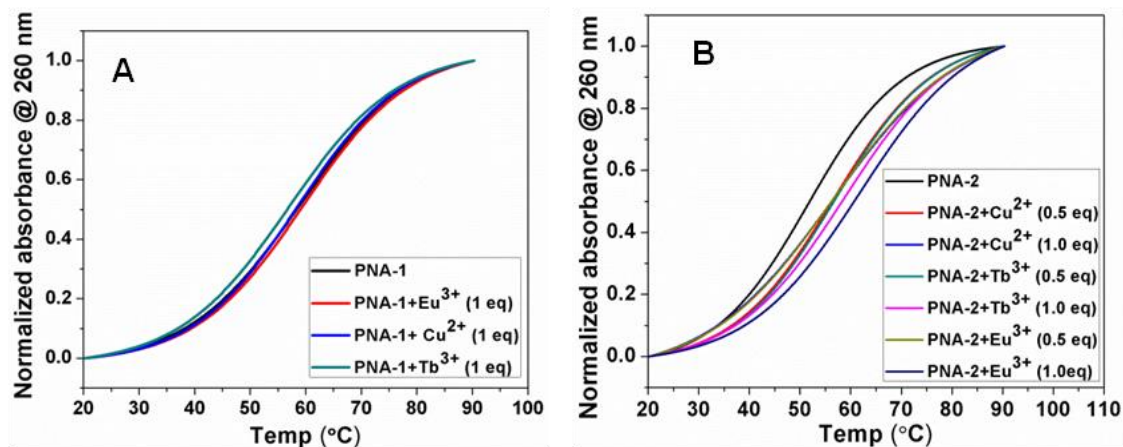


Figure 33. Thermal denaturation profiles (sigmoidal curve) PNA:DNA duplexes derived from self complementary sequences A) PNA-1 and B) PNA-2 in the absence and presence of Eu^{3+} , Cu^{2+} and Tb^{3+} . Solutions were prepared in pH 7.2, 10 mM sodium phosphate buffer and 10 mM NaCl.

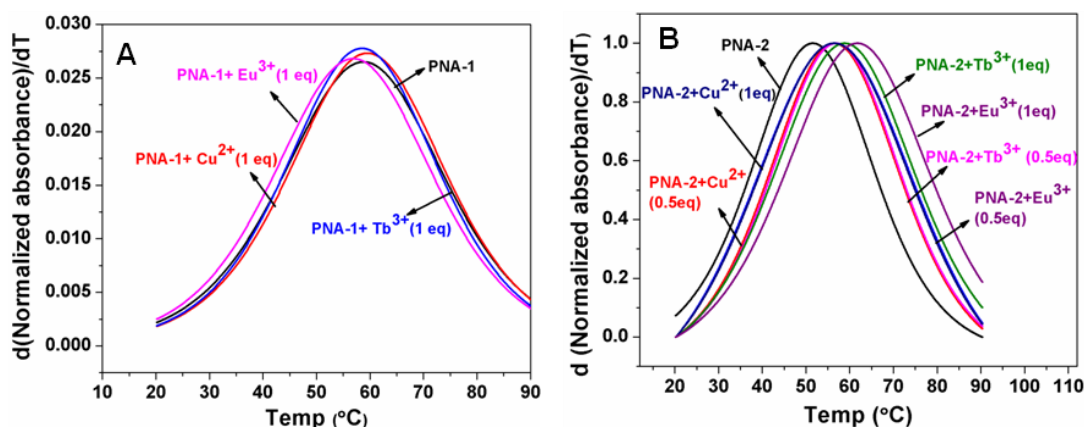


Figure 34. First derivative curve of PNA:DNA duplexes derived from self complementary sequences A) PNA-1 and B) PNA-2 in the absence and presence of Eu^{3+} , Cu^{2+} and Tb^{3+} .

Table 7: T_m ($^{\circ}\text{C}$) of PNA-1 and PNA-2 in the absence and presence of metal salt.

Sr. No	PNA	No Metal	Cu^{2+}		Eu^{3+}		Tb^{3+}	
			(0.5eq)	(1.0 eq)	(0.5eq)	(1.0 eq)	(0.5eq)	(1.0 eq)
1	PNA-1	56	nd	56.0	nd	56.0	nd	55.4
2	PNA-2	51.6	58.7	60.0	56.2	61.0	56.8	58.9
	ΔT_m	-	+7.1	+8.4	+4.6	+9.4	+5.2	+7.2

+ Indicates the stabilization; ΔT_m indicates the difference in T_m of PNA-2 in the absence and presence of metal ion; ($SD = \pm 0.5^{\circ}\text{C}$); nd= not done; PNA-1=H-GCGATCGC-LysNH₂ and PNA-2= GCGA~~X~~TCGC - LysNH₂ (X=MHP).

Figure 35 shows the stabilization of PNA:PNA duplex derived from PNA-2 in antiparallel orientation by metal coordinated base pairing

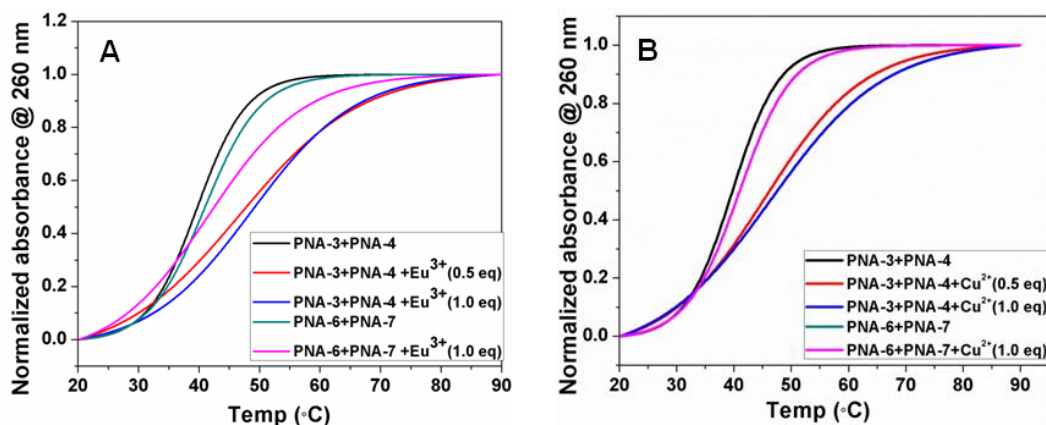


Figure 35. Structure of MHP incorporated PNA:PNA duplex in antiparallel orientation.

1.12.3b Antiparallel PNA:PNA duplexes

The melting curves of antiparallel duplexes PNA-3:PNA-4 (H-ATAGAXCATC-LysNH₂:H-GATGXTCTAT-LysNH₂) and PNA-6:PNA-7 (ATAGATCATC-LysNH₂:H-GATGATCTAT-LysNH₂) showed that the presence of metal salt enhanced the stability of MHP modified duplex PNA-3:PNA-4 (Figure 36). The control duplex PNA-6:PNA-7 showed a melting of (T_m) 40.5 °C in the absence of metal salt and showed no variation in T_m (Table 8) on the individual addition of one equivalent of metal salt (Eu(NO₃)₃, Cu(NO₃)₂ and Tb(NO₃)₃).

The MHP incorporated PNA-3:PNA-4 duplex (Table 8) showed a T_m value 40.0 °C. Addition of Cu²⁺ (0.5 eq.) stabilized the duplex by 6.5 °C. The PNA-3:PNA-4 duplex was further stabilized by 7.8 °C upon increasing the concentration of Cu²⁺ (1.0 eq.). In presence of Eu³⁺ (0.5 eq.), melting temperature of duplex was enhanced by 7.5 °C and with Eu³⁺ (1.0 eq.) showed stabilization by 9 °C. With Tb³⁺ (0.5 eq.), the T_m increased by 6 °C and with Tb³⁺ (1 eq.), the stabilization of duplex was almost similar as that of 0.5 eq. of Tb³⁺ (Table 8). Thus, the addition of metal salts lead to the significant enhancement in the stability of MHP incorporated PNA:PNA duplexes with Eu³⁺ stabilizing the duplex better as compared to Cu²⁺ and Tb³⁺.



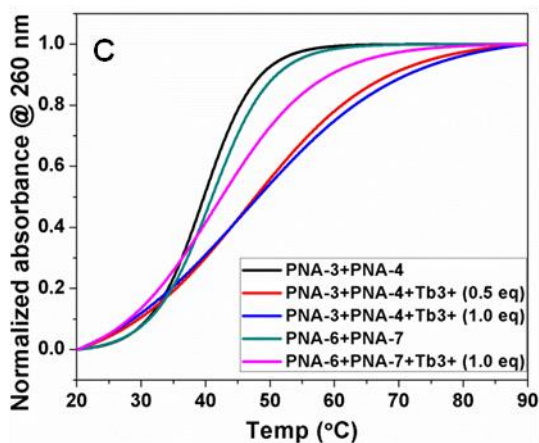


Figure 36. Thermal denaturation profiles of antiparallel PNA:PNA duplexes in the absence and presence of A) Eu^{3+} , B) Cu^{2+} and C) Tb^{3+} . Solutions were prepared in pH 7.2, 10 mM sodium phosphate buffer and 10 mM NaCl.

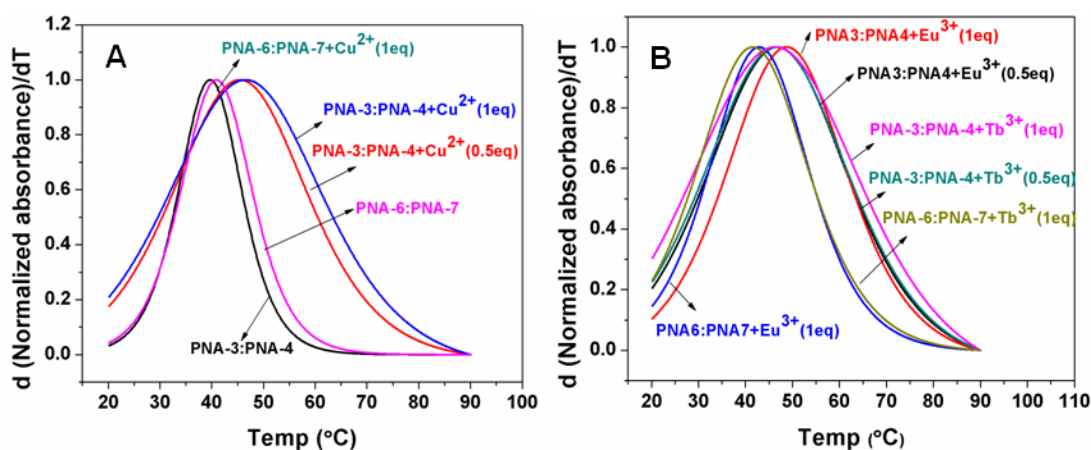


Figure 37. Derivative curves of antiparallel PNA:PNA duplexes in the absence and presence of Eu^{3+} , Cu^{2+} and Tb^{3+} .

Table 8: T_m (°C) of antiparallel PNA:PNA duplexes in the absence and presence of metal salt.

Sr. No.	PNA:PNA duplex	No Metal	Cu^{2+}		Eu^{3+}		Tb^{3+}	
			(0.5eq)	(1.0 eq)	(0.5eq)	(1.0 eq)	(0.5eq)	(1.0 eq)
1	PNA3:PNA-4	40	46.5	47.8	47.5	49.0	46.0	46.5
			(+6.5)	(+7.8)	(+7.5)	(+9.0)	(+6.0)	(+6.5)
2	PNA6:PNA-7	40.5	40.3	nd	41.0	nd	40.8	nd

+ Indicates the stabilization; Values in bracket indicates ΔT_m ; ΔT_m indicates the difference in T_m of PNA-3:PNA-4 duplex in the absence and presence of metal ion; The values are accurate to ± 0.5 °C; nd=not done; PNA-3=H-ATAGAXCATC-LysNH₂; PNA-4=H-GATGXTCTAT-LysNH₂ (X=MHP); PNA-6=H-ATAGATCATC-LysNH₂; PNA-8=H-GATGATCTAT-LysNH₂.

1.12.3c Parallel PNA:PNA duplexes

The melting curves of parallel duplexes PNA-3:PNA-5 (H-ATAGAXCATC-LysNH₂:H-TATCTXGTAG-LysNH₂) and PNA-6:PNA-8 (ATAGATCATC-LysNH₂:H-TATCTAGTAG-LysNH₂) that the presence of metal salts resulted in the enhancement of thermal stability of MHP modified duplex PNA-3:PNA-5 (Figure 38). The control duplex PNA-6:PNA-8 had a melting temperature (T_m) value of 39.2 °C in the absence of metal salt while in the presence of 1.0 equivalent of Cu²⁺, Eu³⁺ and Tb³⁺ there was no change in the T_m . The addition of Cu²⁺ (0.5 eq.) to PNA-3:PNA-5 duplex increased the T_m by 4 °C whereas with Cu²⁺ (1 eq.) the T_m of PNA-3:PNA-5 duplex increased by 6 °C. Upon addition of Eu³⁺ (0.5 eq.) the melting temperature of duplex was enhanced by 5.8 °C and with Eu³⁺ (1 eq.) stabilized the duplex by 7.8 °C. With Tb³⁺ (0.5 eq.) T_m increase was by 4.3 °C and Tb³⁺ ion (1 eq.) enhanced the stability of duplex by 5.7 °C (Table 9). Thus, the addition of metal ions has significantly enhanced the stability of ligand modified PNA duplexes.

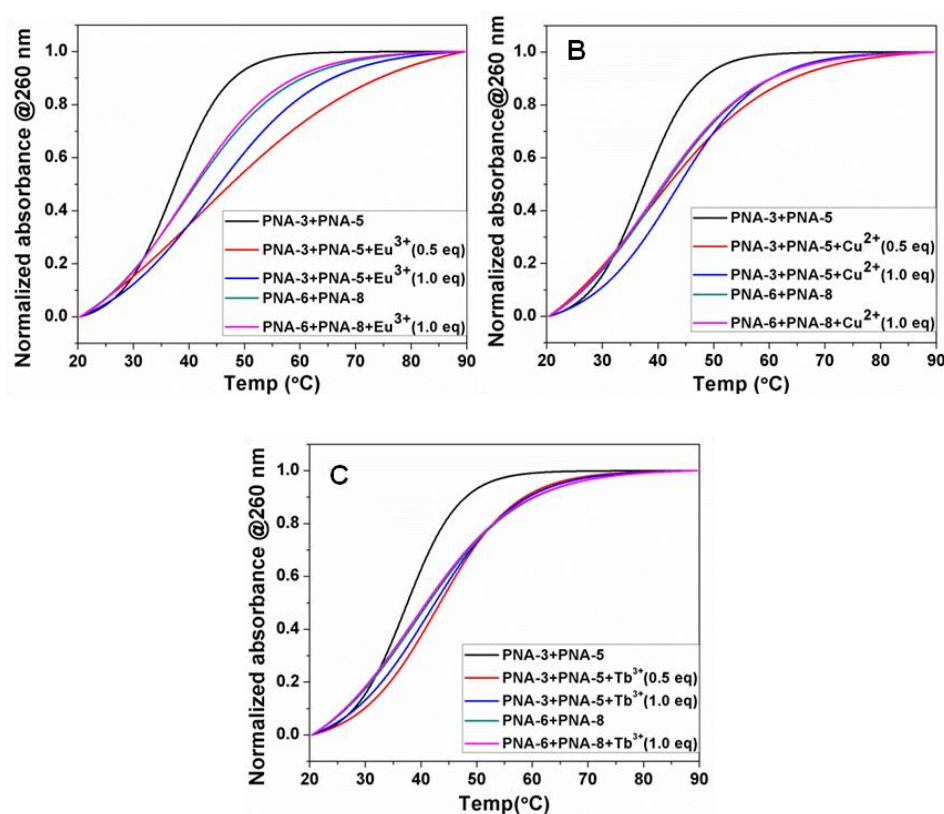


Figure 38. Thermal denaturation profiles of parallel PNA:PNA duplexes with A) Eu³⁺, B) Cu²⁺ and C) Tb³⁺. Solutions were prepared in pH 7.2, 10 mM sodium phosphate buffer and 10 mM NaCl.

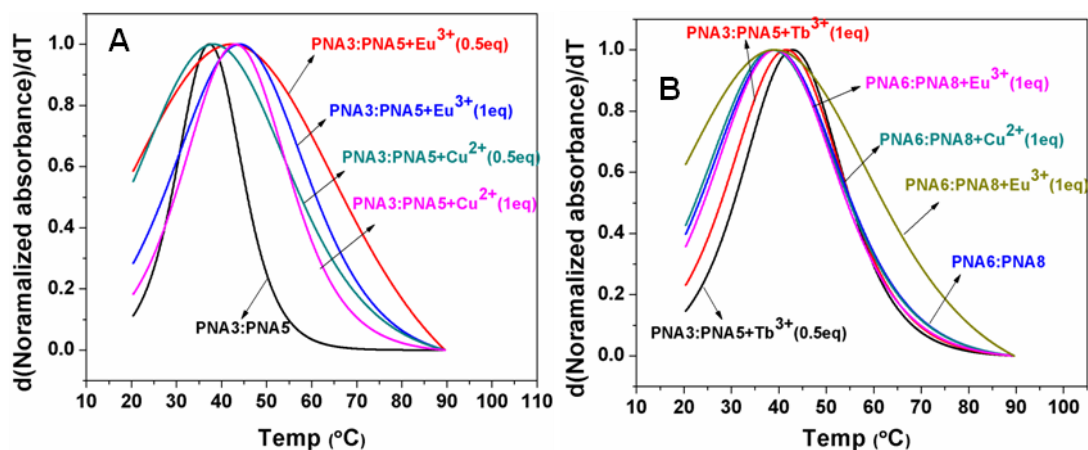


Figure 39. Derivative curves of parallel PNA:PNA duplexes in the absence and presence of Eu^{3+} , Cu^{2+} and Tb^{3+} .

Table 9: T_m ($^{\circ}\text{C}$) of parallel PNA:PNA duplexes in the absence and presence of metal salt.

Sr. No.	PNA:PNA duplex	No Metal	Cu^{2+}		Eu^{3+}		Tb^{3+}	
			(0.5eq)	(1.0 eq)	(0.5eq)	(1.0 eq)	(0.5eq)	(1.0 eq)
1	PNA3:PNA-5	36.2	40.2 (+4.0)	42.2 (+6.0)	42.0 (+5.8)	44.0 (+7.8)	40.5 (+4.3)	41.9 (+5.7)
2	PNA6:PNA-8	39.2	39.1	nd	39.3	nd	38.8	nd

Values in bracket indicates ΔT_m ; + indicates the stabilization; ΔT_m indicates the difference in T_m of PNA-3:PNA-5 duplex in the absence and presence of metal ion; The values are accurate to ± 0.5 $^{\circ}\text{C}$; nd=not done; PNA-3=H-ATAGAXCATC-LysNH₂; PNA-5=H-TATCTXGTAG-LysNH₂ (X=MHP); PNA-6=H-ATAGATCATC-LysNH₂; PNA-8=H-TATCTAGTAG-LysNH₂.

Thus, 2:1 complex formation observed in MALDI-TOF is well supported by melting temperature data resulting in the formation of stabilization of PNA:PNA duplexes by metal ions.

1.13 Comparison of thermal stability of PNA:PNA duplexes

The overall data of previous sections suggests that the thermal stability of MHP-PNA duplexes (both parallel and antiparallel) enhanced upon addition of Cu^{2+} , Eu^{3+} and Tb^{3+} . It is observed that the ΔT_m is higher at 1 eq. of metal ion for the modified self complementary sequence PNA-2 (H-GCGAXTCGC-LysNH₂) indicating that the metal ion is co-ordinating to MHP ligand in the duplex leading to metal mediated base pairing, due to which the MHP-PNA duplexes are more stable as compared to unmodified duplex. Among the three metal salts used, Eu^{3+} stabilized the MHP-PNA:MHP-PNA duplexes better as compared to Cu^{2+} and Tb^{3+} (Figure 40).

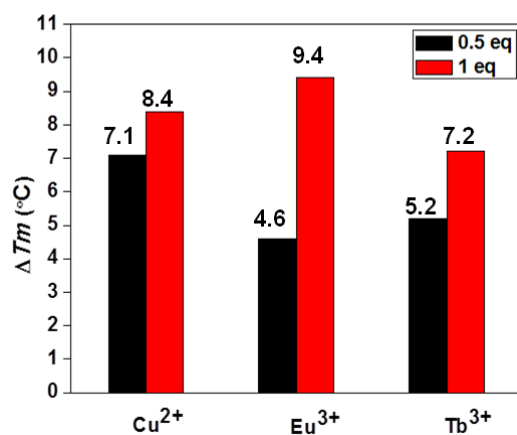


Figure 40. Comparison of ΔT_m (°C) of MHP incorporated PNA:PNA duplex derived from self complementary sequence PNA-2 (H-GCGA~~X~~TCGC-LysNH₂).

Similarly, the addition of metal salts resulted in the stabilization of MHP incorporated parallel and antiparallel PNA:PNA duplexes with Eu³⁺ stabilizing the duplexes better than Cu²⁺ and Tb³⁺. The data clearly suggested that enhancement in the stability of MHP incorporated antiparallel PNA:PNA duplexes is slightly more than MHP incorporated parallel PNA:PNA duplexes. This illustrates that, the metal ion favoring antiparallel orientation more than parallel orientation (Figure 41).

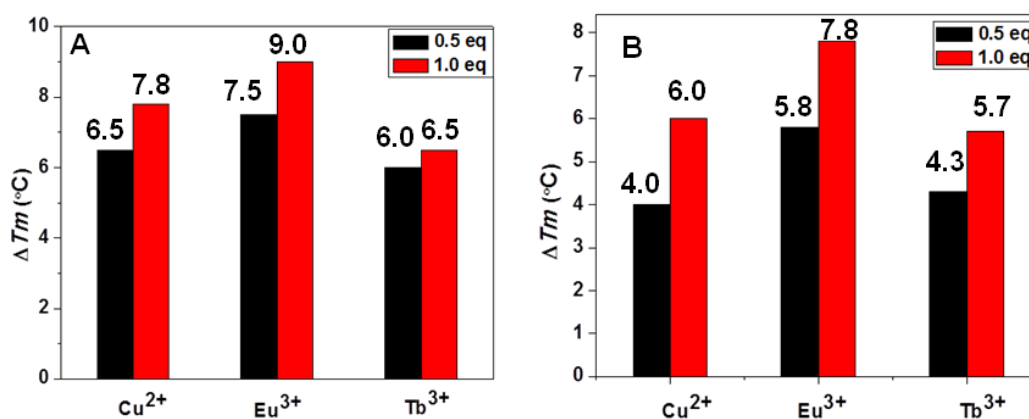


Figure 41. Comparison of ΔT_m (°C) of MHP incorporated PNA:PNA duplexes A) antiparallel and B) parallel orientation.

1.14 Co-ordination chemistry of metal complexes

The incorporation of metals in the artificial nucleobases in the backbone leads to the generation of metal complexes of specific geometry. The artificial nucleobases are generally monodentate, bidentate or tridentate ligands having one, two or three

donor atoms respectively for coordination with transition metals. Shionoya et al.⁶⁵ reported that the bidentate ligand 2-hydroxypyridone forms square planar complexes with Cu^{2+} , monodentate ligand pyridyl forms linear complexes with Ag^+ , bidentate ligand catechol exhibits distorted tetrahedral complexes with B^{3+} etc inside the duplexes. Achim et al.⁶⁶ reported the complexes of different geometries of bipyridine ligand in the PNA backbone with different metal ions. Achim et al.⁴⁵ also reported that the Eu^{3+} in HOPO-PNA duplex retains the five coordinated water molecules.

In view of this, results of the present work states that the 3-hydroxy-2-methyl-4-pyridone in the PNA duplex forms the stable 2:1 complexes with Cu^{2+} , Eu^{3+} and Tb^{3+} . It suggested that geometry of complex formed by PNA with Cu^{2+} is square planar (Figure 42) which is in agreement with the results reported by Shionoya et al.⁶⁵ whereas geometry of complexes formed by PNA with Eu^{3+} and Tb^{3+} indicates that the PNA:PNA duplexes may retain five coordinated water molecules. It implies that Cu^{2+} , Eu^{3+} and Tb^{3+} form stable PNA duplexes.

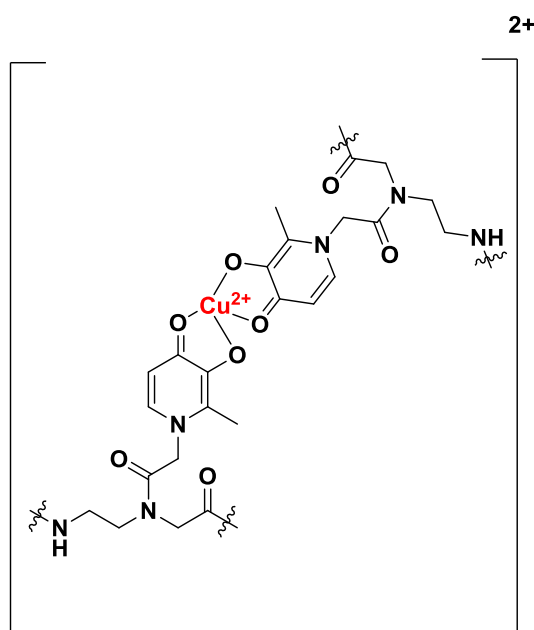


Figure 42. Square planer complex of MHP incorporated PNA:PNA duplex with Cu^{2+} .

1.15 Binding models

To summarize, copper, terbium and europium metal salts revealed possible binding pattern for monomer and oligomer as depicted in Figure 43.

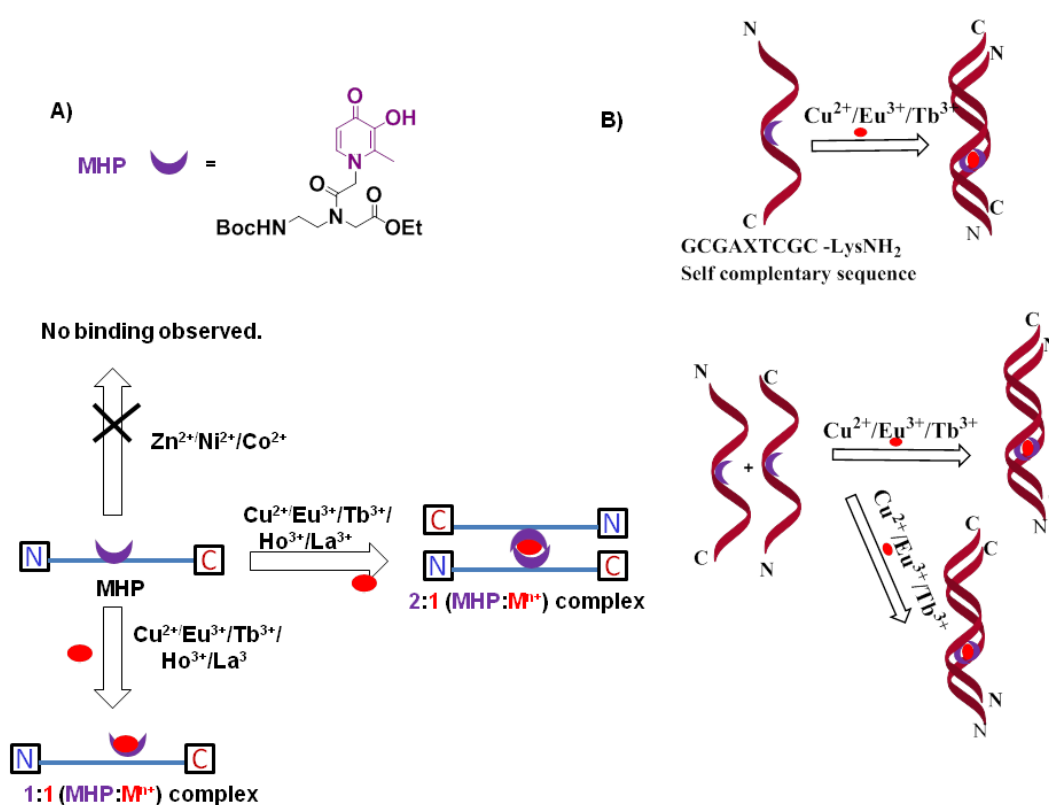


Figure 43. Pictorial representation of possible binding modes of MHP ligand for A) MHP 9 and B) PNA oligomers.

1.16 Conclusion

In conclusion, the synthesis of 3-hydroxy-2-methyl-4-pyridone linked *aeg*-PNA monomer and its incorporation into PNA oligomers at desired position by solid phase peptide synthesis protocol was accomplished successfully. The ligand binds strongly with rare earth metal salts shown by UV-Vis, fluorescence, MALDI-TOF and temperature dependent UV spectroscopic techniques. Thus, present work demonstrates the incorporation of synthetic ligand into PNA oligomers leading to the stabilization of PNA:PNA duplexes via metal mediated base pairing .

The studies here provide the necessary foundation to enable characterization of metal based supramolecular structures and application to design molecular motifs of increased complexity and functions. It can be useful to design PNA based biosensors in addition to development of luminescent materials which may have application in organic light emitting diodes as it binds strongly with lanthanides.

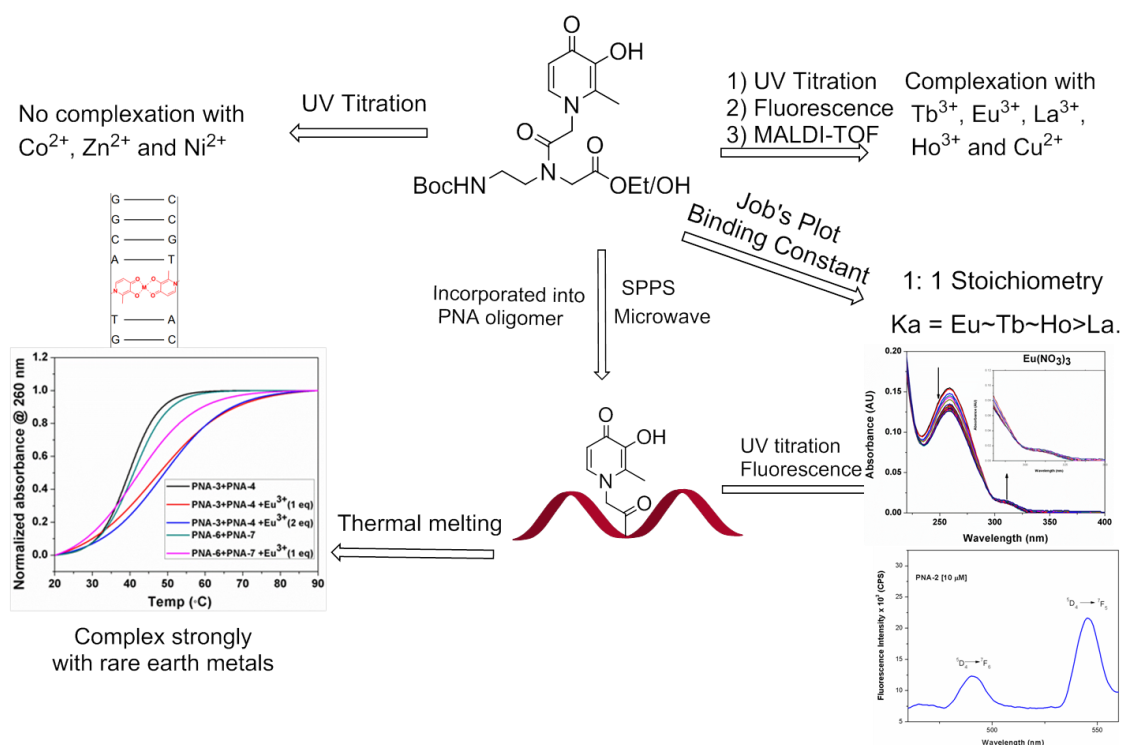


Figure 44. Summary of chapter 1.

1.17 Experimental procedures

This section describes the detailed synthetic procedures and spectral characterization of the rationally designed PNA monomers.

1.17.1 General

The chemicals used were of laboratory or analytical grade. All the solvents used were distilled or dried to carry out various reactions. Reactions were monitored using thin layer chromatography (TLC). Usual workup involved sequential washing of the organic extract with water and brine followed by drying the organic layer over anhydrous sodium sulphate and evaporation of solvent under vacuum. TLCs were carried out on pre-coated silica gel GF₂₅₄ sheets (Merck 5554). TLCs were analysed under UV lamp, by Iodine spray and by spraying with Ninhydrin solution, followed by heating of the plate. Column chromatographic separations were performed using silica gel (60-120 or 100-200 mesh).

Boc-protected aeg-PNA monomers were purchased from ASM Research Chemicals. 4-Methylbenzhydrylamine•HCl (MBHA) resin LL (100-200 mesh) was

obtained from Novabiochem. The unmodified and modified PNA oligomers were synthesized manually by general solid phase PNA synthesis protocol using *Boc*-strategy. Salts and reagents used in buffer preparation such as NaCl, NaH₂PO₄, Na₂HPO₄, etc. were obtained from Sigma-Aldrich. The pH of the buffer solutions was adjusted using NaOH or HCl.

1.17.2 Instrumentation

¹H and ¹³C NMR spectra were recorded using Bruker AC-200 (200 MHz) or JEOL 400 MHz NMR spectrometers. The delta (δ) values for chemical shifts are reported in ppm and are referred to internal standard TMS or deuterated NMR solvents. Mass spectra for reaction intermediates were obtained by Applied Biosystems 4800 Plus MALDI-TOF/TOF mass spectrometry using TiO₂ or 2,5-dihydroxybenzoic acid (DHB) and the integrity of PNA oligomer was checked on the same instrument using DHB or CHCA as matrix. High resolution mass spectra for final PNA monomers were recorded on Synapt G2 High Definition Mass Spectrometry. PNA oligomers were purified on Dionex ICS 3000 HPLC system using semi-preparative BEH130 C18 (10X250 mm) column. Absorption spectra were recorded on a Shimadzu UV-2600 spectrophotometer. UV thermal melting analysis of duplexes was performed on a Cary 300 Bio UV-Vis spectrophotometer. Fluorescence experiments were carried out in a micro fluorescence cuvette (Hellma, path length 1.0 cm) on a Fluoromax-4 spectrofluorometer (Horiba Scientific).

1.17.3 Solid phase protocol

Primarily, MBHA resin hydrochloride salt was neutralized in 50% DIPEA/DCM followed by coupling with 3 equivalents of (Boc/Cl-Cbz) L-lysine, coupling agent HBTU, racemization suppressor HOBt and DIPEA as base to get lysine coupled resin. To avoid deletion of sequences, resin was capped by Ac₂O/Pyridine. The resin was tested by ninhydrin solution to check whether any free amine is present. The observation of no color to the resin was the confirmation that no free amine group is bound to the resin. This was followed by washing of resin several times with DCM and then diethyl ether. The resin bound Boc group was knocked out by using 50% TFA/DCM, followed by neutralization with 10% DIPEA/DCM to get the free amine. The free amine bound resin was tested in ninhydrin solution followed by heating,

which showed the blue colored resin indicating presence of free amine. The free amine was coupled with *aeg*-PNA monomers and heated under microwave condition, which was washed with DMF and DCM. The resin was again tested in ninhydrin. The polyamide oligomers **1** and **2** were cleaved from the resin at final stage using TFA and TFMSA.

1.17.4 Purification of the PNA oligomers by RP-HPLC

PNA purification was carried out on Dionex ICS 3000 HPLC system. For the purification of peptides, semi-preparative BEH130 C18 (10X250 mm) column was used. Purification of PNA oligomers was performed with gradient elution method: A to 50% B in 10 min, 11-20 min: 100% B, 21-25 min: 100% B, 26-30 min: 100% A; A= 0.1% TFA in CH₃CN:H₂O (5:95); B= 0.1% TFA in CH₃CN:H₂O (1:1) with flow rate of 2 mL/min. All the HPLC profiles were monitored at 254 nm and 260 nm wavelength.

1.18 UV titration

The UV spectroscopic measurements were recorded at room temperature. For UV titration at monomeric level, the samples were prepared in 2 mL quantity by dissolving 100 μM of compound in methanol. Solutions of metal salts were prepared by dissolving 10 mM in methanol. 2 mL volume of monomeric solution was transferred to UV cuvette and absorbance was recorded followed by addition of 4 μL of metal salt solution to the cuvette and absorbance was recorded till the saturation point.

For UV titration at oligomer level, 2 μM of PNAs were dissolved in 10 mM HEPES buffer, pH 7.0 and 200 μM of metal salts were prepared in 10 mM HEPES buffer and UV was recorded at room temperature.

1.19 Fluorescence titration

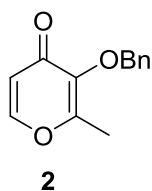
The fluorescence titration of monomer was recorded at room temperature. The samples were prepared by dissolving 10 μM of monomer in methanol and metal salts were prepared at 100 μM concentration in methanol. 2 mL volume of monomeric solution was transferred to fluorescence cuvette and fluorescence was recorded followed by addition of aliquots of 10 μL of metal salt solution to the cuvette and fluorescence was recorded.

1.20 UV- T_m measurement

UV-melting experiments were carried out on Varian Cary 300 UV-spectrophotometer equipped with a peltier. The samples for T_m measurement were prepared by mixing the calculated amounts of respective oligonucleotides in stoichiometric ratio (1:1, for duplex) in sodium phosphate buffer (10 mM) and NaCl (10 mM); pH 7.2 to achieve a final strand concentration of 5 μ M for each strand. The metal salt solutions were prepared in water. The samples were annealed by heating at 90 °C for 10 min. followed by slow cooling to room temperature and then storing at 4 °C for at least 4 to 5 h. The samples (500 μ L) were transferred to quartz cell and equilibrated at the starting temperature for 2 min. The OD at 260 nm was recorded in steps from 20-90 °C with temperature increment of 1 °C/min. Each melting experiment was repeated at least twice. The normalized absorbance at 260 nm was plotted as a function of the temperature. The T_m was determined from the first derivative of normalized absorbance with respect to temperature and is accurate to ± 0.5 °C. The data were processed using Microcal Origin 8.0/8.5. [The concentration of all oligonucleotides were calculated on the basis of absorbance from the molar extinction coefficients of the corresponding nucleobases i.e. T = 8.8 cm²/ μ mol; C = 7.3 cm²/ μ mol; G = 11.7 cm²/ μ mol and A = 15.4 cm²/ μ mol].

1.21 Procedures and spectral data

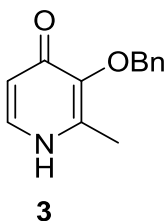
Synthesis of 2-methyl 3-benzyloxy 4-pyrone 2⁵⁸



To a stirred solution of maltol (**1**) (5.0 g, 40 mmol) in methanol (60 mL) sodium hydroxide (2.40 g, 60 mmol) in water (6 mL) was added followed by benzyl bromide (6 mL, 65 mmol), and the mixture was heated to reflux for 12 h. After removal of solvent by rotary evaporation the resultant orange oil was taken up in dichloromethane (30 mL) and washed with 5% (w/v) aqueous sodium hydroxide (5 x 10 mL) and water (2 x 10 mL). The organic fraction was dried over anhydrous sodium sulfate and filtered. The solvent was removed by rotary evaporation to give colorless oil which was triturated

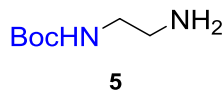
with diethyl ether and cooled at 0 °C for 1 h to give solid product (Yield 6.5 g, 75%). MS (MALDI-TOF) m/z calcd for $C_{13}H_{12}NaO_3$ $[M+Na]^+$ 239.0684, found 239.0429.

Synthesis of 2-methyl 3-benzyloxy 4-pyridone **3**⁵⁸



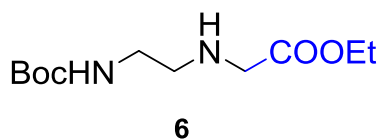
To a solution of compound **2** (4 g, 18 mmol) in ethanol (25 mL) 30% aqueous ammonia (60 mL) was added and the mixture was refluxed for 18 h. Removal of solvent by rotary evaporation gave an oil which solidified on addition of acetone and cooling followed by recrystallization in ethanol gave colorless prisms (Yield 3.2 g, 80%). MS (HR-MS) m/z calcd for $C_{13}H_{14}NO_2$ $[M+H]^+$ 216.1025, found 216.1022.

*N*1- (Boc)-1, 2-diaminoethane (**5**)



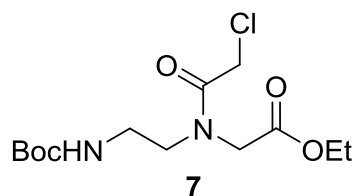
1, 2-diaminoethane (20g, 0.33 mol) was taken in DCM (300 mL) and cooled in an ice-bath. Boc-anhydride (5 g, 35 mmol) in DCM (50 mL) was slowly added with stirring. The mixture was stirred for 12 h and the resulting solution was concentrated to 100 mL. To this solution, water was added and then extracted with DCM. *N*1, *N*2-di-Boc derivative was removed by dissolving in water. The corresponding *N*-mono-Boc derivative was obtained by repeated extraction of aqueous layer with dichloromethane. The collected organic layer was washed with brine followed by drying over anhydrous sodium sulphate. Removal of DCM on rotary evaporator yielded the mono-Boc-diaminoethane (**5**) (3.40 g, 60%) which was used for further reaction without any purification.

Ethyl *N*-(2-Boc-aminoethyl) glycinate (**6**)

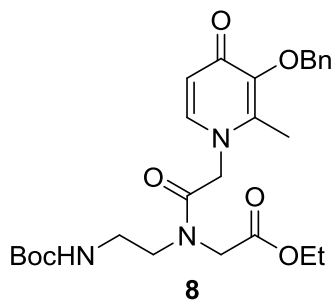


The *N*-(Boc)-1, 2-diaminoethane (**5**) (3.2 g, 20 mmol) was treated with ethyl bromoacetate (2.2 mL, 20 mmol) in acetonitrile (100 mL) in the presence of triethylamine (5.5 mL, 40 mmol) and the mixture was stirred at ambient temperature for 10 h. The completion of reaction was monitored by TLC. After completion of reaction, solvent was removed on rota evaporator. Reaction mixture was then diluted with water (50 mL) and extracted with ethyl acetate (3 x 50 mL), followed by washing with brine. The collected organic layer was dried over anhydrous sodium sulphate and filtered and then concentrated to get crude product. The crude product was used further for next reaction without purification.

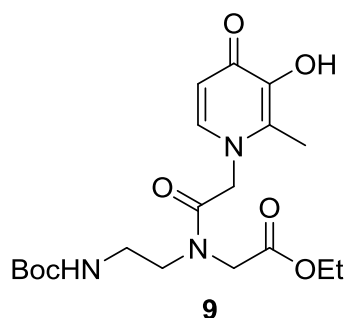
Synthesis of ethyl *N*-(2-Boc-aminoethyl) chloroacetyl glycinate **7**



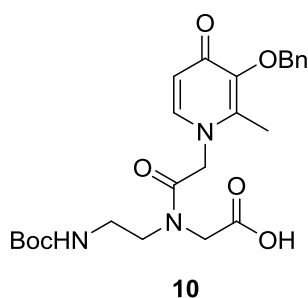
Compound **3** (3 g, 11.5 mmol) was dissolved in dioxane (50 mL) at 0 °C and NaHCO₃ (1.9 g, 23 mmol) in water (50 mL) was added to reaction mixture at 0 °C and stirred for 5 min. To this, chloroacetyl chloride (1.0 mL, 12.6 mmol) was added dropwise and reaction was continued for stirring at 0 °C for another 5 min. After 5 min, the reaction mixture was brought to room temperature and stirred for 1.5 h. After completion of reaction (TLC), dioxane was removed under reduced pressure. Reaction mixture was then diluted with water (25 mL) and extracted with ethyl acetate (3 x 75 mL). The combined organic layer was washed with saturated solution of NaHCO₃ followed by washing with brine. Organic layer was dried over anhydrous sodium sulphate, collected by filtration and concentrated on rotary evaporator. The residual material was purified on column using silica gel in petroleum ether: ethyl acetate (4:1) (Yield 3.2 g, 85%). ¹H NMR (400 MHz, CDCl₃) δ: H 5.02 (bs, 1H), 4.5 (s, 2H), 4.22 (q, 2H), 3.35 (s, 2H), 3.20 (t, 2H), 2.76 (t, 2H), 1.46 (s, 9H), 1.28 (t, 3H) ppm; ¹³C NMR (100 MHz, CDCl₃) δ: 14.1, 28.3, 38.7, 49.7, 61.7, 80.0, 156.1, 167.7, 169.8 ppm.

Synthesis of ethyl N-(2-(3-(benzyloxy)-2-methyl-4-oxopyridin-1(4H)-yl)acetyl)-N-(2-((tert-butoxycarbonyl)amino)ethyl)glycinate **8**

Compound **7** (3 g, 9.3 mmol) was dissolved in dry DMF under inert atmosphere (25 mL) and stirred at 0 °C temperature for 5 min. After 5 min, dry K₂CO₃ and 2-methyl 3-benzyloxy 4-pyridinone (2 g, 9.3 mmol) were added and stirring continued at same temperature. After 5 min, reaction mixture was heated in microwave for 5 min. Completion of reaction was monitored by TLC. After completion of reaction, the hot reaction mixture was allowed to cool at room temperature followed by dilution with water (40 mL) and extracted with ethyl acetate (3 x 75 mL). The combined organic layer was washed with saturated solution of NaHCO₃ (20 mL) and then again washed with water (3 x 40 mL) followed by washing with brine (25 mL). The collected organic layer was dried over anhydrous sodium sulphate, collected by filtration and concentrated on rotary evaporator. The crude product was purified on column using silica gel in petroleum ether: ethyl acetate to give yellowish oil (0.5:4.5) (Yield 3.5 g, 75%). ¹HNMR (CDCl₃, 400 MHz) δ: 8.11 (d, 1H, *J* = 4.7 Hz), 7.44 (m, 2H), 7.34 (m, 3H), 6.75 (mi.) and 6.67 (ma.) (d, 1H, *J* = 5.6 Hz), 5.59 (bs, 1H), 5.07 (ma.) 5.04 (mi.) (s, 2H), 4.9 (ma.) 4.77 (mi.) (s, 2H), 4.26-4.15 (m, 2H, *J* = 7.1 Hz), 4.11 (mi.) 4.03 (ma.) (s, 2H), 3.5 (dt, 2H, *J* = 6 Hz), 3.27 (m, 2H, *J* = 4 Hz), 2.39 (ma.) 2.38 (mi.) (s, 3H), 1.40 (mi.) 1.38 (ma.) (s, 9H), 1.27 (t, 3H, *J* = 8 Hz) ppm; ¹³C NMR (CDCl₃, 100 MHz) δ: 169.7, 167.3, 157.2, 156.0, 153.3, 144.6, 142.1, 140.1, 137.1, 128.4, 128.1, 106.8, 80.0, 74.7, 65.5, 67.1, 62.2, 61.7, 48.5, 38.5, 28.3, 18.9, 14.0 ppm; MS (HRMS-ESI) *m/z* calcd for C₂₆H₃₆N₃NaO₇[M+Na]⁺ 524.2373, found 524.2554.

Synthesis of ethyl N-(2-((tert-butoxycarbonyl)amino)ethyl)-N-(2-(3-hydroxy-2-methyl-4-oxopyridin-1(4H)-yl)acetyl)glycinate 9

Compound **8** (3 g, 6 mmol) was dissolved in ethanol and stirred at room temperature under H₂ atmosphere. To the reaction mixture, 10 % Pd/C on charcoal was added and stirred at same temperature for 6 h. The completion of reaction was monitored by TLC. After completion of reaction, the reaction mixture was filtered on celite-545 pad and filtrate was collected, evaporated to get white solid which was further dried on high vacuum (Yield 2.4 g, 95%). ¹H NMR (CD₃OD, 400 MHz,) δ: 7.80 (d, 1H, *J* = 5.4 Hz), 6.93 (d, 1H, *J* = 8 Hz), 5.09 (mi.) 5.04 (ma.) (s, 2H), 4.23 (m, 4H), 3.5 (t, 2H, *J* = 6 Hz), 2.46 (mi.) 2.40 (ma.) (s, 3H), 1.42 (mi.) 1.38 (ma.) (s, 9H), 1.27(t, 3H, *J* = 8 Hz) ppm; ¹³C NMR (CD₃OD, 100 MHz) δ: ¹³C NMR (CD₃OD, 100 MHz) δ: 175.0, 174.7, 169.6 (ma), 169.1 (mi), 164.9, 158.8, 157.6, 144.9, 143.5, 142.9, 135.9(mi), 135.5 (ma), 130.1, 129.6, 129.6, 109.7 (ma), 109.5 (mi), 80.6, 80.2, 68.25, 52.41,, 39.3, 39.2, 37.1, 28.8, 15.5, 15.2 ppm; MS (MALDI-TOF) *m/z* calcd for C₂₄H₃₁NaN₃O₇ [M+Na] 496.2060, found 496.1967ppm; MS (HRMS-ESI) *m/z* calcd for C₁₉H₃₀N₃O₇ [M+H]⁺ 412.2084, found 412.2084.

Synthesis of N-(2-(3-(benzyloxy)-2-methyl-4-oxopyridin-1(4H)-yl)acetyl)-N-(2-((tert-butoxycarbonyl)amino)ethyl)glycine 10

Compound **8** (1 g, 2 mmol) was dissolved in ethanol and stirred at 0 °C. To this, 10% LiOH (1.5 mL) was added drop wise at the same temperature for 10 min. The completion of reaction was monitored by TLC. After completion of reaction, solvent was removed on rotary evaporator. Ethyl acetate was added to the residue and it was acidified by the addition of saturated aqueous solution of potassium bisulfate till the pH comes down to 3-4. Organic layer was collected and washed with brine solution. The organic layer was concentrated on rotary evaporator to get solid product which was further dried on high vacuum and stored in vacuum dessicator (Yield 0.85 g, 90%). ¹H NMR (400 MHz, CD₃OD) δ: 8.32-8.3 (d, 1H, *J* = 8 Hz), 7.49-7.37 (m, 6H), 5.51-5.32 (s, 2H), 5.3-5.26 (m, 2H), 4.29,4.17(s, 2H,) 3.54-3.51 (m, 2H, *J* = 6 Hz), 3.5, 3.24 (m, 2H), 2.38, 2.29 (s, 3H), 1.43(s, 9H) ppm; ¹³C NMR (CD₃OD, 100 MHz) δ: 174.8 (ma), 174.5 (mi), 169.3 (ma), 168.9 (mi), 164.7, 158.1, 157.4, 144.7, 143.3, 142.7, , 135.7(mi), 135.3 (ma), 129.9, 129.4, 109.4 (ma), 109.3 (mi), 80.4 (ma), 80.0 (mi), 75.7, 68.0, 39.1, 38.9, 36.9, 28.6, 15.3, 14.9 ppm; MS (MALDI-TOF) *m/z* calcd for C₂₄H₃₁NaN₃O₇ [M+Na] 496.2060, found 496.1967.

1.22 References

1. Blackburn, G. M.; Gait, M. J. *Nucleic acids in chemistry and biology*. University Press: Oxford **1990**.
2. Watson, J. D.; Crick, F. H. C. *Nature* **1953**, *171*, 737–738.
3. Crooke, S. T. *Therapeutic Applications of oligonucleotide*. Springer-Verlag: Heidelberg **1995**.
4. Nielsen, P. E.; *Acc. Chem. Res.* **1999**, *32*, 624-630.
5. Hoogsteen, K. *Acta. Crystal.* **1963**, *16*, 907-916.
6. (a) Crick, F. H. C. *J. Mol. Biol.* 1966, *19*, 548-555; (b) Soll, D.; Cherayil, J. D.; Bock, R. M. *J. Mol. Biol.* **1967**, *29*, 97-112.
7. Seeman, N. C.; Rosenberg, J. M.; Rich, A. *Proc. Natl. Acad. Sci. USA.* **1976**, *73*, 604-807.
8. (a) Seeman, N. C. *Trends Biochem. Sci.* **2005**, *30*, 119-125; (b) Seeman, N. C.; Lukeman, P. S. *Rep. Prog. Phys.* **2005**, *68*, 237-270; c) Braun, E.; Keren, K. *Adv. Phys.* **2004**, *53*, 441-496.
9. (a) Zimmermann, N.; Meggers, E.; Schultz, P. G. *J. Am. Chem. Soc.* **2002**, *124*, 13684–13685; (b) Bohme, D.; Dupre, N.; Megger, D. A.; Muller, J. *Inorg. Chem.* **2007**, *46*, 10114–10119; (c) Zhang, L. L.; Meggers, E. *J. Am. Chem. Soc.* **2005**, *127*, 74–75;

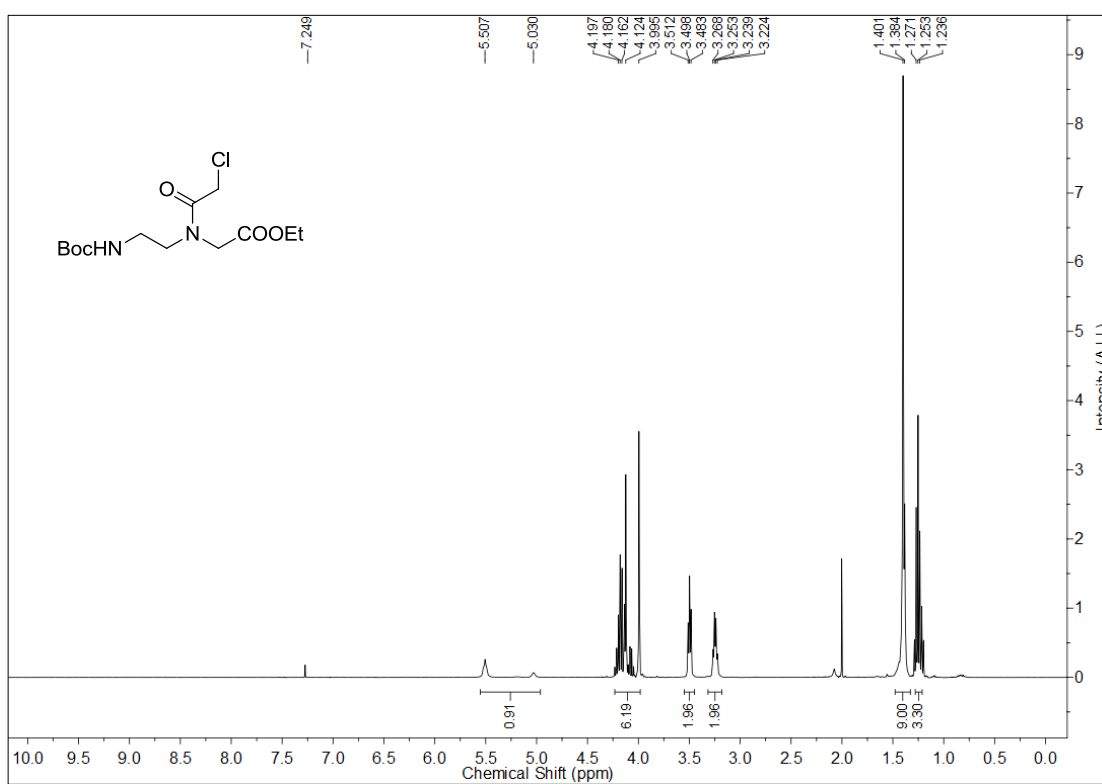
- (d) Shin, D. W.; Switzer, C. *Chem. Commun.* **2007**, 4401–4403; (e) Heuberger, B. D.; Shin, D.; Switzer, C. *Org. Lett.* **2008**, *10*, 1091–1094.
10. He, W.; Franzini R. M.; Achim, C. *Prog. Inorg. Chem.* **2007**, *55*, 545–611.
11. Hirao, I.; Kimoto, M.; Yamashige, R. *Acc. Chem. Res.* **2012**, *45*, 2055–2065.
12. Lee, J. S.; Latimer, L. J. P.; Reid, R. S. *Biochem. Cell Biol.* **1993**, *71*, 162–168.
13. Katz, S. *Biochim. Biophys. Acta*, **1963**, *68*, 240–253.
14. Kuklenyik, Z.; Marzilli, L. G. *Inorg. Chem.* **1996**, *35*, 5654–5662.
15. Liu, J.; Lu, Y. *Angew. Chem. Int. Ed.* **2007**, *46*, 7587–7590.
16. Park, K. S.; Jung, C.; Park, H. G. *Angew. Chem. Int. Ed.* **2010**, *49*, 9757–9760.
17. Takezawa Y.; Shionoya M. *Acc. Chem. Res.* **2012**, *45*, 2066–2076.
18. Tanaka, K.; Shionoya, M. *J. Org. Chem.* **1999**, *64*, 5002–5003.
19. a) Tanaka, K.; Shionoya, M. *Coord. Chem. Rev.* **2007**, *251*, 2732–2742; b) Clever, G. H.; Kaul, C.; Carell, T. *Angew. Chem., Int. Ed.* **2007**, *46*, 6226–6236.
20. Nielsen, P. E.; Egholm, M.; Berg, R. H.; Buchardt, O. *Science* **1991**, *254*, 1497–1500.
21. (a) Nielsen, P. E. *Acc. Chem. Res.* **1999**, *32*, 624–630; (b) Ganesh, K. N.; Nielsen, P. E. *Curr. Org. Chem.* **2000**, *4*, 931–943.
22. Kumar, V. A.; Ganesh, K. N. *Acc. Chem. Res.* **2005**, *38*, 404–412.
23. Percio, A. M.; Farias, L. D.; Dontha, N.; Shiraishi, H.; Cai, X.; Rivas, G.; Nielsen, P. E.; Palecek, E.; Wang, J. *J. Am. Chem. Soc.* **1996**, *118*, 7667–7670.
24. Wang, J. *Biosens. Bioelectron.* **1998**, *13*, 757–762.
25. Wang, J. *Curr. Issues Mol. Biol.* **1999**, *1*, 117–122.
26. Steichen, M.; Decrem, Y.; Godfroid, E.; Buess-Herman, C. *Biosens. Bioelectron.* **2007**, *22*, 2237–2243.
27. Ozkan, D.; Erdem, A.; Kara, P.; Kerman, K.; Gooding, J. J.; Nielsen, P. E.; Ozsoz, M. *Electrochem. Commun.* **2002**, *4*, 796–802.
28. Hashimoto, K.; Ishimori, Y. *Lab Chip*, **2001**, *1*, 61–63.
29. Hejazi, M. S.; Pournaghi-Azar, M. H.; Ahour, F. *Anal. Biochem.* **2010**, *399*, 118–124.
30. Ozkan, D.; Kara, P.; Kerman, K.; Meric, B.; Erdem, A.; Jelen, F.; Nielsen, P. E.; Ozsoz, M. *Bioelectrochemistry*, **2002**, *58*, 119–126.
31. Aoki, H.; Tao, H. *Anal. Sci.* **2008**, *24*, 929–933.
32. Aoki, H.; Tao, H. *Analyst*, **2007**, *132*, 784–791.
33. Palecek, E.; Trefulka, M.; Fojta, M. *Electrochem. Commun.* **2009**, *11*, 359–362.
34. Luo, X.; Lee, M. H.; Hsing, I. M. *Anal. Chem.* **2008**, *80*, 7341–7346.
35. Degefa, T. H.; Kwak, J. J. *Electroanal. Chem.* **2008**, *612*, 37–41.

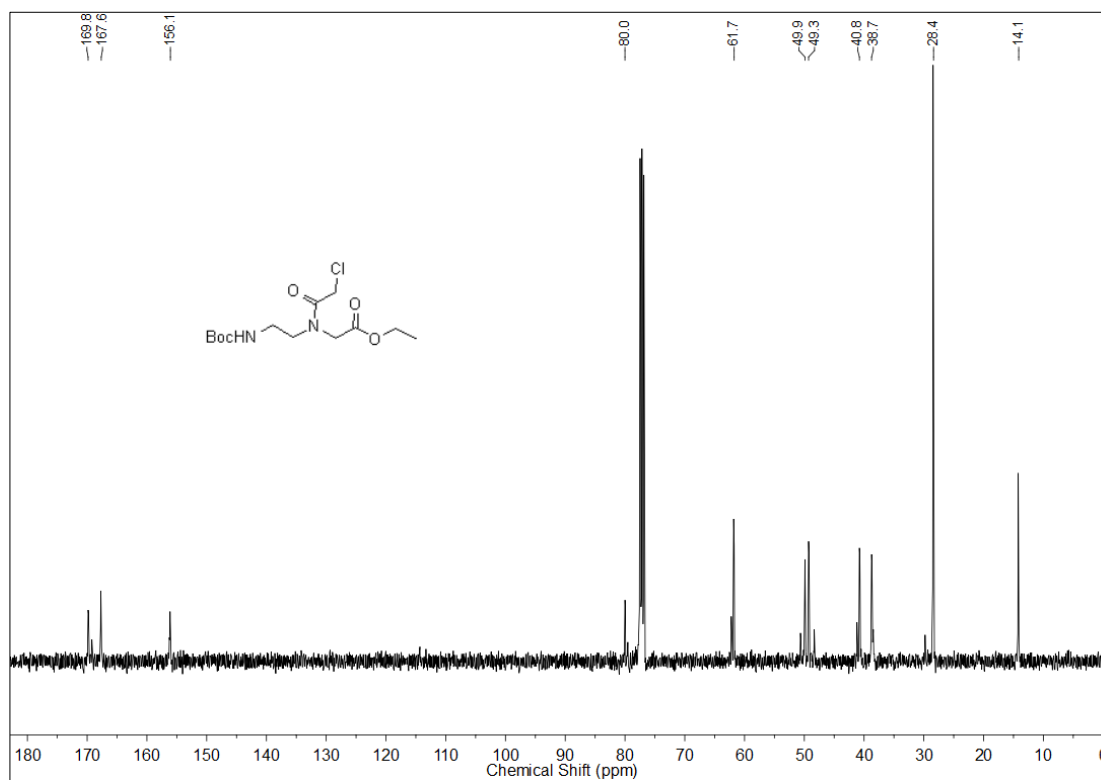
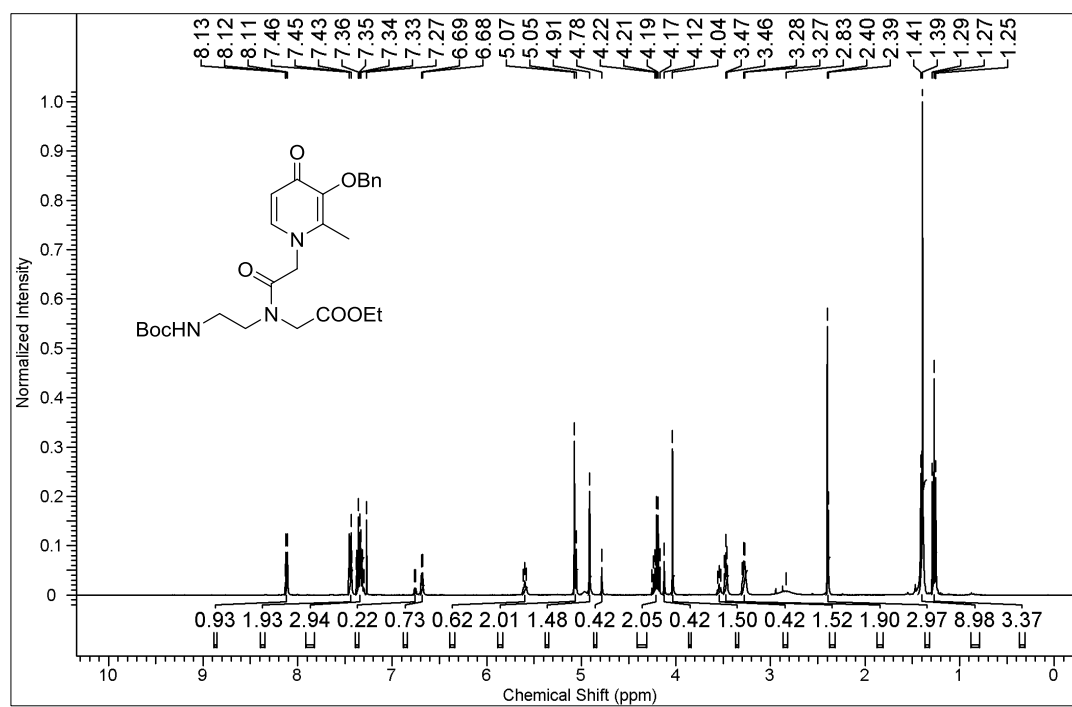
36. Keighley, S. D.; Estrela, P.; Li, P.; Migliorato, P. *Biosens. Bioelectron.* **2008**, *24*, 906-911.
37. Diakowski, P. M.; Kraatz, H. B. *Chem. Commun.* **2009**, 1189-1191.
38. Mateo-Marti, E.; Briones, C.; Pradier, M.; Martin-Gago, J. A. *Biosens. Bioelectron.* **2007**, *22*, 1926-1932.
39. Fussl, A.; Schleifenbaum, A.; Goritz, M.; Riddell, A.; Schlutz, C.; Kramer, R. *J. Am. Chem. Soc.* **2006**, *128*, 5986-5987.
40. Perdicchia, D.; Zinzalla, G.; Licandro, E.; Maiorana, S.; Baldoli, C. *Org. Lett.*, **2002**, *4*, 4341-4344.
41. Zinzalla, G.; Maiorana, S.; Licandro, E.; Giannini, C.; Baldoli, C. *Synlett*, **2004**, *6*, 1044-1048.
42. Salmain, M.; Giannini, C.; Vandoni, B.; Baldoli, C.; Perdicchia, D.; Licandro, E.; Maiorana, S. *J. Mol. Catal. A: Chem.*, **2003**, *204-205*, 165-175.
43. Watson, R. M.; Skorik, Y. A.; Patra, G. K.; Achim, C. *J. Am. Chem. Soc.* **2005**, *127*, 14628-14639.
44. Popescu, D.; Parolin, T. J.; Achim, C. *J. Am. Chem. Soc.* **2003**, *125*, 6354-6355.
45. De Leon, A. R.; Olatunde, A. O.; Morrow, J. R.; Achim, C. *Inorg. Chem.* **2012**, *51*, 12597-12599.
46. Gasser, G.; Hüskens, N.; Köster, S. D.; Metzler-Nolte, N. *Chem. Commun.* **2008**, *45*, 3675-3677.
47. Bazer, S.; Rapireddy, S.; Skorik, Y. A.; Ly Danith, H.; Achim, C. *Inorg. Chem.* **2011**, *50*, 11929-11937.
48. Mokhir, A.; Kra, R.; Wolf, H. *J. Am. Chem. Soc.* **2004**, *126*, 6208-6209.
49. Whitney, A.; Gavory, G.; Balasubramanian, S. *Chem. Commun.* **2003**, 36-37.
50. Murtola, M.; Stromberg, R. *Org. Biomol. Chem.* **2008**, *6*, 3837-3842.
51. Bigey, P.; Sonnichsen, S. H.; Meunier, B.; Nielsen, P. E. *Bioconjugate Chem.* **1997**, *8*, 267-270.
52. Koppelhus, U.; Awasthi, S. K.; Zachar, V.; Holst, H. U.; Ebbesen, P.; Nielsen, P. E. *Antisense and Nucleic Acid Drug Development*, **2002**, *12*, 51-63.
53. Bendifallah, N.; Rasmussen, F. W.; Zachar, V.; Ebbesen, P.; Nielsen, P. E. *Bioconjugate Chem.* **2006**, *17*, 750-758.
54. Wolf, Y.; Pritz, S.; Abes, M.; Lebleu, B.; Oehlke, J. *Biochemistry*, **2006**, *45*, 14944-14954.
55. Turner, Y.; Wallukat, P.; Saalik, B.; Pritz, S.; Oehlke, J. *J. Pept. Sci.* **2010**, *16*, 71-80.
56. Merrifield, R. B. *J. Am. Chem. Soc.* **1963**, *85*, 2149-2154.
57. Anderson, G. W.; Mcgreoger, A. C. *J. Am. Chem. Soc.* **1957**, *79*, 6180-6183.

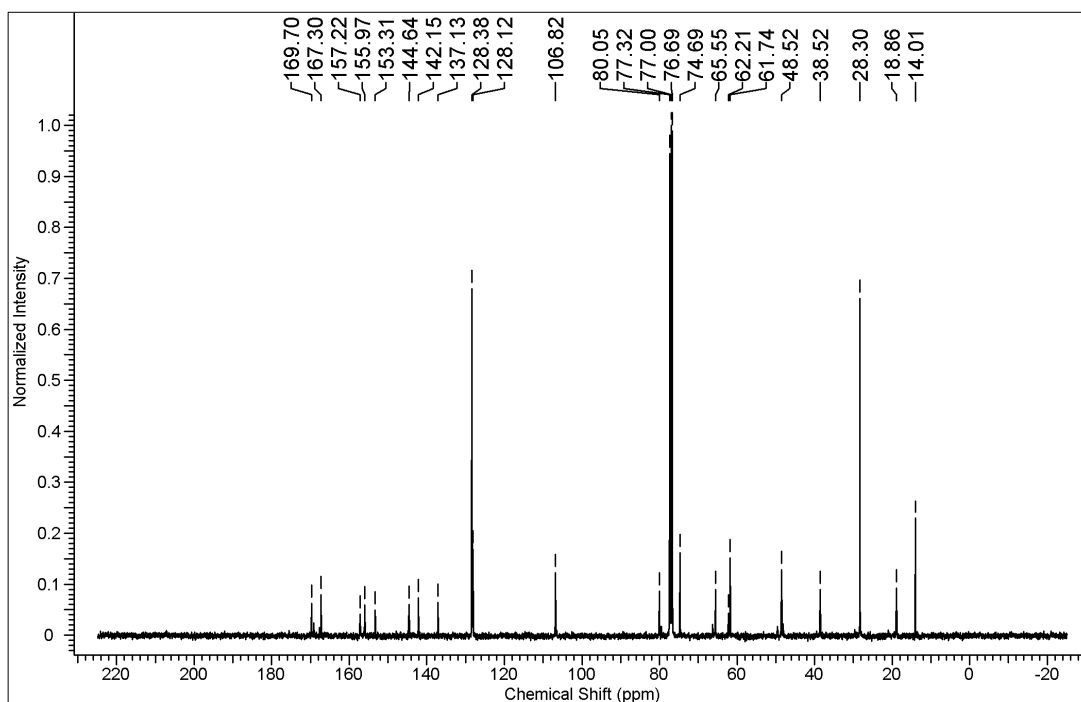
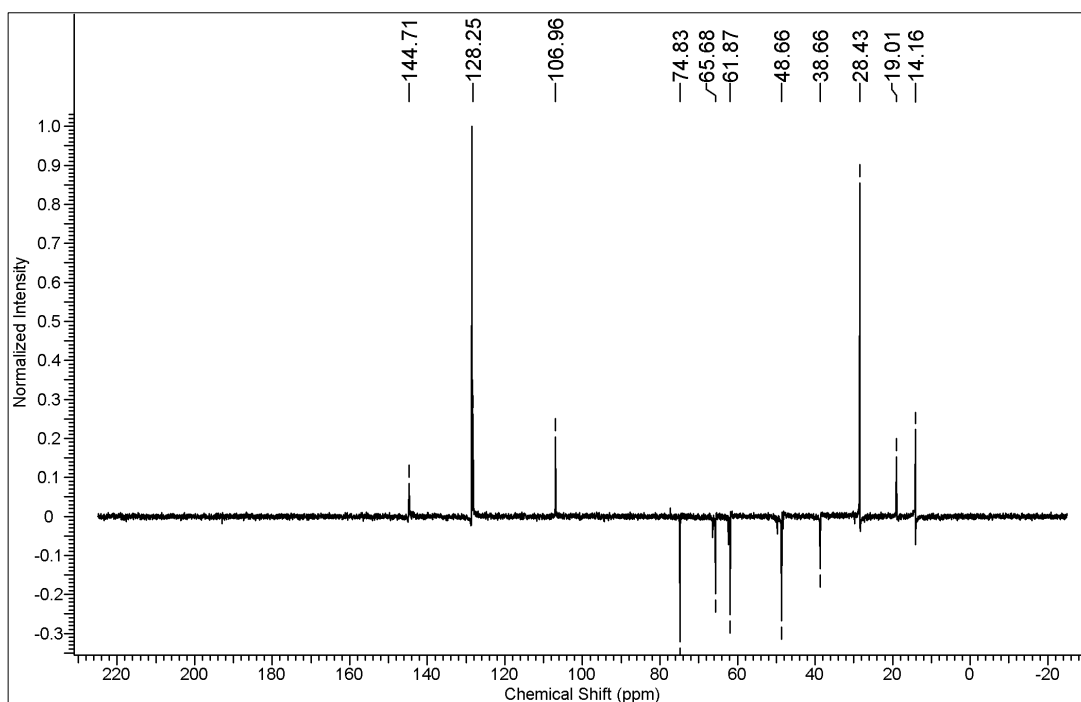
58. Rai B. L.; Dekhordi L. S.; Khodr H.; Jin Y.; Liu Z.; Hider R. C. *J. Med. Chem.* **1998**, *47*, 3347-3359.
59. (a) Erickson, B. W.; Merrifield, R. B. *Solid Phase Peptide Synthesis. In the Proteins*, Vol. II, 3rd ed.; Neurath, H.; Hill, R. L. eds.; Academic Press, New York, **1976**, 255.
(b) Merrifield, R. B.; Stewart, J. M.; Jernberg, N. *Anal. Chem.* **1966**, *38*, 1905-1914.
60. (a) Kaiser, E.; Colescott, R. L.; Bossinger, C. D.; Cook, P. I. *Anal. Biochem.* **1970**, *34*, 595-598 (b) Kaiser, E.; Bossinger, C. D.; Cplscott, R. L.; Olsen, D. B. *Anal. Chim. Acta.* **1980**, *118*, 149-151; (c) Sarin, V. K.; Kent, S. B. H.; Tam, J. P.; Merrifield, R. B. *Anal. Biochem.* **1981**, *117*, 147-157.
61. Dos Santos, C. M. G.; Harte, A. J.; Quinn, S. J.; Gunnlaugsson, T. *Coord. Chem. Rev.* **2008**, *252*, 2512-2527.
62. Bunzli, J. C. G.; Andre, N.; Elhabiri, M.; Muller, G.; Piquet, J. *J. Alloys Compd.* **2000**, *303-304*, 66-74.
63. Iqbal, S. S.; Mayo, M. W.; Bruno, J. G.; Bronk, B V.; Batt, C. A.; Chambers, J. P. *Biosens. Bioelectron.* **2000**, *15*, 549-578.
64. Feng, J.; Shan, G.; Maquieira, A.; Koivunen, M. E.; Guo, B.; Hammock, B. D.; Kennedy, I. M. *Anal. Chem.* **2003**, *75*, 5282-5286.
65. Tanaka, K.; Tasaka, M.; Cao, H.; Shionoya, M. *Supramol. Chem.* **2002**, *14*, 255.
66. Franzini, R. M.; Watson, R. M.; Patra, G. K.; Breece, R. M.; Tierney, D. L.; Hendrich, M. P.; Achim, C. *Inorg. Chem.* **2006**, *45*, 9798.

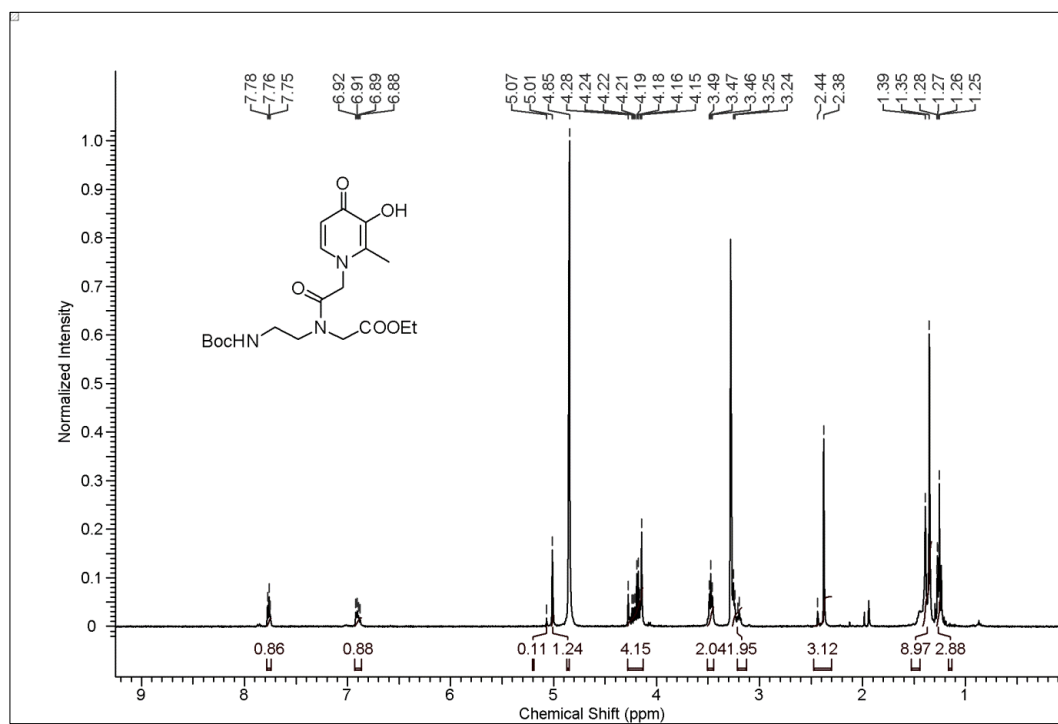
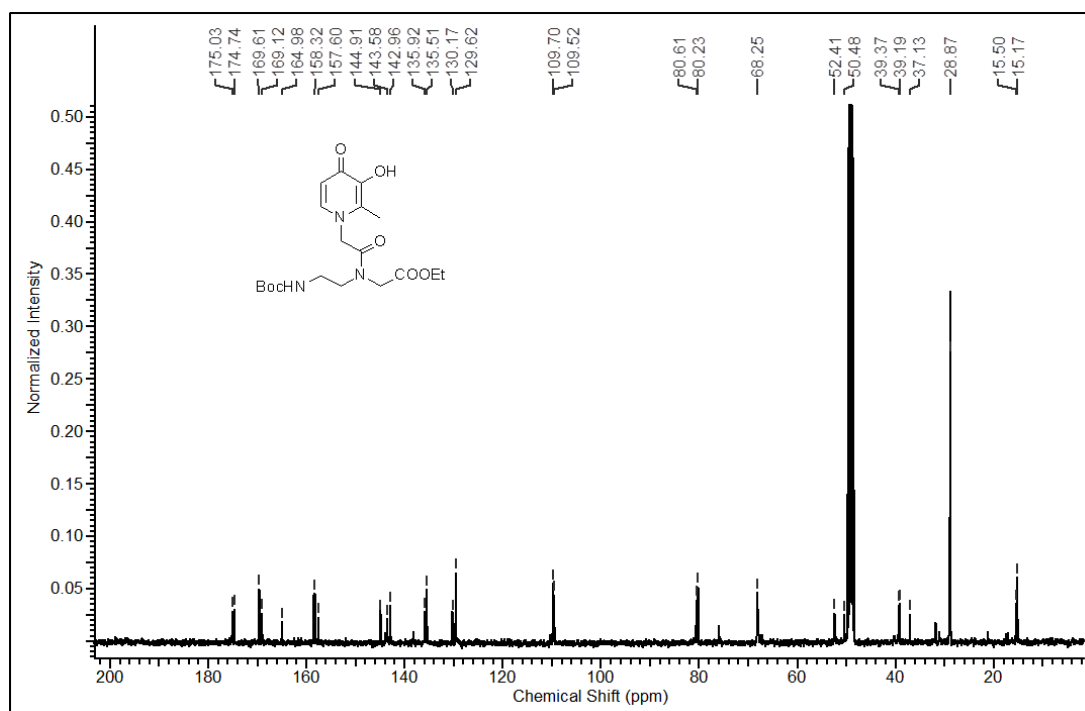
1.23 Appendix-I: Characterization data of synthesized compounds/PNA

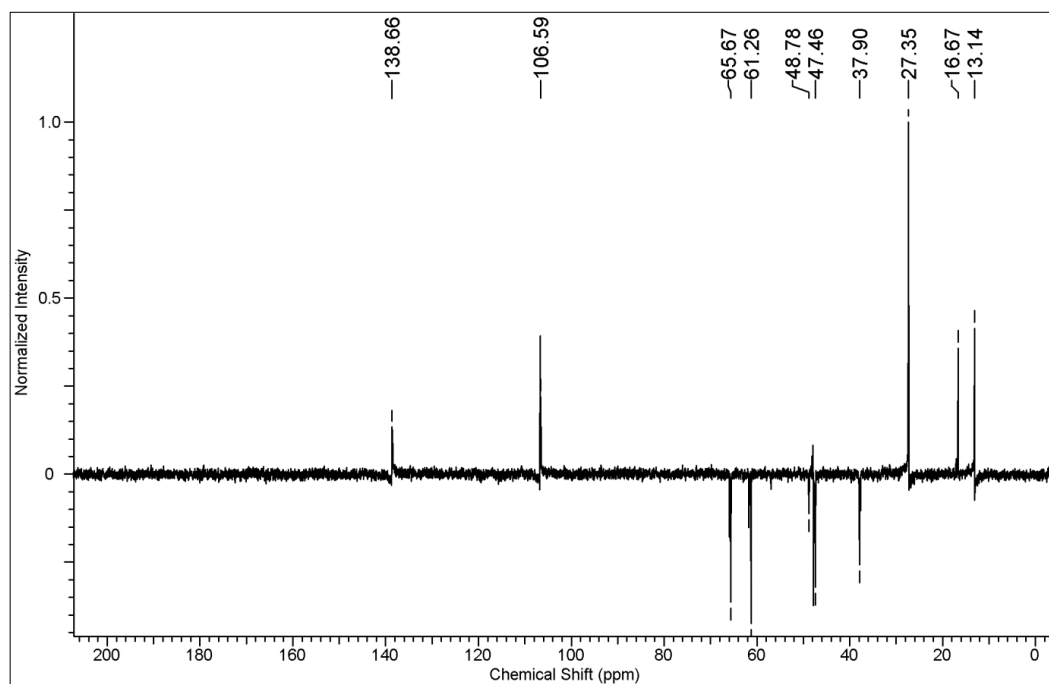
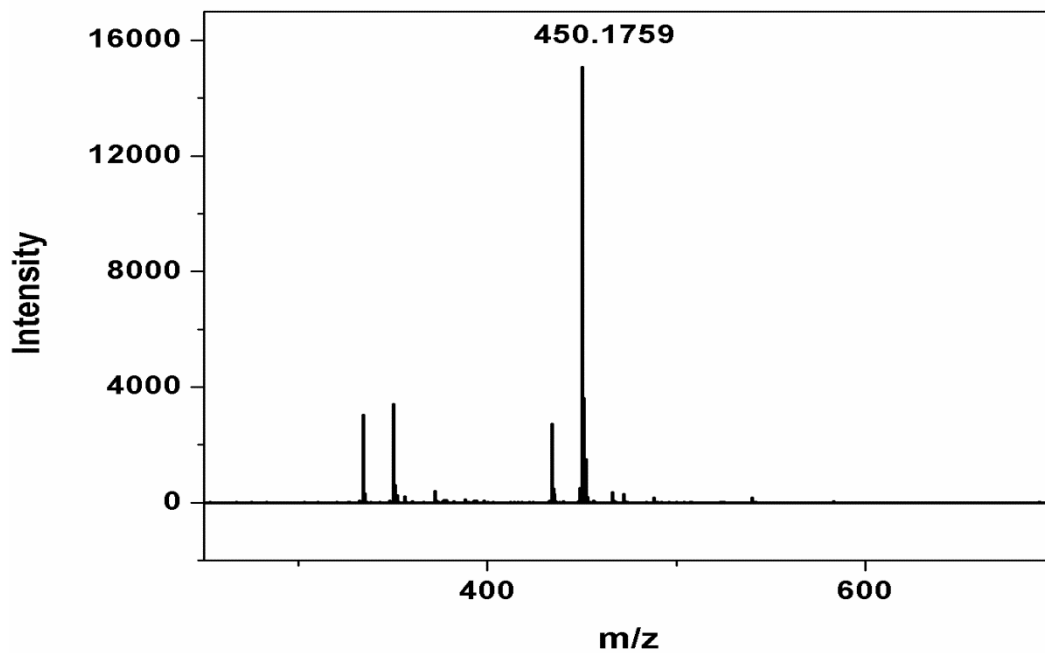
Entry	Table of contents	Page No.
1	^1H , ^{13}C , DEPT, MALDI-TOF of all compounds.	57-62
2	HPLC profiles of all synthesized PNA oligomers	63-67
3	MALDI-TOF mass spectra of all synthesized PNA oligomers	67-71

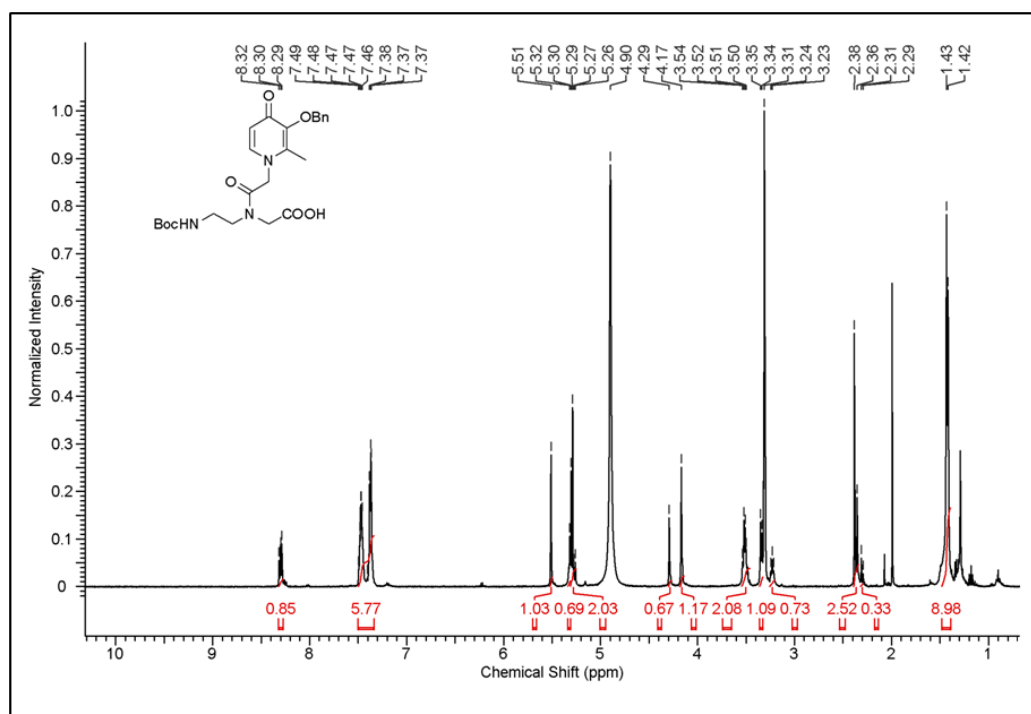
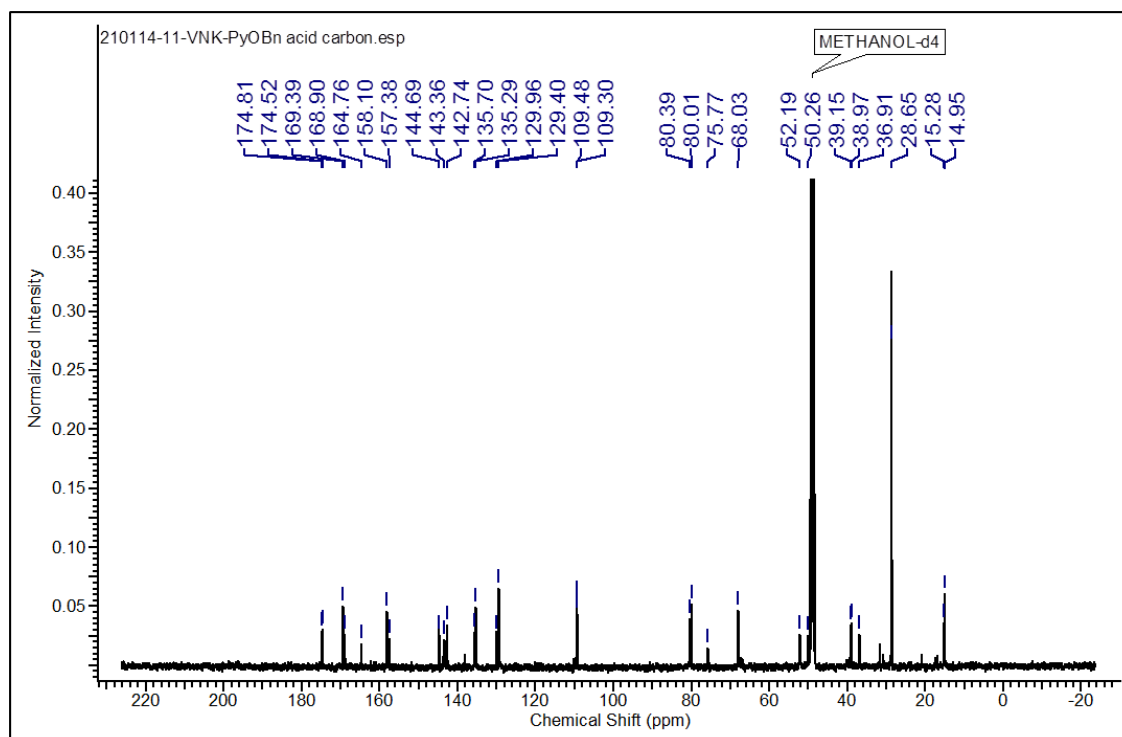
 ^1H NMR of compound 7

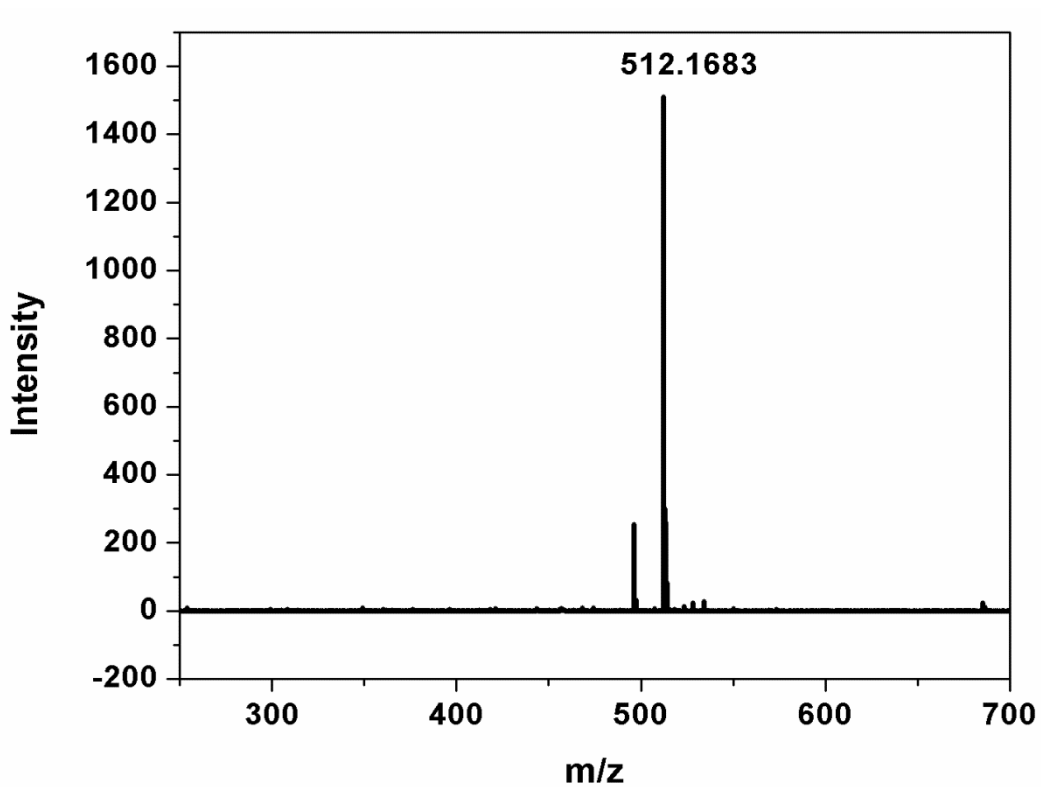
^{13}C NMR of compound 7 **^1H NMR of compound 8**

^{13}C NMR of compound **8**DEPT NMR of compound **8**

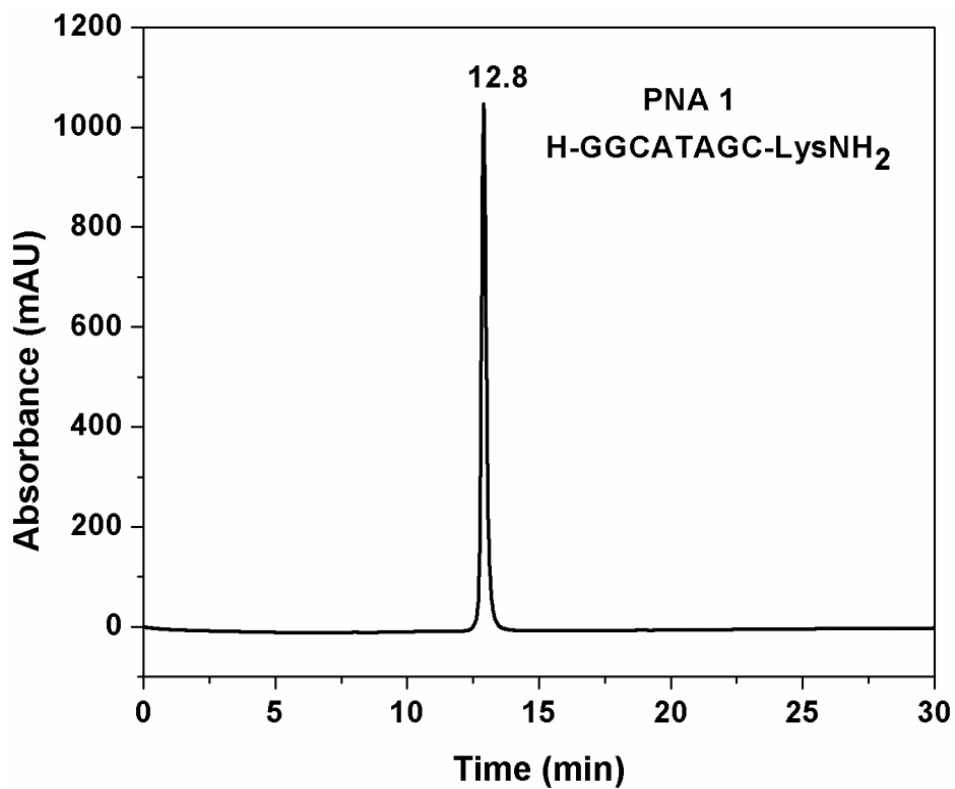
^1H NMR of compound **9** ^{13}C NMR of compound **9**

DEPT NMR of compound **9**MALDI-TOF of compound **9**

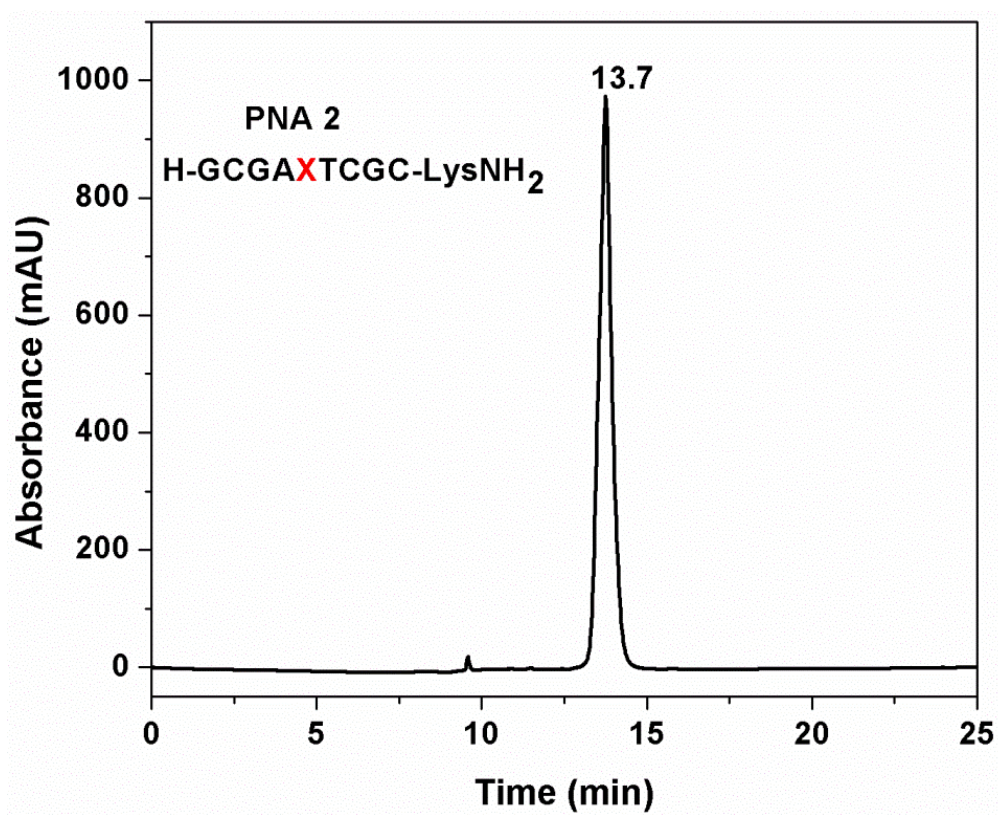
^1H NMR of compound **10** ^{13}C NMR of compound **10**

MALDI-TOF of compound **10**

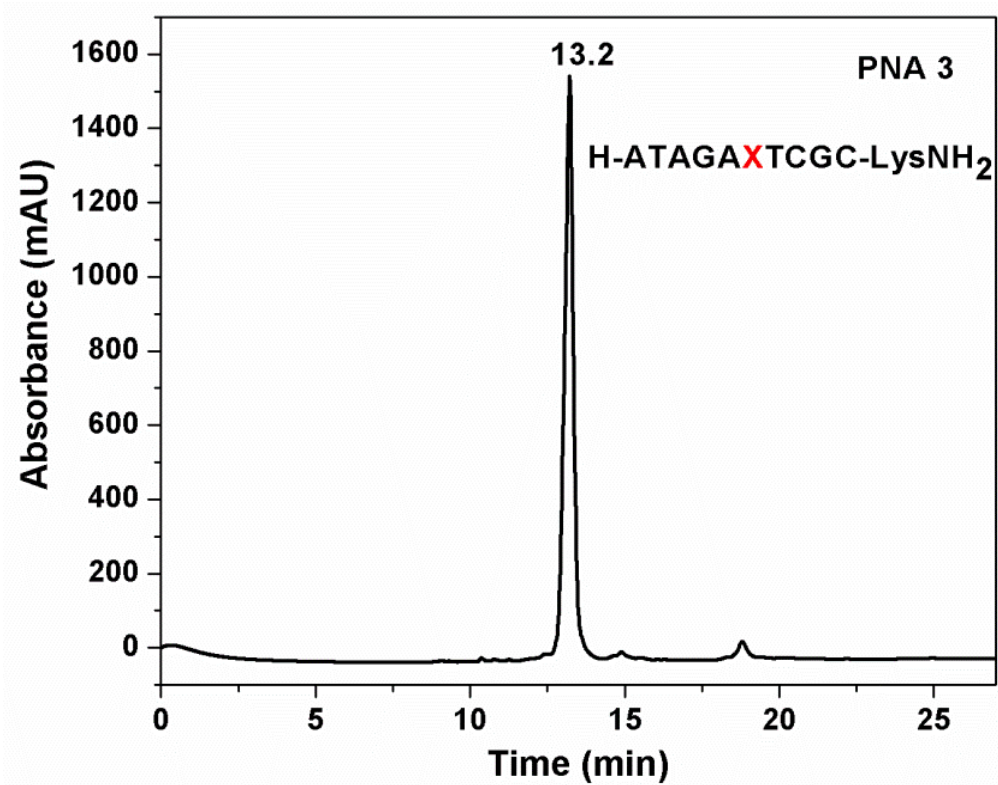
HPLC of PNA-1



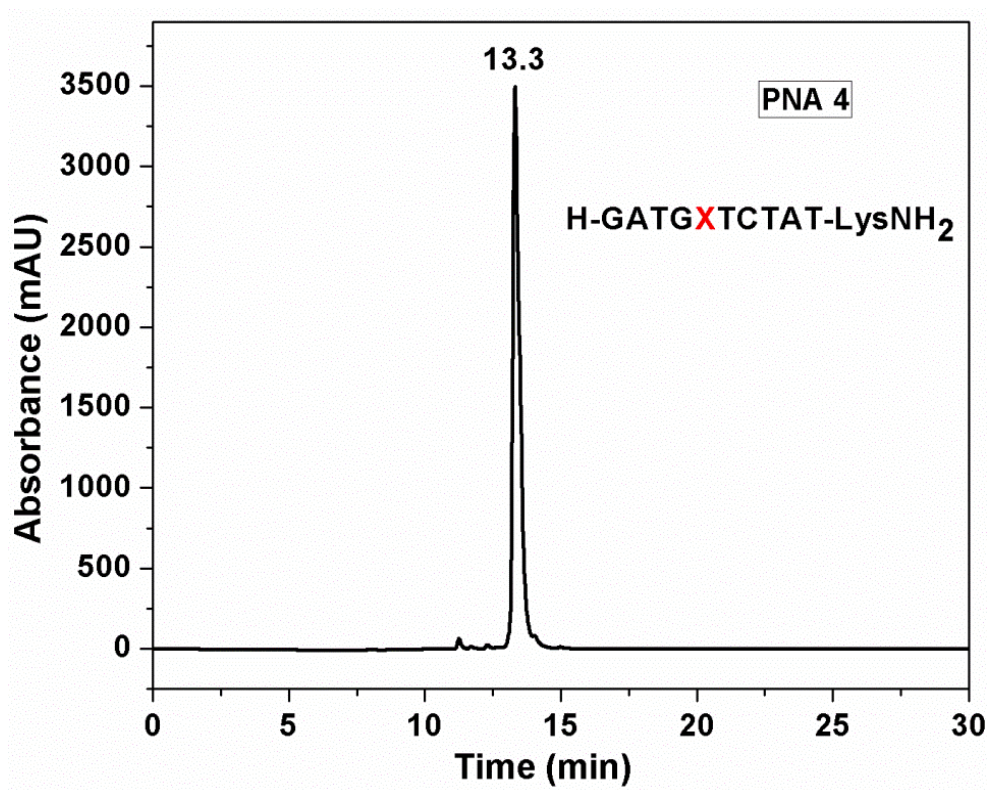
HPLC of PNA-2



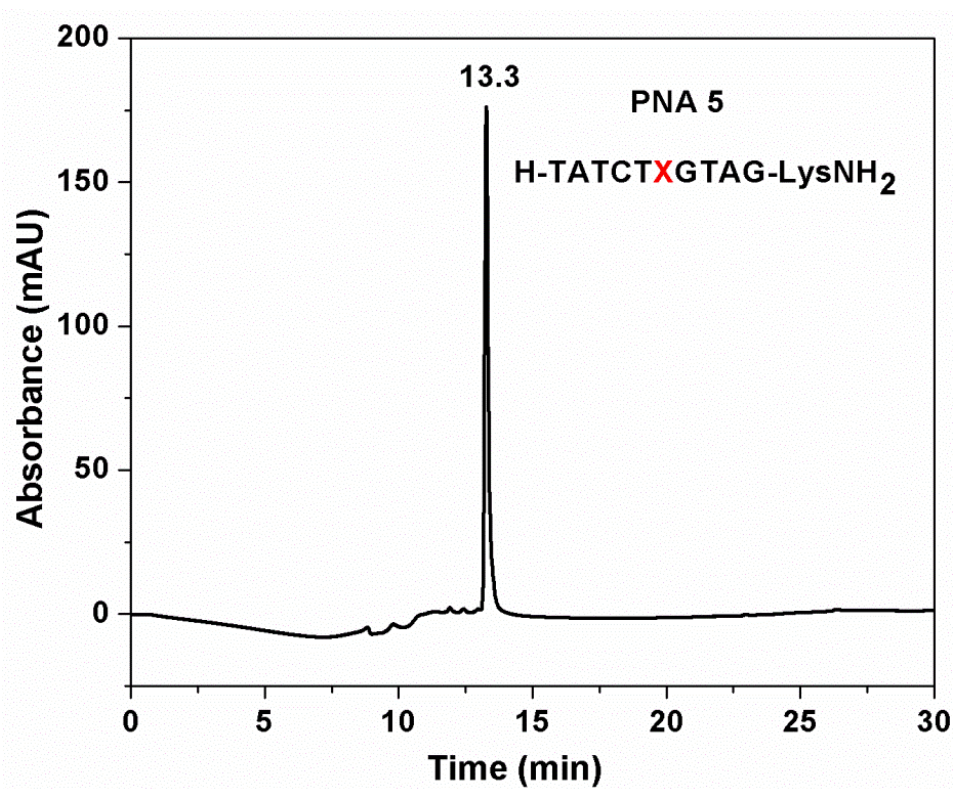
HPLC of PNA-3



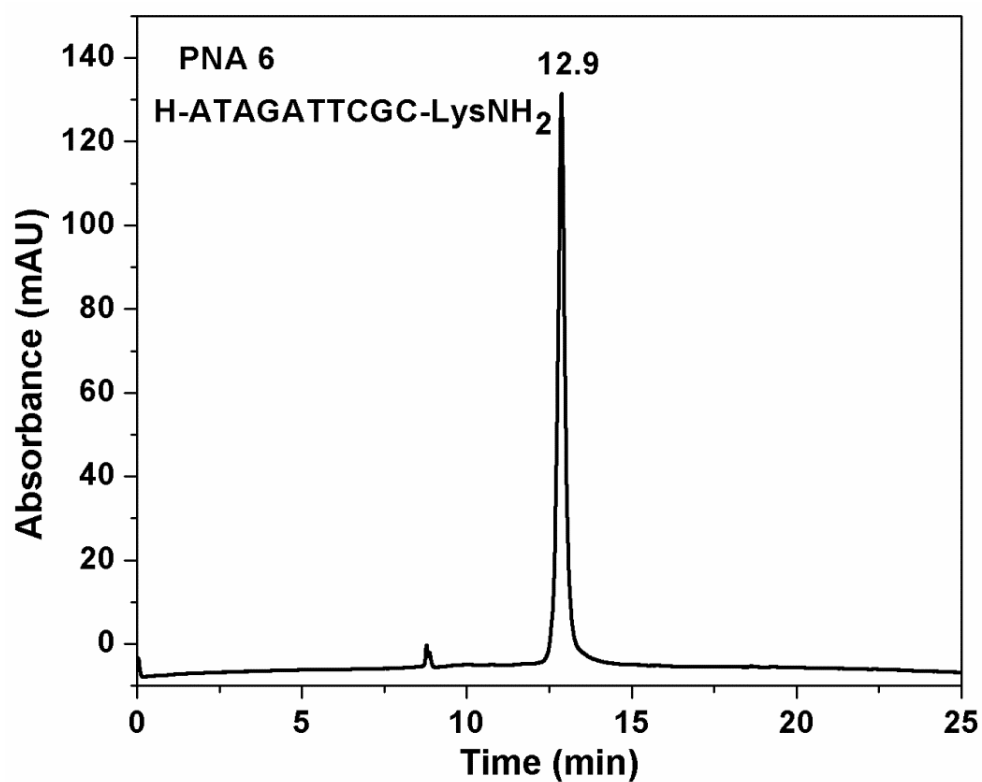
HPLC of PNA-4



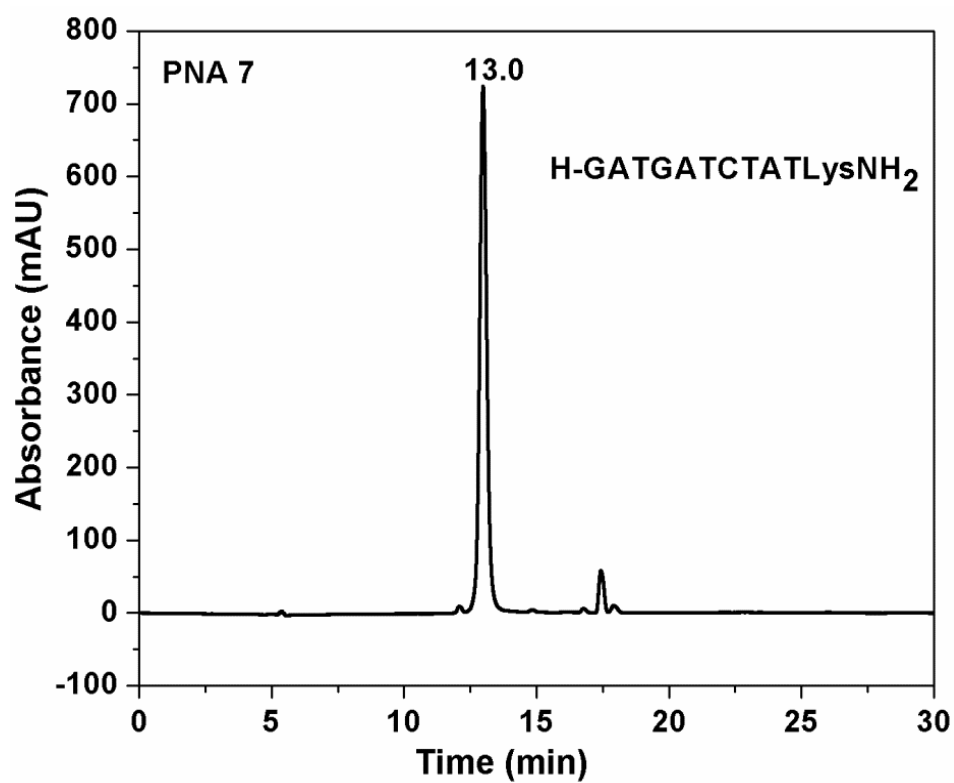
HPLC of PNA-5



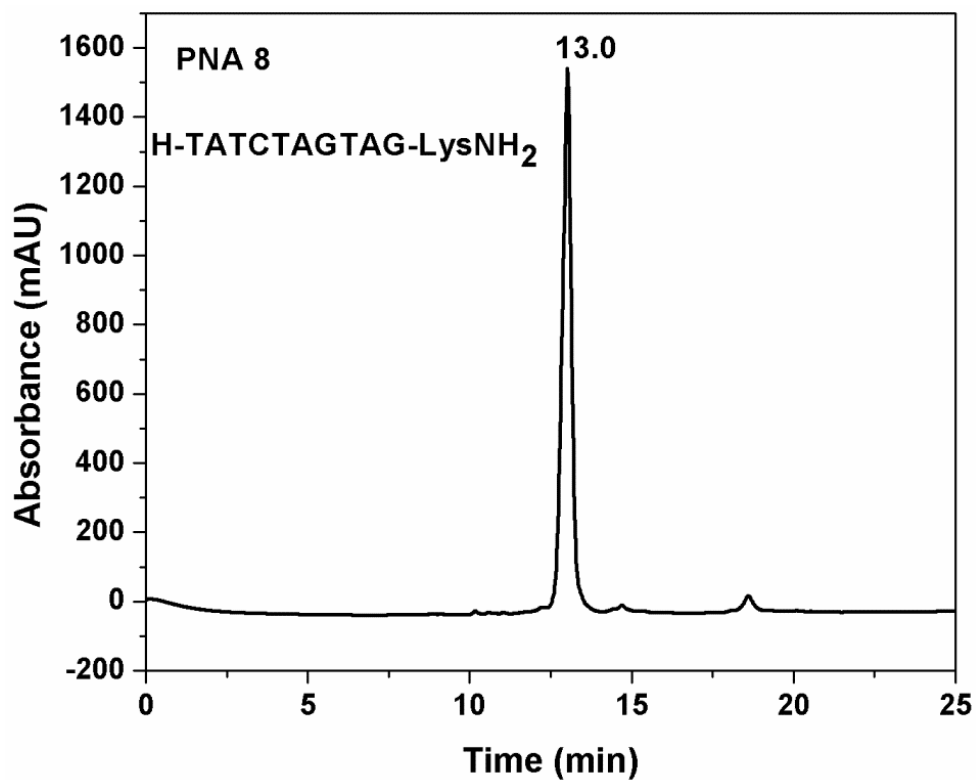
HPLC of PNA-6



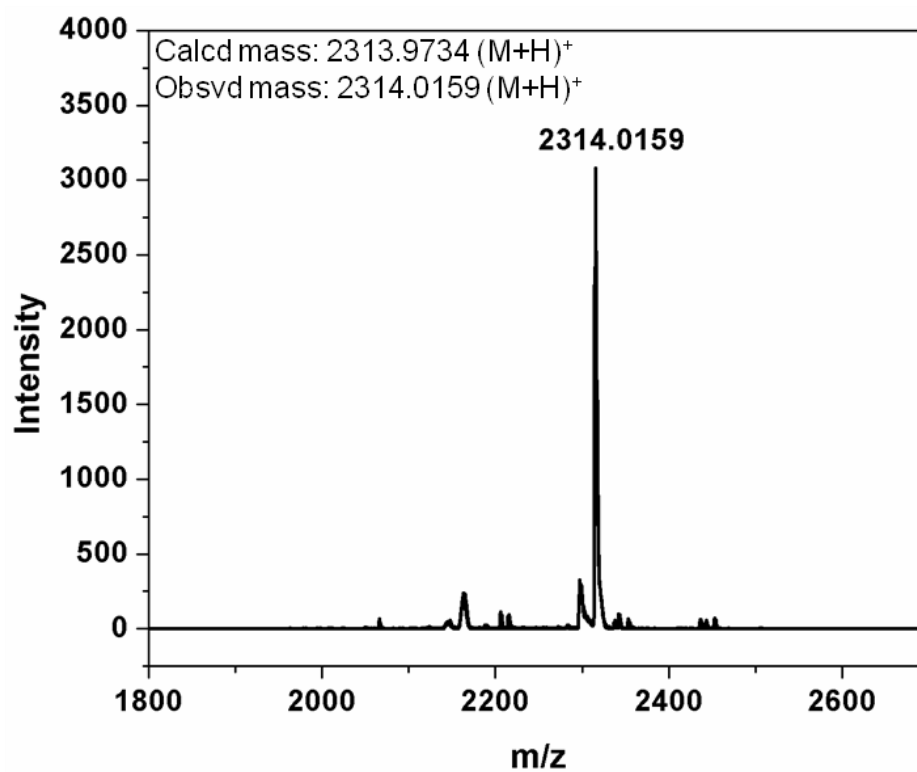
HPLC of PNA-7



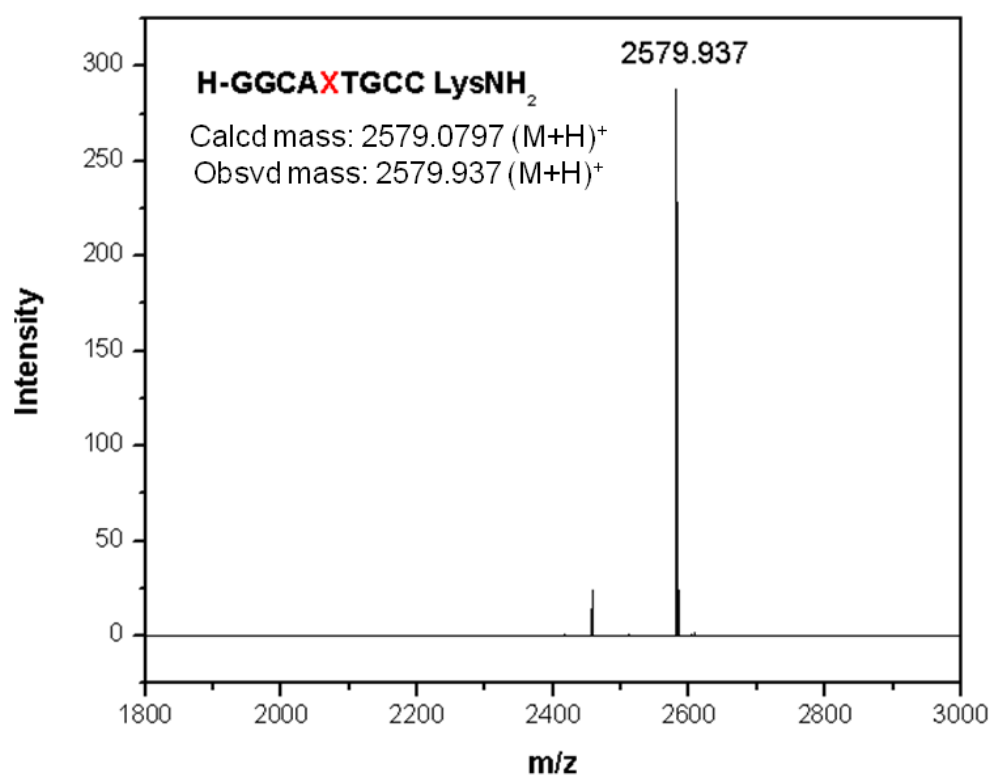
HPLC of PNA-8



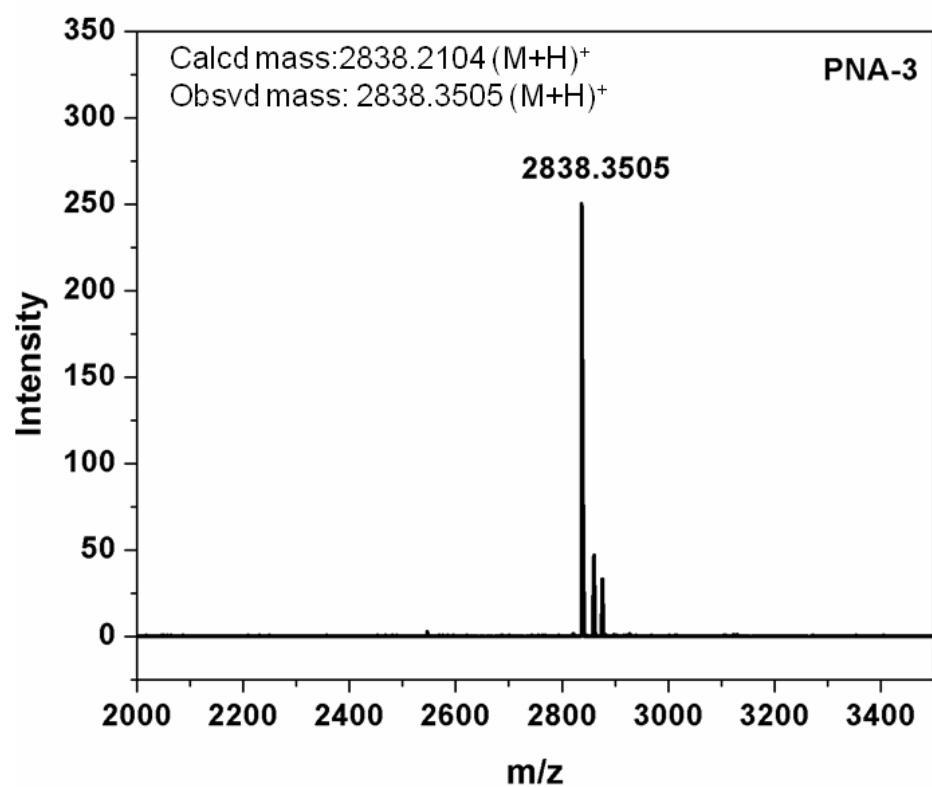
MALDI-TOF of PNA-1



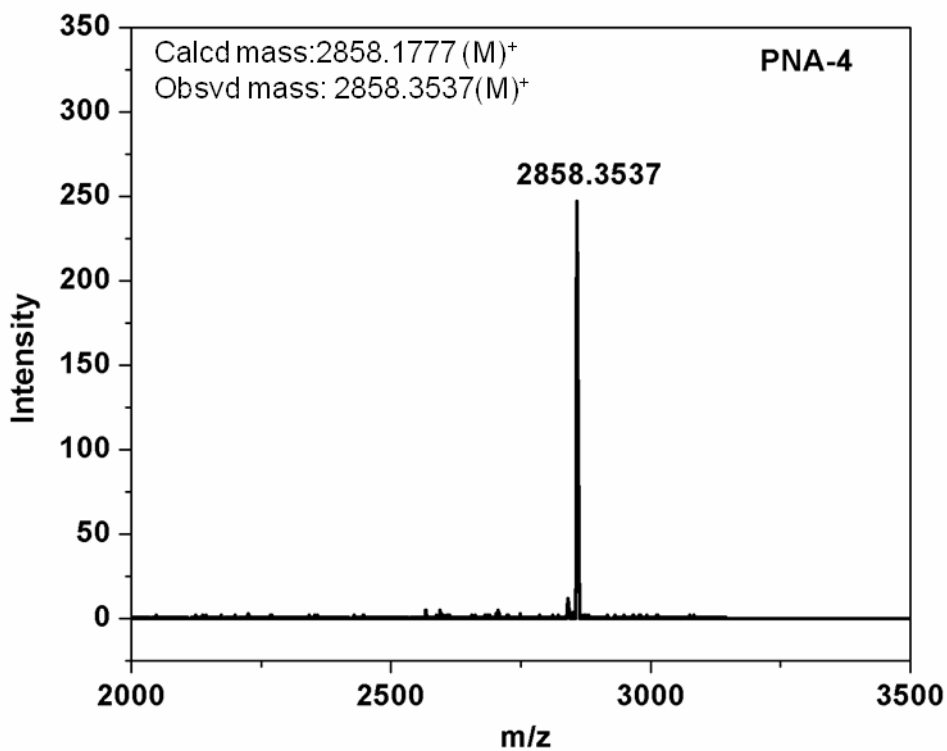
MALDI-TOF of PNA-2



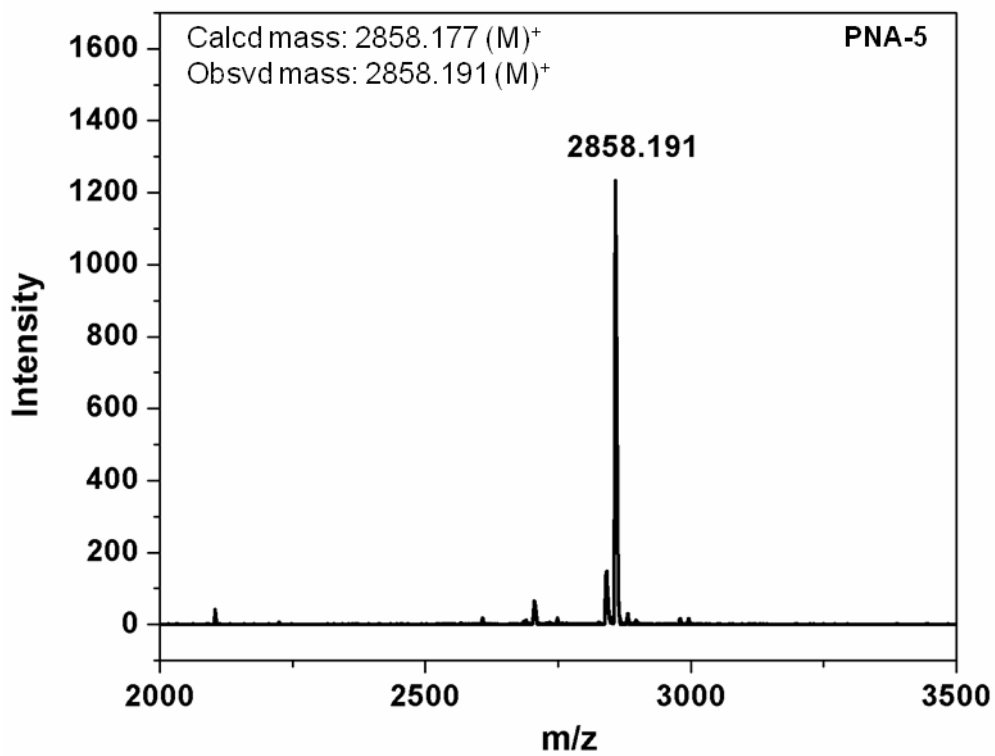
MALDI-TOF of PNA-3



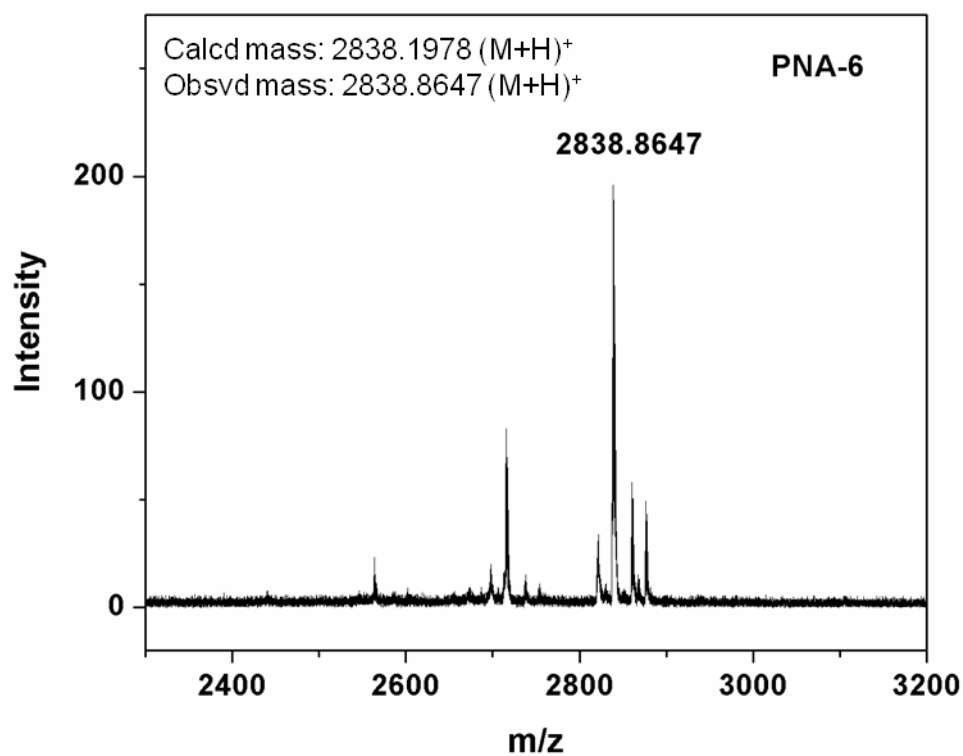
MALDI-TOF of PNA-4



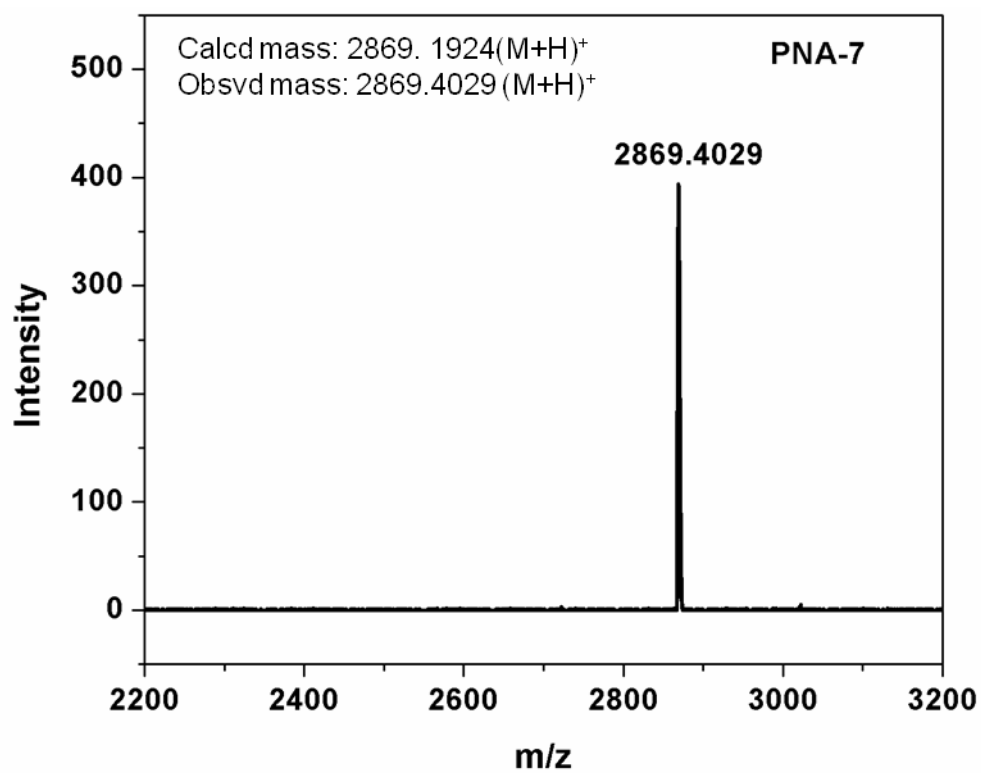
MALDI-TOF of PNA-5



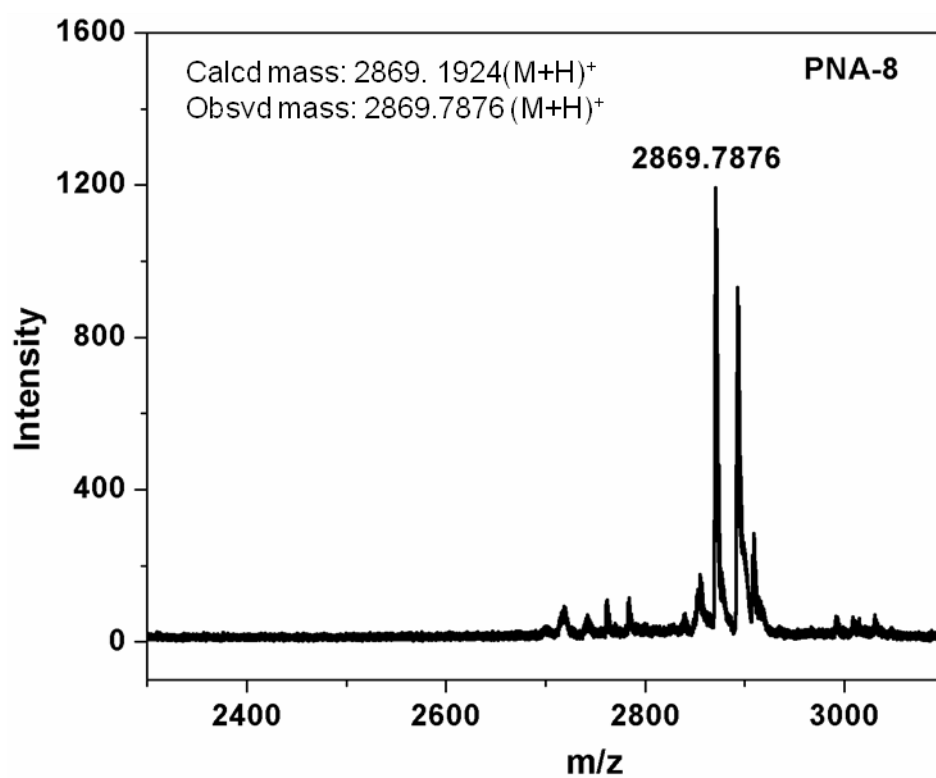
MALDI-TOF of PNA-6



MALDI-TOF of PNA-7

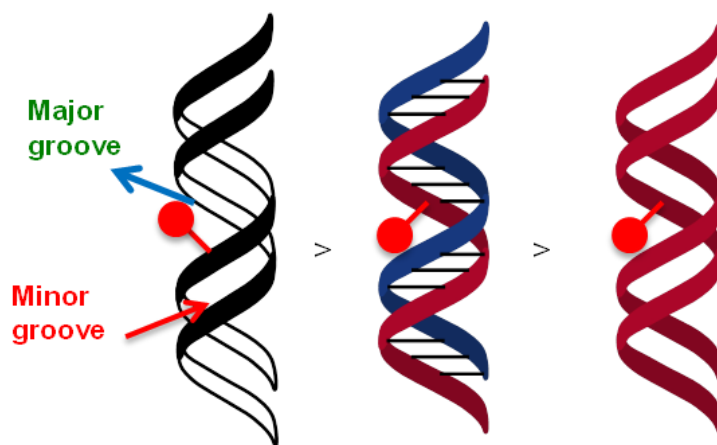


MALDI-TOF of PNA-8



Chapter 2

Polarity Sensing by Fluorescent PNA: Micro-environmental changes in the Major Groove of PNA:DNA/RNA/PNA Hybrids



This chapter describes the synthesis of *aeg*-PNA monomers having hydrophobic, hydrophilic and U-dansyl fluorophore modified bases and their subsequent site specific incorporation into PNA oligomers. The modified PNA oligomers were hybridized with complementary DNA, RNA and PNA to get PNA:DNA/RNA/PNA duplexes for estimation of local dielectric constant by fluorescence spectroscopy.

2.1 Introduction

Nature is versatile as it plays ingenious role in using simpler units in convoluted ways and in various combinations to coordinate complex processes that drives the life. Nucleic acids together with proteins are the most important biopolymers of life. Nucleic acids (DNA and RNA, Figure 1), the essential biopolymers of life are the nature's simple and elegant solution to the problem of storing, retrieving and communicating the genetic information of living organisms, which is the basis of central dogma of molecular biology.¹

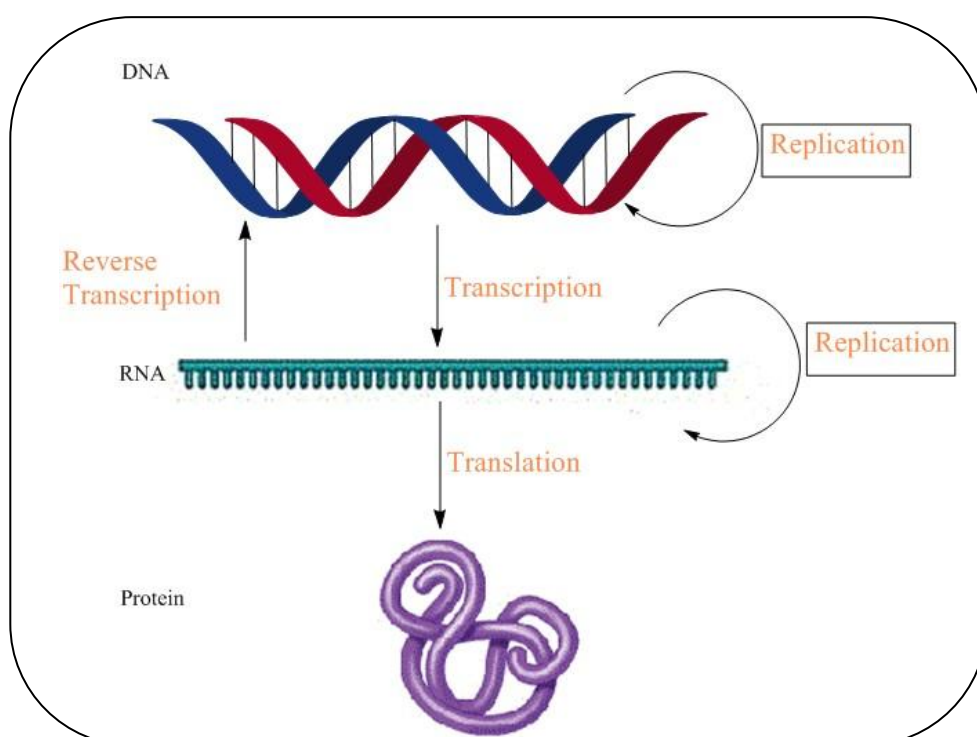


Figure 1. Central dogma of molecular biology.

The discovery of double helical structure of DNA by Watson and Crick in 1953 has led to enormous insights into chemistry and biology of nucleic acids.² One of the most interesting consequences of DNA duplex is the existence of major and minor groove on the opposite faces of the DNA helix (Figure 2). Most specific interactions of DNA with other molecules such as proteins, drugs, water and metal ions takes place in these grooves. Such DNA complexes are induced in the major or minor grooves of DNA via hydrogen bonding, electrostatic and hydrophobic interactions. The two grooves in B-DNA are unequal in size, which is a result of the geometry of the base pairs. The major groove is 22 Å wide and the minor groove is 12 Å wide,³ with the

angle at which two sugars protrude from the base pairs being about 120° . As a result, when base pairs stack on top of each other, the narrow angles between the sugars on one edge of the base pair generates the minor groove and the large angle on other edge generates the major groove.⁴

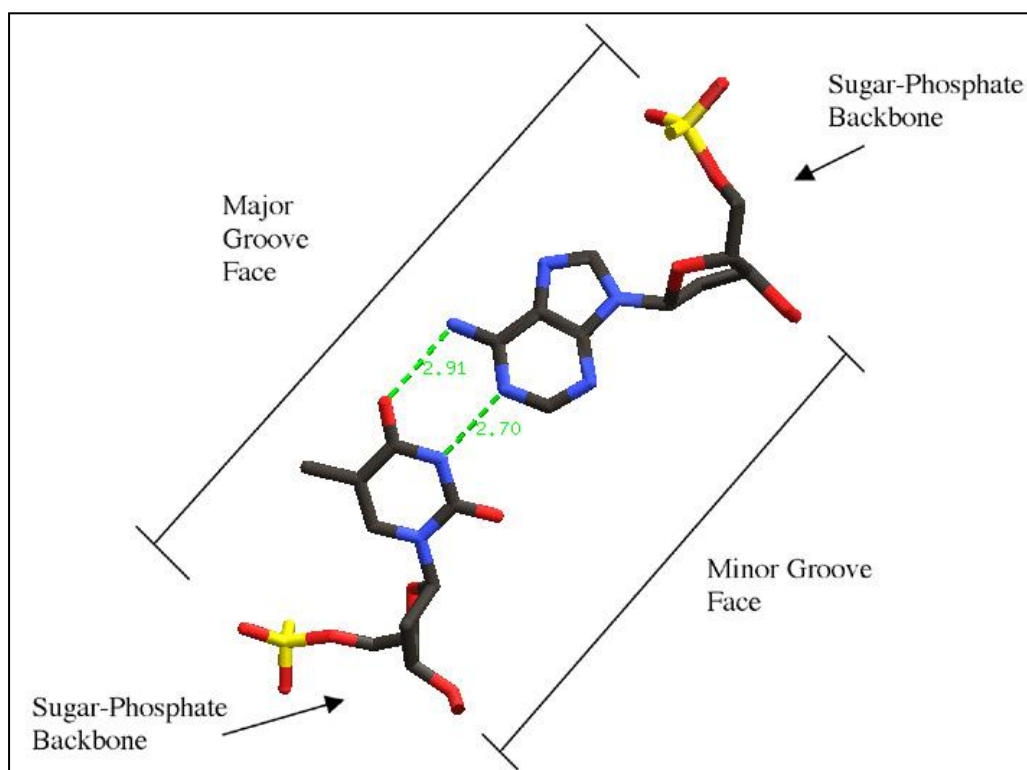


Figure 2. Major and minor groove in DNA.

The major and minor grooves of DNA differ significantly in electrostatic potential, hydrogen bonding characteristics, steric effects and hydration.⁴ The edges of each base pair are exposed in the major and minor grooves, and the characteristic pattern of hydrogen bond donors, acceptors and van der Waals surfaces in the grooves is defined by the type of the base pairs. This pattern (Figure 3) may be termed as code, in which A represents a hydrogen bond acceptor, D a hydrogen bond donor, M a methyl group, and H, a nonpolar hydrogen. The pattern “A D A M” in the major groove signifies an A:T base pair, and “A A D H” stands for a G:C base pair. Likewise, “M A D A” stands for a T:A base pair and “H D A A” is characteristic of a C:G base pair.³

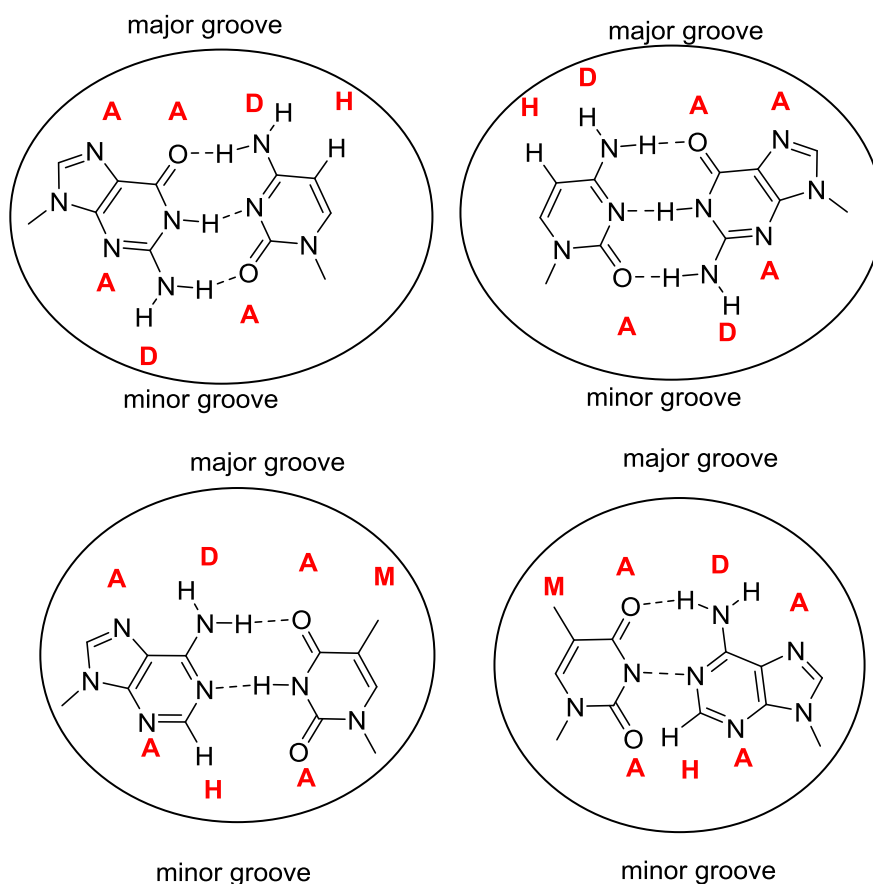


Figure 3. Structural insights of major and minor groove⁴

The salient and significant outcome of these patterns of hydrogen bond donors and acceptors in the base pairs is that the DNA binding molecules can discriminate the A:T base pair from G:C base pair efficiently from the major groove side, while it is not so efficient in the minor groove. Two further features of molecular discrimination are notable. In A:T/T:A base pairs, C5 methyl group of thymine (T) offers substantial hydrophobic recognition in the major groove which is absent in G:C/C:G base pairs. However, in the latter, the N2 amino group of guanine (G) presents a steric block to hydrogen-bond formation at N3 of guanine (G) and C2 carbonyl of cytosine (C) in the minor groove. It is thus possible to distinguish A:T from T:A and G:C from C:G in the major groove since the ordered array of hydrogen bonding sites and hydrophobic center differs among the four pairs.⁵ These patterns are important as they allow proteins to unambiguously recognize DNA sequences. In fact the capability of amino acid side chains of proteins to protrude into the major groove to recognize and bind to specific DNA sequences gives the principal decoding mechanism.

The minor groove offers less chemical information compared to the major groove and the available information is less useful for distinguishing between base pairs. Because of its small size, minor groove is less able to accommodate amino acid side chains. Also, A:T and T:A base pairs and G:C and C:G pairs look similar to one another in the minor groove (Figure 4). The negative electrostatic potential due to phosphate charges is greater in A:T minor groove than in G:C rich regions and this provides an additional important source for A:T specific minor groove recognition.

2.2 Molecular recognition of nucleic acid

Nucleic acids interact reversibly with different types of chemical species that include water, metal ions and their complexes, small organic molecules and proteins. There are three primary ways of interactions:

i) **Electrostatic interaction:** The negative charges on DNA sugar phosphate backbone on the exterior of the helix interact with cationic substrates and are non-specific to DNA sequence (Figure 4A).

ii) **Groove binding:** This arises from the interaction of bound small molecules with the edges of the base pairs in either the major or the minor groove of nucleic acids and mediated by non-covalent forces such as hydrogen bonding and hydrophobic forces (Figure 4B).

iii) **Intercalation:** It originates from the insertion of planar aromatic systems between the base pair stacks, through π - π^* interaction (Figure 4C).

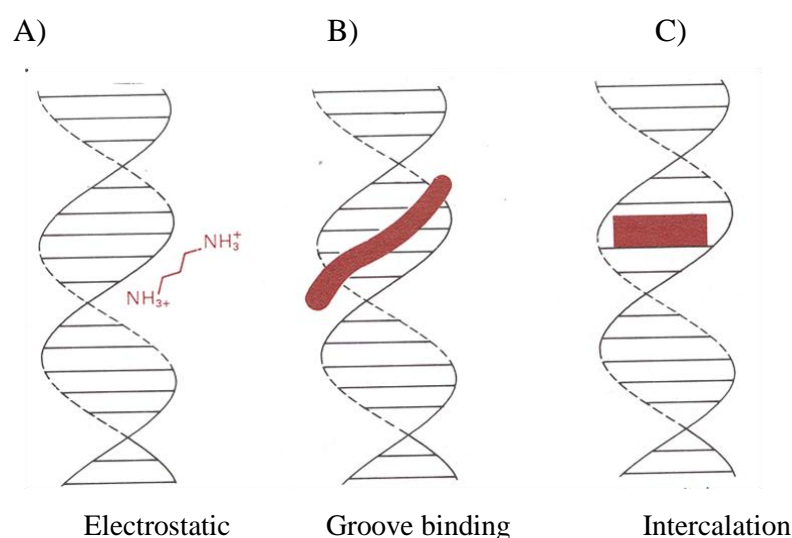


Figure 4. Modes of molecular recognition of nucleic acids.

All the three modes of binding involve slight change in DNA conformations while intercalation may induce major distortion in sugar phosphate geometry and unwinding of helix.

2.3 DNA-Drug interactions in minor groove

Groove binders are a class of molecules that bind to double stranded DNA and play significant role as drugs. As minor groove is narrower than major groove small molecules bind into the minor groove of DNA duplexes. The small molecule-minor groove binding interactions are dominated by the electrostatic, van der Waals, hydrophobic and hydrogen-bonding interactions. The antibiotic drugs netropsin and distamycin (Figure 5) were the first drugs discovered that bind in minor groove of AT rich DNA sequences.

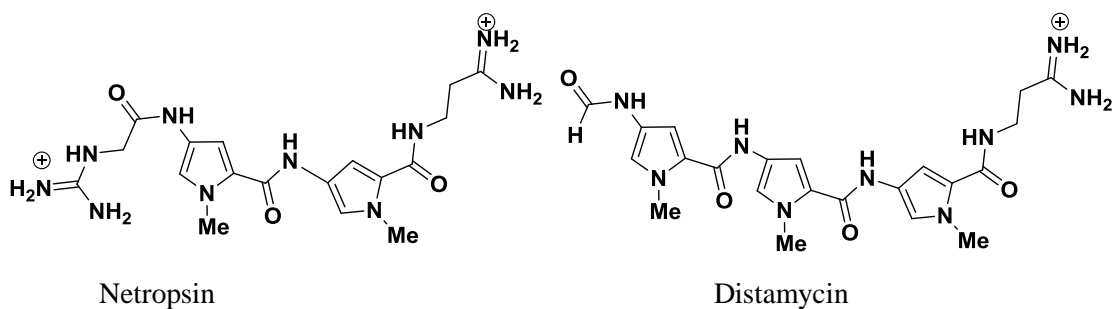


Figure 5. Structures of netropsin and distamycin.

The crystal structure of DNA-netropsin complex led to the structural knowledge of the minor groove binding, providing clear indications of the molecular basis for A:T base pair sequence specific recognition.⁶ The sequence specificity is characterized by key hydrogen-bonds between base pairs and small molecule and also the crescent shape complementarity of small molecule to minor groove. The antitumor antibiotic netropsin binds in minor groove of dodecamer sequence d(CGCGAATTCGCG) by displacing water molecules of the spine of hydration, with each of its three amide NHs forming three-centered hydrogen bonds between adjacent adenine N3 or thymine O2 atoms. The narrow minor groove in AT rich region forces the drug molecule to fit squarely in the center of the groove, with each of its pyrrole rings approximately parallel to the walls of groove in its own region (Figure 6). The two cationic ends of netropsin molecule are centered at bottom of the minor groove, each associated with an N3 of outer adenine

and central base pairs. Distamycin, like netropsin, also specifically binds in AT rich region in minor groove.

The netropsin binding to DNA widens the minor groove slightly and bends the axis at backwards at the side of attachment. Both the deformations illustrate the tightness of fit of the drug molecule into minor groove. Several factors characterize the sequence specificity of minor groove binding drugs. The electrostatic potential in AT rich region is more than GC rich region and the dimensions of AT rich region are narrower and deeper.⁷ The topology at AT rich sites allows easier entrance and greater van der Waals contact by small molecules. In addition to this, the amino group of G in GC protrudes into the groove leading to prohibition of van der Waals contacts as compare to AT rich regions.⁸

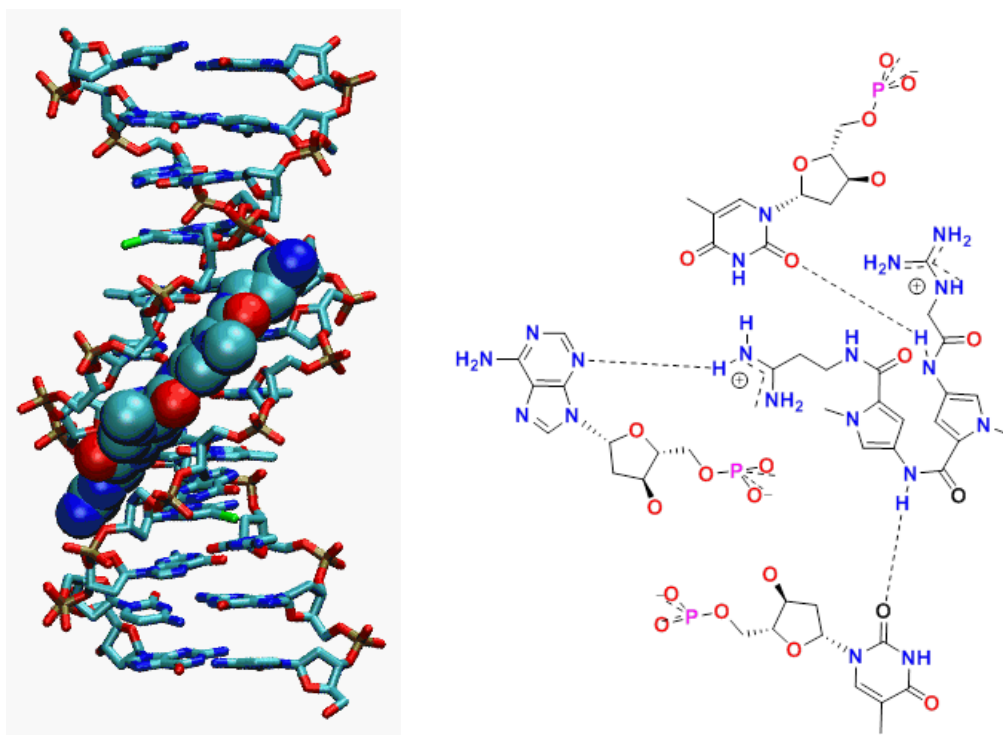


Figure 6. Netropsin binding to AT rich region in DNA.

Mechanism of netropsin binding.

Image obtained from following website

https://commons.wikimedia.org/wiki/File%3ANetropsin_DNA_bound.gif

The understanding of molecular basis of netropsin-DNA interaction in the minor groove of DNA in terms of hydrogen bonding complementarity of H-bond donor-acceptor sites of drug-A:T interaction has led to engineering of lexitropsins, to recognize G:C base pairs as well.⁹ In lexitropsins one or more pyrrole rings are

replaced by imidazole ring (Figure 7), to accommodate acceptor site and prevent steric clash of functional groups.

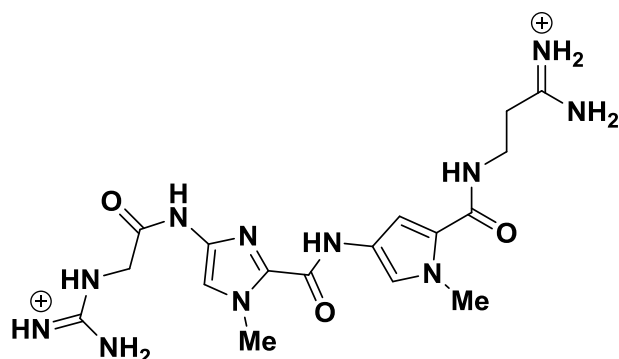


Figure 7. Structure of lexitropsins.

The synthetic bis-(benzimidazole) analog Hoechst 33258 (Figure 8), an antitumor drug is widely used in chromosome staining. It recognizes 3–4 consecutive A/T base-pairs by hydrogen bonding to base edges in 1:1 complex in the minor groove of duplex DNA.¹⁰

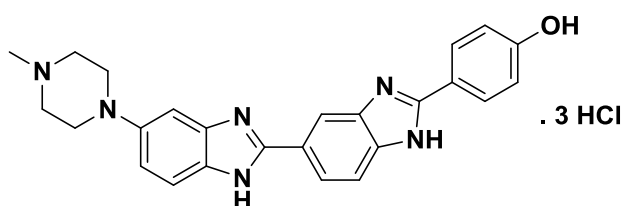


Figure 8. Structure of Hoechst 33258.

There are many small molecules designed to bind into the minor groove of DNA duplexes. Such molecular engineering of DNA binding agents has primary consequences on rational drug design and is emerged as new area in drug development.

2.4 Major groove binders

Major groove is wider as compared to minor groove and therefore allows the binding of large molecules such as proteins, nucleic acids etc. Major groove in DNA duplexes is recognized by proteins through surface complementarity, forming a series of favorable hydrogen bonding, electrostatic and van der Waals interaction between the protein and the base pairs. Nature utilizes protein motifs such as helix-turn-helix, leucine zipper and zinc finger for the major groove recognition of DNA.¹¹

Helix-turn-helix (HTH) recognized as first DNA binding protein motif. Originally found in bacteria, has subsequently been found in hundreds of DNA binding proteins in eukaryotes and prokaryotes. The HTH motif comprises of ~20 amino acid residues characterized by two alpha helices. The residues 1-7 form the first α helix and residues 12-20 forms the second α helix. The two α helices are inclined at 120° to each other, primarily through interaction between two helices. The second helix recognizes the major groove of DNA duplex *via* C-terminal (Figure 9). The hydrophobic residues present at positions 4, 8, 10, 16 and 18 of the second helix helping to form overall hydrophobic core of protein.¹² The widespread existence of HTH motif led to the number of studies to develop methods that can reliably locate the motif within genomic sequences using sequence data.

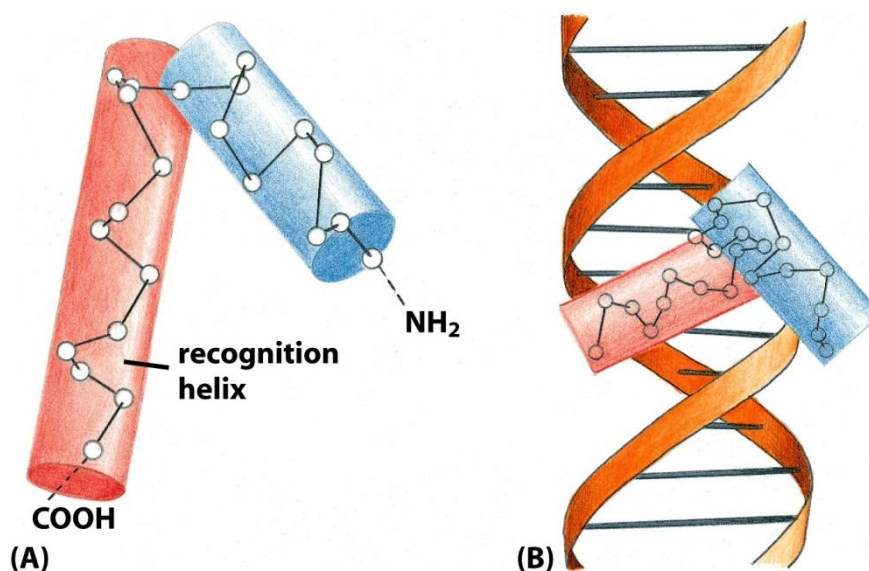


Figure 9. A) Helix-turn –helix and B) Helix-turn-helix binding to the major groove of DNA duplex.

Leucine zipper is observed in many DNA binding proteins consisting periodic repetition of leucine residue at every seventh position. It is formed by the combination of two α helices from separate proteins in coiled-coil manner. The interaction between hydrophobic side chains of amino acid holds the helices together. The two α helices forms the Y shaped structure, which allows their side chains to contact the major groove (Figure 10).¹³

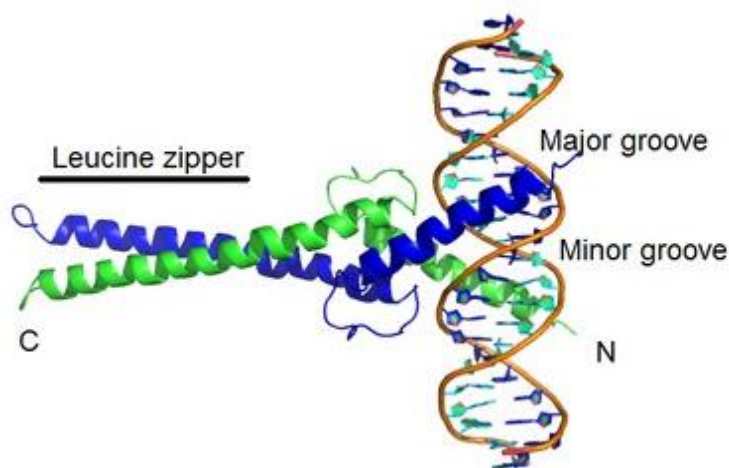


Figure 10. Leucine zipper binding into the major groove of DNA duplex.

Figure obtained from Wikipedia page.

The zinc finger protein motif is involved in transcriptional processes, binding to DNA in sequence specific manner. Zinc finger proteins bind into the major groove of DNA, via a short α -helix spanning 3-4 bases of DNA. In the case of protein such as zif268, successive fingers track the major groove of DNA by center to center between each finger's subsites. Other families of Zn^{2+} co-coordinating proteins binds DNA major groove as dimers. The GAL-4 type protein which contains two structural Zn^{2+} ions per DNA binding domain inserts a helix into the major groove of DNA (Figure 11). There are several families of proteins which recognize DNA major groove through secondary structure.¹⁴

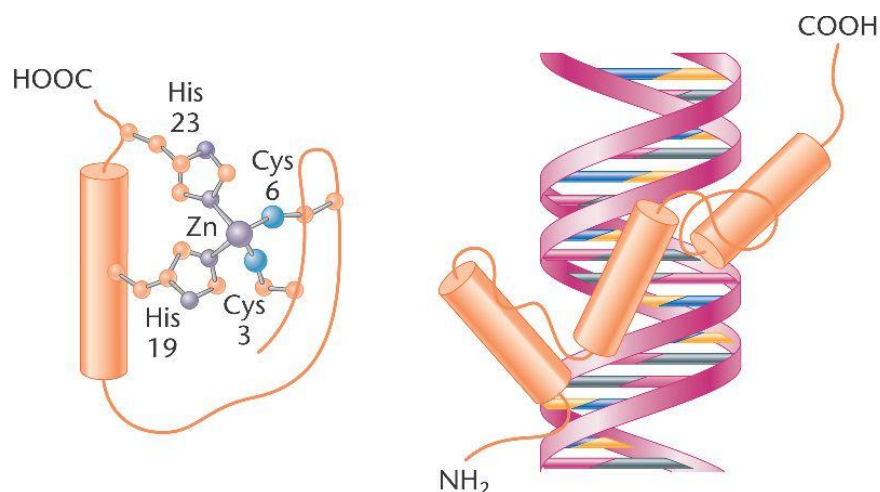


Figure 11. Zinc finger domain binding to DNA. Image obtained from following website

http://bio3400.nicerweb.com/Locked/media/ch17/activator_zinc-finger.html

The DNA binding protein λ repressor forms the helix-turn-helix motif and recognizes the major groove of DNA through N-terminal arm that contacts base pairs. The crystal structure of bacteriophage λ repressor-operator complex led to the finding that hydroxyl group of serine-45 interacts directly with O6 and N7 of a guanine. The carbonyl oxygen atom of the backbone of serine interacts via a water molecule with the N4 atom of complementary cytosine base and O4 of adjacent thymine through the same water molecule.¹⁵

Peptide nucleic acids (PNA), the artificial analog of the DNA also recognizes the major groove of DNA. Homopyrimidine PNA strand invades one of the strand of DNA and forms the PNA₂:DNA triplex.¹⁶ Neomycin, its conjugate with Hoechst 33258 and benzo[f]quino[3,4-b]quinoxaline (BQQ) bind into the major groove of poly(dA):2poly(dT) triplex, small oligomeric triplexes, RNA triplex and hybrid triplexes by stabilizing these structures.¹⁷

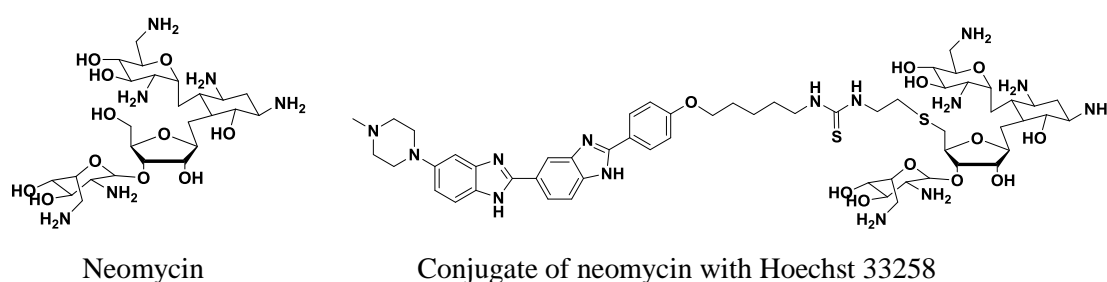


Figure 12. Structure of neomycin and neomycin-Hoechst-33258 conjugate.¹⁷

2.5 Intercalation

DNA intercalation is an important phenomenon, especially with respect to the function of anticancer drugs. Intercalators are small organic molecules or metal complexes that bind through π -stack between two base pair. Intercalation resulting from such insertion of a planar aromatic substituent between DNA base pairs is accompanied by unwinding and lengthening of the DNA double helix.¹⁸ The intercalation process starts with the transfer of interacting molecule from aqueous environment to hydrophobic environment, present in between two adjacent base pairs (Figure 13).

DNA undergoes conformational change to accommodate the ligand, by increasing the vertical separation between two base pairs to create the cavity for

incoming chromophore. This leads to theoretical lengthening of DNA by $\sim 3.4 \text{ \AA/site}$. Once, the drug sandwiches between DNA base pairs, the stability of complex is optimized by compensation with van der Waals and π - π interaction, reduction of coulombic repulsion between the phosphate groups, associated with the increased distance between base pairs, ionic interactions between positively charged groups of ligand and phosphate groups, and hydrogen bonding.

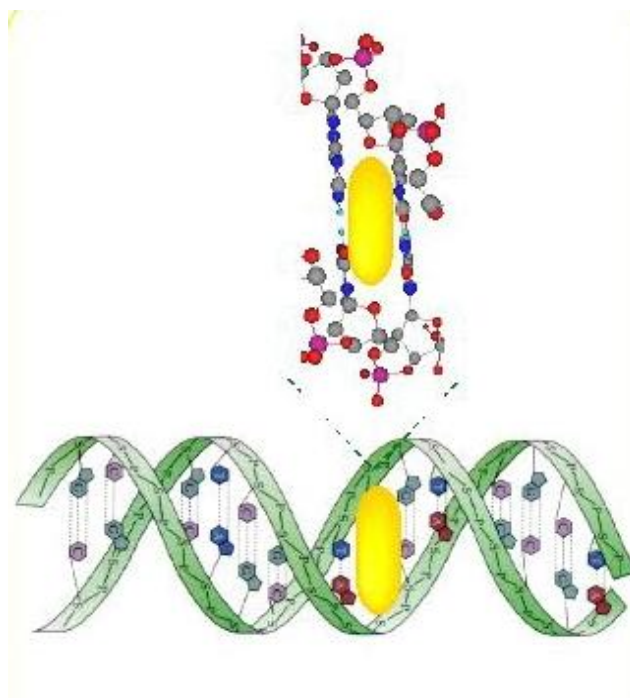


Figure 13. Intercalation in DNA. Image obtained from following website www.photobiology.com/photoiupac2000/pierard/Interactionmain.html

In practice, the net lengthening arising from helical unwinding is much less. This changes the optical properties of both DNA and the intercalators as it interferes in the base stacking.¹⁹ The changes in DNA structure induced by intercalation have been well established by several crystallographic studies of DNA-drug complexes. These involve the distortion of phosphate backbone and rise in base pair separation.²⁰ Solution studies have indicated that at saturating concentrations of intercalating species, binding occurs at most between alternative base pairs on DNA. This observation termed as ‘neighbor exclusion principle’ means that upon binding of an intercalator at one site, it is almost impossible to bind another at adjacent site.²¹ Generally intercalation is less sequence selective than minor groove binding but slightly more specific to C:G base

pairs. Groove binding molecules have greater binding selectivity than intercalator binding as they contact more base pairs in the groove.

Intercalators are of two types namely, monofunctional and bifunctional intercalator. Monocation form of ellipticine intercalates into DNA, which leads to inhibition of RNA polymerase, DNA polymerase, RNA methylase, and topoisomerase II. There are many other anticancer, antitumor drugs such as chartreusin, elsamicin A and their analogs, which are intercalators (Figure 14).

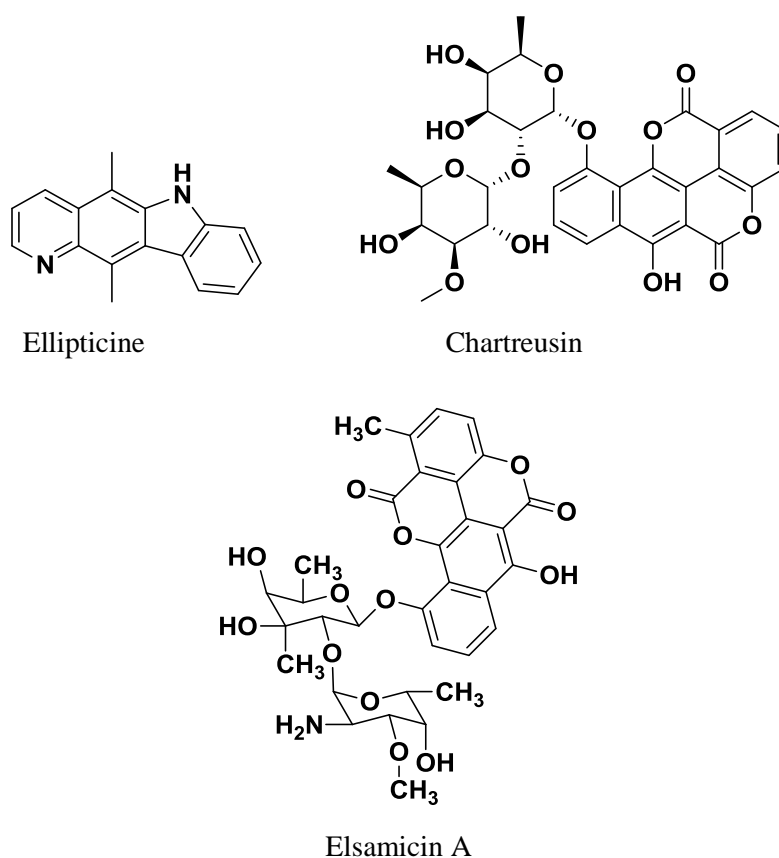


Figure 14. Structure of ellipticine, Chartreusin, Elsamicin A.

The binding selectivity of intercalators has been elegantly enhanced by linking them covalently to oligonucleotides at specific sequences.^{22,23} The hybrid molecules combining intercalation with groove binding have been reported to obtain selective DNA recognition.^{24,25} This has been developed into versatile method to achieve targeted DNA cleavage via oligonucleotide directed triple helix formation.²⁶ The cleavage is induced by attaching EDTA.Fe complex to a homopyrimidine strand

that binds to corresponding homopyrimidine-homopurine tracts within double helical DNA via triple helix formation (Figure 15).²⁷



Figure 15. Triplex forming oligonucleotide conjugate.

Specificity in binding of nucleic acid results from molecular contacts between the bound ligand and the edges of base pairs on the floor of the groove. Many proteins exhibit binding specificity with nucleic acid primarily via major groove interactions while smaller molecules in general bind in the minor groove. For sequence-specific recognition of DNA by ligands, the major groove offers greater discrimination among A:T and C:G base pairs through different arrangements of available hydrogen-bond donor and acceptor sites. While most of the non-intercalating DNA binding drugs interact through the DNA minor groove, the larger proteins engage DNA mostly from the major groove side. This binding may lead to change in the polarity of grooves of DNA duplexes. The major and minor grooves differ in polarity which can be determined by experimental methods (fluorescence spectroscopy)^{28,29} and then proved by theoretical studies.³⁰

2. 6 Fluorescence spectroscopy

Local variations in the structure and dynamics of biomolecules play important roles in mediating the interactions between biomolecules. In particular, monitoring the microenvironmental change in conformation, polarity, viscosity, and charge around the DNA surface is essential in order to understand the mechanisms driving the biological events in cells. In case of DNA, the polarity of major and minor groove of nucleic acids

plays an important role in the binding of proteins and small molecules that considerably influence the gene regulation.

Fluorescence spectroscopy has been widely used for the study of structure and dynamics of micro-heterogeneous systems-colloid particles, micelles, liquid crystals, artificial and natural membranes, polymers, and biological macromolecules. While polarity of various solvents is a bulk property, in biopolymers, folding generates several local structures or pockets which may differ in local polarity.

2.7 Solvent polarity and local environment effects

Solvent polarity and the local environment have intense effect on fluorescence properties of fluorophore. Stokes shift is the inverse difference in wavelength between positions of the band maxima of the absorption and emission spectra of same transition. The stokes shift ($\Delta\nu$) is given by the equation,

$$\Delta\nu = \frac{1}{\lambda_{ex}} - \frac{1}{\lambda_{em}}$$

The fluorescence emission spectra of many fluorophore are sensitive to solvent polarity and local environment.³¹ This polarity dependence occurs from, i) difference in the dipole moment of fluorophore in the ground and excited state and ii) specific interactions such as hydrogen-bonding, charge-transfer interactions etc. between the fluorophore and the solvent molecules.

The local polarity changes around the excited fluorophore due to reorientation of solvent molecules are reflected by the orientation polarity of the solvent molecules. Orientation polarity contributes more to the emission spectral shifts in the absence of solvent-fluorophore specific interactions. The general solvent effect caused by the physico-chemical interactions between fluorophore and the solvent molecules is described by Lippert equation.^{32,33} This equation describes the Stokes shift ($\Delta\nu$) in terms of the changes in dipole moment.

$$\Delta\nu = \frac{2\Delta\mu^2}{hca^3} \times f$$

where $\Delta\mu$ is the difference in dipole moment between the excited and the ground states of the fluorophore, h is Planck's constant, c is the speed of light and a is

the radius of the cavity in which the fluorophore resides. Since for a given fluorophore, a and $\Delta\mu$ remains constant, the above equation implies that the Stokes shift is directly proportional to solvent polarity (f) changes. The general solvent effects are governed by the orientation polarity (f), derived from the refractive index (n) and dielectric constant (ϵ) of the medium.^{32,33}

$$f = \frac{\epsilon - 1}{2\epsilon + 1} - \frac{n^2 - 1}{2n^2 + 1}$$

Stokes shift as a function of orientation polarity must show a linear behavior if the general solvent effects predominate over special solvent effects. The orientation polarity obtained from the measured Stokes shifts are interpolated to give dielectric constant of the medium.

2.8 Solvent polarity scale

Solvent polarity is defined as overall solvation capacity of solvents, which depends on specific and nonspecific intermolecular interactions between solute ions and solvent molecules. However, it excludes that interaction which leads to definite chemical alteration of solvent molecules. There are several scales available for measuring solvent polarity scale. The most comprehensive scales among solvent polarity scales derived from various physicochemical parameters are based on solvatochromic method.³⁴

The $E_T(30)$ scale of Dimroth and Reichardt³⁵ is most popularly used for solvent polarity scale. $E_T(30)$ values are based on the pyridinium *N*-phenolate betaine dye and represents the molar electronic transition energies (E_T) measured in kcal/mol at room temperature and normal pressure (1 bar).

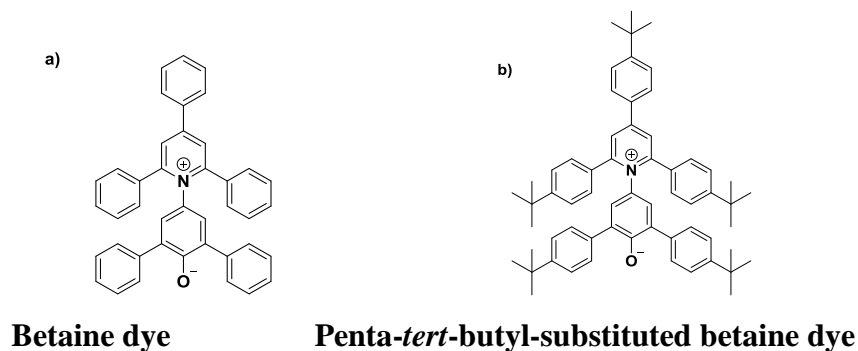


Figure 16. Structure of betaine dye and Penta-*tert*-butyl-substituted betaine dye.

In addition to $E_T(30)$ values, normalized E_T^N values have been introduced. They are defined according to following equation as dimensionless figures, using water and tetramethylsilane (TMS) as extreme polar and nonpolar solvents respectively. Hence, the scale ranges from 0.000 for TMS, the least polar solvent to 1.000 for water, the most polar solvent.

$$E_T^N = \frac{E_T(\text{solvent}) - E_T(\text{TMS})}{E_T(\text{water}) - E_T(\text{TMS})} = \frac{E_T(\text{solvent}) - 30.7}{32.4}$$

For nonpolar solvents, penta-*tert*-butyl--substituted betaine dye with appropriate solubility is appropriate for the measurement of polarity. The excellent linear correlation between the E_T values of both the betaine dyes for solvents, in which both dyes are soluble, allows the calculation of $E_T(30)$ values according to following equation,

$$E_T(30) \text{ (kcal mol}^{-1}\text{)} = \{[28591/\lambda'_{\text{max}} \text{ (nm)}] - 1.808\}/0.9424$$

In above equation λ'_{max} corresponds to the wavelength of the absorption maximum of substituted dye. Lower $E_T(30)$ value corresponds to nonpolar solvent and higher $E_T(30)$ value corresponds to polar solvent and $E_T(30)$ values for various solvents range from 27 to 64.7 kcal mol⁻¹.³⁶

2. 9 Characterization of polarity in grooves

The major and minor grooves in nucleic acids differ in polarity. The minor groove of DNA:DNA duplexes is hydrophobic in nature whereas major groove is hydrophilic in character. Minor groove interacts with small molecule drugs and major groove interacts with large molecules such as proteins and nucleic acids (Figure 17).

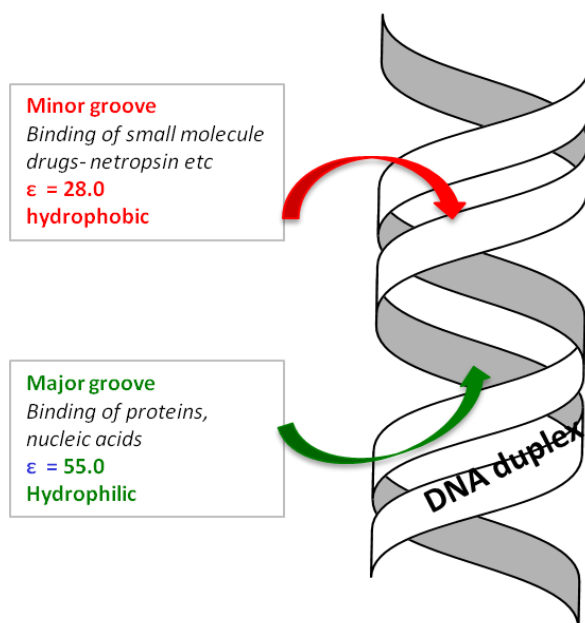


Figure 17. Major and minor groove in DNA duplex.

Breslauer et al.²⁹ were the first to investigate the polarity of grooves by experimental method. Hoechst 33258, a highly fluorescent environment-sensitive drug selectively binds to AT rich regions in minor groove and induces sequence specific structural changes in the resulting DNA complex. Comparison of the fluorescence properties of Hoechst 33258 bound DNA duplex with that of free Hoechst 33258 lead to finding that minor groove is hydrophobic and nonpolar with the dielectric constant $\approx 20D$.

Ganesh et al.²⁸ characterized the polarity of major groove by covalently incorporating environment sensitive dansyl fluorophore into DNA oligomers having different environment. Dansyl conjugated 5-aminouridine was incorporated into Dickerson's dodecamer DNA sequence having hydrophobic and hydrophobic environment surrounding the dansyl fluorophore. The 5-NH₂ group in 5-aminouridine resides in major groove and hence the linked dansyl would report the microenvironment of major groove. Any changes in the local polarity of major groove would affect the Stokes shift. The orientation polarity was computed as a function of Stokes shift and exhibited a linear relationship that was interpolated to give dielectric constant. It was found that the ϵ of major groove was $\approx 55D$, which is more hydrophilic and polar as compared to the minor groove. This result was supported from theoretical calculations by Pack et al. by using numerical Poisson-Boltzmann method.³⁰ By

embedding the polarity sensitive U^{DNS} in different sequence context, Ganesh et al. shown that polarity of the major groove is also sensitive to the DNA sequence.³⁷ This resulted in the finding that polarity of the major groove of DNA changes with local environment surrounding fluorophore.

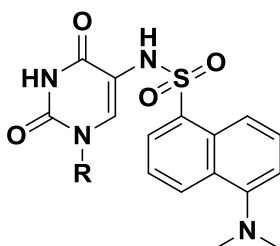


Figure 18. Structure of 5-amidodansyluridine.

Majima et al.^{38,39} introduced the environment sensitive fluorophore dan (6-dimethylamino-2-acyl-naphthalene)-modified bases to B-DNA and Z-DNA and determined the polarity of grooves by fluorescence spectroscopy. After comparing the Stokes shift and dielectric constant of both DNA, it was found that major and minor groove of Z-DNA were more hydrated than B-DNA. The dielectric constant of major and minor groove of DNA was 61 and 30 respectively while that of Z-DNA was 74 and 43 respectively. Saito and co-workers⁴⁰ demonstrated the major groove polarity of DNA duplexes by incorporating fluorescent nucleobase $^{\text{DNC}}U$ into DNA. The estimation of dielectric constant of DNA duplexes by fluorescence spectroscopy led to the finding that major groove was more polar when compared to other reports. Tor et al.⁴¹ estimated the major groove polarity of DNA duplex in terms of $E_{T(30)}$ by introducing emissive furan-containing nucleoside into DNA and found that major groove of DNA was nonpolar as compared to previous reports. All of these research groups used fluorescence spectroscopy to determine the polarity of the major groove and minor groove.

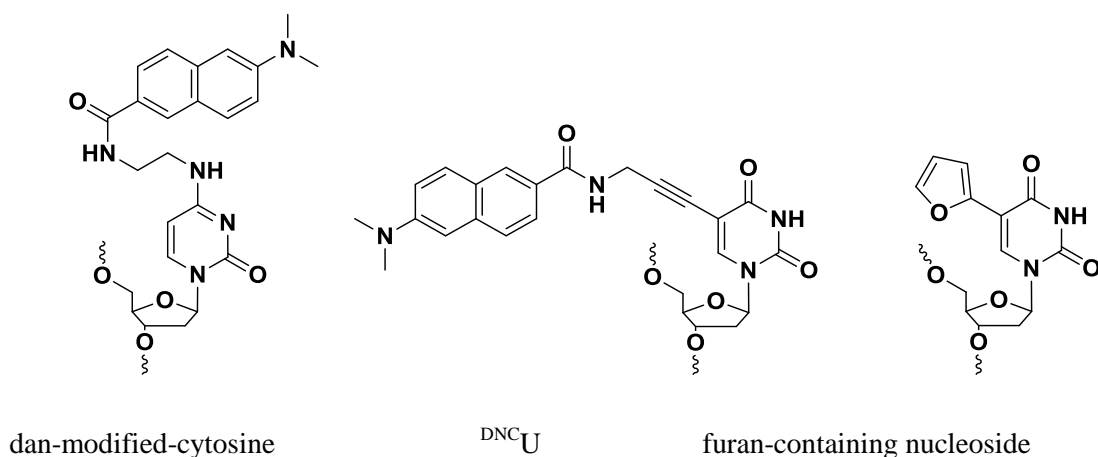


Figure 19. Structure of emissive nucleosides.³⁸⁻⁴¹

Till date several groups have explored the polarity of major groove of DNA duplexes. In view of growing interest in biological and material applications of DNA duplexes with RNA/PNA/XNA and modified nucleic acids it is relevant to study how the polarity of grooves changes with the structural diversity of complementary DNA analogues. This fluorescence strategy can be used also for the determination of major groove polarity of PNA:DNA/RNA/PNA duplexes, as PNA having a nonpolar backbone will affect the major groove polarity being structurally different than DNA/RNA.⁴²

2.10 Present work: Rationale and objective

PNA has great potential for nucleic acid based therapeutics and in this context, it is important to study characterization of the major groove of its duplex with complementary DNA/RNA/PNA. The polyamide backbone of PNA is more hydrophobic compared to the sugar-phosphate backbone of DNA/RNA. Based on previous work, the objective involved incorporation of 5-aminouracil *aeg*-PNA monomer site specifically into different PNA sequences and its fluorescent derivative.

Objectives of the present work are

1. Synthesis of hydrophilic (5-aminouracil) and fluorescent 5-amidodansyluracil *aeg*-PNA monomers

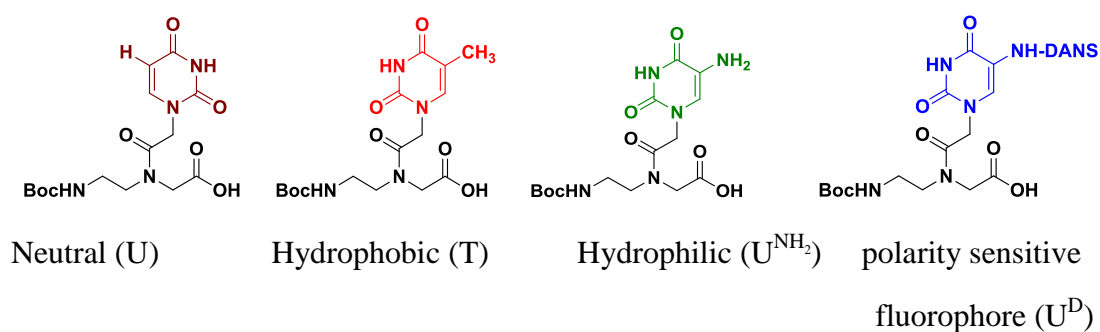


Figure 20: Structure of desired monomers.

- Incorporation of the above PNA monomers into PNA oligomers in such a way that 5-amidodansyluracil is flanked by hydrophobic, hydrophilic or neutral environment. This is achieved via flanking fluorescent monomer (U^D) with PNA units containing U, T and U^{NH_2} bases.
- Hybridization of these modified PNA oligomers with complementary DNA, RNA and PNA and to determine the stability of duplexes.
- Determining the change in major groove polarity through Stokes shift measurements.
- Studying the comparative effects of PNA backbone on the major groove polarity of PNA:DNA/RNA/PNA duplexes.

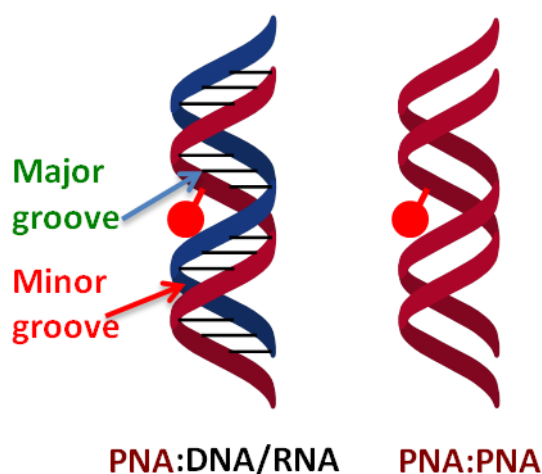


Figure 21. PNA:DNA/RNA and PNA/PNA duplexes.

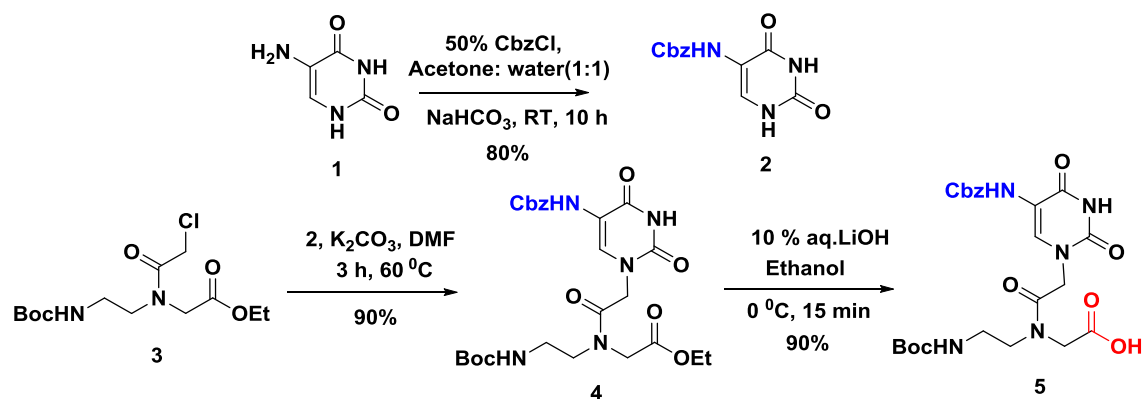
2.11 Results and discussion

The required monomers were synthesized and incorporated into sequence dependent PNA oligomers, in which dansyl fluorophore was flanked by different bases. These PNA oligomers were hybridized with complementary DNA, RNA and PNA to form PNA:DNA, PNA:RNA and PNA:PNA duplexes respectively. The polarity of major groove of these duplexes was determined by calculating dielectric constants from Stokes shift.

2.11.1 Synthesis of ethyl *NI*-Boc-aminoethyl-5-NHCbz uracil glycine (*5NHCbzU-aeg*)

The commercially available 5-aminouracil was treated with 50% benzyl chloroformate in toluene to obtain Cbz protected 5-aminouracil (**2**) (Scheme 1). This compound was reacted with the *N/C*-protected aminoethyl glycyl chloroacetamide compound (**3**) to give the protected PNA monomer (**4**). This ester upon hydrolysis with 10% aq. LiOH gave the desired acid monomer **5**.

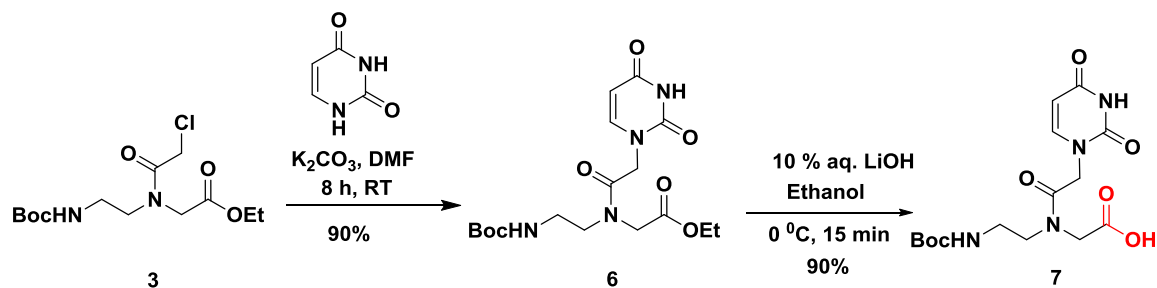
Scheme 1:



2.11.2 Synthesis of ethyl *NI*-Boc-aminoethyl-5-uracil glycine (*U-aeg*)

Compound **3** was reacted with commercially available uracil base (Scheme 2) to give compound **6**, which upon hydrolysis with 10% aq. LiOH gave the desired *aeg*-PNA-U monomer **7**.

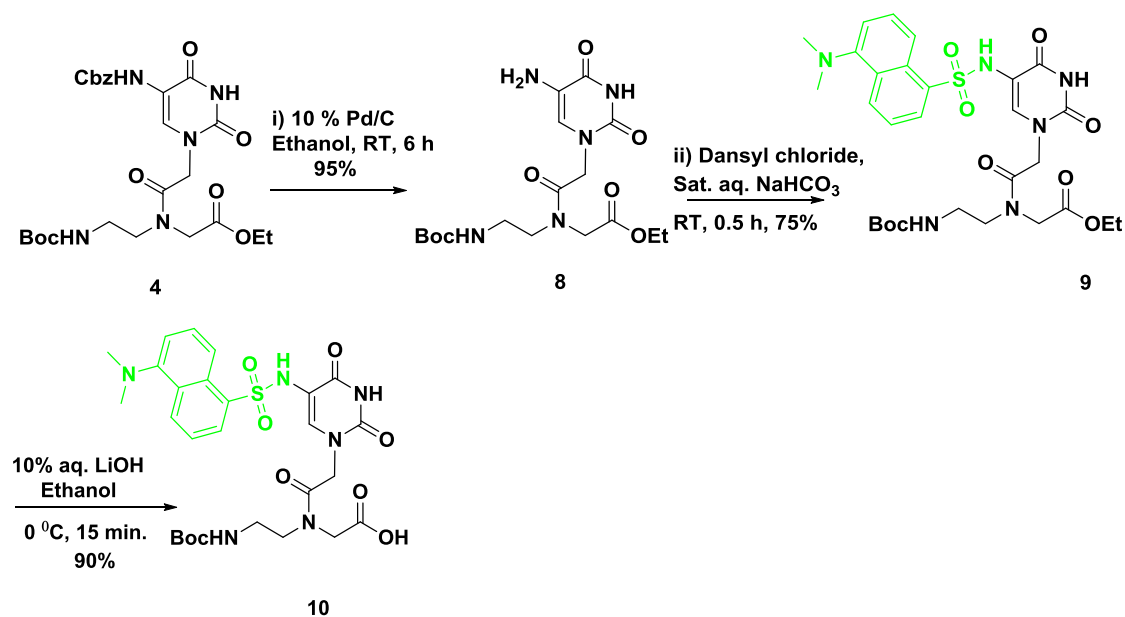
Scheme 2:



2.11.3 Synthesis of ethyl *NI*-Boc-aminoethyl-5-NH-dansyl uracil glycine (*5NHDNSU-aeg*)

Compound **4** on hydrogenated with 10% Pd/C in ethanol to obtain Cbz deprotected 5-amino-uracil **8** (Scheme 3), which on subsequent reaction with dansyl chloride gave the ester **9**. This upon hydrolysis with 10% aq. LiOH yielded the desired 5-amidodansyl-U-PNA monomer acid **10**.

Scheme 3:



All the compounds are characterized by ^1H , ^{13}C , HR-MS spectral techniques and compounds **4**, **5**, **6**, **7**, **9** and **10** are characterized by UV-vis and fluorescent spectroscopic techniques. Compound **4** displayed two distinct absorption bands at 240 nm and 292 nm. Compound **5** exhibited only one absorption band at 284 nm. Both compounds **6** and **7** showed the absorption band at 263 nm whereas compound **9** and **10**

exhibited two distinct absorption maxima at 257 nm and 340 nm and emission band at 532 nm. ^1H NMR of ester compound **4** showed two peaks at 7.17 ppm (minor) and 7.13 ppm (major) for C6 proton and quartet and triplet peaks characteristic to ethyl group at 4.20-4.28 ppm and 1.27-1.32 ppm respectively. ^1H NMR of acid compound **5** exhibited two peaks for *Boc* group at 1.44 ppm (major) and 1.42 ppm (minor) and disappearance of peaks at 4.20-4.28 ppm and 1.27-1.32 ppm suggesting the conversion of ester to acid functionality. Ester compound **6** showed two doublet peaks for C6 proton of uracil at 7.21 ppm (minor) and 7.16 ppm (major) with coupling constant $J=10$ Hz. It also exhibited doublet for C5 proton at 5.73 ppm with coupling constant $J=8$ Hz. ^1H NMR of acid compound **7** displayed slightly deshielding of C6 proton of uracil having peak at 7.46 ppm with coupling constant $J=6$ Hz and also disappearance of quartet and triplet group indicating the absence of ethyl ester. Compound **9** showed two peaks in the region 4.21-30 ppm and 1.33 ppm corresponding to quartet and triplet respectively. It also showed two singlet peaks for *Boc* group at 1.47 ppm (major) and 1.44 ppm (minor). All the intermediates showed two peaks for the proton in same chemical environment which may be arise by the presence of rotamer formed due to rotation of tertiary amide. NMR, HR-MS, UV and fluorescence spectra are shown in Appendix-II.

2.11.4 Synthesis of PNA oligomers

The synthesized PNA monomers were incorporated into the desired *aeg*-PNA sequence by solid phase peptide synthesis (SPPS) protocol using Boc strategy, on MBHA resin, which is amenable to acidic conditions. In the synthesis of all oligomers, orthogonally protected (Boc/Cl-Cbz) L-lysine was selected as the C-terminal spacer-amino acid, which is linked to the resin through amide bond. The amine loading on the resin was suitably lowered from 0.67 mmol/g to 0.35 mmol/g by partial acylation of free amines on the resin with calculated amount of acetic anhydride.⁴³ The residual free amine groups available on the resin for further coupling was confirmed by Kaiser's test before starting synthesis. The deprotection of the *t*-Boc and the completion of coupling reaction were monitored by Kaiser's test.⁴⁴ The *t*-Boc deprotection leads to a positive Kaiser's test, where the resin beads show blue color (Ruhemann's purple). On the other hand, resin beads were colorless after completion of coupling reaction indicating a negative Kaiser's test. The free amine was subsequently coupled to PNA acid monomer by using HBTU/HOBt, DIPEA in DMF. The coupling reactions were done on solid

support under microwave conditions (25 watts, 75 °C, for 5 min.). The deprotection, neutralization and coupling steps were repeated till the synthesis of desired length of oligomer was achieved. The PNA oligomers were then cleaved from the solid support (MBHA resin), using trifluoromethanesulphonic acid (TFMSA) in the presence of trifluoroacetic acid to give *aeg*-PNA oligomers having amide group at C terminus (Figure 22). After cleavage, the polyamide oligomers obtained in solution were precipitated by addition of cold diethyl ether.

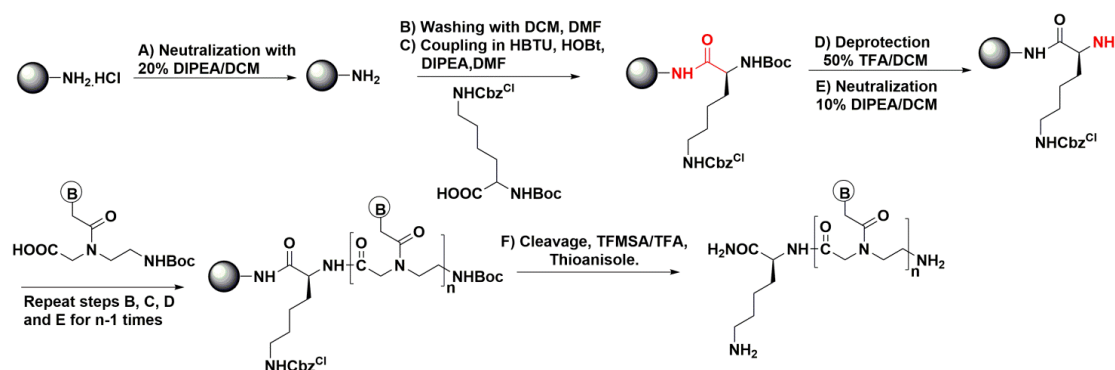


Figure 22: Scheme for the synthesis of PNA oligomers.

2.11.5 Design of PNA sequences

PNA sequences were designed in such a way that the dansyl fluorophore is flanked by hydrophobic (T), neutral (U) or hydrophilic environment (U^{NH_2}) of adjacent bases. PNA-1 is nonfluorescent sequence whereas PNA-2 to PNA-6 has dansyl fluorophore (U^D) and PNA-7 is complementary antiparallel PNA sequence to make PNA:PNA duplexes. In PNA-2 the U-dansyl fluorophore is flanked on either side by hydrophobic thymine (T) bases and in PNA-3, it is flanked by hydrophobic (T) and neutral (U) bases. PNA-4 has the dansyl fluorophore (U^D) flanked on both sides by neutral uracil (U) bases. In PNA-5, the dansyl fluorophore (U^D) is flanked by hydrophilic (U^{NH_2}) bases whereas in PNA-6 dansyl fluorophore (U^D) is flanked by hydrophobic thymine (T) and hydrophilic (U^{NH_2}) bases (Figure 23). The base triplets having dansyl fluorophore is flanked by hydrophobic, neutral or hydrophilic environment are shown in color in the Table 1.

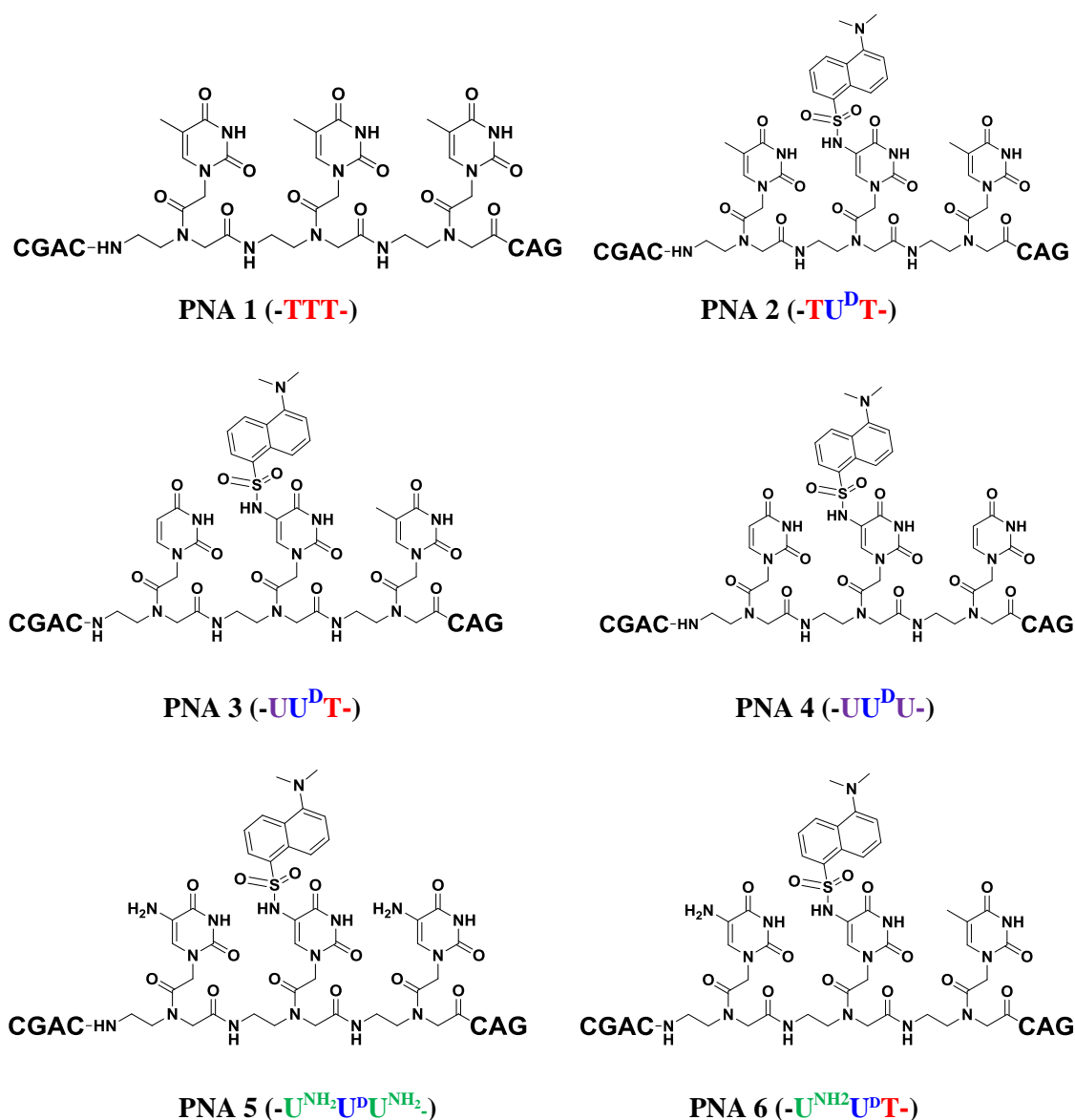


Figure 23: PNA sequences showing the structure of base triplets.

Table 1: PNA sequences

Entry	Sequence code	PNA sequence	Monomers used
1	PNA 1	H-CGAC TTT CAG LysNH ₂	A/G/C/T/U = aeg PNA
2	PNA 2	H-CGAC TU^DT CAG LysNH ₂	
3	PNA 3	H-CGAC UU^DT CAG LysNH ₂	
4	PNA 4	H-CGAC UU^DU CAG LysNH ₂	
5	PNA 5	H-CGAC U^{NH₂}U^DU^{NH₂} CAG LysNH ₂	
6	PNA 6	H-CGAC U^{NH₂}U^DT CAG LysNH ₂	
7	PNA 7	H-CTG AAA GTCG LysNH ₂	

2.11.6 Purification and characterization of PNA oligomers

The synthesized PNA oligomers were purified by reverse phase high performance liquid chromatography (RP-HPLC) on a semi-preparative C18 column using acetonitrile/water gradient elution. The purity of PNA oligomers was checked by reinjecting the sample on analytical C18 column. The integrity of the synthesized PNA oligomers was confirmed by MALDI-TOF mass spectrometry using 2,5-dihydroxybenzoic acid (DHB) as matrix. The calculated and observed molecular weights for all PNAs with their molecular formula and HPLC retention times are shown in Table 2. The HPLC and MALDI-TOF spectra of the PNA oligomers are shown in Appendix-II. MALDI-TOF of modified PNA oligomers PNA 2-6 showed mass less than 300 which might be due to the fragmentation of dansyl group.

Table 2: MALDI-TOF and retention time (Rt) of purified PNA oligomers

Entry	Sequence code	Mol. Formula	Calcd. mass	Obsvd. mass	Retention time (min)
1	PNA 1	C ₁₁₃ H ₁₅₁ N ₅₉ O ₃₂	2832.197	2832.4500	13.2
2	PNA 2	C ₁₁₇ H ₁₄₈ N ₅₉ O ₃₂	2831.1767	2831.0874	13.0
3	PNA 3	C ₁₁₁ H ₁₄₇ N ₅₉ O ₃₂	2818.1689	2818.2815	12.9
4	PNA 4	C ₁₁₀ H ₁₄₄ N ₅₉ O ₃₂	2803.1454	2803.2864	12.7
5	PNA 5	C ₁₁₀ H ₁₄₆ N ₆₁ O ₃₂	2833.1672	2833.6022	12.5
6	PNA 6	C ₁₁₁ H ₁₄₇ N ₆₀ O ₃₂	2832.1720	2832.3088	12.6
7	PNA 7	C ₁₁₄ H ₁₄₈ N ₆₃ O ₃₀	2879.1992	2879.3357	12.9

2.12 Solvent dependent fluorescence study

In order to examine the change in dansyl fluorophore conjugated compound **9** with respect to alteration in the dielectric constant, the UV-visible and fluorescence spectroscopic measurements were performed in the solvents having different polarity (Figure 24, Table 3). It was observed that emission wavelength of compound **9** varies from nonpolar (dioxane) to polar solvent (methanol).

In methanol, compound **9** showed the two distinct absorption maxima at 257 nm and 340 nm attributed to the base and dansyl fluorophore respectively. When the solvent polarity decreased from methanol to dioxane, the highest and lowest absorption bands were slightly affected. However, the emission maximum and intensity were influenced by solvent polarity (Figure 24). When a solution of **9** in dioxane was excited at 341 nm, a strong fluorescence band was observed in visible region at 503 nm. As the

polarity of solvent changed from dioxane to methanol, the compound **9** exhibited bathochromic shift (from 503 to 532 nm) and nearly 10 fold quenching in the fluorescence (Figure 24). The observation of bathochromic shift (red) results with increase in solvent polarity is termed as positive solvatochromism. This is caused by differential solvation of the ground and first excited state of fluorophore. Positive solvatochromism results from a better stabilization of the molecule in the first excited state relative to that in the ground state.³⁶ Polar solvents stabilize the excited state better as compared to non-polar solvents. The change in shift of emission band with change in solvent polarity for the compound **9** indicated that dansyl fluorophore is sensitive to surrounding environment. The intensity of emission is higher in nonpolar solvents compared to polar solvents.

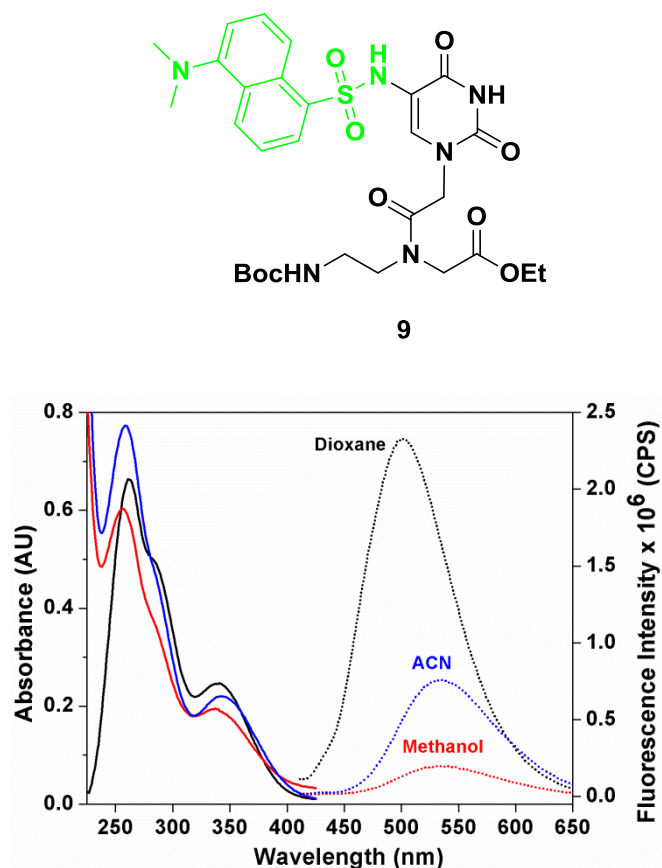


Figure 24. UV and fluorescence spectra of compound **9** in the solvents of different polarity.

Table 3: λ_{ex} and λ_{em} in different solvents

Solvent	λ_{ex} (nm)	λ_{em} (nm)	Dielectric* constant (ϵ)	$E_{T(30)}$ *
1,4 –Dioxane	341	503	2.25	36.0
Acetonitrile	344	540	37.5	45.6
Methanol	340	530	32.7	55.4

*Values are taken from literature.³⁶

Thus, fluorescence spectra of 5-amidodansyl indicated that its excitation/emission properties are reasonably sensitive to the microenvironment.

2.13 Biophysical studies

In this section temperature dependent UV spectroscopy (T_m) was used to study the thermal stabilities of hybrids derived from modified PNAs towards their complementary antiparallel DNA/RNA/PNA and circular dichroism (CD) studies employed to examine if the modifications alter the secondary duplex structures in the modified PNA:DNA/RNA/PNA hybrids.

2.13.1 Thermal melting of PNA/DNA, PNA/RNA and PNA/PNA duplexes

The thermal stability of PNA/DNA, PNA/RNA and PNA/PNA duplexes was studied by temperature dependent UV studies. The different synthesized PNA decamers were hybridized with complementary antiparallel DNA in 10 mM phosphate buffer and 10 mM sodium chloride. These samples were then annealed by heating at 90 °C for 3 min (In case of PNA:PNA duplexes samples were heated for 10 min) followed by slow cooling to room temperature and then refrigerated at 4 °C for at least 4 to 5 h to make duplexes. The thermal stability (T_m) of these duplexes was examined by UV-melting at 260 nm. The temperature absorbance curves were sigmoidal and T_m derived from midpoint of derivative curve.

2.13.1a PNA:DNA duplexes

The T_m derived from midpoint of derivative plots of various PNA:DNA hybrids are shown in Figure 25, Table 4. The unmodified duplex PNA-1:DNA has T_m value of 46.5 °C. The T_m was slightly increased by 1.4 °C in the PNA-2:DNA duplex where dansyl fluorophore is flanked by two hydrophobic thymines (T). The PNA-3:DNA duplex was slightly destabilized by 0.7 °C where dansyl fluorophore is flanked by neutral (U) and hydrophobic environment (T). The T_m of PNA-4:DNA duplex was slightly stabilized by 0.8 °C where dansyl fluorophore is flanked by neutral uracil (U) bases. The PNA-5:DNA duplex where dansyl group is flanked by two hydrophilic U^{NH_2} bases was slightly stabilized by 0.4 °C and is least stabilized duplex as compared to other modified duplexes. The T_m of PNA-6:DNA duplex was stabilized by 2.2 °C where dansyl fluorophore is flanked by hydrophobic thymine (T) and hydrophilic 5-aminouracil (U^{NH_2}) bases. From temperature dependent UV spectroscopy, it was found that modified PNA:DNA duplexes except PNA-3:DNA duplex are slightly stabilized as compared to unmodified duplex of PNA-1:DNA. Thus the modified PNA:DNA duplexes are stable and T_m variation with the changes with sequence are only marginal compared to unmodified duplex.

The ΔT_m changes in the order PNA-6:DNA ($U^{NH_2}U^DT$) > PNA-2:DNA (TU^DT) > PNA-4 :DNA (UU^DU) > PNA-5:DNA ($U^{NH_2}U^DU^{NH_2}$) > PNA-1:DNA (TTT) > PNA-3:DNA (UU^DT).

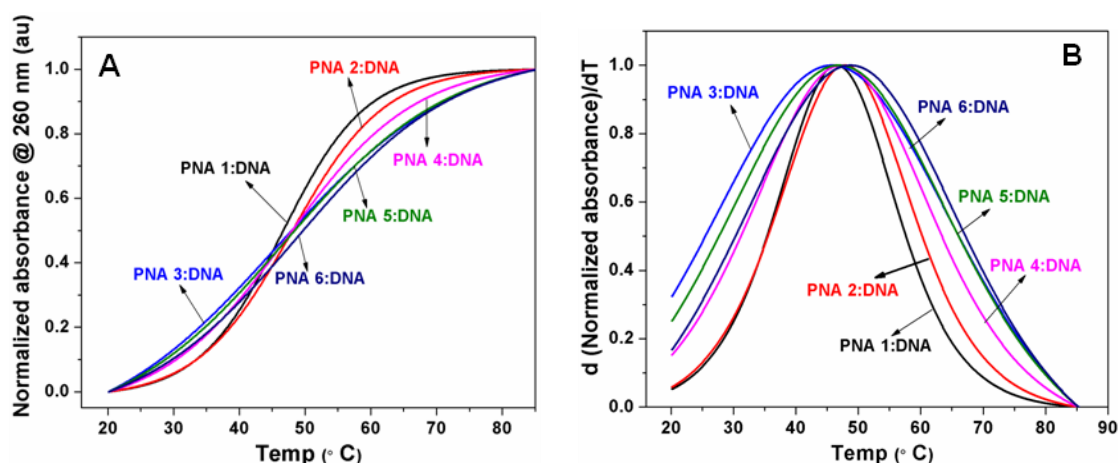


Figure 25. Melting curves of PNA/DNA duplexes A) Sigmoidal curve and B) Derivative curve.

Table 4: T_m of PNA:DNA duplexes.

Entry	Sequence code	PNA sequence	UV- T_m (°C)	ΔT_m (°C)
1	PNA 1	H-CGAC TTT CAG LysNH ₂	46.5	-
2	PNA 2	H-CGAC TU^DT CAG LysNH ₂	47.9	+1.4
3	PNA 3	H-CGAC UU^DT CAG LysNH ₂	45.8	-0.7
4	PNA 4	H-CGAC UU^DU CAG LysNH ₂	47.3	+0.8
5	PNA 5	H-CGAC U^{NH₂}U^DU^{NH₂} CAG LysNH ₂	46.9	+0.4
6	PNA 6	H-CGAC U^{NH₂}U^DT CAG LysNH ₂	48.7	+2.2

$U^D = 5NHDNSU$ -aeg; $U = U$ -aeg; $U^{NH_2} = 5NH_2U$ -aeg; ΔT_m indicates the difference between T_m of PNA:DNA duplexes and PNA-1:DNA; Values are accurate to ± 0.5 °C; (-) and (+) indicates destabilization and stabilization respectively. DNA = 3'-GCTG AAA GTC-5'.

2.13.1b PNA:RNA duplexes

The melting temperature curves of PNA:RNA duplexes are shown in Figure 26 and T_m values are given in Table 5. The unmodified duplex PNA-1:RNA has T_m value of 56.8 °C. The PNA-2:RNA duplex was destabilized by 9.8 °C where dansyl fluorophore is flanked by two hydrophobic thymine (T) residues. When dansyl fluorophore is flanked by hydrophobic thymine (T) and neutral uracil (U), the PNA-3:RNA duplex was destabilized by 2.8 °C but more stabilized as compare to PNA-2:RNA duplex. The melting temperature of PNA-4:RNA duplex was destabilized by 2.0 °C where dansyl fluorophore on either side is flanked by neutral uracil (U) bases. In the PNA-5:RNA duplex where dansyl group is flanked by two hydrophilic 5-aminouracil (U^{NH_2}) bases, the destabilization observed by 1.8 °C and least destabilized duplex as compared to other modified PNA:RNA duplexes. The PNA-6:RNA duplex where dansyl fluorophore flanked by hydrophobic thymine (T) and hydrophilic (U^{NH_2}) bases was destabilized by 6.8 °C. From temperature dependent UV spectroscopy it was found that i) modified PNA:RNA duplexes are more stabilized than PNA:DNA duplexes, ii) PNA:RNA duplexes were more destabilized upon incorporation with modified bases such as U, U^{NH_2} and U^D . Thus the modified PNA:RNA duplexes were stable but destabilized when they were modified.

The ΔT_m changes in the order PNA-1:RNA (TTT) > PNA-5:RNA ($U^{NH_2}U^DU^{NH_2}$) > PNA-4:RNA (UU^DU) > PNA-3:RNA (UU^DT) > PNA-6:RNA ($U^{NH_2}U^DT$) > PNA-2:DNA (TU^DT).

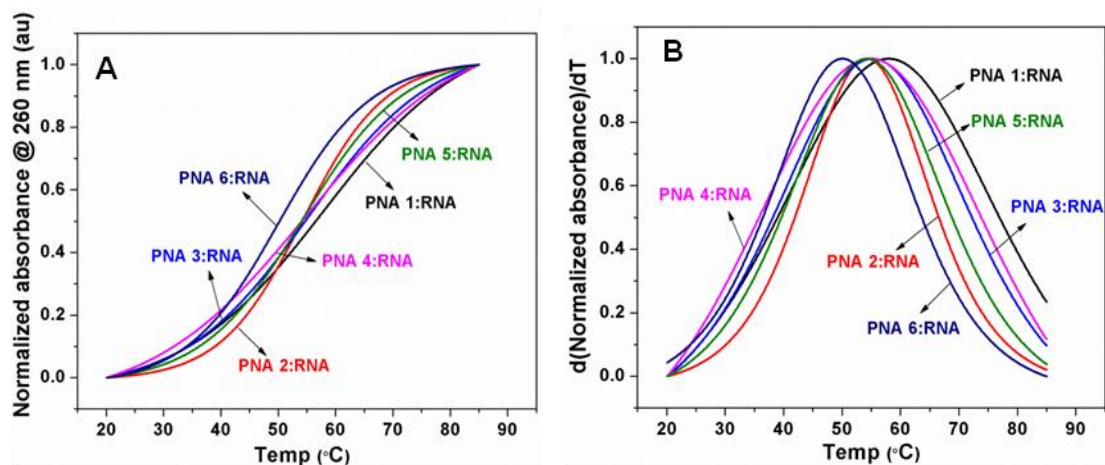


Figure 26. Melting curves of PNA/RNA duplexes A) Sigmoidal curve and B) Derivative curve.

Table 5: T_m of PNA:RNA duplexes.

Entry	Sequence code	PNA sequence	UV- T_m (°C)	ΔT_m (°C)
1	PNA 1	H-CGAC TTT CAG LysNH ₂	56.8	-
2	PNA 2	H-CGAC TU^DT CAG LysNH ₂	47.0	-9.8
3	PNA 3	H-CGAC UU^DT CAG LysNH ₂	54.0	-2.8
4	PNA 4	H-CGAC UU^DU CAG LysNH ₂	54.8	-2.0
5	PNA 5	H-CGAC U^{NH₂}U^DU^{NH₂} CAG LysNH ₂	55.0	-1.8
6	PNA 6	H-CGAC U^{NH₂}U^DTCAG LysNH ₂	50.0	-6.8

U^D = 5NHDNSU-aeg; **U** = U-aeg; **U^{NH₂}** = 5NH₂U-aeg; ΔT_m indicates the difference between T_m of PNA:DNA duplexes and PNA-1:DNA; Values are accurate to ± 0.5 °C; (-) indicates destabilization. RNA = 3'-GCUG AAA GUC-5'.

2.13.1c PNA:PNA duplexes

The temperature absorbance curves are shown in Figure 27 and the T_m derived from midpoint of derivative plots given in Table 6. It was found from thermal melting curves that PNA:PNA duplexes were more stable as compared to PNA:DNA and PNA:RNA duplexes. The unmodified duplex PNA-1:PNA has T_m value of 60.0 °C and found to be more stable as compared to PNA-1:DNA and PNA-1:RNA duplexes. The T_m of PNA-2:PNA duplex where dansyl fluorophore flanked by two hydrophobic thymine (T) bases, was destabilized by 9.0 °C. In the PNA-3:PNA duplex destabilization by 4.6 °C was observed where dansyl fluorophore flanked by neutral (U) and hydrophobic (T) bases. The PNA-4:PNA duplex was destabilized by 4.0 °C where dansyl fluorophore on either side flanked by neutral (U) bases. The PNA-5:PNA duplex where dansyl fluorophore is flanked by two hydrophilic 5-aminouracil (U^{NH₂}) bases, was destabilized by 12.2 °C. The T_m of PNA-6:PNA duplex was destabilized by 12.0

°C where dansyl group flanked by hydrophobic thymine (T) and hydrophilic 5-aminouracil (U^{NH_2}) bases. From temperature dependent UV spectroscopy, it was found that in modified PNA:PNA duplexes the presence of hydrophilic 5-NH₂ group next to the dansyl fluorophore destabilized the PNA :PNA duplexes.

The ΔT_m changes in the order PNA-1:PNA (TTT) > PNA-4:PNA (UU^DU) > PNA-3:PNA (UU^DT) > PNA-2:PNA (TU^DT) > PNA-6:PNA ($U^{NH_2}U^DU$) > PNA-5:PNA ($U^{NH_2}U^DU^{NH_2}$).

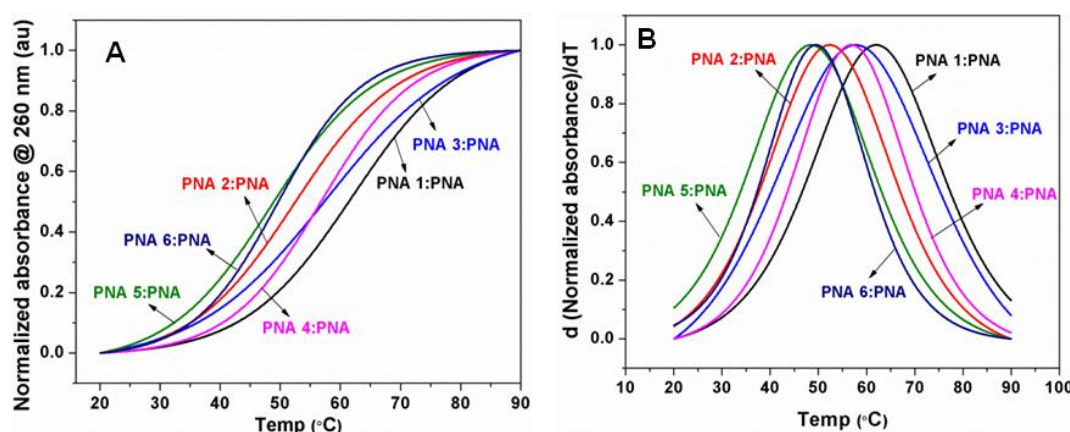


Figure 27. Melting curves of PNA/PNA duplexes A) Sigmoidal curve and B) Derivative curve.

Table 6: T_m of PNA:PNA duplexes.

Entry	Sequence code	PNA sequence	UV- T_m (°C)	ΔT_m (°C)
1	PNA 1	H-CGAC TTT CAG LysNH ₂	60.0	-
2	PNA 2	H-CGAC TU^DT CAG LysNH ₂	51.0	-9.0
3	PNA 3	H-CGAC UU^DT CAG LysNH ₂	55.4	-4.6
4	PNA 4	H-CGAC UU^DU CAG LysNH ₂	56.0	-4.0
5	PNA 5	H-CGAC U^{NH₂}U^DU^{NH₂} CAG LysNH ₂	47.8	-12.2
6	PNA 6	H-CGAC U^{NH₂}U^DT CAG LysNH ₂	48.0	-12.0

$U^D = 5NHDNSU$ -aeg; $U = U$ -aeg; $U^{NH_2} = 5NH_2U$ -aeg; ΔT_m indicates the difference between T_m of PNA:DNA duplexes and PNA-1:DNA; Values are accurate to ± 0.5 °C; (-) indicates destabilization. PNA = GCTG AAA GTC written from C to N terminus.

2.13.1d Comparison of UV- T_m of PNA:DNA, PNA:RNA and PNA:PNA duplexes

The comparison of T_m of PNA:DNA, PNA:RNA and PNA:PNA duplexes is given in the Table 7. It is generally observed that PNA:PNA duplexes are more stable compared to PNA:DNA and PNA:RNA duplexes except for PNA-5:PNA and PNA-6:PNA duplex having U^{NH_2} substitution.

When dansyl fluorophore is flanked by hydrophobic thymine (T) and neutral (U) bases, order of stability of duplexes is PNA:PNA>PNA:RNA>PNA:DNA whereas in case of dansyl fluorophore is flanked by hydrophilic base 5-aminouracil (U^{NH_2}) the stability order of duplexes is, PNA:RNA>PNA:PNA>PNA:DNA. Thus from T_m data, it is evident that T_m of PNA:DNA, PNA:RNA and PNA:PNA duplexes vary with change in local base sequence (Figure 28, Table 7).

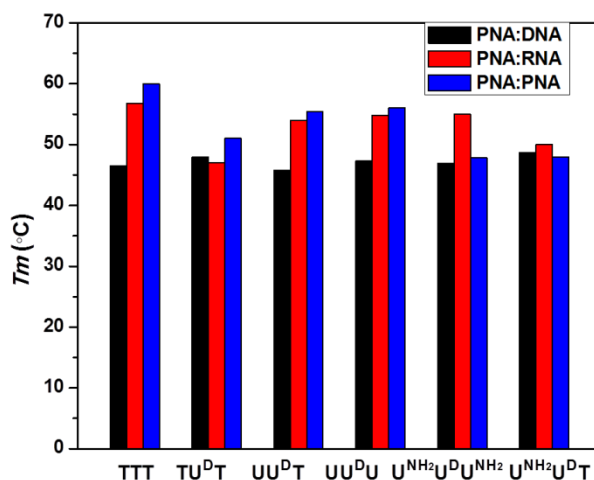


Figure 28. Comparative T_m of PNA:DNA, PNA:RNA and PNA:PNA duplexes.

Table 7: Comparison of T_m of PNA:DNA, PNA:RNA and PNA:PNA duplexes.

Sr. No.	Sequence code	PNA	PNA: DNA duplex	PNA: RNA duplex	PNA: PNA duplex
1	PNA-1	-TTT-	46.5	56.8	60.0
2	PNA-2	-TU ^D T-	47.9	47.0	51.0
3	PNA-3	-UU ^D T-	45.8	54.0	55.4
4	PNA-4	-UU ^D U-	47.3	54.8	56.0
5	PNA-5	-U ^{NH₂} U ^D U ^{NH₂} -	46.9	55.0	47.8
6	PNA-6	-U ^{NH₂} U ^D T-	48.7	50.0	48.0

2.13.2a Circular dichroism (CD) of PNA:DNA/RNA duplexes

CD spectroscopy provides the structural information of many types of chiral biomacromolecules that possess UV-Vis absorbing chromophore. Circular dichroism is the difference between the absorption of left handed and right handed circularly polarized light and is measured as a function of wavelength. Although detailed structural information not available from CD, it can provide a reliable estimation of

overall conformational state of biopolymers and any structural changes induced by modification when compared to that of reference samples. The CD of single stranded PNA oligomers and their hybrids with complementary DNA and RNA was recorded to examine the effect of modifications on the secondary structures of PNA:DNA and PNA:RNA duplexes. PNA being achiral shows insignificant CD signature but exhibit characteristic CD signature upon hybridization with complementary DNA and RNA (Figure 29). CD of PNA:DNA and PNA:RNA duplexes was recorded in 10 mM phosphate buffer and 10 mM sodium chloride at ambient temperature.

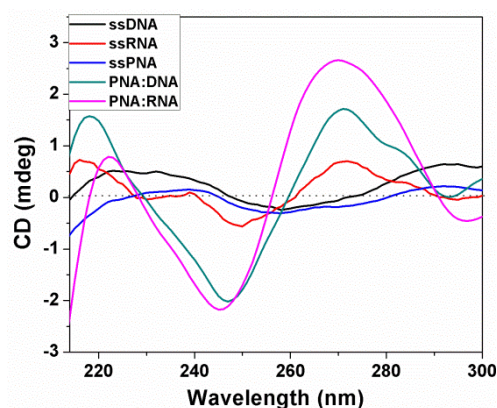


Figure 29. Representative CD profile of ssDNA, ssRNA, ssPNA, PNA:DNA and PNA:RNA.

The formation of PNA:DNA duplexes results in two positive bands with maxima one in the region of 265 to 270 nm and another band between 215 to 220 nm. PNA:DNA duplexes also showed negative maxima at 240 to 250 nm with cross-over points at approximately 230 and 260 nm. CD profile of PNA:RNA duplexes showed two positive bands with maxima one in the region 265 to 275 nm (higher intensity) and another band of very low intensity in the region 220 to 225 nm. PNA:RNA duplexes also exhibited negative band at 239 to 251 nm. Thus, CD signature of PNA/DNA and PNA/RNA duplexes showed that the chemical modification at C-5 doesn't alter any of the duplex structures PNA:DNA and PNA:RNA (Figure 30).

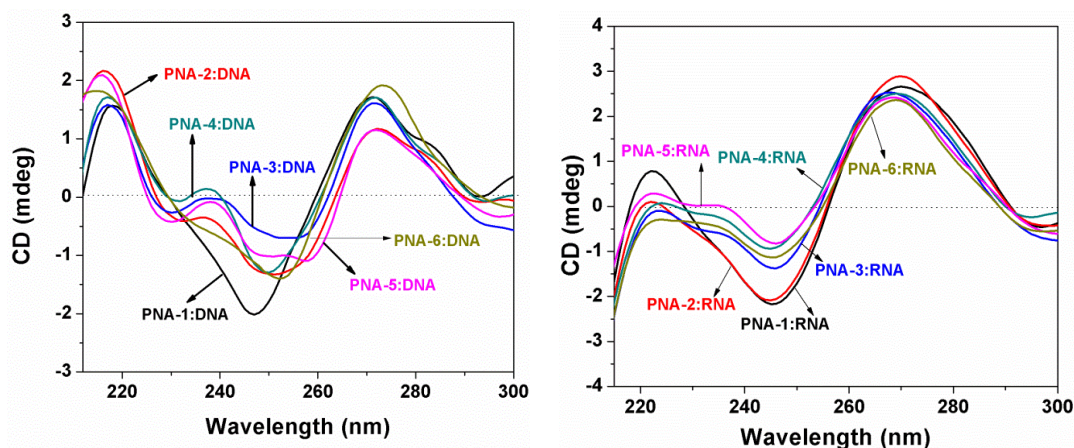


Figure 30. CD profiles of PNA/DNA and PNA/RNA duplexes.

2.13.2b Circular dichroism (CD) of PNA:PNA duplexes

PNA:PNA duplexes form equal amounts of left-handed and right-handed helices due to the absence of a chiral unit. The attachment of chiral lysine to the C-terminus of the PNA strand leads to the preferred handedness of the duplex.⁴⁶ The CD signature of PNA:PNA duplexes also depends on the subsequent base attached to lysine. Guanine or cytosine attached to lysine in the PNA strand generally exhibits a helical conformation of PNA:PNA duplexes.⁴⁶

CD spectroscopic measurements of PNA1-6:PNA duplexes were recorded at ambient temperature. The unmodified PNA-1:PNA duplexes exhibited a positive band at 239 nm and a negative band at 260 nm along with one maximum at 292 nm, indicating the formation of a double-helical structure (Figure 31A). The modified PNA2-6:PNA duplexes showed a blue shift of the maximum at 227 nm. The PNA2-6:PNA duplexes also exhibited a minimum at 260 nm and a maximum at 295 nm. From the CD data, it was observed that chemical modification at C5 slightly alters the helicity of modified PNA:PNA duplexes. However, they remain in the duplex form as that of B-DNA.

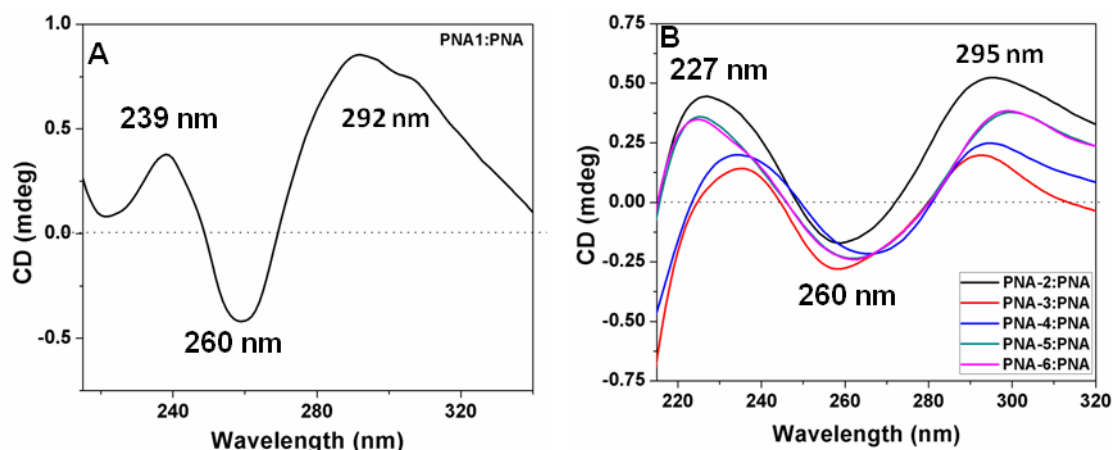


Figure 31. CD signature of A) PNA-1:PNA duplex and B) Modified PNA2-6:PNA duplexes.

2.14 Determination of dielectric constant as a measure of polarity

In order to estimate the dielectric constant of the major groove in PNA:DNA/RNA/PNA duplexes using U-dansyl as fluorescent probe, the fluorescence parameters (λ_{ex} and λ_{em}) of the compound **9** were measured in media of different dielectric constants generated by varying ratios of dioxane:water. The dioxane:water solvent system was used (rather than the organic solvents) to record fluorescence of compound **9** to compare its Stokes shift with that of PNA oligomers **2-6**, that dissolve in water. Thus recording the fluorescence of compound **9** in dioxane:water solvent system helps to compute the dielectric constants of duplexes.

To find the possible effects of sequence on the major groove polarity, oligonucleotides were designed by successively replacing **T**'s adjacent to the fluorescent nucleobase probe **U^D** with 5-aminouracil (**U^{NH₂}**) and uracil (**U**), to induce polarity changes around the 5-substituent region in the major groove of PNA. Thus in PNA-**2** sequence (**-TU^DT-**), dansyl fluorophore is flanked on either side by hydrophobic **T**s and successive replacement of these two **T**'s by neutral **U** gives PNA-**3** (**-UU^DT-**) and PNA-**4** (**-UU^DU-**) respectively. The successive replacement of thymine by hydrophilic **U^{NH₂}** resulted in PNA-**5** (**-U^{NH₂}U^DU^{NH₂}-**) and PNA-**6** (**-U^{NH₂}U^DT-**). The complementary nonfluorescent PNA oligomer PNA-**7** was used to form PNA:PNA duplexes.

The Stokes shift ($\Delta\nu$) at various dielectric constants was calculated from measuring the λ_{ex} and λ_{em} in different composition of dioxane:water and the orientation

polarity (f) and dielectric constant (ϵ) were taken from the literature.⁴⁵ The plot of Stokes shift against orientation polarity (f), exhibited linear relationship suggesting the dominant influence of general solvent effects on the observed fluorescence properties of compound **9** (Figure 32). Assuming that such a correlation of orientation polarity and dielectric constant for dansyl fluorophore in the monomer is valid for incorporated dansyl in PNA decamers, the observed Stokes shift of duplexes of these PNA with complementary DNA/RNA/PNA in buffer can be used to estimate the major groove polarity of these duplexes using Lippert equation. Using an identical procedure with Hoechst 33258, the polarity of minor groove in DNA has been estimated.²⁹

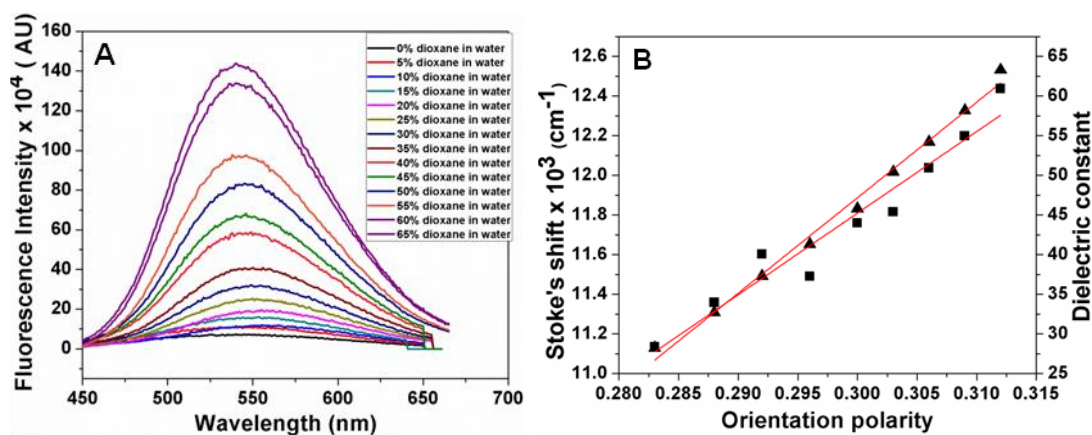
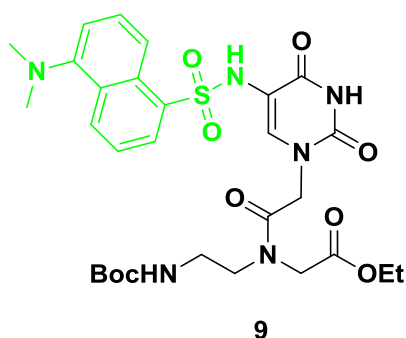


Figure 32. (A) Fluorescence spectra of compound **9** in different solvents and (B) Combined plot of Stoke's shift (\blacksquare) versus orientation polarity and dielectric constant (\blacktriangleleft) versus orientation polarity.

Table 8: Dielectric constant, orientation polarity and Stokes shift for compound 9.

% 1,4-Dioxane in water	Dielectric constant* (ε)	Orientation polarity (f)*	λ_{ex} (nm)	λ_{em} (nm)	Stoke's shift (cm-1)
0	78.5	0.320	328	540	11969
5	72.5	0.317	328	547	12206
10	67.0	0.314	328	557	12534
15	63.0	0.312	328	554	12437
20	58.2	0.309	332	558	12199
25	54.2	0.306	332	553	12037
30	50.4	0.303	333	549	11816
35	45.8	0.300	334	550	11759
40	41.3	0.296	334	542	11490
45	37.3	0.292	335	548	11602
50	32.7	0.288	337	546	11358
55	28.2	0.283	338	542	11135
60	24.0	0.277	338	540	11067
65	20.0	0.270	338	540	11067

*Values are taken from literature.⁴⁵

2.15 Determination of dielectric constants of PNA:DNA/RNA/PNA duplexes

After calculation of Stokes shift of compound **9** and plotting them against orientation polarity with dielectric constant, the fluorescence spectra of different PNA oligomers and their corresponding duplexes with complementary DNA, RNA and PNA were recorded in both single strand and duplex form. The data showed considerable variations in fluorescence parameters (λ_{ex} and λ_{em}) dependent on solvent. The Stoke's shift derived from this data has been used to calculate local dielectric constant through the orientation polarity employing Lippert equation for each of the PNA/DNA, PNA/RNA and PNA/PNA duplexes.

$$f = \frac{\varepsilon - 1}{2\varepsilon + 1} - \frac{n^2 - 1}{2n^2 + 1}$$

2.15.1 PNA:DNA duplexes

The values of derived local ε from for different hybrids are shown in Table 9. In the major groove of the PNA-2:DNA duplex U-dansyl fluorophore is flanked by the two hydrophobic thymines on either side (-TU^DT-), the local dielectric constant was

found **39.5D**. Upon replacing one of the thymine by uracil (devoid of 5-Me), the local dielectric constant increased by 2.5 units to **42.0D** in duplex PNA-3:DNA (-U^DT-). When the other thymine was also replaced by uracil in PNA-4:DNA (-U^DU-) duplex, the local dielectric constant slightly increased by 1.7 unit to **43.6D**. Upon replacing both thymine with the hydrophilic 5-aminouracil as in PNA-5:DNA duplex (-U^{NH₂}U^DU^{NH₂}-), the local dielectric constant considerably enhanced to **50.7D** but when one hydrophilic 5-aminouracil was replaced by thymine, the local dielectric constant found to be **44.0D** in PNA-6:DNA duplex (-U^{NH₂}U^DT-).

The local dielectric constant (ϵ) of PNA-2:DNA (-T^DT-) duplex was found to be nearly equal as compared to **40D** observed for the DNA:DNA duplex d(GGTGA T^DT AAGCG): d(CGCTTAAATCACC) reported by Ganesh et al.³⁷ where U-dansyl was flanked by same local environment as that of PNA-2:DNA duplex. When compared with the ϵ of self complementary sequence CGCGAAU^DTCGCG where U-dansyl was flanked by one T and one A, the ϵ of PNA-2:DNA duplex (**40 D**) was found to be considerably less by 14.5 units. The ϵ of PNA-5:DNA (-U^{NH₂}U^DU^{NH₂}-, **50.7D**) and PNA-6:DNA (-U^{NH₂}U^DT-, **44.0D**) duplexes were also compared with the DNA:DNA (**61.0D** and **56.1D** respectively) duplexes where U-dansyl is flanked by similar bases as that of PNA-5:DNA and PNA-6:DNA duplexes and found that DNA:DNA duplexes are more hydrated than PNA:DNA duplexes.

Thus, the results of present work are in good agreement with earlier reports and indicate that local polarity in major groove of PNA:DNA duplexes is sequence dependent and microenvironment sensitive. In comparison with local dielectric constant of DNA:DNA (**40D** to **61D**) duplexes, the local dielectric constant of PNA:DNA duplexes are relatively less, which suggests that neutral hydrophobic backbone of PNA influences the local polarity of PNA:DNA duplexes. Figure 33 shows the fluorescence spectra of PNA:DNA duplexes and plot determination of dielectric constant from Stokes shift.

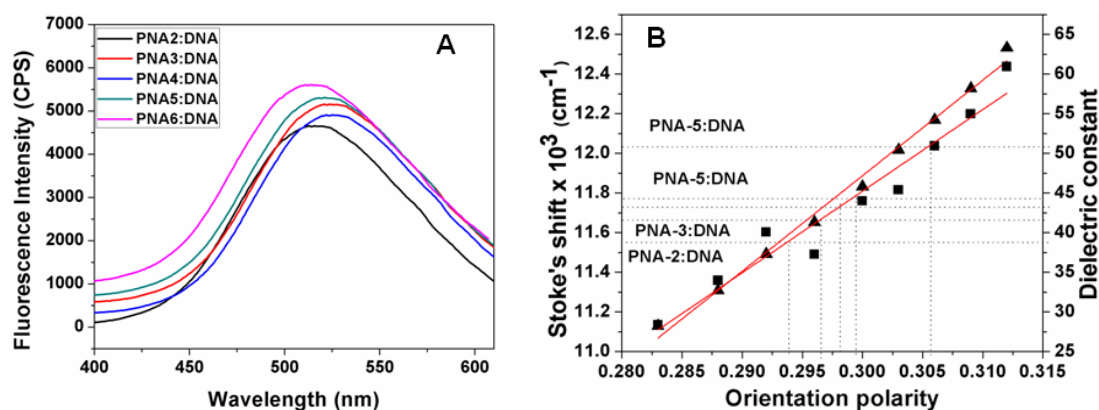


Figure 33. A) Fluorescence spectra of PNA:DNA duplexes and B) Combined plot of Stokes shift (■) versus orientation polarity and dielectric constant (▲) versus orientation polarity of PNA:DNA duplexes. Fluorescence measurements were recorded in 10 mM phosphate buffer (pH 7.2) containing 10 mM NaCl.

Table 9: Dielectric constants of PNA:DNA duplexes

PNA No.	PNA	λ_{ex} (nm)	λ_{em} (nm)	Stoke's shift (cm ⁻¹)	Orientation polarity (f)	Dielectric constant (ϵ)	ϵ of DNA:DNA*
PNA-2	-TU ^D T-	323	516	11580	0.293	39.5	40.0
PNA-3	-UU ^D T-	325	524	11686	0.297	42.0	-
PNA-4	-UU ^D U-	325	525	11722	0.298	43.6	-
PNA-5	-U ^{NH₂} U ^D U ^{NH₂} -	320	521	12057	0.306	50.7	61.0
PNA-6	-U ^{NH₂} U ^D T-	319	510	11740	0.298	44.0	56.1

* ϵ obtained from the literature.³⁷

2.15.2 PNA:RNA duplexes

The values of derived local ϵ for PNA:RNA hybrids are shown in Table 10. It was observed that in the major groove of the PNA-2:RNA duplex (-TU^DT-) having U-dansyl flanked by two hydrophobic thymines, the local dielectric constant was **35.9D**. This was considerably less compared to **39.5D** of PNA-2:DNA duplex (-TU^DT-) and also less than DNA:DNA duplexes suggesting it is less polar as compared to PNA:DNA and DNA:DNA duplexes.

Upon replacing one of thymines by unsubstituted uracil, the local dielectric constant increased to **38.7D** in PNA-3:RNA duplex (-UU^DT-), while replacing both adjacent thymines by uracil in PNA-4:RNA duplex (-UU^DU-), the local dielectric constant was further enhanced to **44.1D**. The local dielectric constant increased to **52.5D** after replacing both thymines with hydrophilic 5-aminouracil as in PNA-5:RNA

duplex ($-\text{U}^{\text{NH}_2}\text{U}^{\text{D}}\text{U}^{\text{NH}_2}-$). When one thymine was replaced with 5-aminouracil, the local dielectric constant was found to be **46.3D** in PNA-6:RNA duplex ($-\text{U}^{\text{NH}_2}\text{U}^{\text{D}}\text{T}-$).

In comparison with local polarity of PNA/DNA duplexes, it was found that PNA/RNA duplexes derived from PNAs 4-6 were more polar. This result may arise from the 2' hydroxyl group present in the major groove of RNA which enhances the local polarity of PNA/RNA duplexes. The results overall indicated that the local dielectric constant of PNA:RNA duplexes changes with the change in local sequence except PNAs-2:RNA and PNA-3:RNA duplex. The probable reason behind this anomalous behavior is not yet predicted. Figure 34 shows the fluorescence spectra of PNA:DNA duplexes and plot for the determination of dielectric constant of PNA:RNA duplexes.

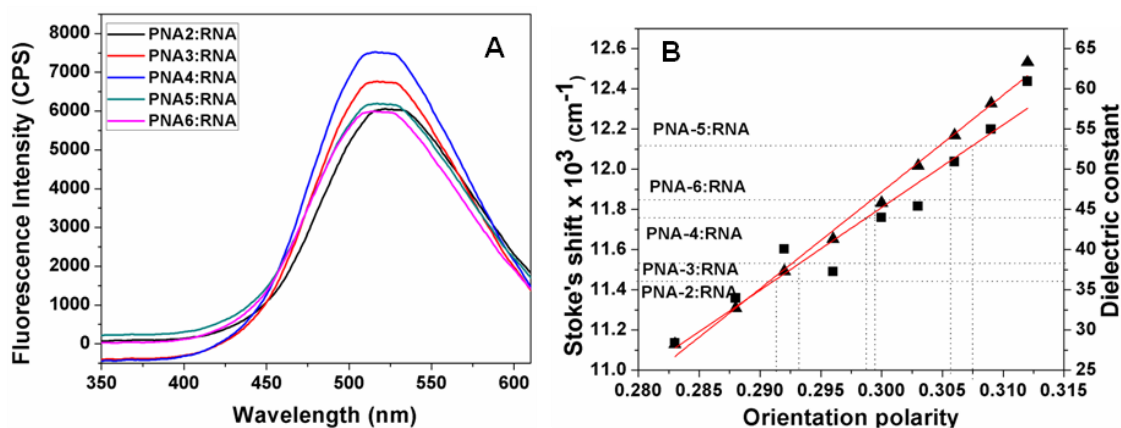


Figure 34. Combined plot of Stokes shift (■) versus orientation polarity and dielectric constant (▲) versus orientation polarity of PNA:RNA duplexes. Fluorescence measurements were recorded in 10 mM phosphate buffer (pH 7.2) containing 10 mM NaCl.

Table 10: Dielectric constants of PNA:RNA duplexes.

PNA No.	PNA	λ_{ex} (nm)	λ_{em} (nm)	Stoke's shift (cm ⁻¹)	Orientation polarity (f)	Dielectric constant (ε)
PNA-2	$-\text{TU}^{\text{D}}\text{T}-$	327	522	11424	0.290	35.9
PNA-3	$-\text{UU}^{\text{D}}\text{T}-$	324	517	11522	0.293	38.7
PNA-4	$-\text{UU}^{\text{D}}\text{U}-$	321	516	11773	0.298	44.1
PNA-5	$-\text{U}^{\text{NH}_2}\text{U}^{\text{D}}\text{U}^{\text{NH}_2}-$	318	517	12104	0.307	52.5
PNA-6	$-\text{U}^{\text{NH}_2}\text{U}^{\text{D}}\text{T}-$	320	515	11833	0.301	46.3

2.15.3 PNA:PNA duplexes

The local dielectric constants of PNA:PNA duplexes are given in Table 11. It was observed that in the PNA-2:PNA-7 duplex (-**TU^DT**-) having U-dansyl flanked by two thymines, the local dielectric constant was **28.8D** which is much lower compared to dielectric constant of **39.5D** of PNA-2:DNA duplex and **35.9D** of PNA-2:RNA duplex. This dielectric constant was also found to be less than dielectric constant (**40.0D**) of DNA:DNA duplexes reported by Ganesh et al.³⁷

When one of the thymines was replaced by unsubstituted uracil, the local dielectric constant increased to **32.0D** in PNA-3:PNA-7 duplex (-**UU^DT**-) and upon replacing both thymines by uracil, the local dielectric constant was further enhanced to **35.9D** in PNA-4:PNA-7 duplex (-**UU^DU**-). Replacing both thymines with hydrophilic 5-aminouracil as in PNA-5:PNA-7 duplex (-**U^{NH₂}U^DU^{NH₂}**-), the local dielectric constant increased to **43.1D** and when only one thymine was replaced by 5-aminouracil, the local dielectric constant was found to be **39.4D** in PNA-6:PNA-7 duplex (-**U^{NH₂}U^DT**-).

The comparative data on dielectric constants of PNA:PNA duplexes indicates that the polarity of major groove in PNA:PNA duplexes is dependent on local environment. Figure 35 shows the fluorescence spectra of PNA:PNA duplexes and plot for the determination of dielectric constant of PNA:PNA duplexes.

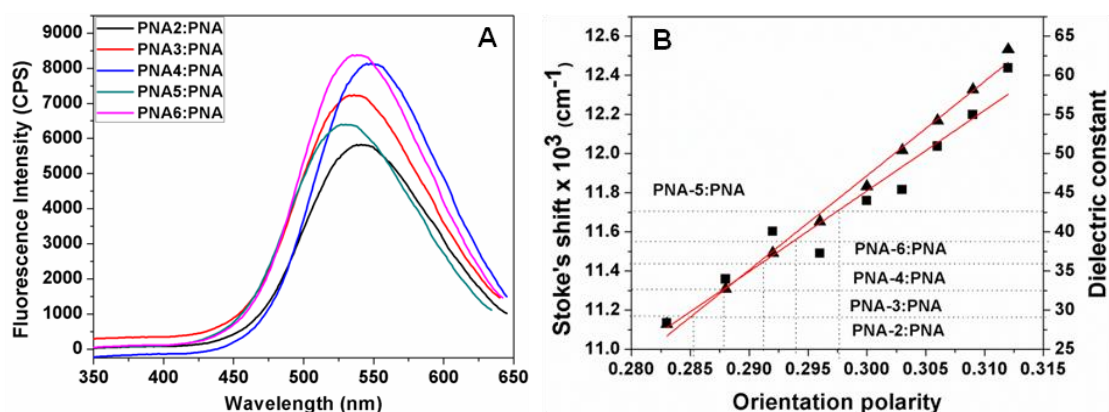


Figure 35. A) Fluorescence spectra of PNA:PNA duplexes and B) Combined plot of Stokes shift (■) versus orientation polarity and dielectric constant (◄) versus orientation polarity of PNA:PNA duplexes. Fluorescence measurements were recorded in 10 mM phosphate buffer (pH 7.2) containing 10 mM NaCl.

Table 11: Dielectric constants of PNA:PNA duplexes.

PNA No.	PNA	λ_{ex} (nm)	λ_{em} (nm)	Stoke's shift (cm-1)	Orientation polarity (f)	Dielectric constant (ϵ)
PNA-2	-T ^U T-	337	541	11189	0.284	28.8
PNA-3	-U ^U T-	334	536	11284	0.287	32.0
PNA-4	-U ^U U-	337	548	11425	0.290	35.9
PNA-5	-U ^{NH₂} U ^D U ^{NH₂} -	327	530	11714	0.297	43.1
PNA-6	-U ^{NH₂} U ^D T-	332	538	11587	0.294	39.4

2.16 Comparison between dielectric constants of PNA:DNA, PNA:RNA, PNA:PNA and DNA:DNA duplexes

The comparative local dielectric constants of PNA:DNA, PNA:RNA and PNA:PNA duplexes measured from Stokes shift of U-dansyl probe indicated that the dielectric constant in these duplexes is sequence selective and varies with local environment. The local dielectric constant in PNA:PNA duplexes increases when U-dansyl fluorophore is flanked by relatively more hydrophilic uracil/5-aminouracil (U/U^{NH₂}) in comparison with that flanked by hydrophobic thymine. This observation of increasing trend of dielectric constants is similar in PNA:DNA, PNA:RNA and PNA:PNA duplexes.

The major groove in PNA:PNA duplexes was found to be more nonpolar when local environment surrounding the U-dansyl fluorophore is hydrophobic whereas more polar when local environment is hydrophilic with flanking U/U^{NH₂}. The major groove in PNA:DNA duplexes is also nonpolar (**39.5D**) when local environment is hydrophobic and more polar when local environment is hydrophilic (**50.7D**). The major groove in PNA:RNA duplexes showed trend (**35.9D**) similar to PNA:PNA and PNA:DNA duplexes with U-dansyl fluorophore is surrounded by thymine being nonpolar and relatively polar when U-dansyl fluorophore surrounded by hydrophilic U^{NH₂} (**52.5D**).

When the dielectric constant of PNA:DNA, PNA:RNA and PNA:PNA duplexes were compared with the dielectric constant of DNA:DNA duplexes,³⁷ it was found that the major groove of DNA:DNA duplexes is more polar as compared to these duplexes. The dielectric constants of PNA:DNA and PNA:RNA duplexes were found to be less or equal to dielectric constant of DNA:DNA duplexes and that of PNA:PNA duplexes

were very less than DNA:DNA duplexes (Figure 36). The comparison of dielectric constant of PNA:DNA, PNA:RNA, PNA:PNA and DNA:DNA duplexes is given in Table 12.

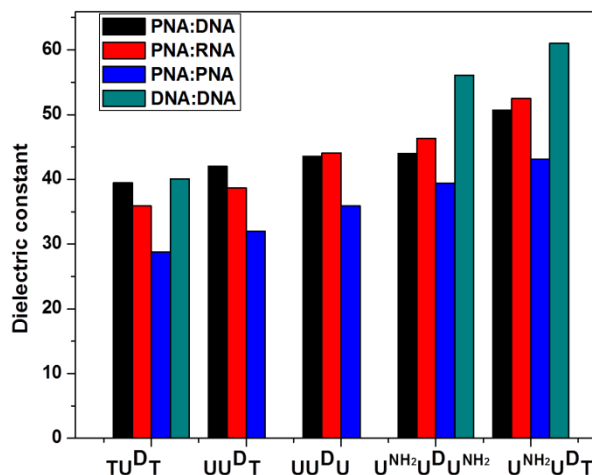


Figure 36. Comparison of dielectric constants of DNA:DNA, PNA:DNA/RNA/PNA duplexes.

Table 12: Comparison of dielectric constants

Duplex	-TU ^D T-	-UU ^D T-	-UU ^D U-	-U ^{NH₂} U ^D T-	-U ^{NH₂} U ^D U ^{NH₂} -
PNA:PNA	28.8	32.0	35.9	39.4	43.1
PNA:DNA	39.5	42.0	43.6	44.0	50.7
PNA:RNA	35.9	38.7	44.1	46.3	52.5
DNA:DNA*	40.1	-	-	56.1	61.0

* Values are taken from the literature.³⁷

2.17 Summary

In summary, this chapter describes the synthesis of different PNA monomers carrying hydrophobic, hydrophilic and U-dansyl modified nucleobases and their incorporation into PNA oligomers followed by the polarity determination of PNA:DNA/RNA/PNA duplexes and their comparison with DNA:DNA duplexes (Figure 37). Results showed that major groove of PNA:PNA duplexes are comparatively nonpolar as compared to PNA:DNA, PNA:RNA and DNA:DNA duplexes. Results also showed that major groove of DNA:DNA duplexes is more polar as compared to PNA:DNA/RNA/PNA duplexes. This may be due to the hydrophobic backbone of PNA as compared to DNA and RNA. Thus, Backbone also plays an important role in dielectric constant.

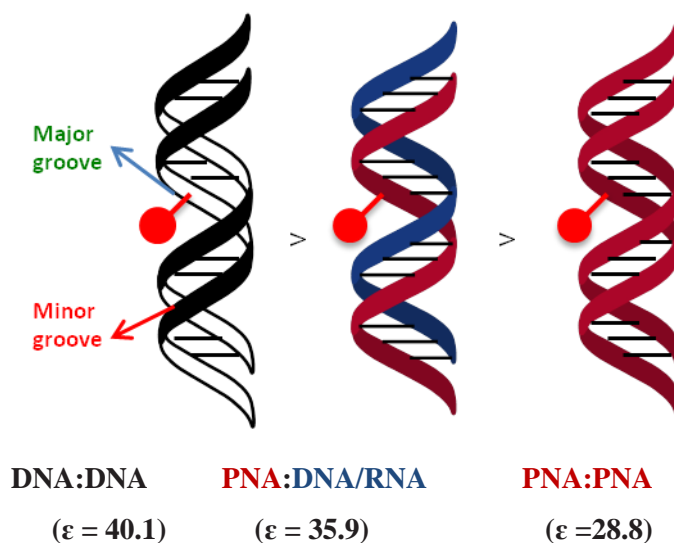


Figure 37. Comparison of polarity of DNA:DNA and PNA:DNA/RNA/PNA duplexes.

2.18 Experimental methods

2.18.1 Chemicals

The chemicals used were of laboratory or analytical grade. All the solvents used were distilled or dried to carry out various reactions. Reactions were monitored using thin layer chromatography (TLC). Usual workup involved sequential washing of the organic extract with water and brine followed by drying the organic layer over anhydrous sodium sulphate and evaporation of solvent under vacuum. TLCs were carried out on pre-coated silica gel GF₂₅₄ sheets (Merck 5554). TLCs were analysed under UV lamp, by Iodine spray and by spraying with Ninhydrin solution, followed by heating of the plate. Column chromatographic separations were performed using silica gel (60-120 or 100-200 mesh).

2.18.2 Instrumentation

¹H and ¹³C NMR spectra were recorded using Bruker AC-200 (200 MHz) or JEOL 400 MHz NMR spectrometers. The delta (δ) values for chemical shifts are reported in ppm and are referred to internal standard TMS or deuterated NMR solvents. Mass spectra for reaction intermediates were obtained by Applied Biosystems 4800 Plus MALDI-TOF/TOF mass spectrometry using TiO₂ or 2,5-dihydroxybenzoic acid (DHB) and the integrity of PNA oligomer was checked on the same instrument using

DHB or CHCA as matrix. High resolution mass spectra for final PNA monomers were recorded on Synapt G2 High Definition Mass Spectrometry. PNA oligomers were purified on Dionex ICS 3000 HPLC system using semi-preparative BEH130 C18 (10X250 mm) column. Absorption spectra were recorded on a Shimadzu UV-2600 spectrophotometer. UV thermal melting analysis of duplexes was performed on a Cary 300 Bio UV-Vis spectrophotometer. Fluorescence experiments were carried out in a micro fluorescence cuvette (Hellma, path length 1.0 cm) on a Fluoromax-4 spectrofluorometer (Horiba Scientific).

2.18.3 Solid phase protocol

MBHA resin hydrochloride salt was neutralized in 50% DIPEA/DCM followed by coupling with 3 equivalents of (Boc/Cl-Cbz) L-lysine, coupling agent HBTU, racemization suppressor HOBt and DIPEA as base to get lysine coupled resin. To avoid deletion of sequences, resin was capped by Ac₂O/Pyridine. The resin was tested by ninhydrin solution to check whether any free amine is present. The observation of no color to the resin was the confirmation that no free amine group is bound to the resin. This was followed by washing of resin several times with DCM and then diethyl ether. The resin bound Boc group was knocked out by using 50% TFA/DCM, followed by neutralization with 10% DIPEA/DCM to get the free amine. The free amine bound resin was tested in ninhydrin solution followed by heating, which showed the blue colored resin indicating presence of free amine. The free amine was coupled with *aeg* PNA monomers and heated under microwave condition, which was washed with DMF and DCM. The resin was again tested in ninhydrin. The polyamide oligomers were cleaved from the resin at final stage using TFA and TFMSA.

2.18.4 Purification of the PNA oligomers by RP-HPLC

PNA purification was carried out on Dionex ICS 3000 HPLC system. For the purification of peptides, semi-preparative BEH130 C18 (10X250 mm) column was used. Purification of PNA oligomers was performed with gradient elution method: A to 50% B in 10 min, 11-20 min: 100% B, 21-25 min: 100% B, 26-30 min: 100% A; A= 0.1% TFA in CH₃CN:H₂O (5:95); B= 0.1% TFA in CH₃CN:H₂O (1:1) with flow rate of 2 mL/min. All the HPLC profiles were monitored at 254 nm wavelength. Fluorescent PNA oligomers were monitored on both 254 and 310 nm wavelengths.

2.19 Biophysical studies

2.19.1 UV- T_m measurements

UV-melting experiments were carried out on Varian Cary 300 UV-spectrophotometer equipped with a peltier. The samples for T_m measurement were prepared by mixing the calculated amounts of respective oligonucleotides in stoichiometric ratio (1:1, for duplex) in sodium phosphate buffer (10 mM) and NaCl (10 mM); pH 7.2 to achieve a final strand concentration of 2 μ M for each strand. The samples were annealed by heating at 90 °C for 5 min. followed by slow cooling to room temperature and then storing at 4 °C. The samples (500 μ L) were transferred to quartz cell and equilibrated at the starting temperature for 2 min. The OD at 260 nm was recorded in steps from 20-90 °C with temperature increment of 1 °C/min. Each melting experiment was repeated at least twice. The normalized absorbance at 260 nm was plotted as a function of the temperature. The T_m was determined from the first derivative of normalized absorbance with respect to temperature and is accurate to \pm 0.5 °C. The data was processed using Microcal Origin 8.0/8.5. [The concentration of all oligonucleotides were calculated on the basis of absorbance from the molar extinction coefficients of the corresponding nucleobases i.e. T = 8.8 cm²/ μ mol; C = 7.3 cm²/ μ mol; G = 11.7 cm²/ μ mol and A = 15.4 cm²/ μ mol].

2.19.2 Circular dichroism

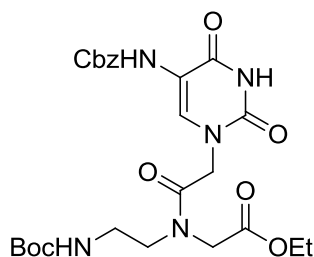
CD spectra were recorded on JASCO J-815 spectropolarimeter connected with a peltier. The calculated amounts for PNA oligomers and the complementary DNA/RNA/PNA were mixed together in stoichiometric ratio (1:1, for duplex) in sodium phosphate buffer (10 mM) and NaCl (10 mM); pH 7.2 to achieve a final strand concentration of 5 μ M for each strand. The samples were annealed by heating at 90 °C for 5 min. followed by slow cooling to room temperature and then transferred to refrigerator for at least 4 to 5 h. To record the CD spectra of PNA:DNA/RNA/PNA duplexes and single stranded PNAs, the temperature of circulating water was kept at 25 °C. The CD spectra were recorded as an accumulation of 10 scans from 350 to 190 nm using 2 mm cell, a resolution of 0.1 nm, band-width of 1 nm, sensitivity of 2 m deg, response of 2 sec and a scan speed of 50 nm/min.

2.19.3 UV-visible and fluorescence studies

UV-Visible spectra for all PNA oligomers and complementary oligonucleotides were recorded on Shimadzu UV-2600 spectrophotometer and for fluorescence studies, experiments were performed on Horiba Jobin Yvon Fluorolog 3 spectrophotometer. The samples for fluorescence spectra were prepared by mixing calculated amounts of PNA and DNA/RNA/PNA in stoichiometric ratio (1:1, for duplex) in sodium phosphate buffer (10 mM) and NaCl (10 mM); pH 7.2 to achieve a final strand concentration of 5 μ M for each strand. The annealed samples were used to record fluorescence spectra in a rectangular quartz cell at ambient temperature.

2.20 Procedures and spectral data

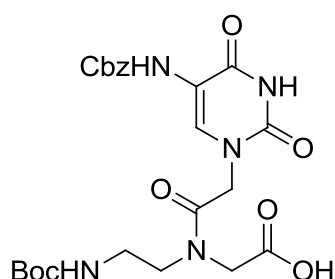
Ethyl 2-(2-(5-(((benzyloxy)carbonyl)amino)-2,4-dioxo-3,4-dihydropyrimidin-1(2H)-yl)-N-(2-(((tert-butoxycarbonyl)amino)ethyl)acetamido)acetate 4



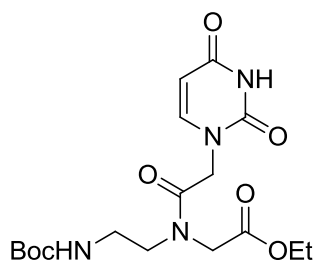
Compound **3** (3 g, 9.3 mmol) was dissolved in dry DMF under inert atmosphere (25 mL) and stirred at 0 °C temperature for 5 min. After 5 min, dry K₂CO₃ and 5-benzyloxyaminouracil (2 g, 9.3 mmol) was added and stirring continued at the same temperature. After 5 min, reaction mixture was moved to oil bath and heated at 60 °C for 2 h. Completion of reaction was monitored by TLC. The hot reaction mixture was allowed to cool at room temperature and then reaction mixture was diluted with water (40 mL) and extracted with ethyl acetate (3 x 75 mL). The combined organic layer was washed with saturated solution of NaHCO₃ (20 mL) and then again washed with water (3 x 40 mL) followed by washing with brine (25 mL). The collected organic layer was dried over anhydrous sodium sulphate, collected by filtration and concentrated on rota evaporator. The crude product was purified on column using silica gel in petroleum ether: ethyl acetate (1.5:3.5) (Yield 3.5 g, 75%). ¹H NMR (400 MHz, CDCl₃) δ : 9.82 (bs, 1H), 8.03 (bs, 1H), 7.44-7.33 (m, 5H), 7.17 (mi.) 7.13 (ma.) (s, 1H), 5.64(bs, 1H),

5.16 (mi.) 5.15 (ma.), (s, 2H), 4.61 (ma.) 4.47 (mi.) (s, 2H,) 4.28 (mi.) 4.20 (ma.) (q, 2H, $J = 8$ Hz), 4.05 (s, 2H), 3.53 (t, 2H, $J = 6$ Hz), 3.33 (t, 2H, $J = 8$ Hz), 1.45 (ma.) 1.43 (mi.) (s, 9H), 1.32 (mi.) 1.27 (ma.) (t, 3H, $J = 6$ Hz) ppm; ^{13}C NMR (100 MHz, CDCl_3) δ : 169.4, 169.0, 167.03, 159.7, 156.1, 152.9, 149.1, 135.7, 129.6, 128.5, 128.1, 114.8, 80.0, 67.3, 62.3, 61.6, 48.8, 38.8, 28.3, 14.0 ppm; MS (HRMS-ESI): m/z calcd for $\text{C}_{25}\text{H}_{33}\text{N}_5\text{O}_9\text{Na}$ 547.2278, found 570.2175 (M+Na), 448.1895 (M-Boc).

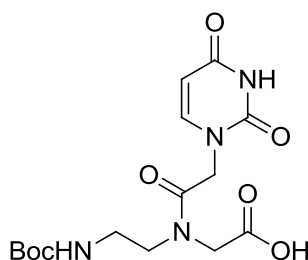
2-(2-(5-(((Benzyloxy)carbonyl)amino)-2,4-dioxo-3,4-dihydropyrimidin-1(2H)-yl)-N-(2-((tert-butoxycarbonyl)amino)ethyl)acetamido)acetic acid 5



Compound **4** (1 g, 2 mmol) was dissolved in ethanol and stirred at 0 °C. To this, 10% LiOH (1.5 mL) was drop wise added at the same temperature for 10 min. The completion of reaction was monitored by TLC. After completion of reaction, solvent was removed on rotary evaporator. Ethyl acetate was added to the residue and it was acidified by addition of saturated aqueous solution of potassium bisulfate till the pH comes down to 3-4. Organic layer was collected and washed with brine solution. The organic layer was concentrated on rota evaporator to get solid product which was further dried on high vacuum and stored in vacuum dessicator (Yield 0.85 g, 90%). ^1H NMR (400 MHz, CD_3OD) δ : 7.93 (d, 1H, $J = 12$ Hz), 7.39-7.30 (m, 5H), 5.15 (ma.) 5.05 (mi.) (s, 2H), 4.77 (ma.), 4.6 (mi.) (s, 2H), 4.26 (mi.) 4.11 (ma.) (s, 2H), 3.52-4.47 (m, 2H), 3.29-3.21 (m, 2H), 1.44 (ma.) 1.42 (mi.) (s, 9H) ppm; ^{13}C NMR (100 MHz, CD_3OD) δ : 173.0, 170.3, 169.9, 162.5, 158.7, 156.1, 151.8, 138.2, 135.0, 129.9, 129.5, 129.4, 115.9, 81.0, 68.4, 49.1, 39.4, 31.1, 29.0 ppm; MS (HRMS-ESI): m/z calcd for $\text{C}_{23}\text{H}_{29}\text{N}_5\text{O}_9$ 547.2278, found 570.2175 (M+Na), 448.1895 (M-Boc).

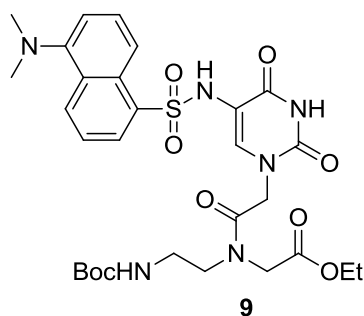
Ethyl 2-(N-(2-((tert-butoxycarbonyl)amino)ethyl)-2-(2,4-dioxo-3,4-dihydropyrimidin-1(2H)-yl)acetamido)acetate 6

Compound **3** (3 g, 9.3 mmol) was dissolved in dry DMF under inert atmosphere (25 mL) and stirred at 0 °C temperature for 5 min. After 5 min, dry K₂CO₃ and uracil (2 g, 9.3 mmol) was added and stirring continued at same temperature for 4 h. Completion of reaction was monitored by TLC. The hot reaction mixture was allowed to cool at room temperature and then reaction mixture was diluted with water (40 mL) and extracted with ethyl acetate (3 x 75 mL). The combined organic layer was washed with saturated solution of NaHCO₃ (20 mL) and then again washed with water (3 x 40 mL) followed by washing with brine (25 mL). The collected organic layer was dried over anhydrous sodium sulphate, collected by filtration and concentrated on rota evaporator. The crude product was purified on column using silica gel in petroleum ether: ethyl acetate (1.5:3.5) (Yield 3.5 g, 75%). ¹H NMR (400 MHz, CDCl₃) δ: 7.21 (mi.) 7.16 (ma.) (d, 1H, J = 10 Hz) 5.73(d, 1H, J = 8 Hz), 5.55 (br, 1H), 4.61 (ma.) 4.46 (mi.) (s, 2H), 4.26-4.18 (m, 2H), 4.05 (s, 2H), 3.54 (t, 2H, J = 6 Hz), 3.33 (t, 2H, J = 8 Hz), 1.45 (ma.) 1.44 (mi.) (s, 9H), 1.33 (mi.) 1.27 (ma.) (t, 3H, J = 6 Hz) ppm. ¹³C NMR (100 MHz, CDCl₃) δ: 169.6, 167.1, 163.5, 155.9, 150.9, 145.0, 102.3, 80.0, 62.3, 61.7, 49.1, 47.8, 38.6, 28.3, 14.0 ppm. MS (HRMS-ESI): m/z calcd for C₁₇H₂₆N₄O₇Na 421.1698, found 421.1696, 299.1355 (M-Boc).

2-(N-(2-((tert-butoxycarbonyl)amino)ethyl)-2-(2,4-dioxo-3,4-dihydropyrimidin-1(2H)-yl)acetamido)acetic acid 7

Compound **6** (1 g, 2 mmol) was dissolved in ethanol and stirred at 0 °C. To this, 10% LiOH (1.5 mL) was drop wise added at the same temperature for 10 min. The completion of reaction was monitored by TLC. After completion of reaction, solvent was removed on rotary evaporator. Ethyl acetate was added to the residue and it was acidified by addition of saturated aqueous solution of potassium bisulfate till the pH comes down to 3-4. Organic layer was collected and washed with brine solution. The organic layer was concentrated on rota evaporator to get solid product which was further dried on high vacuum and stored in vacuum dessicator (Yield 0.85 g, 90%). ¹H NMR (400 MHz, CD₃OD) δ: 7.46 (ma.) 7.43 (mi.) (d, 1H, *J* = 6 Hz), 5.67 (d, 1H, *J* = 8 Hz), 4.78 (ma.), 4.6 (mi.) (s, 2H), 4.28 (mi.) 4.11 (ma.) (s, 2H), 3.53-4.45 (m, 2H), 3.30-3.21 (m, 2H), 1.44 (ma.) 1.43 (mi.) (s, 9H) ppm; ¹³C NMR (100 MHz, CD₃OD) δ: 171.2, 168.6, 168.2, 165.5, 157.1, 151.4, 146.5, 100.8, 79.2, 48.2, 38.0, 27.3 ppm; MS (HRMS-ESI): *m/z* calcd for C₁₅H₂₂N₄O₇Na 393.1385, found 393.1386, 271.1041 (M-Boc).

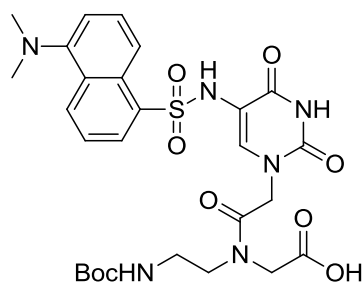
Ethyl-2-(N-(2-((tert-butoxycarbonyl)amino)ethyl)-2-(5-(5-(dimethylamino)naphthalene-1-sulfonamido)-2,4-dioxo-3,4-dihydropyrimidin-1(2H)-yl)acetamido)acetate **9**



To the Compound **4** (3 g, 6 mmol) dissolved in ethanol, 10 % Pd/C on charcoal was added under H₂ atmosphere and stirred at room temperature for 6 h. The completion of reaction was monitored by TLC. The reaction mixture was filtered on celite-545 pad and filtrate was collected, evaporated to get solid product. This compound was dissolved in DMF and kept at 0 °C for 5 min. To the resultant solution, saturated aqueous sodium bicarbonate solution and dansyl chloride was added and stirring continued for half an hour. The completion of the reaction was monitored by TLC. After completion of reaction, reaction mixture was diluted with water (40 mL) and

extracted with ethyl acetate (3 x 75 mL) washed with brine (25 mL). The collected organic layer was dried over anhydrous sodium sulphate, collected by filtration and concentrated on rota evaporator. The crude product was purified on column using silica gel in petroleum ether: ethyl acetate (1:4) (Yield 3.5 g, 75%). ^1H NMR (400 MHz, CDCl_3) δ : 8.66 (br, 1H), 8.42 (br, 1H), 8.21 (mi.) 8.17 (ma.) (d, 1H, $J = 8$ Hz), 7.63-7.52 (m, 3H), 4.60 (ma.) 4.45 (mi.) (s, 2H,) 4.30- 4.21 (m, 2H, $J = 8$ Hz), 4.16-4.06 (m, 2H), 3.52 (t, 2H, $J = 8$ Hz), 3.33 (m, 2H,), 2.98 (2s, 6H), 2.08 (mi.) 2.06 (ma.) (br, 1H), 1.47 (ma.) 1.44 (mi.) (s, 9H), 1.33 (t, 3H, $J = 6$ Hz) ppm; ^{13}C NMR (100 MHz, CDCl_3) δ : 169.6, 166.8, 160.2, 156.2, 149.5, 134.1, 130.2, 129.7, 128.5, 112.5, 80.1, 62.4, 61.8, 49.1, 48.7, 45.6, 38.8, 28.4, 14.2 ppm; MS (HRMS-ESI): m/z calcd for $\text{C}_{29}\text{H}_{39}\text{N}_6\text{O}_9\text{S}$ 646.2421, found 647.25 (M+H), 547.1971 (M-Boc).

2-(N-(2-((tert-butoxycarbonyl)amino)ethyl)-2-(5-(5-(dimethylamino)naphthalene-1-sulfonamido)-2,4-dioxo-3,4-dihydropyrimidin-1(2H)-yl)acetamido)acetic acid 10



Compound **9** (1 g, 2 mmol) was dissolved in ethanol and stirred at 0 °C. To this, 10% LiOH (1.5 mL) was drop wise added at the same temperature for 10 min. The completion of reaction was monitored by TLC. After completion of reaction, solvent was removed on rotary evaporator. Ethyl acetate was added to the residue and it was acidified by addition of saturated aqueous solution of potassium bisulfate till the pH comes down to 3-4. Organic layer was collected and washed with brine solution. The organic layer was concentrated on rota evaporator to get solid product which was further dried on high vacuum and stored in vacuum dessicator (Yield 0.85 g, 90%). ^1H NMR (400 MHz, CDCl_3) δ : 8.53 (d, 1H, $J = 12$ Hz), 8.42 (d, 1H, $J = 8$ Hz), 8.20 (d, 1H, $J = 8$ Hz), 7.57-7.48 (m, 3H), 7.22 (d, 1H, $J = 8$ Hz), 4.73 (ma.) 4.56 (mi.) (s, 2H), 4.23 (mi.) 4.1 (ma.) (s, 2H,), (m, 2H), 3.48 (t, 2H, $J = 6$ Hz), 3.19 (t, 2H,), 2.85 (s, 6H), 1.99 (mi.) 1.97 (ma.) (s, 1H), 1.43 (ma.) 1.41 (mi.) (s, 9H), 1.33 (t, 3H, $J = 6$ Hz) ppm;

^{13}C NMR (100 MHz, CDCl_3) δ : 172.8, 169.3, 162.6, 158.6, 153.0, 151.9, 142.3, 136.7, 131.1, 129.2, 124.4, 121.2, 116.5, 113.4, 86.8, 50.03, 45.9, 39.4, 30.9, 28.9 ppm; MS (HRMS-ESI): m/z calcd for $\text{C}_{27}\text{H}_{35}\text{N}_6\text{O}_9\text{S}$ 618.2108, found 619.2183 (M+H), 519.1659 (M-Boc).

2.21 References

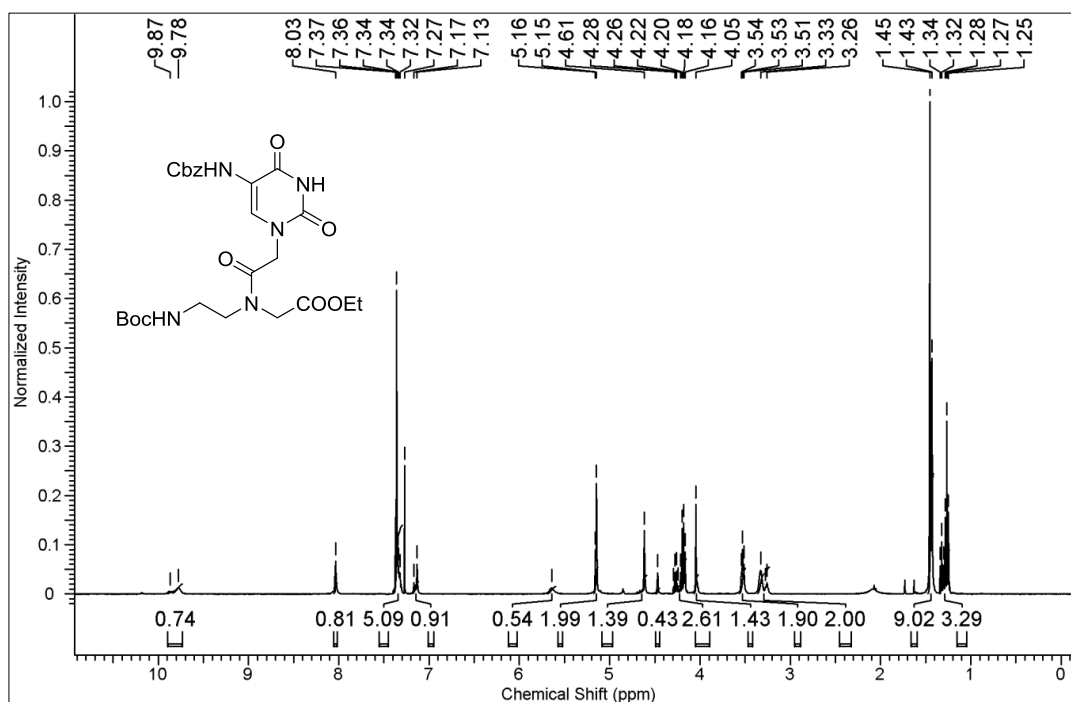
1. Nielsen, P. E.; *Acc. Chem. Res.* **1999**, *32*, 624-630.
2. (a) Watson, J. D.; Crick, F. H. C. *Nature*, **1953**, *171*, 737-738; (b) Crick, F. H. C. *J. Mol. Biol.* **1966**, *19*, 548-555; (c) Soll, D.; Cherayil, J. D.; Bock, R. M. *J. Mol. Biol.* **1967**, *29*, 97-112.
3. Dickerson, R. E. *Sci. Amer.* **1983**, *249*, 94-111.
4. *Molecular biology of gene*, chapter 6, page 10.
5. Seeman, N. C.; Rosenberg, J.M.; and Rich, A. *Proc. Natl. Acad. Sci. USA*, **1976**, *73*, 804-808.
6. Kopka, M. L.; Yoon C.; Goodsell D.; Pjura P.; Dickerson R. E. *Proc. Natl. Acad. Sci. USA*, **1985**, *82*, 1376-1380.
7. Pullman, B.; Pullman, A. *Stud. Biophys.*, **1981**, *86*, 95-102.
8. Bailly, C.; Payet, D.; Travers, A. A.; Waring, M. J. *Proc. Natl. Acad. Sci. USA*, **1996**, *93*, 13623-13628.
9. (a) Lown, J. W., Krowicki, K., Bhat, U. G., Skorobogaty, A., Ward, B., Dabrowiak, J. *C. Biochemistry*, **1986**, *25*, 7408., (b) Paul, A.; Bhattacharya, S. *Current Science*, **2012**, *102*, 212-231.
10. Harshman, K. D.; Dervan, P. B. *Nucl. Acids Res.* **1985**, *13*, 4825-4835.
11. Neidle, S. *Nucleic Acid Structure and Function*, Oxford press, Oxford, **2002**.
12. Alberts, B. *Molecular Biology of the Cell*, 5th Edition, Garland Science, **2008**.
13. Hakoshima, T. *Encyclopedia of Life Sciences*, **2005**, 1-5.
14. Garvie, C. W.; Wolberger C.; *Mol. Cell*, **2001**, *8*, 938-946.
15. Beamer, L. J.; Pabo, C. O. *J. Mol. Biol.* **1992**, *227*, 177-196.
16. a) Nielsen, P. E.; Egholm, M.; Buchardt O. *J. Mol. Recog.* **1994**, *7*, 165-170; b) Cherney, D. Y.; Belotserkovskii, B. P.; Frank-Kamnetskii, M. D.; Egholm, M.; Buchardt O.; Berg, R.H.; Nielsen, P. E. *Proc. Natl. Acad. Sci. USA*, **1993**, *90*, 1667-1670.
17. (a) Arya D. P.; Willis, B. *J. Am. Chem. Soc.* **2003**, *125*, 12398-12399., (b) Arya D. P.; Xue, L.; Willis, B. *J. Am. Chem. Soc.* **2003**, *125*, 10148-10149.

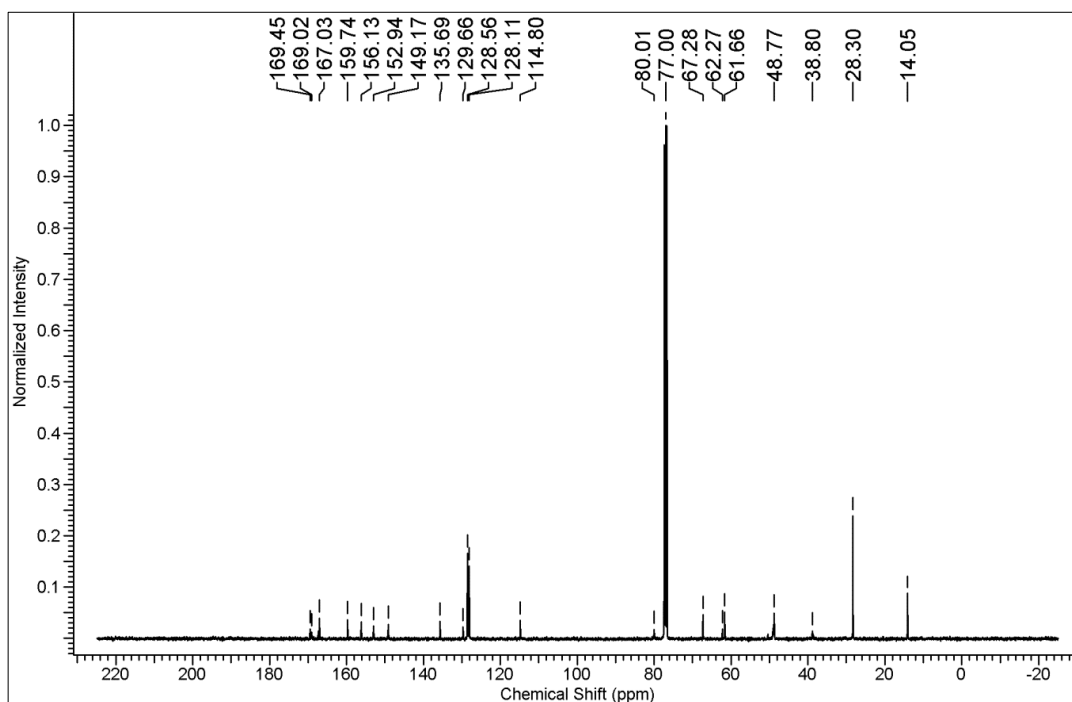
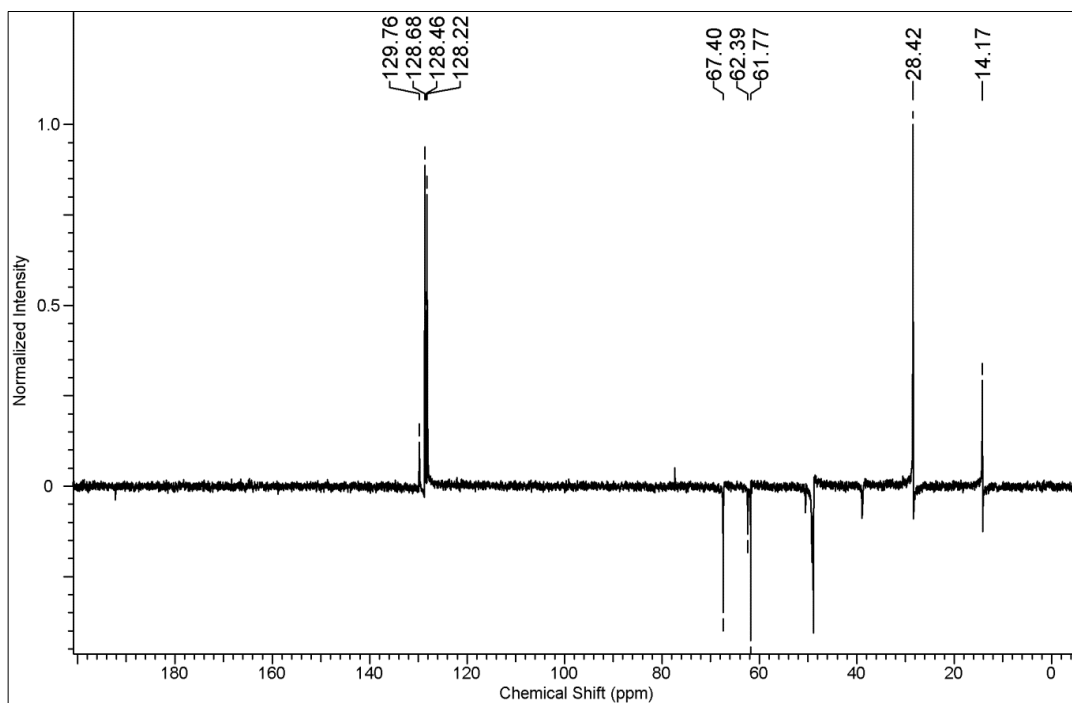
18. Waring, M. J.; Wakelin, L. P. G. *Comprehensive medicinal chemistry*. ed. Sammes, P. G. **1990**, Pergamon press, Oxford.
19. Porumb, H. *Prog. Biophys. Mol. Biol.* **1978**, *34*, 175-195.
20. Neidle, S.; Pearl, L. H.; Skelly, J. V. *Biochem. J.* **1987**, *243*, 1-13.
21. Rao, S. N.; Kollman, P. A. *Proc. Natl. Acad. Sci. USA*, **1987**, *84*, 5735-5739.
22. (a) Helene C.; Garestier, M. T.; Saison, T.; Takasugi, M.; Toulme, J. J.; Thuong, N. T. *Biochimie*, **1985**, *67*, 777-783; (b) Helene, C. *Pure & Appl. Chem.* **1994**, *66*, 663-669.
23. (a) Vlassov, V. V.; Zarytova, V. F.; Kutiyavin, A. V.; Mameav, S. V.; Podyminogin, M. A. *Nucleic Acids Research*, **1986**, *14*, 4065-4076; (b) Vlassov, V. V.; Gaidamakov, S. A.; Zarytova, V. F.; Knorre, D. G.; Levina, A. S.; Nikonova, A. A.; Podust, L. M.; Fedorova, O. S. *Gene*, **1988**, *73*, 313-322.
24. Nielsen, P. E. *Bioconjugate Chem.* **1991**, *2*, 1-12.
25. Bailey, C.; Henichart, J. P. *Bioconjugate Chem.* **1991**, *2*, 379-393.
26. Dervan, P. B. *Nature*, **1992**, *359*, 87-88.
27. Moser, H. E.; Dervan, P. B. *Science*, **1987**, *238*, 645-650.
28. Barawkar, D. A.; Ganesh, K. N. *Nucleic Acids Research*, **1995**, *23*, 159-164.
29. Jin, R.; Breslauer, K. J. *Proc. Natl. Sci. Acad. USA*, **1988**, *85*, 8939-8942.
30. Lamm, G.; Pack, G. R. *J. Phys. Chem.* **1997**, *101*, 959-965.
31. Lakowicz, J. R. *Principles of fluorescence spectroscopy*, Springer, Third edition, page 205-213.
32. Lippert, V. E. *Z Electrochem*, **1957**, *61*, 962-975.
33. Mataga N.; VKaifu Y.; Koizumi M. *Bull. Chem. Soc. Jpn.* **1956**, *29*, 465-470.
34. Bunsel, E.; Rajagopal, S. *Acc. Chem. Res.* **1990**, *23*, 226-231.
35. (a) Dahne, S.; Shob, F.; Nolte, K. D.; Radeaglia, R. *Ukr. Khim. Zh.* **1976**, *41*, 1170-1176; (b) Dahne, S.; Shob, F.; Nolte, K. D.; Radeaglia, R. *Chem. Abstr.* **1976**, *84*, 43086j.
36. Reichardt, C. *Chem. Rev.* **1994**, *94*, 2319-2358.
37. Jadhav, V. R.; Barawkar, D. A.; Ganesh, K. N. *J. Phys. Chem. B*, **1999**, *103*, 7383-7385.
38. T. Kimura, K. Kawai, T. Majima, *Org. Lett.* **2005**, *7*, 5829-5832.
39. T. Kimura, K. Kawai, T. Majima, *Chem. Commun.* **2006**, 1542-1544.
40. A. Okamoto, K. Tainaka, I. Saito, *Bioconjugate Chem.* **2005**, *16*, 1105-1111.
41. Sinkeldam, R. W.; Greco, N. J.; Tor, Y. *ChemBioChem*, **2008**, *9*, 706-709.
42. Nielsen, P. E.; Egholm, M.; Berg, R.H.; Buchardt O. *Science*, **1991**, *254*, 1497-1500.

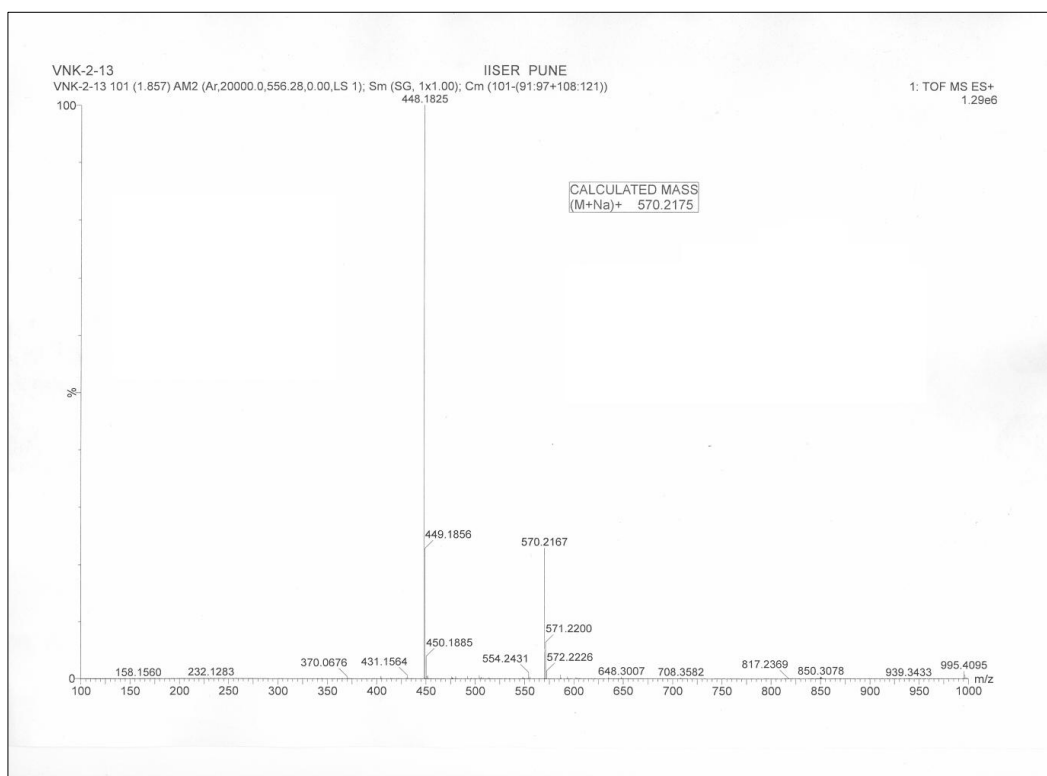
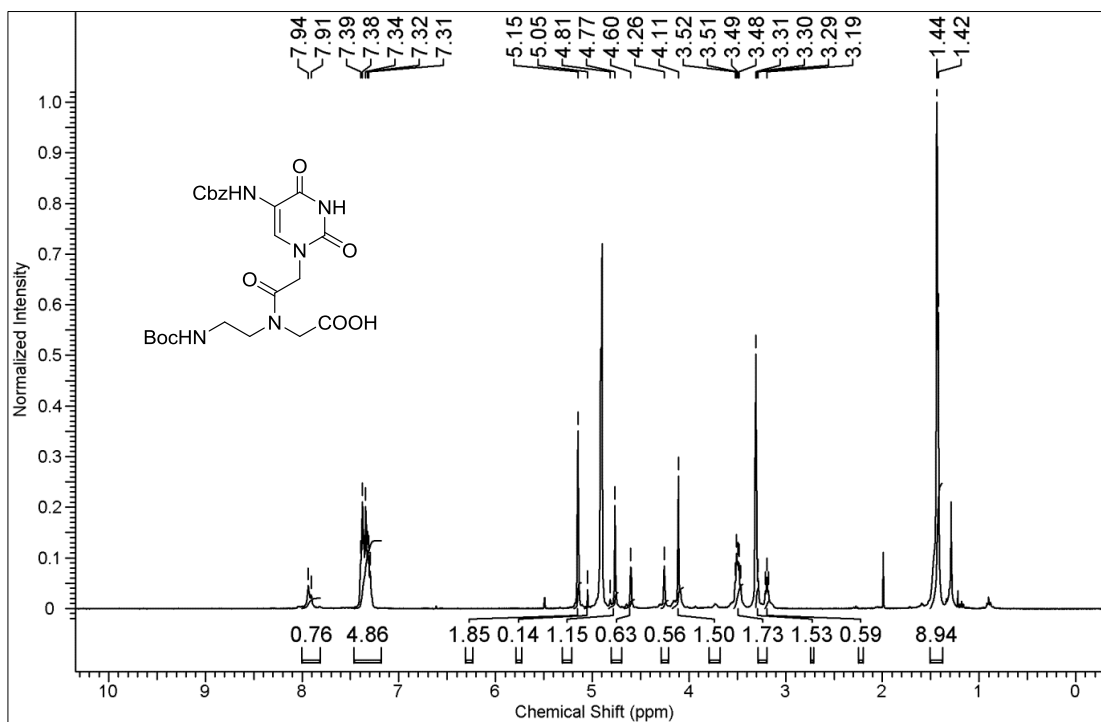
43. (a) Erickson, B. W.; Merrifield, R. B. *Solid Phase Peptide Synthesis. In the Proteins*, Vol. II, 3rd ed.; Neurath, H.; Hill, R. L. eds.; Academic Press, New York, **1976**, 255.
(b) Merrifield, R. B.; Stewart, J. M.; Jernberg, N. *Anal. Chem.* **1966**, *38*, 1905-1914.
44. (a) Kaiser, E.; Colescott, R. L.; Bossinger, C. D.; Cook, P. I. *Anal. Biochem.* **1970**, *34*, 595-598 (b) Kaiser, E.; Bossinger, C. D.; Cplescott, R. L.; Olsen, D. B. *Anal. Chim. Acta.* **1980**, *118*, 149-151; (c) Sarin, V. K.; Kent, S. B. H.; Tam, J. P.; Merrifield, R. B. *Anal. Biochem.* **1981**, *117*, 147-157.
45. Frank, F.; Ives, D. J. G. *Q. Rev. (London)*, **1966**, *20*, 1-45.
46. Wittung, P.; Nielsen, P. E.; Buchardt, O.; Nordbn, B.; *Nature*, **1994**, *368*, 561-563.

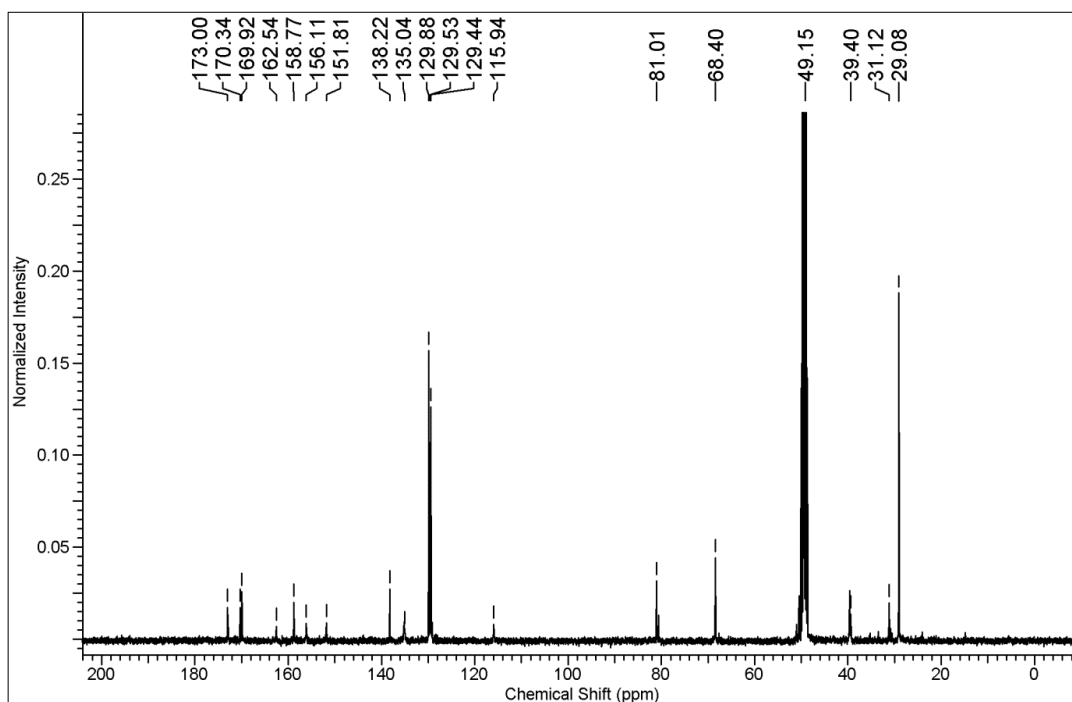
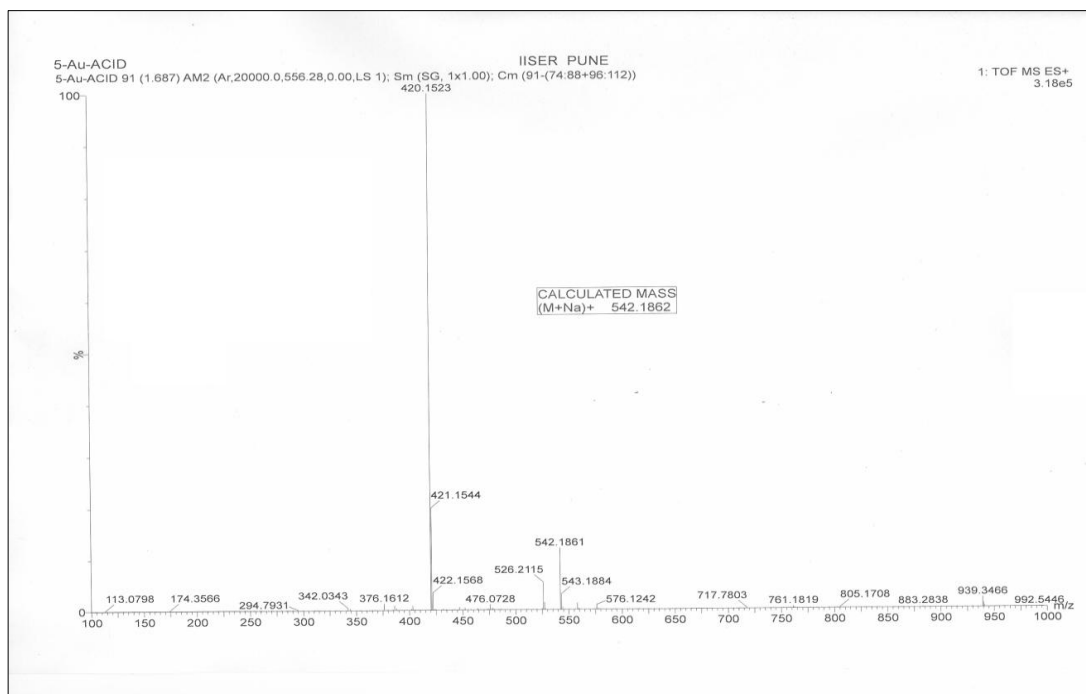
2.18 Appendix II: Characterization data of synthesized compounds/PNA

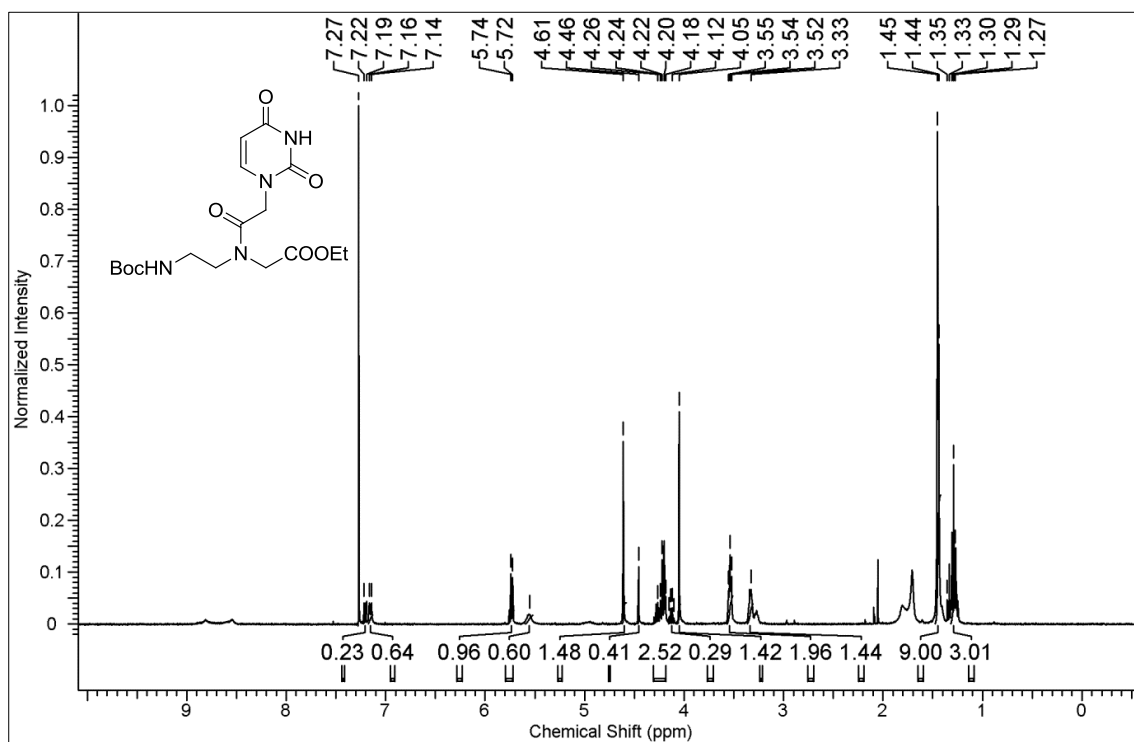
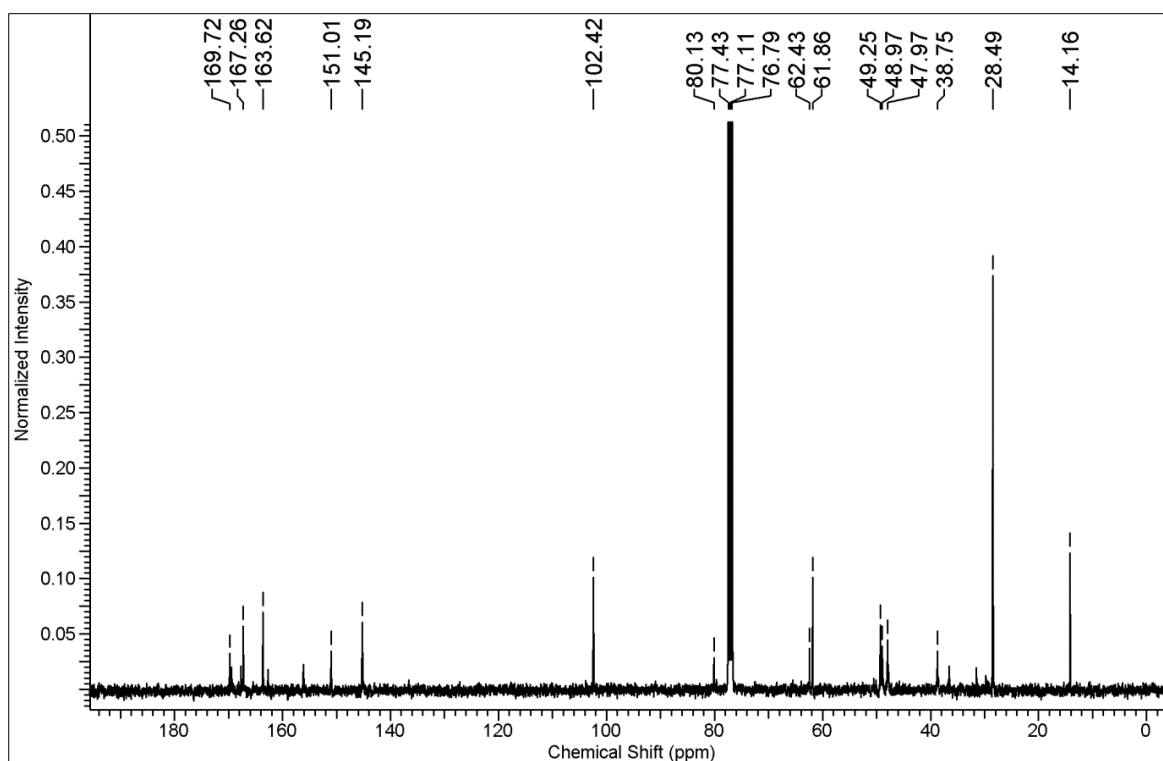
Sr. No.	Description of spectral characterization	Page No.
1	^1H NMR, ^{13}C NMR, HR-MS of all compounds	130-140
2	UV-Vis spectra of compounds 4-9	140
3	HPLC spectra of PNAs 1-7	141-144
4	MALDI-TOF spectra of PNAs 1-7	144-147

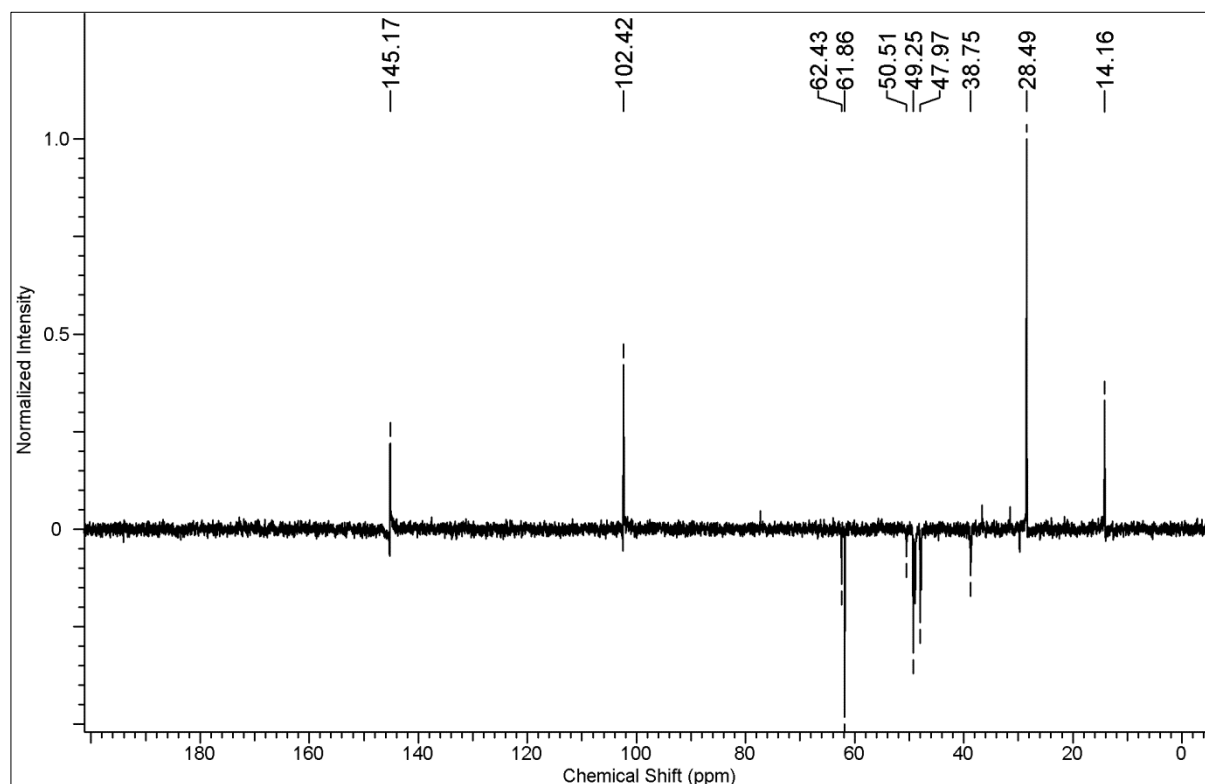
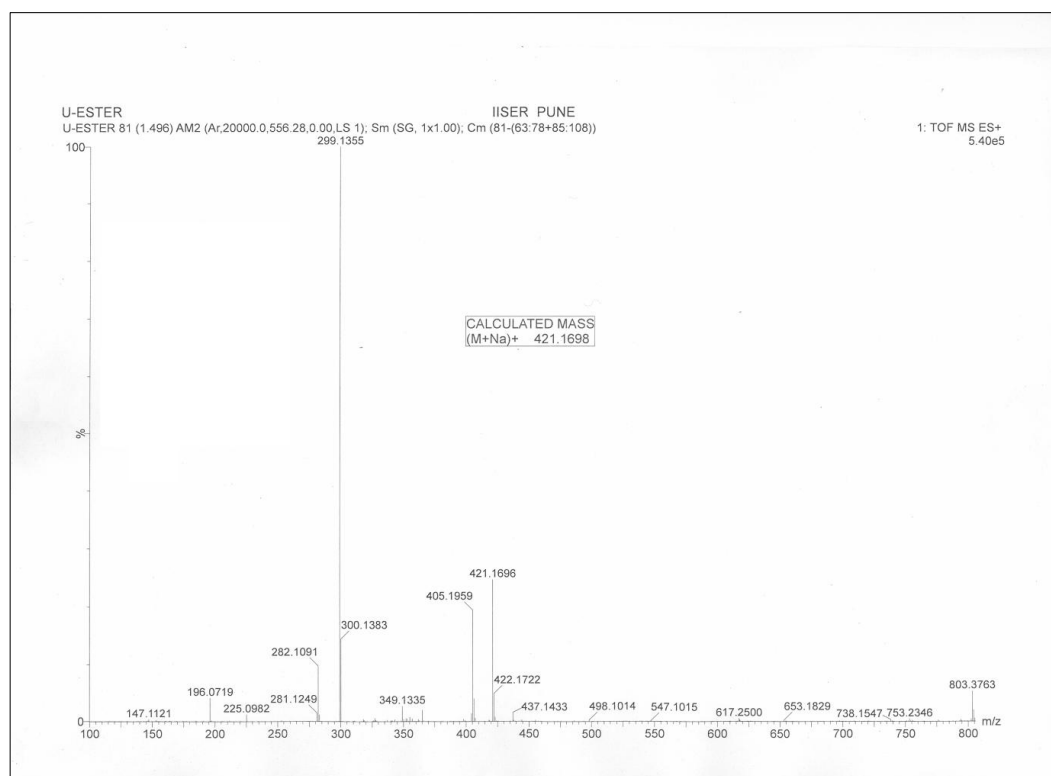
 ^1H NMR of compound 4

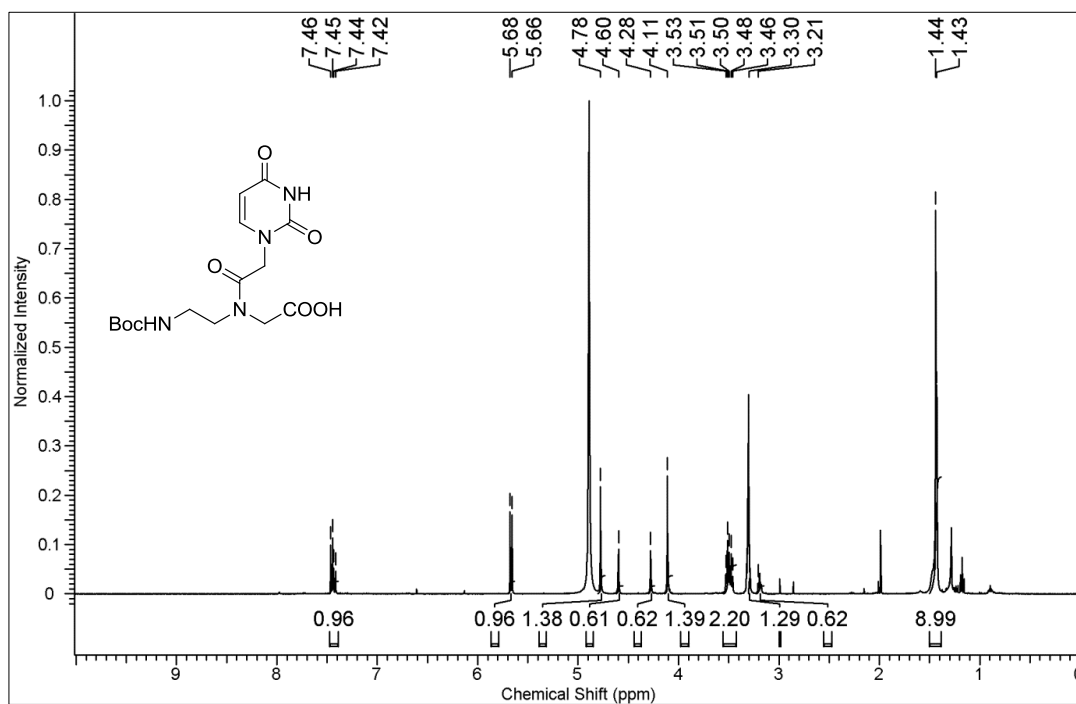
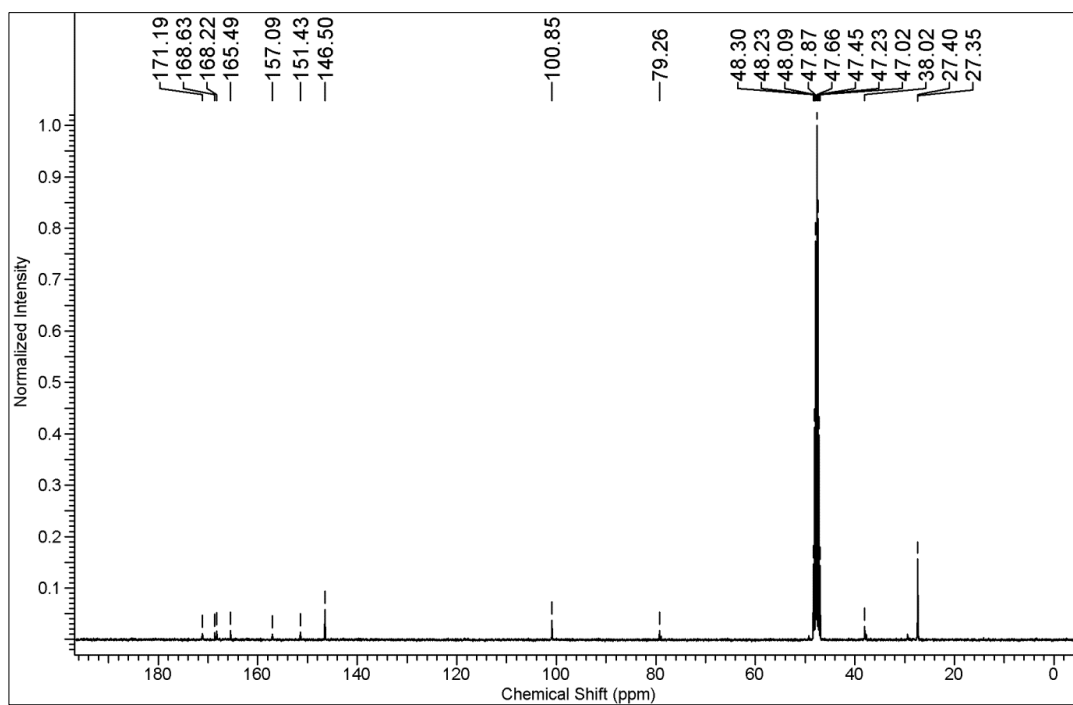
^{13}C NMR of compound 4**DEPT NMR of compound 4**

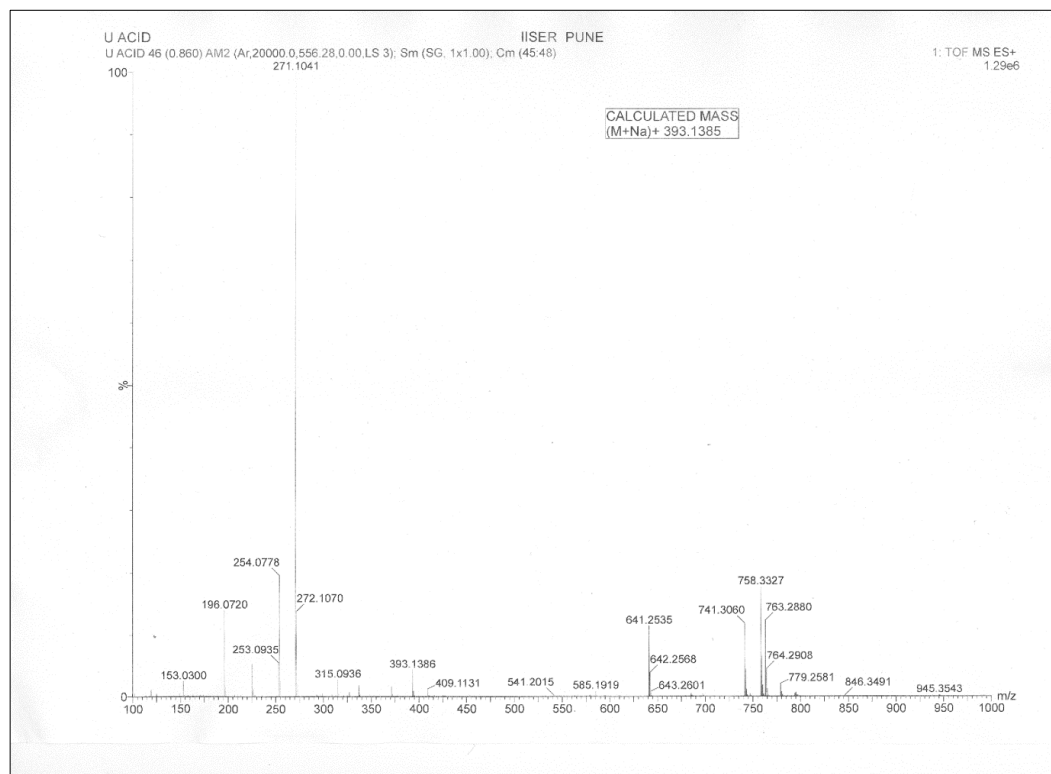
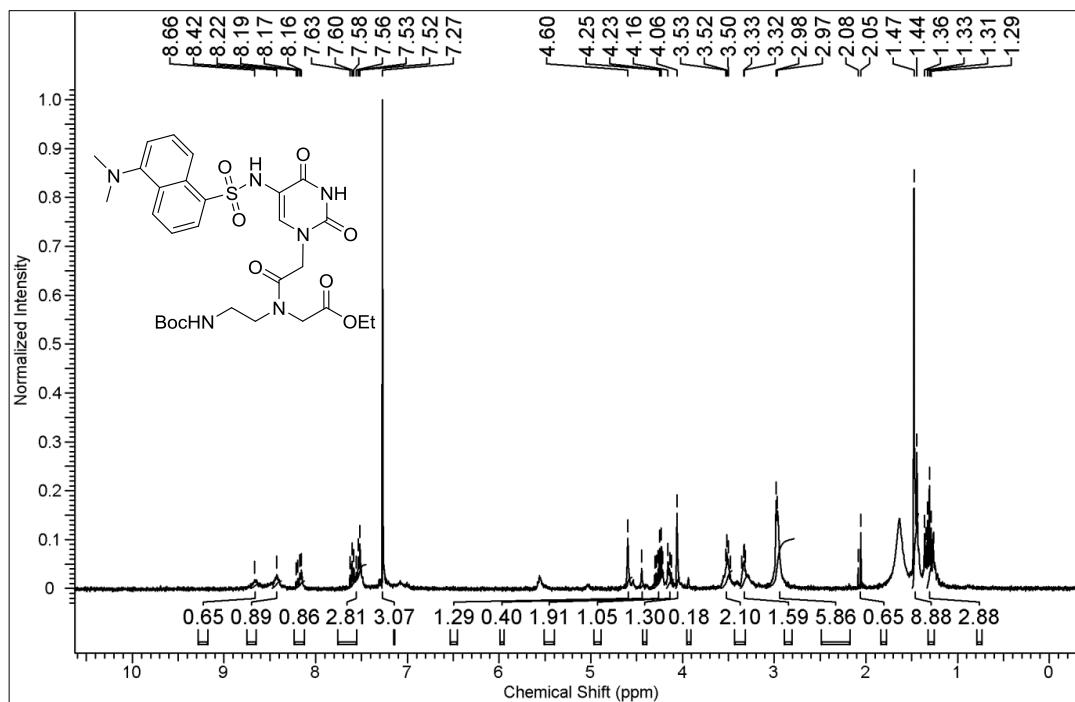
HR-MS (ESI) of compound 4**¹H NMR of compound 5**

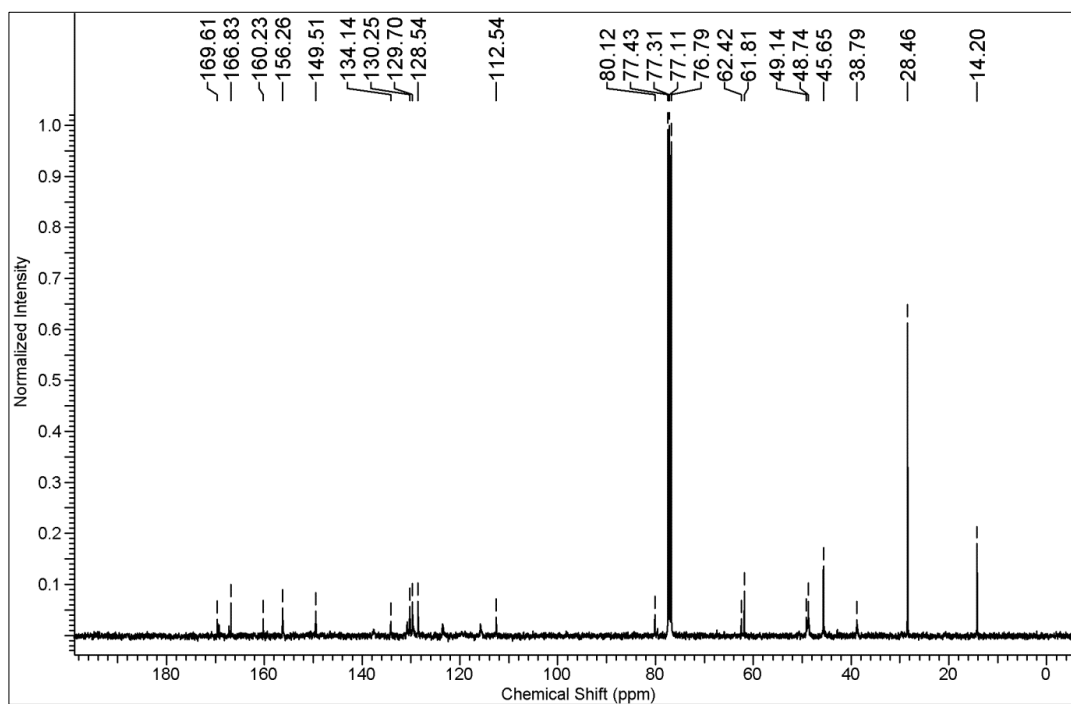
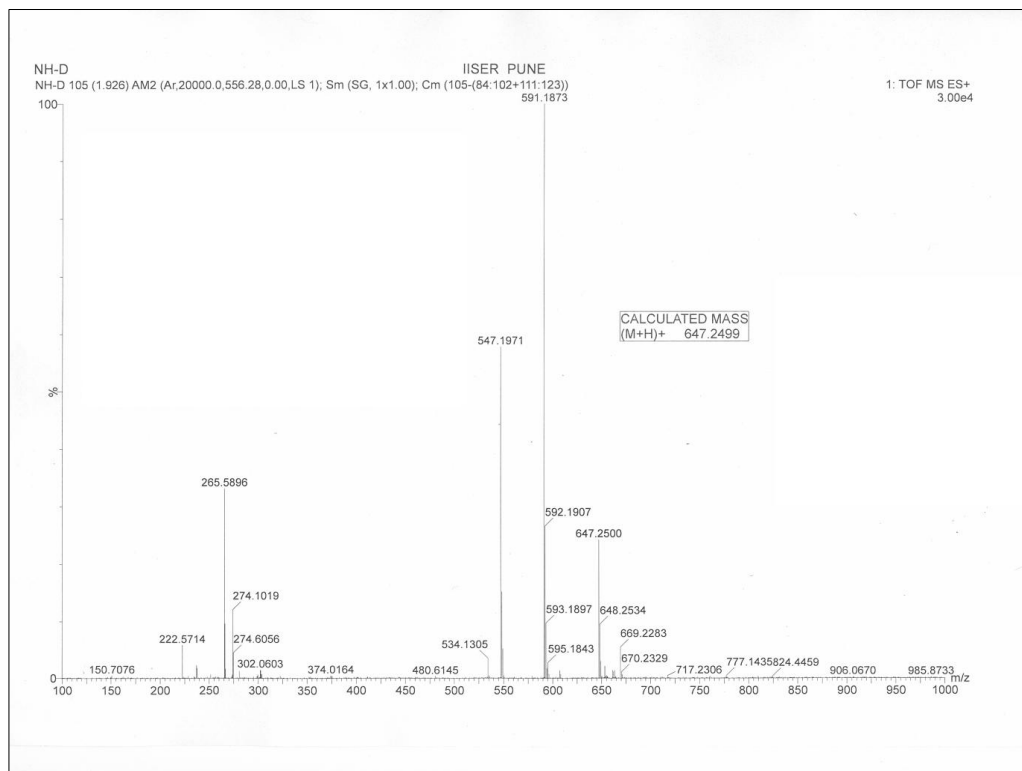
^{13}C NMR of compound 5**HR-MS (ESI) of compound 5**

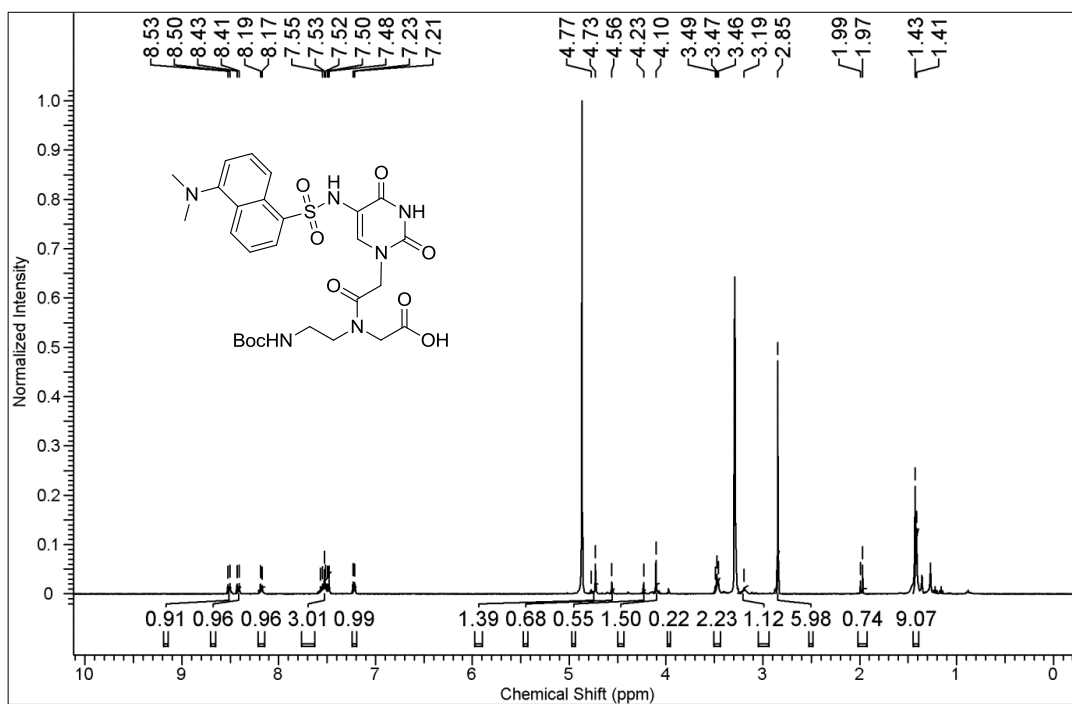
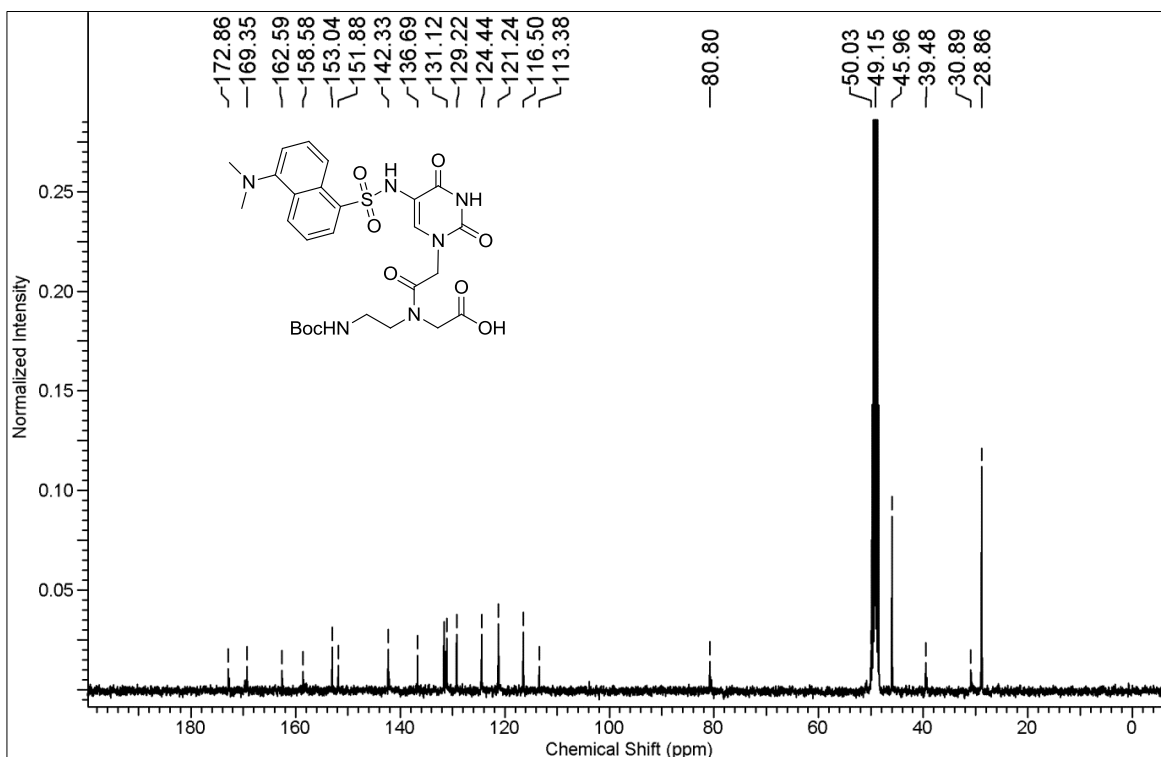
^1H NMR of compound 6 **^{13}C NMR of compound 6**

DEPT NMR of compound 6:**HR-MS (ESI) of compound 6**

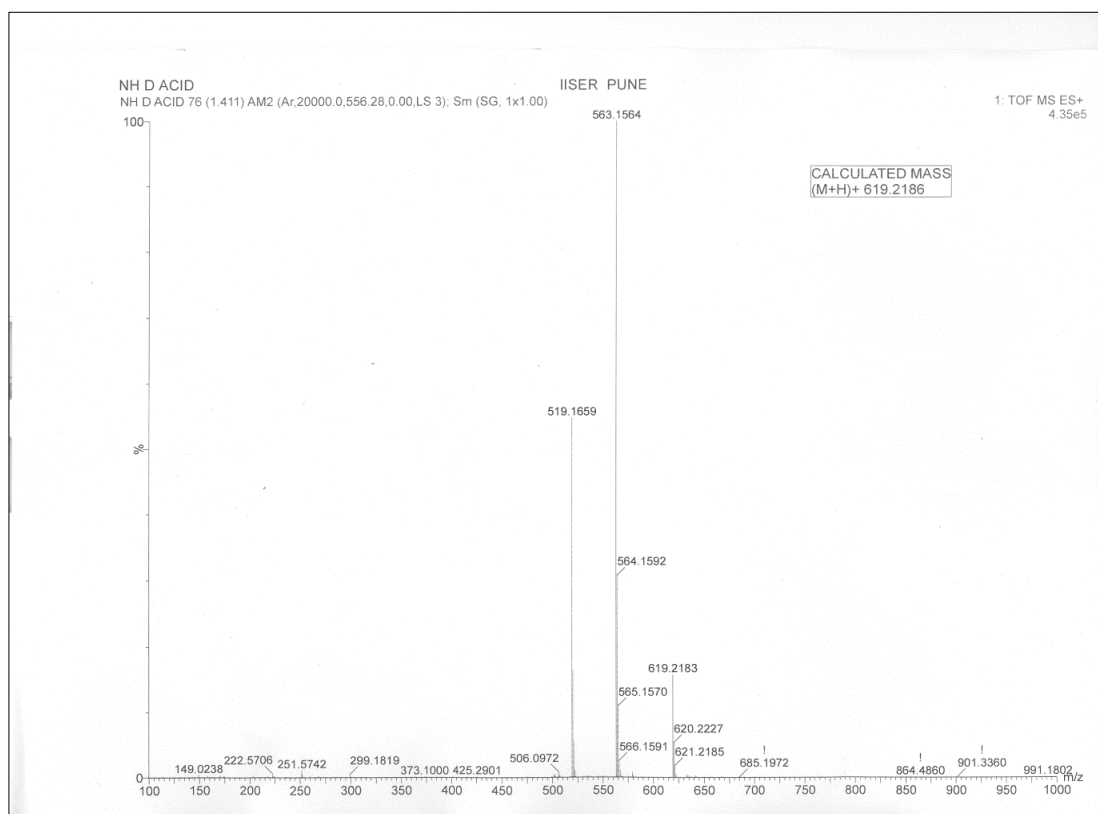
^1H NMR of compound 7 **^{13}C NMR of compound 7**

HR-MS (ESI) of compound 7**¹H NMR of compound 9**

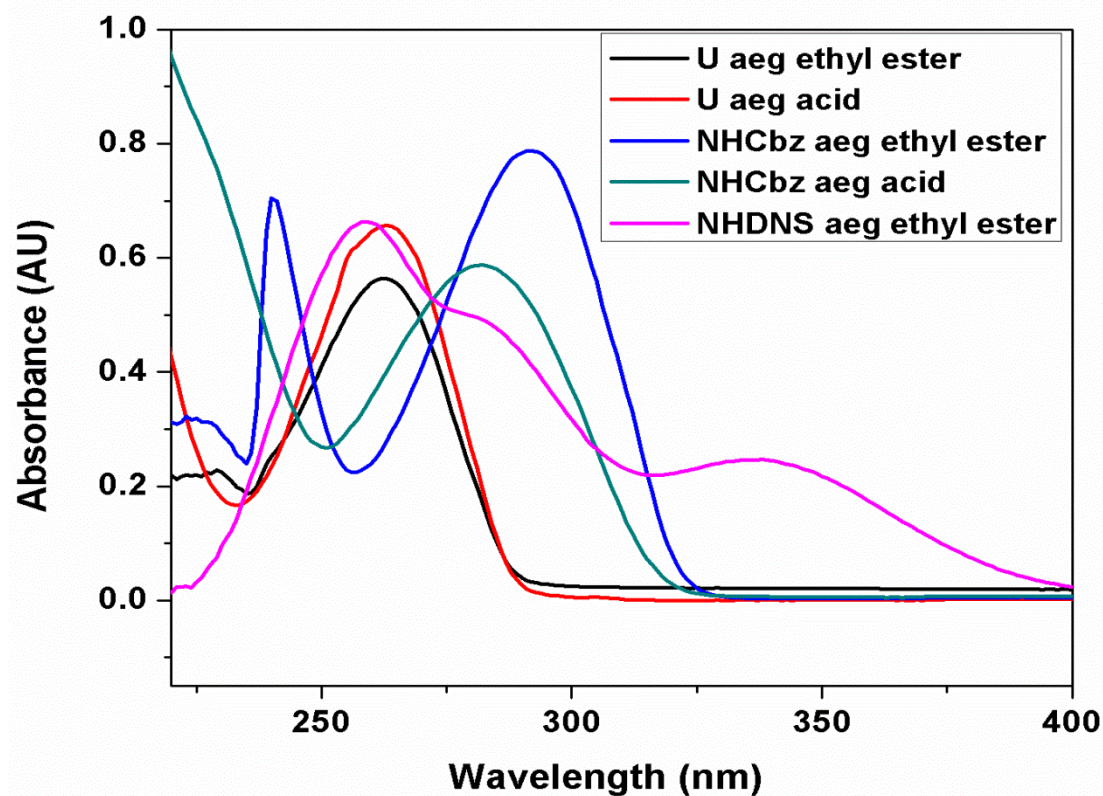
^{13}C NMR of compound 9**HR-MS (ESI) of compound 9**

^1H NMR of compound 10 **^{13}C NMR of compound 10**

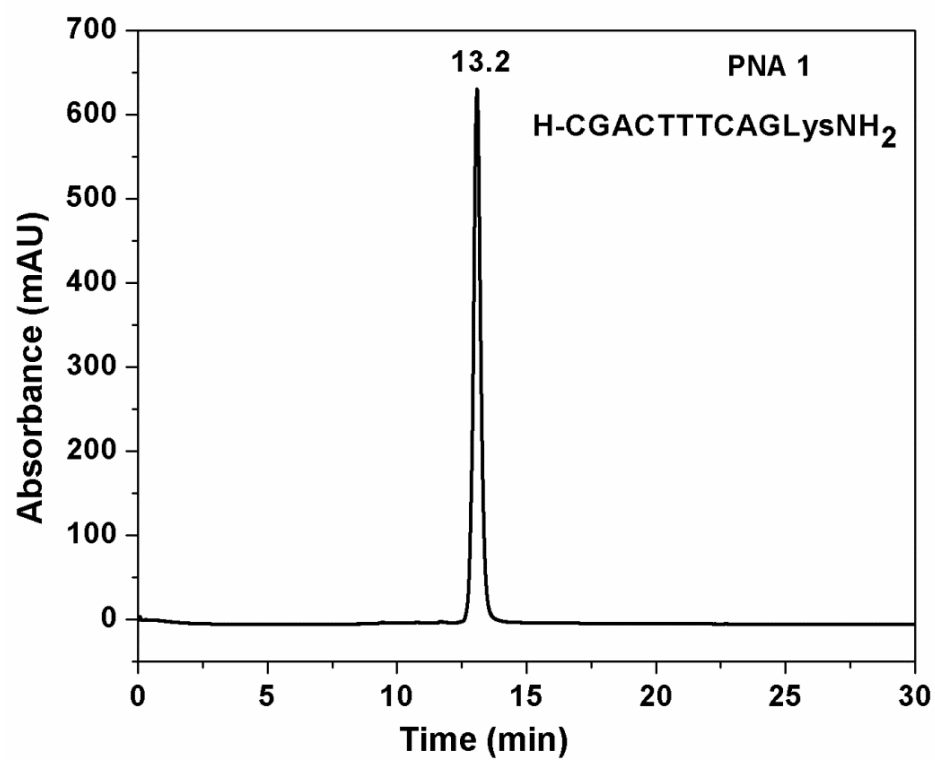
HR-MS (ESI) of compound 10



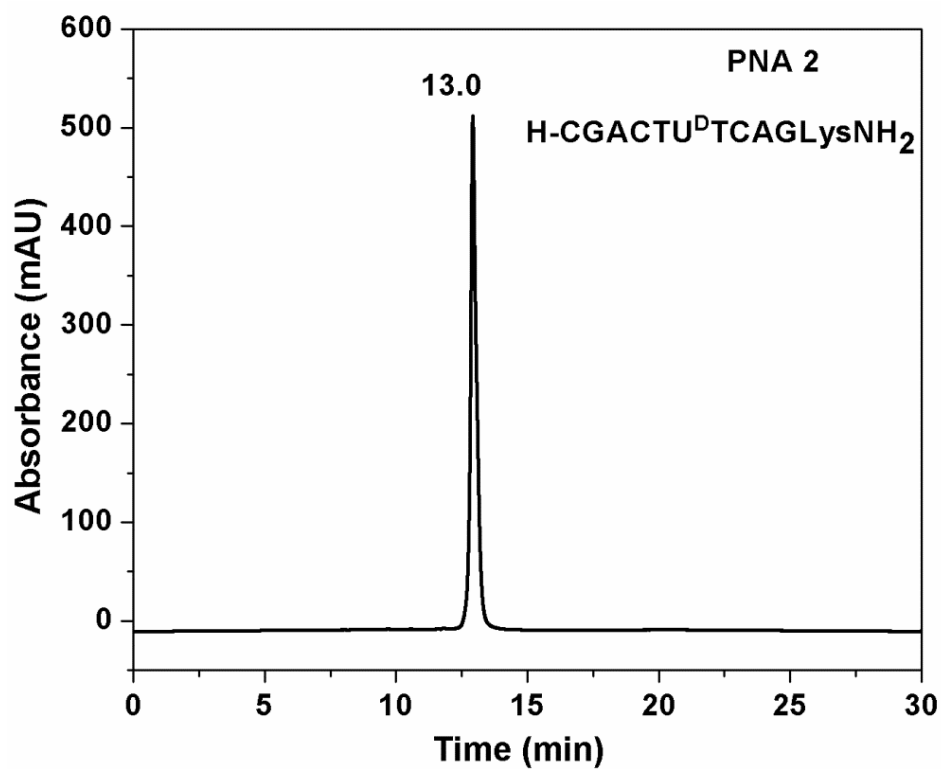
UV-Vis spectra of compounds 4-9



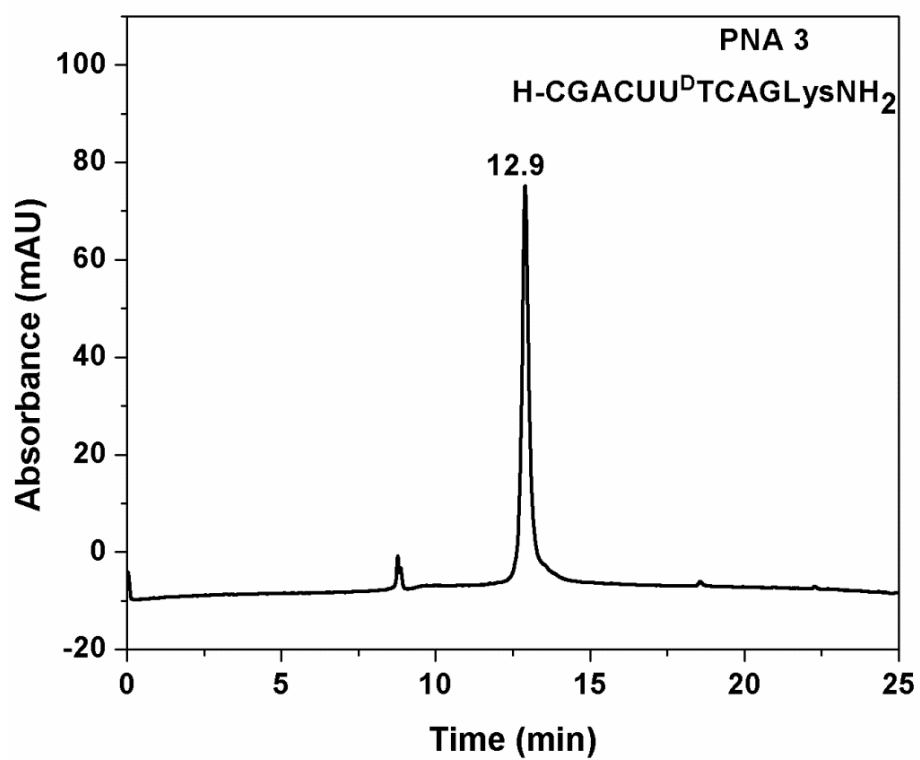
HPLC of PNA-1



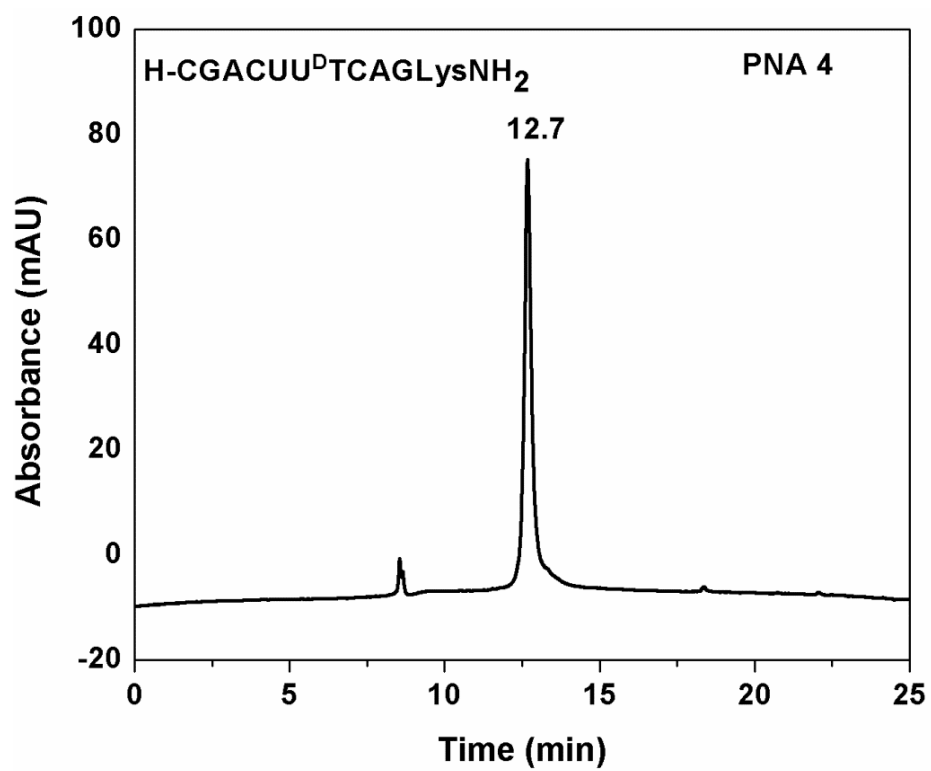
HPLC of PNA-2



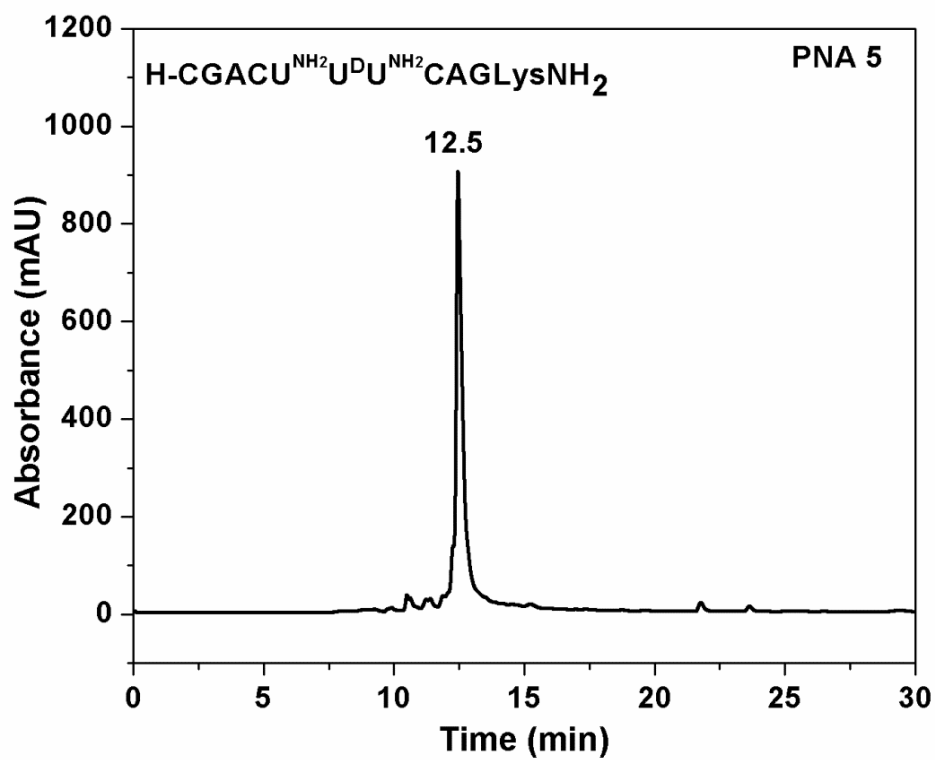
HPLC of PNA-3



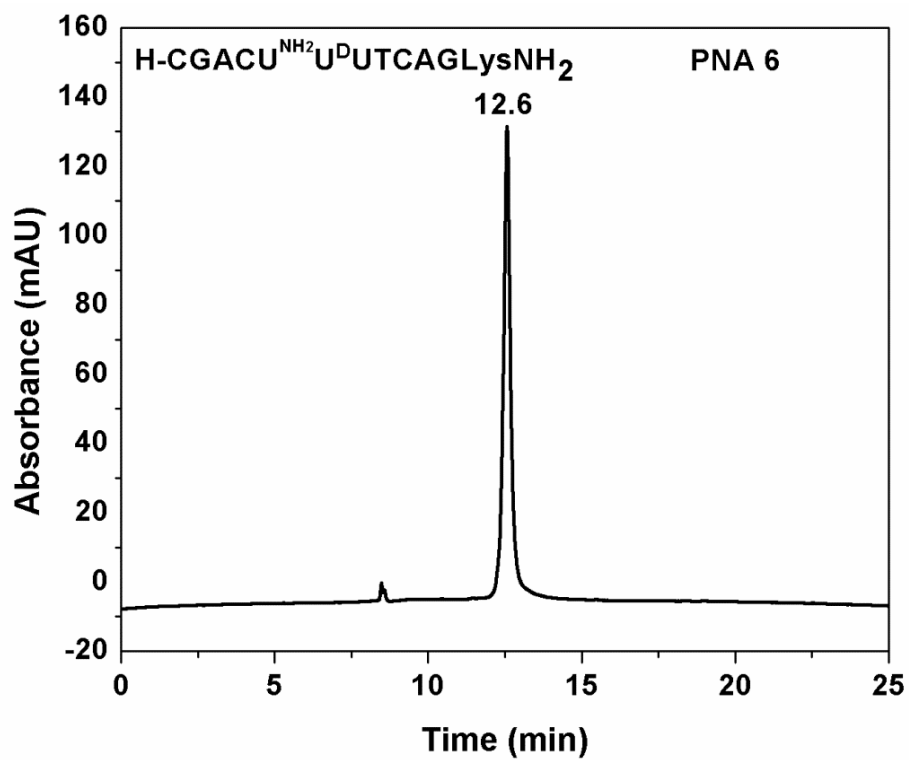
HPLC of PNA-4



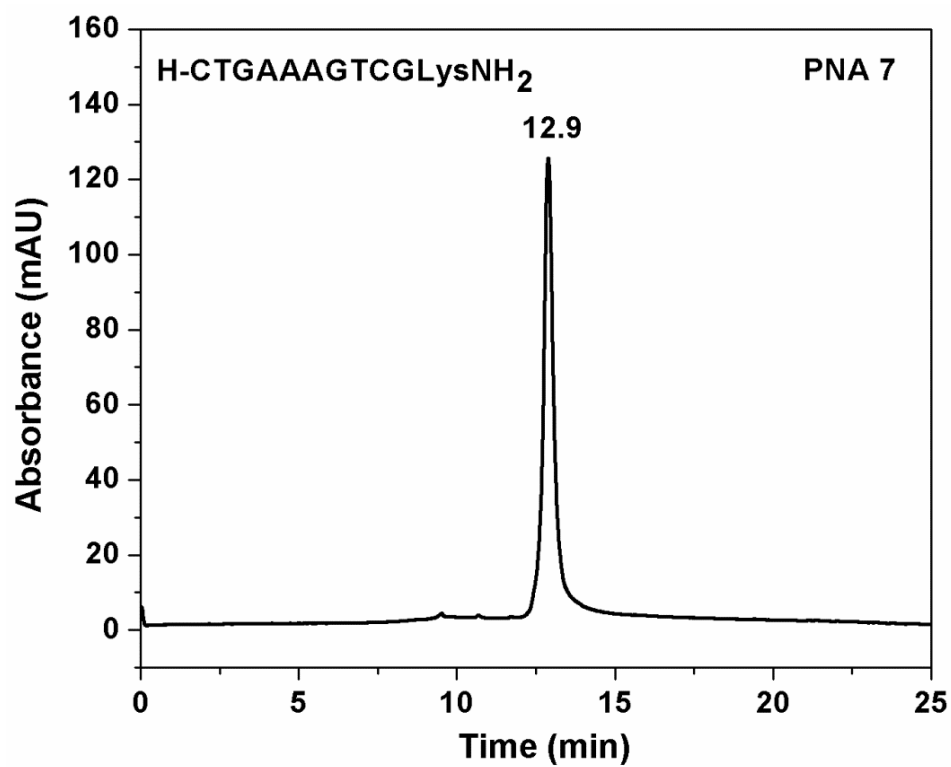
HPLC of PNA-5



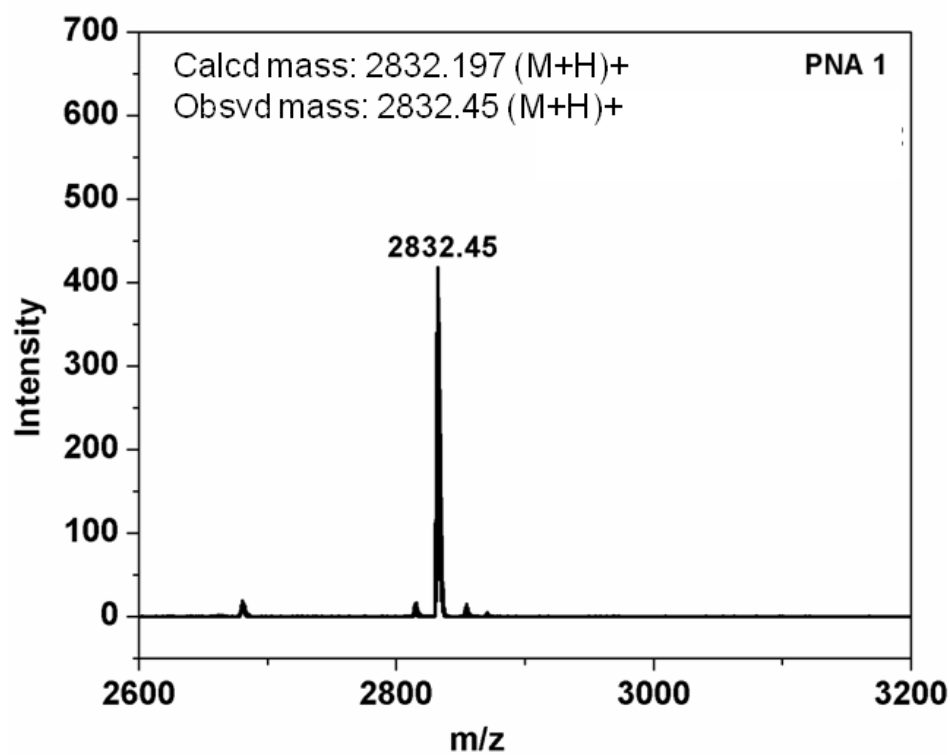
HPLC of PNA-6



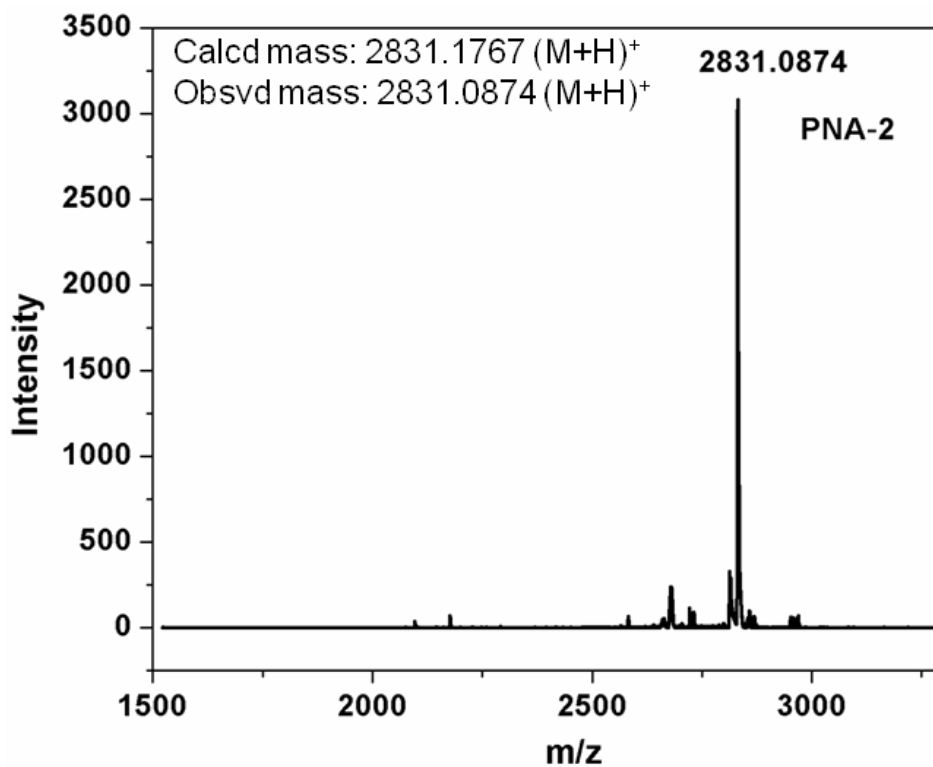
HPLC of PNA-7



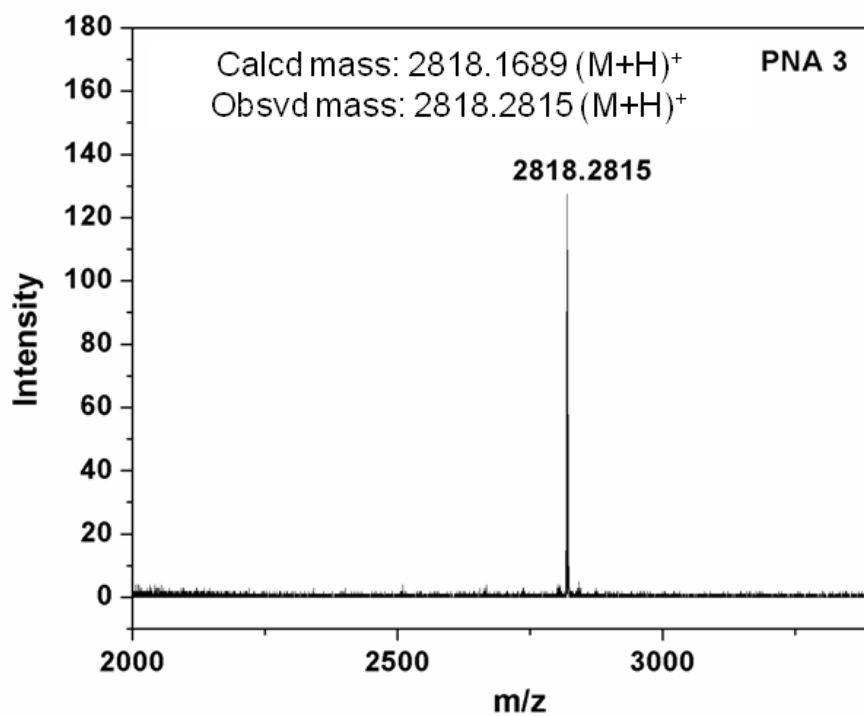
MALDI-TOF of PNA-1



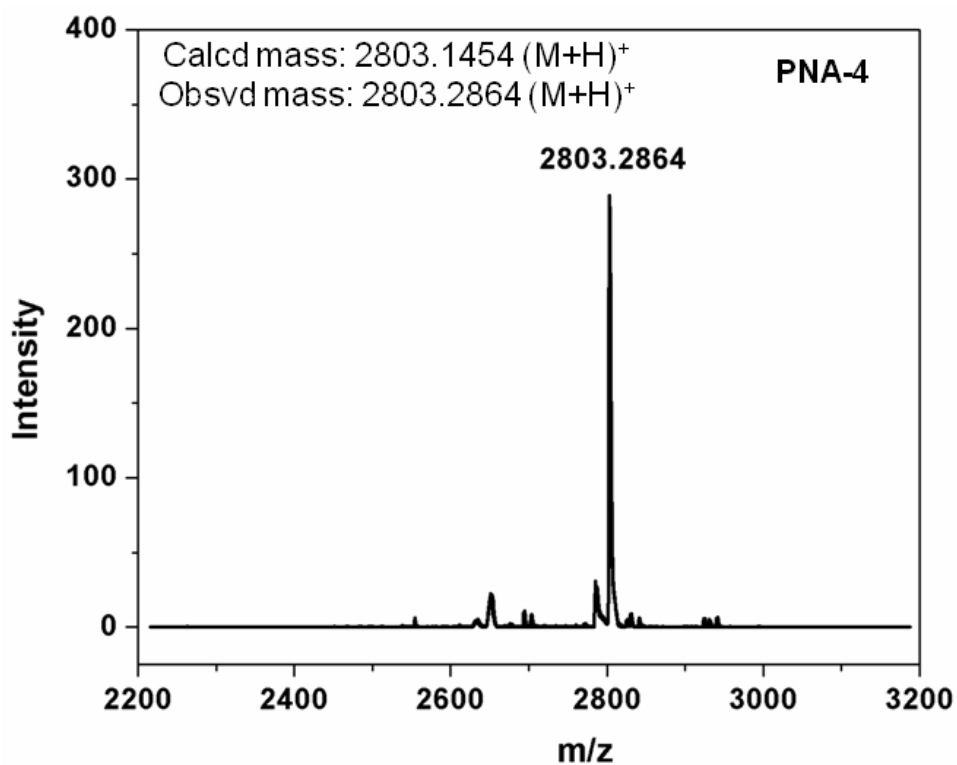
MALDI-TOF of PNA-2



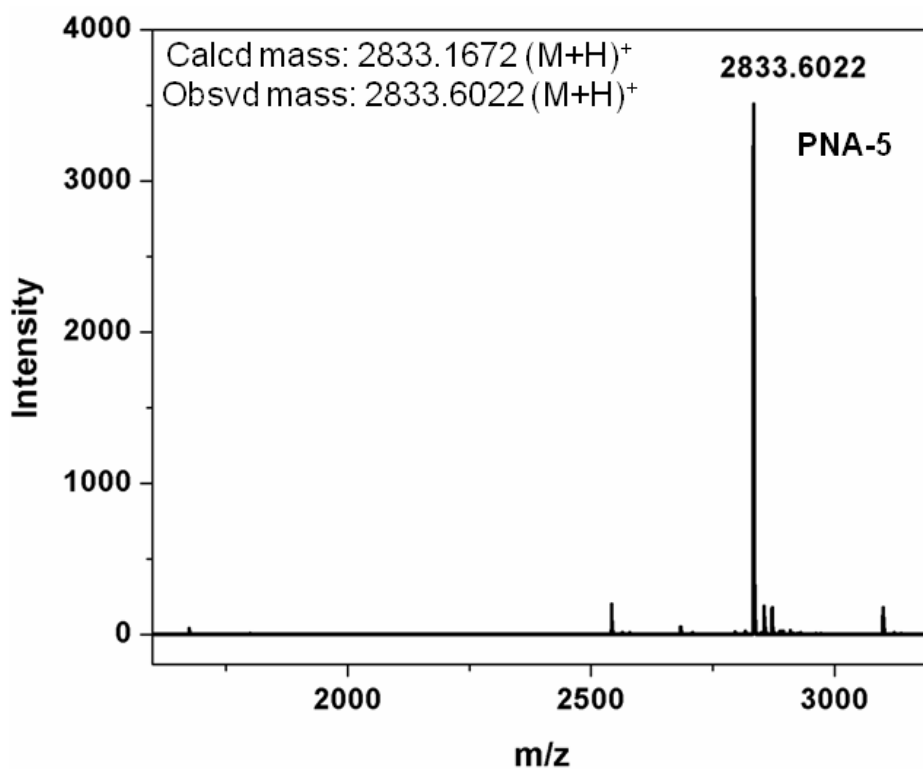
MALDI-TOF of PNA-3



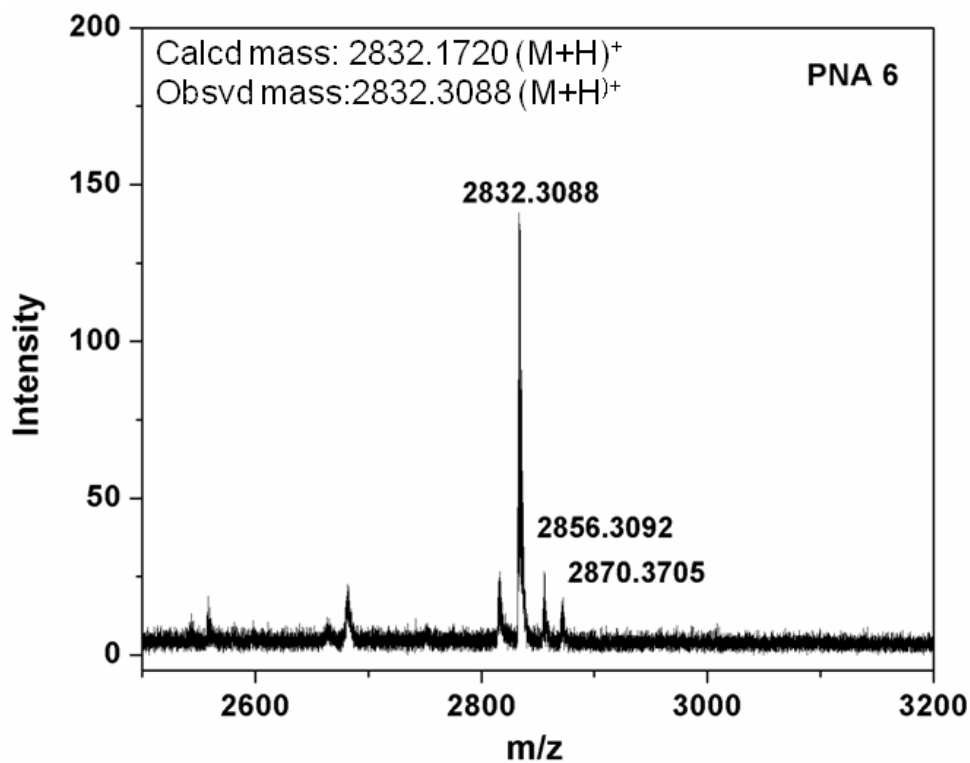
MALDI-TOF of PNA-4



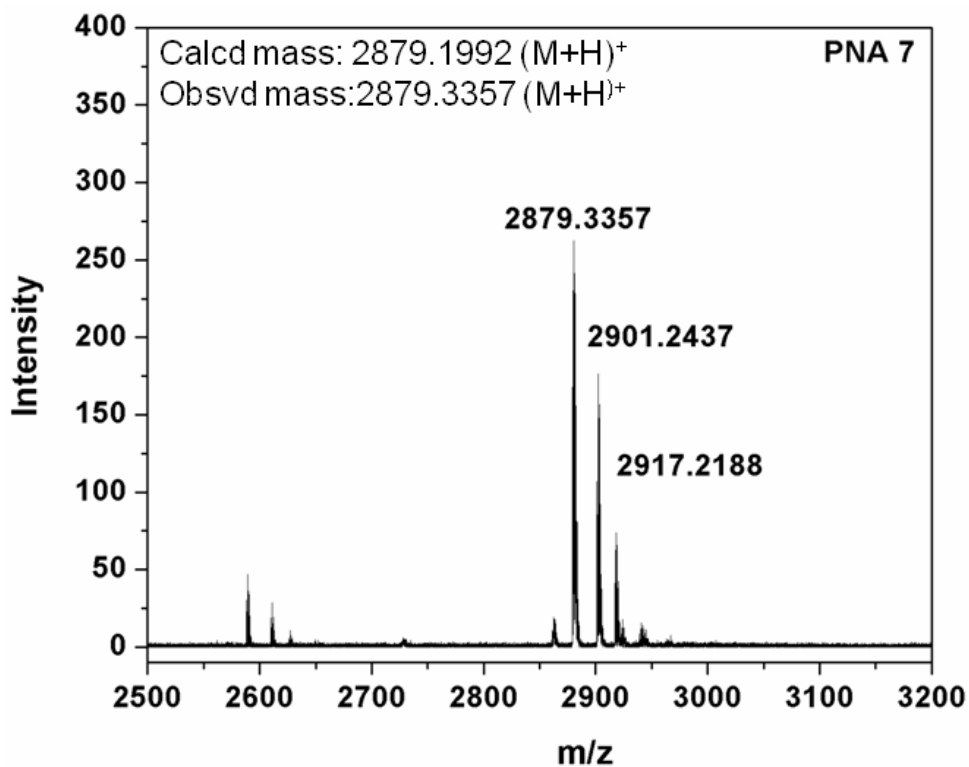
MALDI-TOF of PNA-5



MALDI-TOF of PNA-6



MALDI-TOF of PNA-7



Chapter 3

Biophysical Studies of Tetraplex Formation of Base Modified aeg-PNA hexamers

This chapter includes two sections. Section 3A deals with the utilization of 5-aminouracil linked to aeg-PNA backbone for the tetraplex formation and section 3B deals with the use of PNA tetraplexes for studying host-guest interactions.

Section 3A. Biophysical studies of tetraplexes of 5-aminouracil linked *aeg*-PNA

3A.1 Introduction

Nucleic acids are versatile molecules in forming various such as hairpin, duplexes, triplexes, tetraplexes and higher order structures. Among these, quadruplexes are an important class of self assembled structure observed in telomeres formed by self association of guanine (G).¹⁻² These are guanine rich DNA sequences present at the end of eukaryotic chromosomes (Figure 1) that protects them from deterioration or fusion with neighboring chromosomes. The guanine rich sequences of DNA form four stranded structures through Hoogsteen hydrogen bonds.³ The sequences d(TTTTGGGG), d(TTGGGG) and d(TTAGGG) present in *Oxytricha*, *Tetrahymena* and humans respectively form telomeric structures.⁴ The regular short repeat sequences leading to G-quadruplexes of DNA fall into the general motif d(T3-(T/A)-G3-4).⁵

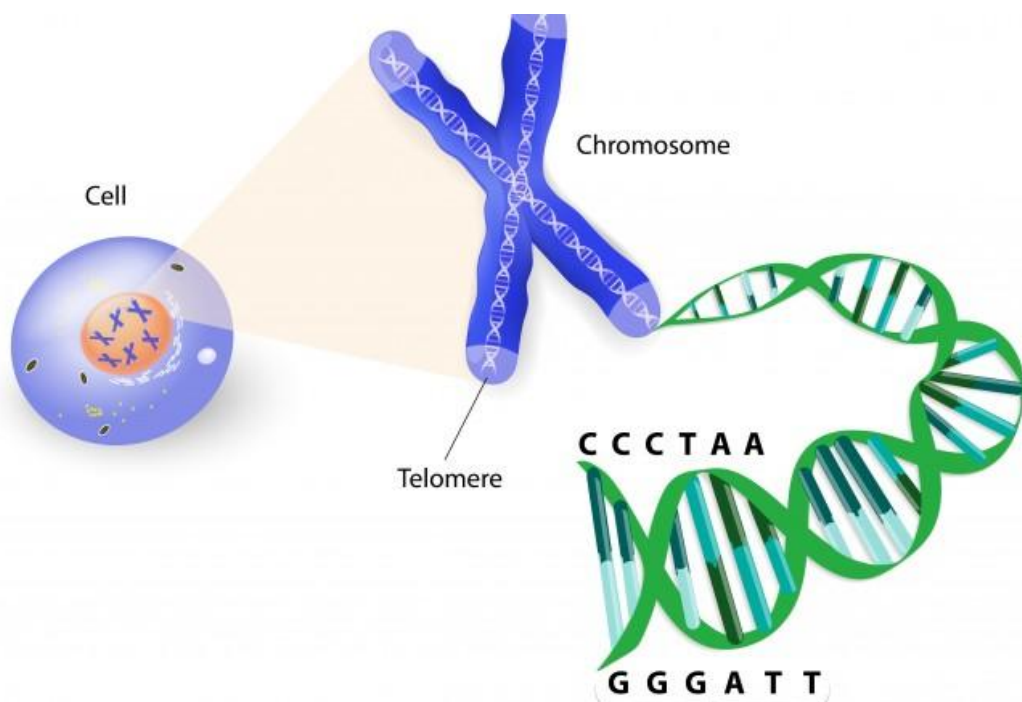


Figure 1. Typical structure of cell nucleus.

Ref: Image obtained from website: <http://thirdage-assets.thirdage.com/field/image/telomere-730x430.jpg>

While DNA secondary structures such as hairpins and cruciforms are stabilized by Watson-Crick complementary base pairing, the higher order DNA structures triplexes and quadruplexes are stabilized by Hoogsteen hydrogen bonding. It is reported that the G-rich sequences in DNA form quadruplex structures in presence of monovalent cations (Na^+ , K^+ etc) at physiological conditions.⁶ These quadruplex structures exhibit diverse topologies, depending on cation, glycosidic conformation, and relative orientation of strands (Figure 2).^{7,8} The central cavity of G-quadruplex is occupied by monovalent cations which neutralize the electrostatic repulsion between guanine O6 oxygens and thus stabilize the structure.⁹ The stability of quadruplex structure by monovalent cation follows the order, $\text{K}^+ > \text{Na}^+ > \text{Li}^+$.¹⁰ The crystal structure of telomeric sequence 5'-TGGGGT-3', found in *Tetrahymena* has shown formation of parallel stranded G-tetrads in the presence of Na^+ , Ca^{2+} , K^+ or Tl^+ .¹¹⁻¹³ Around 376,000 DNA G-quadruplex sequences are present in human genome and the presence of G-quadruplex in human cells is now well established.^{14,15} This has provided the basis for the mechanism of their role in normal and diseased states¹⁶⁻¹⁸ since they play vital role in regulation of replication, transcription and recombination processes.¹⁹

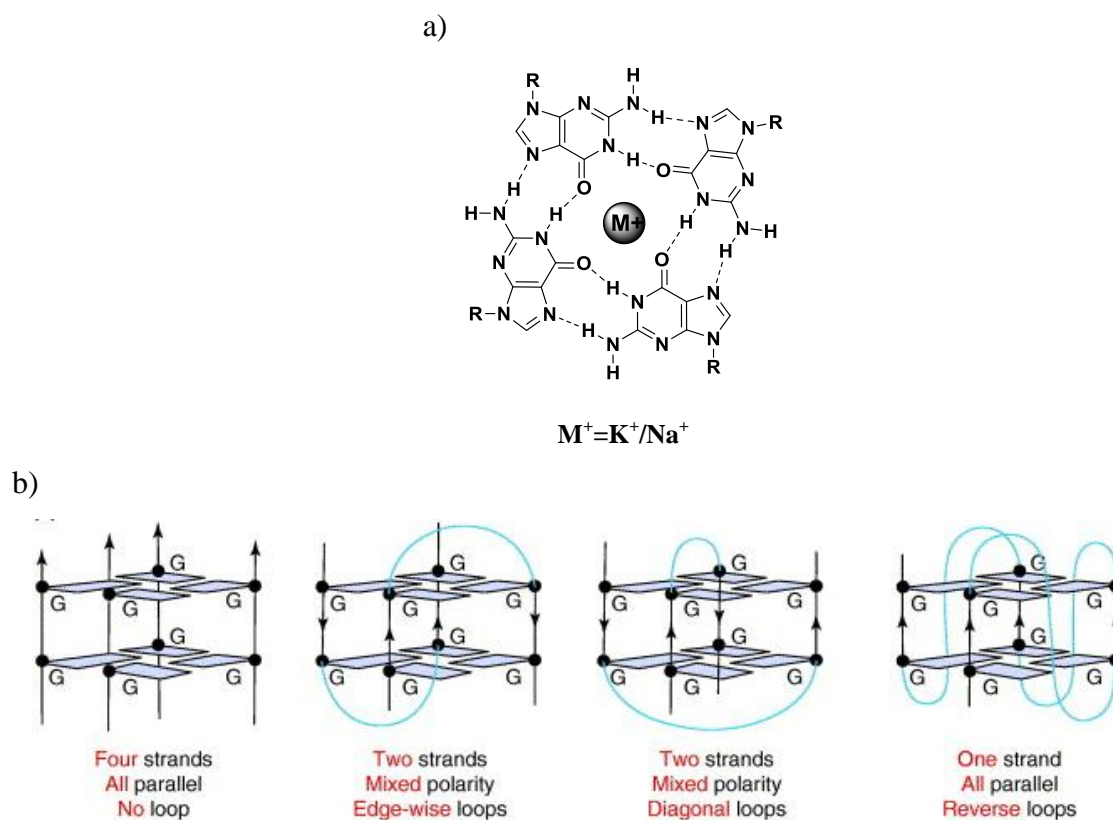


Figure 2. a) Hydrogen bonding pattern in G- quadruplex, b) G-quadruplex topologies.

Like DNA, G-tetrad formation is also observed in RNA. Kim et al.²⁰ in 1991 found that a 19-mer sequence of 5S rRNA in *Escherichia coli* forms a G-quadruplex. RNA quadruplexes are also observed in 3' untranslated region of insulin like growth factor II mRNA.²¹ The RNA tetrad of r(UGGGGU)₄ forms parallel stranded structure like DNA in the presence of Sr²⁺.²² RNA quadruplexes are found to be thermodynamically more stable than their DNA counterparts under near physiological conditions.^{23,24} The high resolution structural analysis of telomeric repeat RNA sequence TERRA showed that the 2'-hydroxyl stabilizes quadruplex via intramolecular hydrogen-bonding contributing to formation of parallel stranded RNA quadruplex.²⁵

3A.2 Characterization of G-tetrad formation in DNA

Many techniques and established methodologies have been used to characterize G-tetrad structure. These include chemical probing, NMR, crystallography, circular dichroism, Raman spectroscopy, gel electrophoresis, ultraviolet absorption, and ESI-mass spectroscopy.

3A.2.1 Nuclear Magnetic Resonance

G-quadruplexes exhibit characteristic NMR spectra.²⁶ The number of imino proton resonances corresponds to the number of guanosine residues involved in quadruplex formation. This observation is used to distinguish quadruplexes from other secondary structures. The chemical shift of imino protons of guanine residue involved in quadruplex formation is around 10.5-12 ppm. The first detailed NMR study of a G-quartet structure was done on the oligomer d(GGTTTTTGG). These studies found that the glycosidic torsion angle alternated between syn and anti for each adjacent pair of guanines along the strand.²⁷

Qualitative NMR studies showed that the nature and stability of telomeric DNA G-quadruplexes differs according to monovalent cation present in the central cavity. The sequences d(TTGGGG)₄ and d(TTAGGG)₄ were studied in sodium phosphate or potassium phosphate buffer. The study showed a complex NMR spectrum suggesting the presence of multiple species at higher concentration required for NMR studies. The NMR spectrum was distinct in sodium and potassium buffer. Temperature dependence of imino proton chemical shift indicated that the G-quadruplexes were most stabilized

by K^+ as compared to Na^+ , with imino protons still observable for quadruplex of d(TTGGGG)₄ in presence of K^+ .²⁸

3A.2.2 X-Ray Crystallography

X-ray crystallographic analysis of d(GGGGTTTTGGGG) supported the basic features postulated for G-quadruplex.²⁹ X-ray study showed the presence of alternate *syn-anti-syn-anti* along the strand of quadruplex. The thymidines are situated on opposite ends of G-quartet structure in head-to-tail manner, which is unlike to structure postulated by NMR. The detail structure of G-quartet is studied by X-ray crystallography. It was observed that base geometry is distorted from ideal square planar arrangement of guanines. The crystal structure of telomeric sequence 5'-TGGGGT-3' found in *Tetrahymena* is shown in Figure 3.¹³

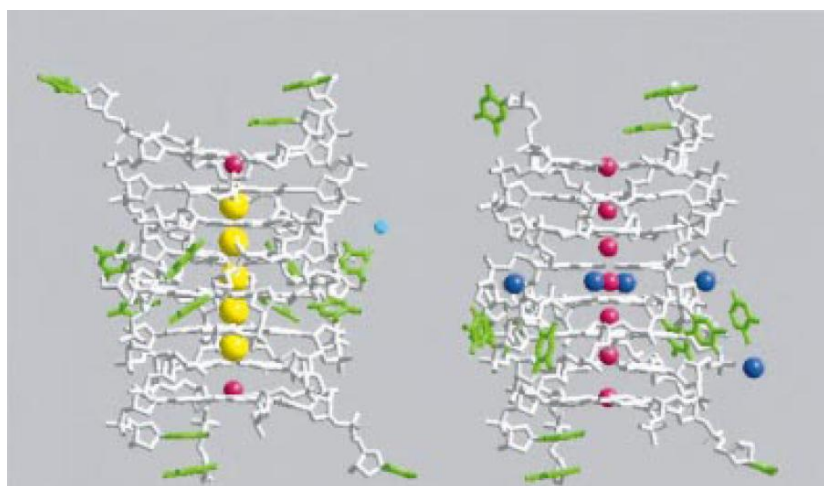


Figure 3. X-ray crystal structure of d(TG4T) in the presence of monovalent metal ion.¹³

3A.2.3 Nondenaturing electrophoresis

The folded structures can be rapidly identified as compared to unfolded single stranded DNA structures under stringent native conditions. Nondenaturing (native) gel is a simple but powerful method for the analysis of telomeric DNA structures. Electrophoretic mobility is dependent on the size, shape, and charge of the molecule as it passes through the gel matrix. DNA fragments adopting secondary structures migrate differently than unfolded single stranded DNA of the same length under denaturing conditions. Therefore, this technique is used to distinguish different structures formed

by DNA. The stability of quadruplexes is sensitive to buffering condition and temperature used during experiment.³⁰

3A.3 Thermal denaturation by UV and CD spectroscopy

The thermal denaturation of DNA can be monitored by hyperchromicity resulting from unstacking of bases and dissociation of duplex DNA. Thermal denaturation by UV or CD is used to monitor quadruplex formation.

3A.3.1 UV spectroscopy

The UV spectra of G-rich DNA sequences typically exhibit bands in the range 260 nm to 280 nm. Upon folding of telomeric repeats, a characteristic change in absorbance occurs. Generally, melting temperature of DNA and RNA duplexes are monitored at 260 nm, at which maximum absorption is observed. For DNA and RNA duplexes approximate 25% change in absorbance occurs at 260 nm between folded and unfolded state. However, this difference is just 4% for quadruplexes. Therefore, melting temperature of quadruplexes is monitored at 295 nm as denaturation exhibits 50% change in absorbance. Formation of G quadruplex can be easily confirmed by UV melting. G-quadruplexes show reverse sigmoidal curve at 295 nm in relation to melting curve of DNA/RNA duplexes.^{31,32}

3A.3.2 CD spectroscopy

The circular dichroism (CD) spectroscopy of telomeric DNAs is diagnostic of the conformation and sensitive to base stacking geometry. Two basic profiles of CD spectra are generally observed for telomeric DNAs i.e. type 1 and type 2. CD spectra of typical parallel quadruplex exhibits type 1 CD spectrum showing absorption maxima at 264 nm and minima at 240 nm with additional positive band at 290 nm differentiating it from single and double stranded quadruplexes. The CD spectra of DNA and RNA quadruplexes are similar to A-form duplexes. However, these two structural motifs can be differentiated by positive or negative band at 210 nm. A-form duplexes are characterized by negative band at 210 nm whereas parallel quadruplexes exhibits positive band at this wavelength. Antiparallel quadruplexes exhibits characteristic type 2 CD signature showing positive band at 295 nm and a negative band at 265 nm.^{33,34}

The presence of multiple conformations and mixture of parallel and antiparallel quadruplexes often make it difficult to assign structures by CD data alone. CD spectroscopy can also provide information on conformational changes induced by altering solution conditions. It is also possible to follow the kinetics of quadruplex formation by CD spectroscopy.³⁵

3A.4 Polymorphism in DNA G-quartet

The structure of quadruplexes found by NMR and X-ray analysis illustrated the polymorphic nature of G-quartets. Several structures are formed by G-rich sequences making difficult to identify and recognize structures in certain conditions. The interesting feature of G-quartet is that the same bases can be assembled in various ways with same basic hydrogen-bonding leading to the polymorphism. The following types of polymorphism are found in telomeric DNA.

- 1. Parallel vs antiparallel strands:** The relative orientations of strands forming G-quartet is fundamental source of structural variation. The four strands that make tetrameric complex can associate in different ways. All strands may be parallel, three parallel strands and one antiparallel or two pairs of adjacent parallel strands or alternate antiparallel strands (Figure 4).³⁶

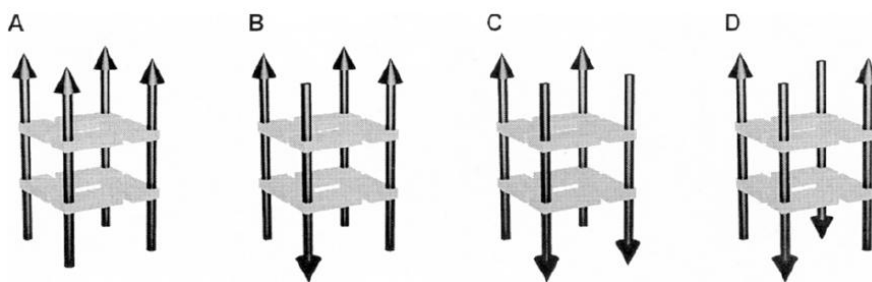


Figure 4. Orientation of quadruplex. A) All strands are parallel; B) three parallel and one antiparallel; C) two pairs of adjacent parallel strands and D) alternate antiparallel strands.

- 2. Strand stoichiometry:** The same oligomer can form different types of structures by association of one,³⁷ two³⁸ or four strands.³⁹ A telomeric DNA sequence containing four repeats can form an intramolecular quadruplex, dimer or true quadruplex (Figure 5). The formation of stable structure among all possibilities depends on strand concentration.

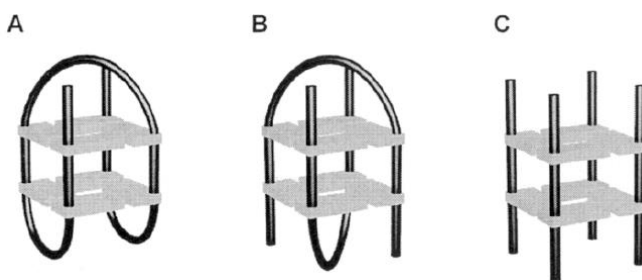


Figure 5. Various strand stoichiometries A) one strand gives unimolecular quadruplex, b) two strand give bimolecular quadruplex and C) four strand give tetrameric quadruplex.

3. **Glycosidic conformation:** The bases in DNA duplex are exclusively in *anti* conformation whereas guanines in G-quartets are observed in both *syn* and *anti* conformation. Basically, a string of four guanine residues can adopt different combinations of glycosidic conformations. The only observed patterns thus far are all-*anti* and alternating *syn-anti*. Guanines involved in the same quartet have the same glycosidic conformation in parallel orientation, while guanines on antiparallel strands have opposite glycosidic conformation (Figure 6).⁴⁰ The glycosidic conformation changes the relative orientation of the bases on adjacent G-quartets, and thus can affect the stacking energy between G-quartets. Thus adjacent guanines in the same G-quartet can have the same or the opposite glycosidic torsion angle depending upon whether their constituent strands are parallel or antiparallel.

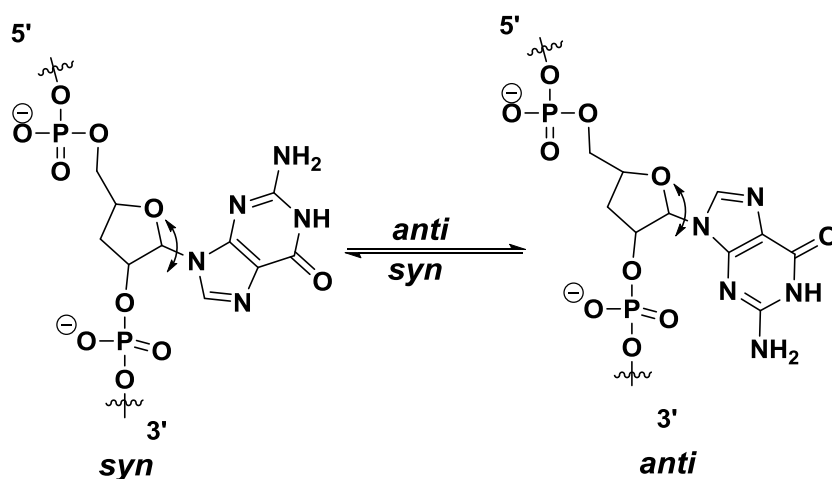


Figure 6. Rotation around glycosidic conformation enables guanines to interconvert between *syn* and *anti* conformation.

- 4. Loop geometry:** Depending on whether the G-quartet formation is unimolecular or bimolecular, the G-strings can connect in different ways. For example, in bimolecular quadruplexes loops connect diagonally or edgewise.⁴¹

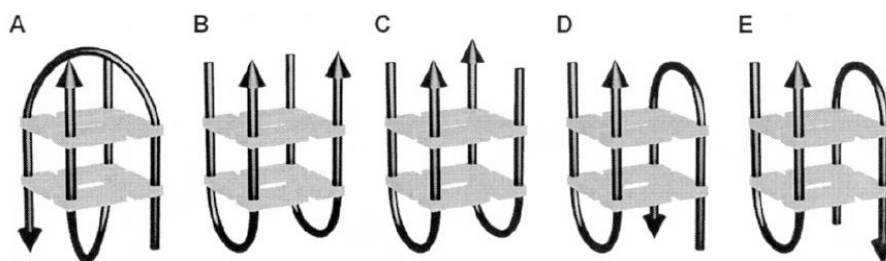


Figure 7. Loop geometry in quadruplexes.

- 5. Ion-binding geometry:** Probably the most important characteristic of quadruplex structures is the selective interaction with metal ion that occupies the position in central cavity. The metal ions may interact with the G-quartet structures in different ways and in different stoichiometries. It is well established from the crystal structure of d(GGGGTTTTGGGG) with K^+ ion that the G-quartet structure is stabilized by K^+ ion. The electron density for the positive ion is found in between the second and third G-quartet levels.⁴²

3A.5 Other quadruplex forming sequences

Along with telomeric sequences, there are other sequences which form the tetrameric structure. This section describes such sequences which can form quadruplex structures.

3A.5.1 The i-motif

The i-motif is formed from cytosine rich sequences by intercalated hemiprotonated C-C⁺ base pairs. Under normal physiological conditions, cytosine rich sequences make the duplex DNA. However, in acidic conditions below pH 4.5 or at higher temperature, the cytosine rich sequences unfold and refold into i-motif structure. The human telomeric sequence (5'-TTAGGG-3'): (5'CCCTAA-3') forms the i-motif in antiparallel orientation with hemiprotonated C-C⁺ base pairing.⁴³ Recently, the formation of double quadruplex structure with i-motif and G₄ domains on the same strand was reported.⁴⁴

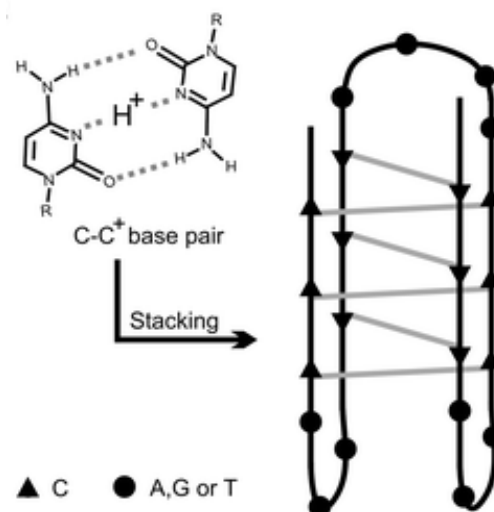


Figure 8. i-motif formation in DNA.

3A.5.2 G:C tetrads

The G:C tetrads came into the picture after discovery of the fragile X syndrome and associated $d(\text{CGG})_n:d(\text{CCG})$ repeat sequences. Initial studies indicated the formation of parallel stranded motif stabilized by methylation of cytosine bases. NMR analysis revealed head-to-tail hairpin arrangement via a lateral loop with *syn-anti-syn-anti* conformation similar to the telomeric G-rich bimolecular quadruplex structures.⁴⁵

3A.6 Applications of G-quadruplexes

Quadruplex structural motif is formed by telomeres, immunoglobulin region and regulatory region of oncogenes.⁴⁶ Thus, inhibition of the G-quadruplex is a promising target for anticancer drug design. The supramolecular architecture of G-quartets has also led to the development of interesting and functional non-covalent assemblies such as, G-wire, ion-channels and self assembled ionophores. In recent years considerable efforts have been directed towards the synthesis and investigation of new DNA analogs with improved binding properties with nucleic acids other than the natural canonical counterparts. Search for more stable quadruplexes from modified analogs of DNA may also help in understanding the formation of quadruplex.

In literature, many reports of G quadruplex formation by modified oligonucleotides⁴⁷ such as, locked nucleic acids (LNA)⁴⁸ and peptide nucleic acids (PNA)⁴⁹⁻⁵¹ have been well studied. Since, PNA was developed to mimic the Watson-Crick and Hoogsteen base pairing; they can participate in the formation of G

quadruplex in two ways: (1) G-rich PNAs forming quadruplexes alone or in presence of DNA templates and (2) self assembly of G-rich sequences of PNA-DNA chimeras. Armitage et al.⁵² have discussed the formation of PNA2:DNA2 hybrid quadruplexes by strand invasion and overhang effect. The quadruplex formation by PNA-DNA chimeras -5'TGGG3'-t, 5'TGG3'-gt, t-5'GGGT3' and tg-5'GGT3' where lower and upper case letters indicate PNA and DNA residues respectively, have been reported.⁵³ Balsubramanian et al.⁵⁴ reported the quadruplex formation by TG₃ homo oligomer PNA at pH 7.4 by electrospray ionization mass spectrometry (ESI-MS) and confirmed by ¹H NMR and thermal stability measurements by UV absorbance. Ganesh et al.⁵⁵ reported the PNA quadruplexes formation by incorporating modified PNA monomer into hexameric sequence TGGGGT and also they reported the tetraplex formation of PNA sequence TC₈ through i-motif.⁵⁶

3A.7 Rationale and objective of present work

5-Aminouracil is a modified nucleobase which can be a mimic of purines. 5-Aminouracil can form H-bonds from both sides just like purines.

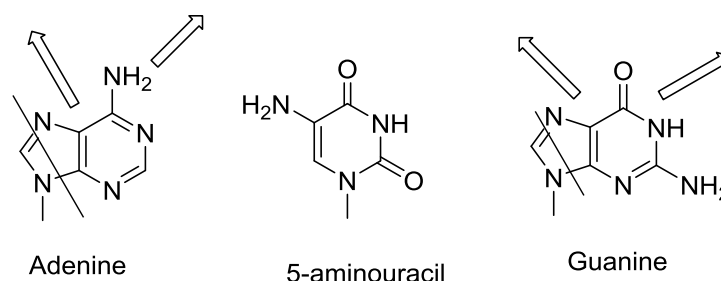


Figure 9. Structural similarity between purines and 5-aminouracil.

5-Aminouracil has the same number of H-bond donors and acceptors as that of guanine. The only difference is that two H-bond donors and two acceptors in guanine are in successive manner, whereas H-bond donors and acceptors in 5-aminouracil alternate in their sequential arrangement (Figure 11). The hydrophilic 5-aminouracil incorporated DNA has been used to alter the polarity of major groove when U^{NH₂} replaced the hydrophobic 5-CH₃ of thymine in DNA and in PNA in chapter 2.

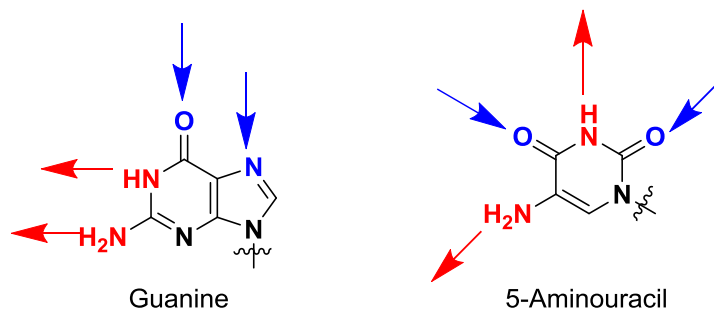


Figure 10. Comparison of hydrogen-bond acceptors and donors in guanine and 5-aminouracil.

5-Aminouracil can make a quartet structure given the number of H-bond acceptors and H-bond donor as that of guanine as shown in Figure 11.

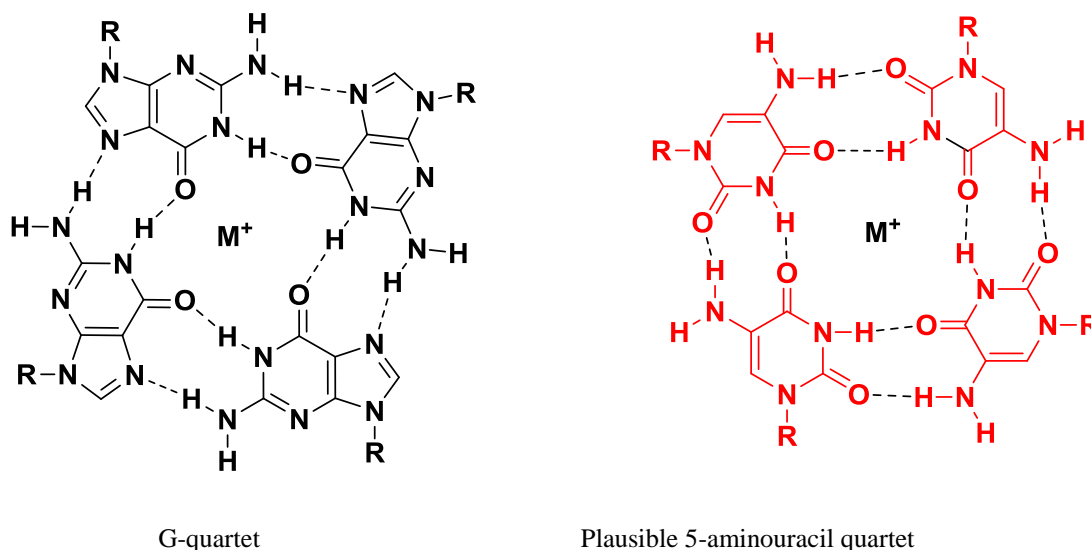
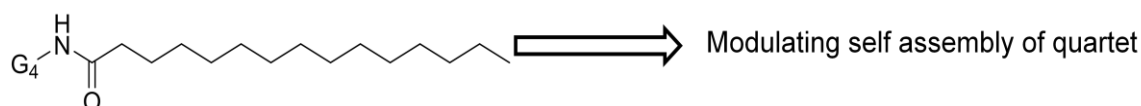


Figure 11. G-quartet structure and plausible 5-aminouracil quartet structure.

1. 5-Aminouracil incorporated PNA oligomer is explored for formation of quartet structure.
2. To modulate the self-assembly of quartet formation by the conjugation of fatty acid to PNA oligomer.



In this context, 5-aminouracil modified *aeg*-PNA monomer was synthesized and incorporated into PNA oligomers ($TU^{NH_2}U^{NH_2}U^{NH_2}U^{NH}T$, where, U^{NH_2} is 5-

aminouracil). The fatty acid chain was conjugated to PNA oligomers at N-terminus to induce aggregation that may from the self-assembly. The quartet formation of PNA oligomers was studied by biophysical techniques (CD) and the self assembled structures were examined by FESEM.

3A.8 Result and discussion

This section describes the synthesis of 5-aminouracil *aeg*-PNA monomer followed by its incorporation into PNA sequence by solid phase peptide synthesis and biophysical studies of tetraplex formation.

3A.8.1 Synthesis of monomers

The synthesis of *N*-Boc protected *aeg*-5-aminobenzoyloxyuracil and *N*-Boc protected *aeg*-uracil PNA monomers was achieved as per experimental procedures described in Chapter 2 and using the commercially available *N*-Boc protected *aeg*-guanine PNA monomer.

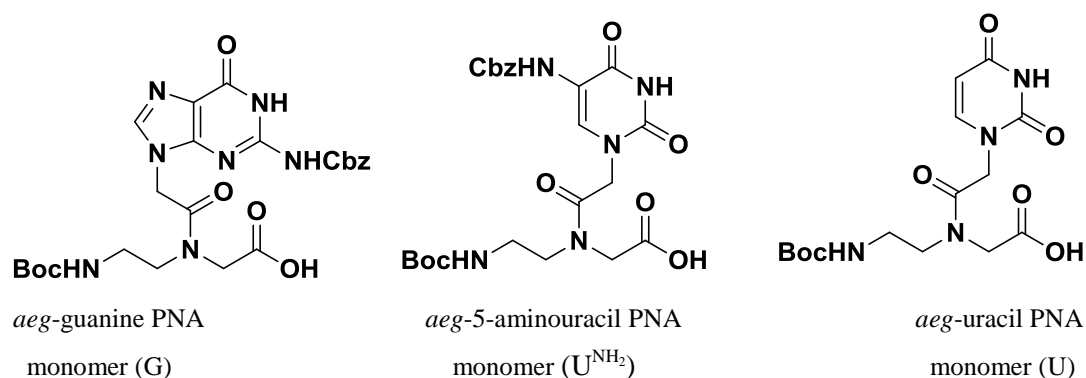


Figure 12. Structure of desired monomers.

3A.8.2 Synthesis and characterization of PNA oligomers

The *N*-Boc protected monomers were incorporated into PNA oligomers through established solid phase peptide synthesis protocol as described in Chapters 1 and 2. The synthesized oligomers were purified by RP-HPLC and characterized by MALDI-TOF mass spectroscopy (Table 1). MALDI-TOF mass spectra and HPLC profile of all PNA oligomers are shown in Appendix III. In addition to 5-amino-U-PNA for comparison, the oligo-U-PNA and oligo-G-PNA were also synthesized.

Table 1: MALDI-TOF of PNA hexamers.

Sequence Code	PNA sequence	Mol. formula	Calcd mass	Obsvd mass
PNA-1	H-TGGGGT LysNH ₂	C ₇₂ H ₉₇ N ₃₉ O ₂₁	1842.7643	1842.9417
PNA-2	H-T(U ^{NH₂}) ₄ T LysNH ₂	C ₆₈ H ₉₆ N ₃₁ O ₂₅	1746.7194	1746.9674
PNA-3	H-TUUUUT LysNH ₂	C ₆₈ H ₉₃ N ₂₇ O ₂₅	1686.6758	1686.6497

G = *aeg*-guanine ; U^{NH₂} = *aeg*-5-aminouracil; U = *aeg*-uracil.

3A.8.3 Biophysical studies of PNA oligomers

The formation of quadruplex by the synthesized oligomers was studied by CD spectroscopy.

3A.8.3a CD spectroscopy

Circular dichroism (CD) of PNA oligomers was recorded in sodium phosphate buffer (10 mM, pH 7.2) at 25 μ M concentration. All of the PNA oligomers exhibited no characteristic CD signature suggesting the absence of self-assembled structure formation by PNAs **1-3**. Addition of NaCl (100 mM) to the solution of PNAs **1-3** resulted in the observation of characteristic CD signature by PNA-**1** and PNA-**2** whereas PNA-**3** did not show any significant CD signature.

CD profile of PNA-**1** (TGGGGT-LysCONH₂) exhibited negative band at 236 nm and positive band at 258 nm along with one positive band around 300 nm indicating the self-association of guanine to form the self-assembled structure. CD spectra of PNA-**2** H-T(U^{NH₂})₄T LysCONH₂ showed the maxima at 234 nm and minima at 261 nm along with one positive band around 300 nm suggesting the formation of self-assembled structure whereas PNA-**3** (H-TUUUUT-LysCONH₂) did not show any significant CD signature (Figure 13). These results suggested the possibility of U forming self assembled structure with band at 300 nm indicated to be tetraplex in nature.

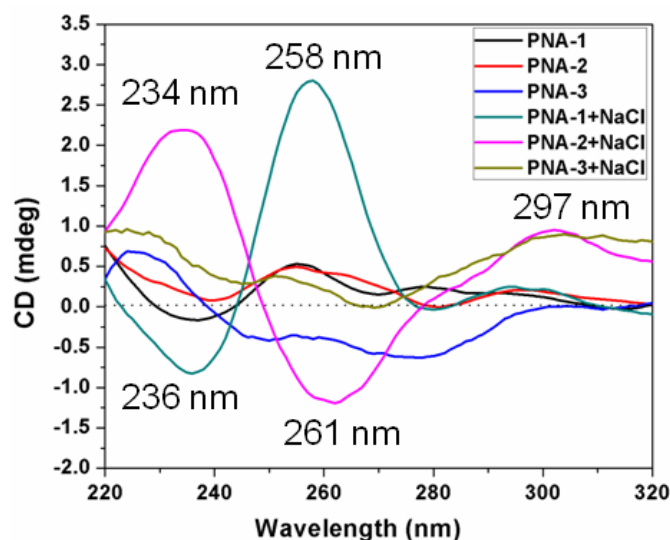


Figure 13. CD profile of PNAs 1-3 in the absence and presence of NaCl in phosphate buffer. CD spectra were recorded in sodium phosphate buffer (10 mM, pH 7.2) containing 100 mM NaCl at 25 μ M concentration.

When CD profile of PNA-2 (U^{NH_2}) is compared with literature reports of DNA G-quadruplexes, it is seen that PNA-2 exhibits type II CD signature suggesting the formation of self-assembled structure in antiparallel orientation. This may arise from C5-amino group being engaged in hydrogen bonding to form the tetraplex type of structure. This characteristic CD pattern was absent in PNA-3 (U) due to lack of hydrogen bond donor system like guanine or U^{NH_2} .

Since tetraplex formation is formed by Na^+/K^+ , the effect of cation on self-assembled structure of PNA-2 (U^{NH_2}) was examined.

3A.8.3b Salt dependent CD spectroscopy

To examine the effect of monovalent metal ion on the formation of tetraplex, salt dependent CD spectroscopic measurements of PNA-2 H-T(U^{NH_2})₄T LysCONH₂ was recorded. Figure 14 shows the CD profile of PNA-2 measured in presence of NaCl and KCl (100 mM) at 10 °C. The CD profiles of PNA-2 (U^{NH_2}) were similar in presence of Na^+/K^+ , except for intensity differences. PNA-2 (U^{NH_2}) exhibited more intensity for negative band at 263 nm and positive band at 305 nm in the presence of NaCl as compared to KCl suggesting the more stabilization of self-assembled structure by Na^+ ion.

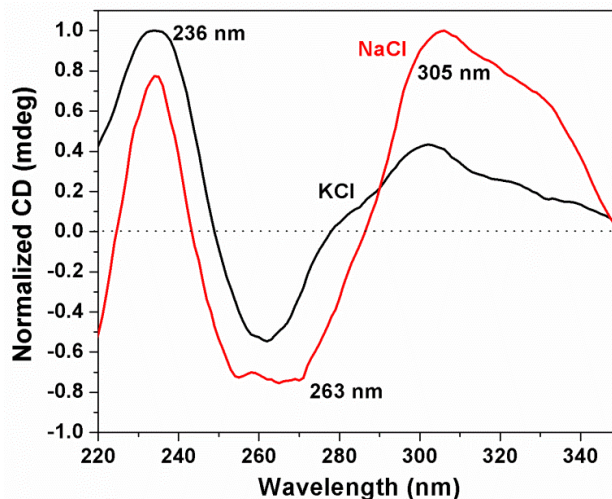


Figure 14. CD profile of PNA-2 (U^{NH_2}) in the presence of NaCl and KCl. CD spectra were recorded in sodium phosphate buffer (10 mM, pH 7.2) containing 100 mM NaCl and potassium phosphate buffer (10 mM, pH 7.2) containing 100 mM NaCl at 25 μ M concentration.

3A.8.3c pH dependent CD study of PNA-2 (U^{NH_2})

The property of self assembled structure of PNA-2 (U^{NH_2}) was examined at pH 5.1, 6.0 and 7.2 to find the effect of pH on the PNA-2. At physiological pH (7.2), one positive band and one negative band at 234 nm and 261 nm appeared respectively along with one positive band at 302 nm. When pH was lowered to 6.0, the bands characteristic of self-assembled structure disappeared. Upon further decreasing pH to 5.1, the CD profile was similar to what observed at pH 6.0. It suggested that the self-assembled structure is formed at physiological pH.

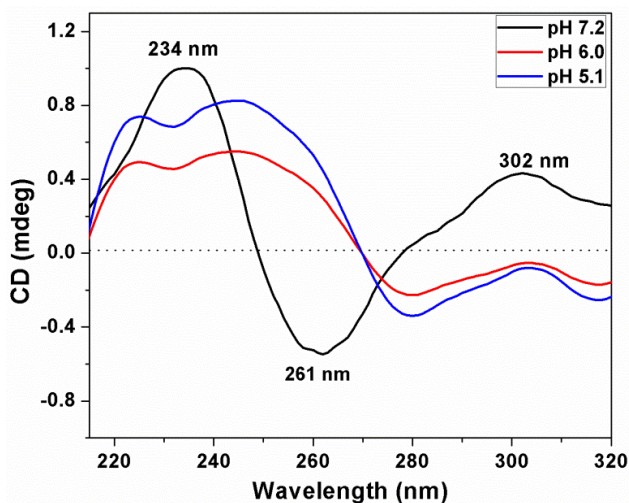


Figure 15. pH dependent CD profiles of PNA-2 (U^{NH_2}). CD spectra were recorded in sodium phosphate buffer (10 mM of different pH) containing 100 mM NaCl at 25 μ M concentration.

3A.8.3d Concentration dependent CD of PNA-2 (U^{NH_2})

Concentration dependent CD spectroscopic measurements of PNA-2 (U^{NH_2}) were carried out to find the concentration at which PNA-2 (U^{NH_2}) self assembles to form the tetraplex structure. For this purpose concentration of PNA-2 (U^{NH_2}) was varied from 5 μ M, 15 μ M to 25 μ M and CD was recorded in phosphate buffer (10 mM, pH 7.2) containing sodium chloride (100 mM) at 10 $^{\circ}$ C. It was observed that PNA-2 (U^{NH_2}) showed CD bands in positive region which suggest that 5 μ M is not enough concentration to form self assembled structure. After increasing the concentration to 15 μ M, PNA-2 (U^{NH_2}) displayed bands at 300 nm which became more prominent upon increasing the concentration to 25 μ M. The characteristic CD pattern of positive band at 234 nm and negative band at 260 nm along with positive band around 300 nm suggested the formation of self assembled structure at 25 μ M (Figure 16).

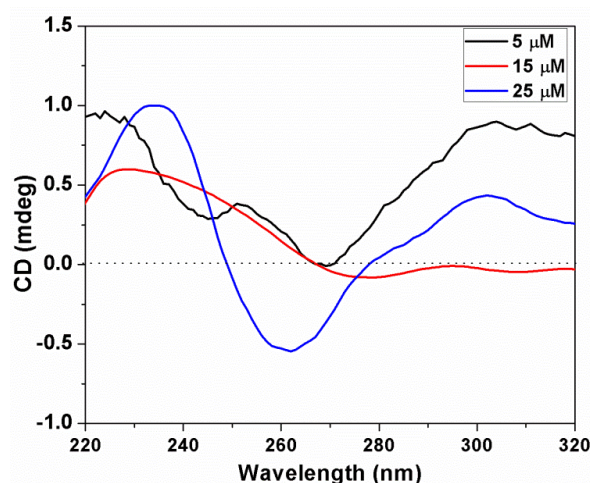


Figure 16. Concentration dependent CD profile of PNA-2 (U^{NH_2}). CD spectra were recorded in sodium phosphate buffer (10 mM, pH 7.2) containing 100 mM NaCl at different concentration.

Thus CD spectroscopic measurements suggested the formation of self-assembled structure by PNA-2 (U^{NH_2}) at physiological pH, at 25 μ M concentration and stabilized by Na^+ ion. The possible H-bonding pattern or 4-carbonyl arrangement required for monovalent cation coordination of 5-aminouracil is similar to G-tetrad. While this thesis was submitted, Galeone et al.⁵⁷ recently showed that 5-aminouracil DNA tetrad contributes to stabilize the DNA G-tetrad studied by CD, NMR, Gel electrophoresis and molecular modeling. This work supports our hypothesis that 5-aminouracil may form tetraplex structure. However, more experimental is needed to

prove that 5-aminouracil form the self assembled structure which can be studied by NMR and X-ray crystallography may provide further insights for structural evidence. However, these studies require more amount of material. Therefore these studies were not performed due to lack of enough concentration of 5-aminouracil PNA.

3A.9 Modulating the self-assembly of tetraplex formation by fatty acid conjugation to PNA oligomers

Self assembly is an attractive tool to develop functional nanomaterial.⁵⁷⁻⁶⁰ The biopolymers nucleic acid and proteins form a wide range of supramolecular assemblies, displaying interesting properties. Depending on the nature of assemblies, the bioactive peptides linked to lipophilic groups create self-assembled nanostructures, which has drawn attention for their promising applications in biomedical science.⁶¹

A peptide nucleic acid/peptide amphiphilic conjugates have been reported to self-assemble into nanostructures bind to the DNA with high affinity and high specificity.⁶² Schneider et al.⁶³ have reported PNA amphiphiles that form micelles and recognizes the DNA oligomers. Zhang et al.⁶⁴ recently reported the peptide nucleic acid amphiphiles forming micelles which make stable PNA:PNA duplex. Recently Gazit et al.⁶⁵ have developed the CG, GC and GG di-PNAs and found that this guanine containing di-PNAs form well ordered architectures exhibiting optical properties. Ganesh et al.⁶⁶ recently shown the increase in the cellular uptake of PNAs conjugated with perfluoroundecanoyl moiety in NIH 3T3 and HeLa cells via nanoparticle formation.

In this context, herein the fatty acid chain was conjugated with PNA hexamers to enhance the self-assembly leading to tetraplex structures.

3A.10 Synthesis and characterization of fatty acid chain conjugated PNA hexamers

The undecanoyl and perfluoroundecanoyl chain was conjugated to corresponding PNA oligomers through solid phase peptide synthesis (Figure 17). The synthesized oligomers were purified by RP-HPLC and characterized by MALDI-TOF mass spectroscopy. The formation of self assembled structure was studied by CD spectroscopic measurements and FESEM techniques (Table 2).

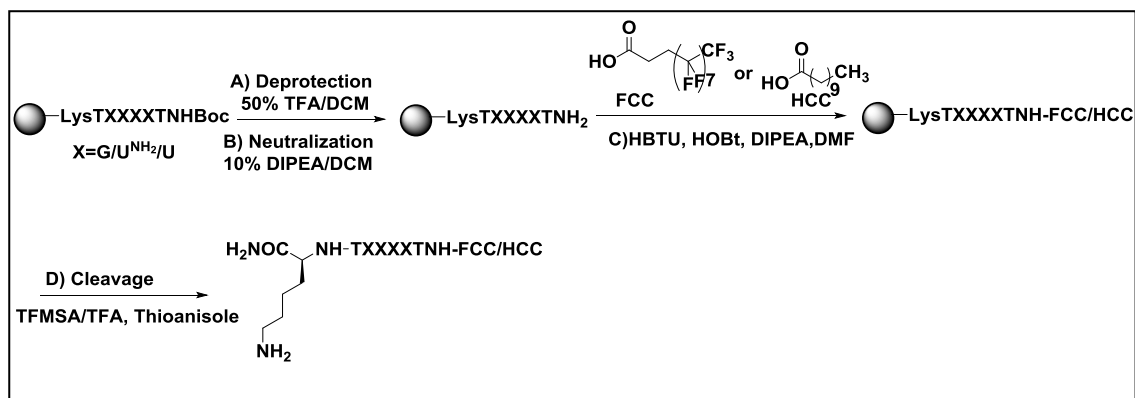


Figure 17. Solid phase synthesis of fatty acid chain conjugated PNA hexamers.

Table 2: MALDI-TOF mass of fatty acid chain conjugated PNA hexamers.

PNA	PNA sequence	Mol formula	Calcd mass	Obsvd mass
PNA-4	CF ₃ -(CF ₂) ₇ -(CH ₂) ₂ -CONHTG ₄ TKNH ₂	C ₈₃ H ₉₉ F ₁₇ N ₃₉ O ₂₂	2316.7555	2316.6396
PNA-5	CH ₃ -(CH ₂) ₉ -CONHTG ₄ T KNH ₂	C ₈₃ H ₁₁₆ N ₃₉ O ₂₂	2010.9157	2010.8900
PNA-6	CF ₃ -(CF ₂) ₇ -(CH ₂) ₂ -CONH T(U ^{NH₂}) ₄ T KNH ₂	C ₇₉ H ₉₉ F ₁₇ N ₃₁ O ₂₆	2220.71	2220.8210
PNA-7	CH ₃ -(CH ₂) ₉ -CONHT(U ^{NH₂}) ₄ T KNH ₂	C ₇₉ H ₁₁₆ N ₃₁ O ₂₆	1914.8708	1914.9725
PNA-8	CF ₃ -(CF ₂) ₇ -(CH ₂) ₂ -CONHTU ₄ T KNH ₂	C ₇₉ H ₉₅ F ₁₇ N ₂₇ O ₂₆	2160.6670	2160.5957
PNA-9	CH ₃ -(CH ₂) ₉ -CONHTU ₄ T KNH ₂	C ₇₉ H ₁₁₂ N ₂₇ O ₂₆	1854.8272	1854.9534

K = L-Lysine

3A.11 CD spectroscopy of fatty acid chain conjugated PNA hexamers

CD spectroscopic measurements of fatty acid chain conjugated PNA hexamers were recorded in sodium phosphate buffer (10 mM, pH 7.2) containing NaCl (100 mM) at 25 μM concentration to examine the effect of fatty acid chain conjugation on the tetraplex. Perfluoroundecanoyl conjugated PNA-4 (FCC-G) exhibited the maxima at 228 nm and one minima at 263 nm in addition to one maxima at 302 nm suggesting that perfluoroundecanoyl chain does not affect on the tetraplex formation. Hydrocarbon chain undecanoyl conjugated PNA-5 (HCC-G) showed two positive bands at 228 nm and 302 nm along with negative band at 273 nm exhibiting shifting of band by 10 nm as compared to PNA-4 (FCC-G). It shows that hydrocarbon undecanoyl chain influences the tetraplex structure. However, FCC-G and HCC-G showed different CD pattern as that of G-rich PNA-1. The possible reason may be that the fatty acid chain increases the aggregation of molecule due to which CD pattern might be different

The FCC conjugated PNA-6 (FCC-U^{NH₂}) displayed a maxima at 228 nm and minima at 263 nm along with one positive band around 302 nm suggesting G-

quadruplex formation. The HCC chain conjugated PNA-7 (HCC-U^{NH₂}) exhibited similar types of bands as that of HCC chain conjugated PNA-5 (HCC-G) displaying the shifting of band by 10 nm as compared to PNA-6 (FCC-U^{NH₂}). The FCC conjugated PNA-8 (FCC-U) and HCC conjugated PNA-9 (HCC-U) didn't show any characteristic CD signature suggesting that there is no formation of tetraplex structure by these PNA hexamers (Figure 18). Thus, fatty acid chain conjugation favored the tetraplex formation by U^{NH₂}-PNA.

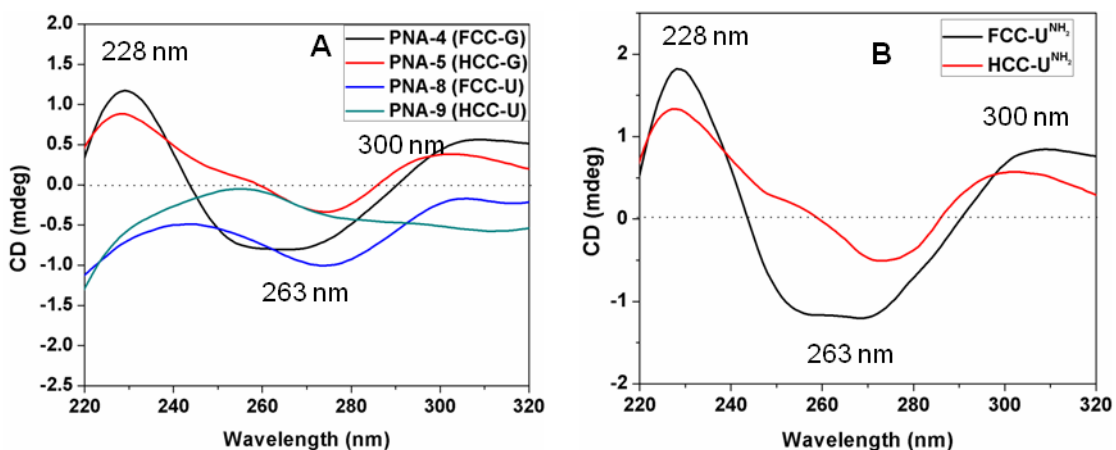


Figure 18. CD profile of fatty acid chain conjugated PNA hexamers A) G and U-PNA B) U^{NH₂} PNA.

The fluoroalkyl chain is more hydrophobic as compared to its counterpart hydrocarbon chain. Therefore aggregation in fluoroalkyl chain conjugated PNA may be more as compared to hydrocarbon chain conjugated PNA and thus have different effects.

3A.12 Characterization of self assembled structure by FESEM

Field emission scanning electron microscopy (FESEM) was employed to observe the self assembled structures formed by synthesized PNA oligomers. The individual PNA oligomers (40 μ M) were heated at 90 $^{\circ}$ C for 10 min and allowed to cool slowly at room temperature and further used for recording the microscopic pictures.

The oligomers PNA 1 (G-PNA), PNA 2 (U^{NH₂}-PNA) and PNA 3 (U-PNA) showed nanoparticle formation in the range 50-300 nm. The guanine linked PNA hexamer PNA-1 has showed uniform nanoparticle formation in the range 50-60 nm. The modified PNA oligomer PNA-2 (U^{NH₂}-PNA) exhibited the self-assembled structure

in the range of 300-320 nm whereas PNA-3 (U-PNA) exhibited the formation of nanoparticle of size 165 nm (Figure 19).

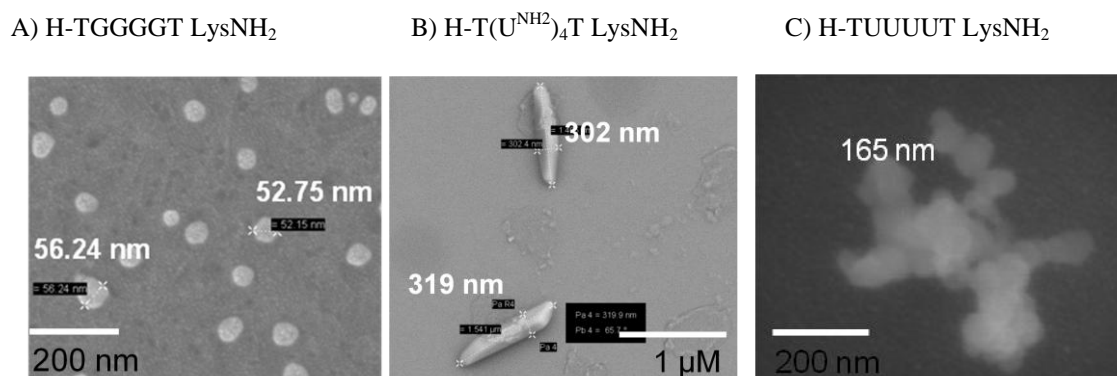


Figure 19. FESEM images of A) PNA-1, B) PNA-2 and C) PNA-3.

The fluoroalkyl undecanoyl chain (FCC) conjugated PNA oligomers PNA-4, PNA-6 and PNA-8 displayed the formation of nanoparticle varying from 80 to 550 nm range. The PNA-4 (FCC-G) showed the increase in the nanoparticle size to 180-190 nm as compared to PNA-1 (G-PNA) suggesting that the fluorinated hydrocarbon chain promote the self-assembly. 5-Aminouracil linked FCC conjugated PNA-6 (FCC-U^{NH₂}) had more ordered nanoparticle of uniform size around 85 nm as compared to the PNA-2 (U^{NH₂}, 300-320 nm) suggesting that fluorocarbon chain enhanced the nanoparticle formation and leading to well ordered morphology. The FCC conjugated PNA-8 (FCC-U) showed polydispersed nanoparticles with random size indicating that the self assembled structure but in disordered manner (Figure 20).

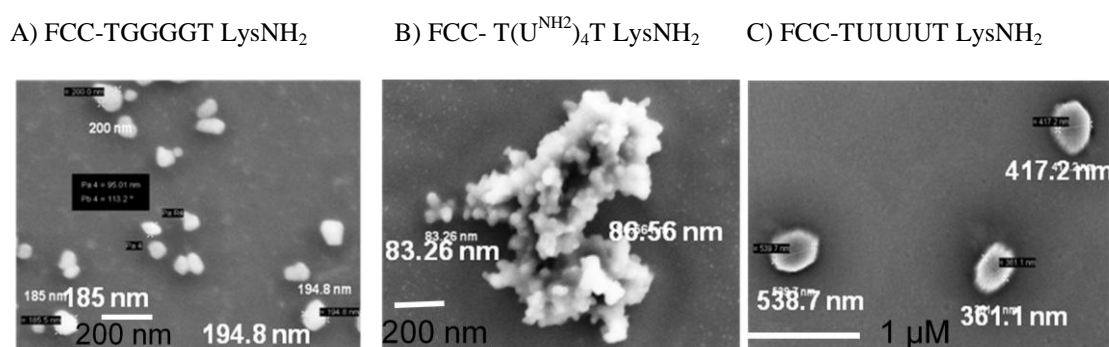


Figure 20. FESEM images of A) PNA-4, B) PNA-6 and C) PNA-8.

The hydrocarbon chain undecanoyl (HCC) conjugated PNA-5 (HCC-G) has increased nanoparticle size (288 nm) as compared to PNA-1 (G-PNA, 52 nm) and FCC

conjugated PNA-4 (FCC-G, 185 nm). This suggested the ability of hydrocarbon chain to promote self assembled nanoparticle formation. The HCC conjugated 5-aminouracil linked PNA-7 (HCC-U^{NH₂}) showed the nanoparticle formation of size 176 nm and PNA-9, a HCC conjugated PNA oligomer formed nanoparticles that are not uniform in size (Figure 21).

A) HCC-TGGGGTLysNH₂ B) HCC- T(U^{NH₂})₄T LysNH₂ C) HCC-TUUUUT LysNH₂

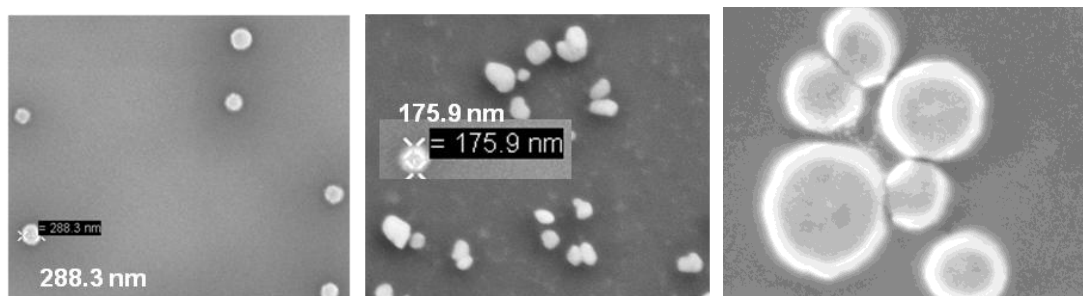


Figure 21. FESEM images of A) PNA-5, B) PNA-7 and C) PNA-9.

Table 3: Size of nanoparticles formed by different PNA hexamers

Sr. No.	PNA	Size (nm)
1	PNA-1 (G-PNA)	50-60
2	PNA-2 (U ^{NH₂} -PNA)	300-320
3	PNA-3 (U-PNA)	165
4	PNA-4 (FCC-G-PNA)	180-190
5	PNA-5 (HCC-G-PNA)	288
6	PNA-6 (FCC-U ^{NH₂} -PNA)	85
7	PNA-7 (HCC-U ^{NH₂} -PNA)	176
8	PNA-8 (FCC-U-PNA)	Random
9	PNA-9 (HCC-U-PNA)	Random

The above results indicate that the self assembly of PNA oligomers can be enhanced by the conjugation of hydrocarbon chain and fluoroalkyl chain effects are relatively more for U^{NH₂}-PNAs that can form tetraplex. The self-assembly properties of tetraplex derived by 5-aminouracil may lead to develop rationalized creation of nanostructure as G-quadruplex and their structural motifs have potential applications.

3A.13 Summary

In summary, this section deals with the synthesis of different PNA hexamers by employing standard solid phase peptide synthesis protocol and their studies by CD spectroscopy and FESEM technique. Results showed that U^{NH_2} -PNAs may form tetraplex structure like guanine. From concentration and pH dependent CD measurements it was observed that U^{NH_2} form tetraplex structure (25 μM) at physiological pH and FESEM revealed that U^{NH_2} -PNA forms well ordered nanoparticle of uniform size (85 nm). Formation of tetraplex structure by U^{NH_2} -PNAs may be due to the presence of NH_2 group at C5 of 5-aminouracil which are self associating to form tetraplex structure.

Thus, this section demonstrated that 5-aminouracil may form tetraplex type of structure and also formation of self assembled structures were promoted upon conjugation of fatty acid chain. However, to confirm whether 5-aminouracil favors the tetraplex formation like guanine, more techniques like NMR, X-ray crystallography are needed to study.

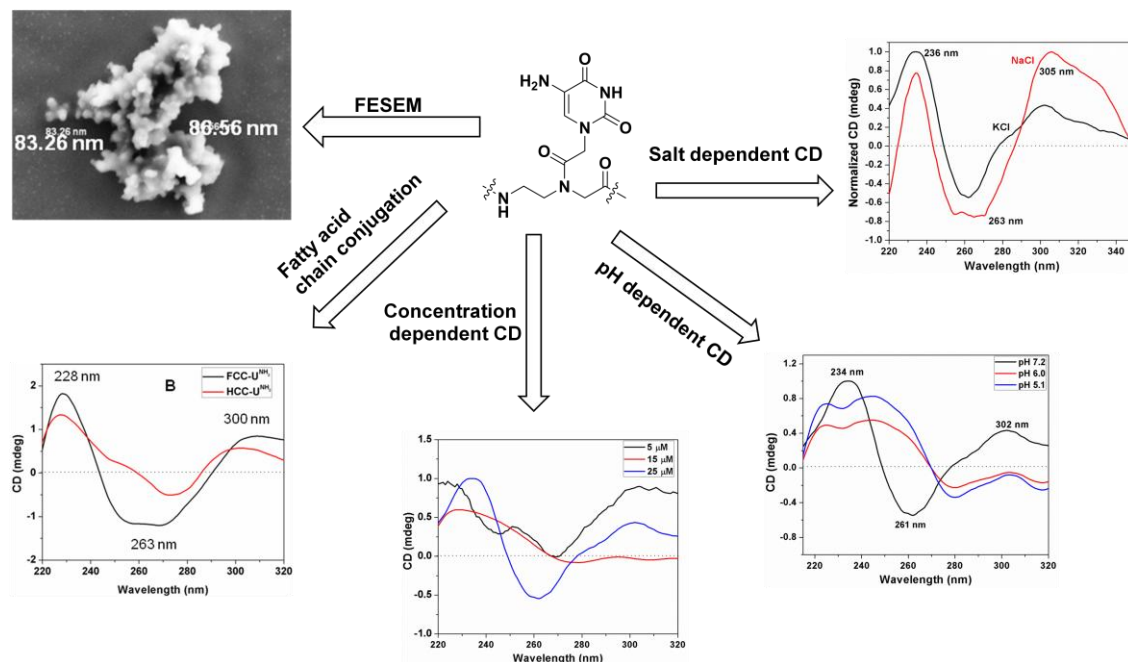


Figure 23. Summary of section 3A

The next section deals with the host-guest interaction of PNA tetraplex with β -cyclodextrin.

**Section 3B. Host-Guest Complexation of
Adamantyl-G₄ PNA Quadruplex With Sugar
Capped β -Cyclodextrin to Study Carbohydrate-
Protein Interaction**

3B.1 Introduction

Carbohydrates play critical role in numerous physiological as well as pathological cell functions owing to their structural complexity and ubiquitous nature. They are important receptors in cell-cell interactions and cell-matrix interactions and are requisite for leucocytes extravasation during inflammation and lymphocyte recirculation.⁶⁷ Many microorganisms such as, bacteria, viruses and their toxins have evolved to bind carbohydrates on the cell surface, which is prerequisite for infection to occur.^{68,69} Carbohydrates interact with various protein families including lectins, antibodies, sugar transporters and enzymes. Generally, these carbohydrate-protein interactions are quite weak and not specific. Therefore nature has developed multivalent systems to communicate the carbohydrate-protein interactions (Figure 21).

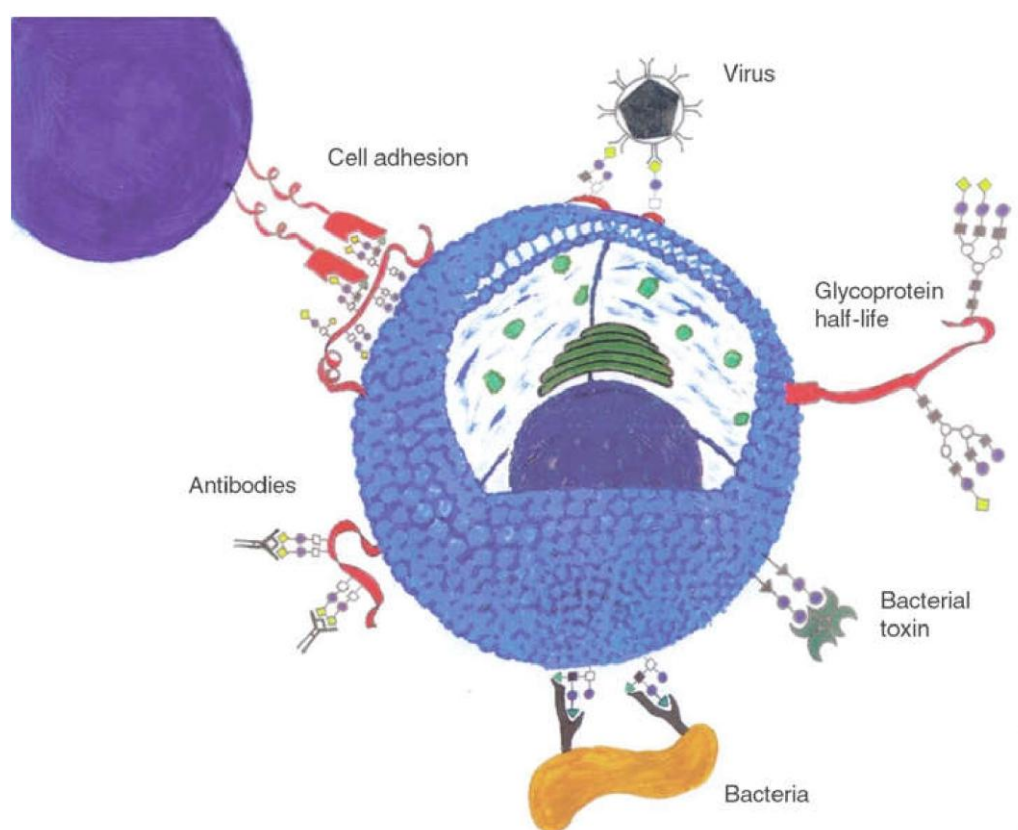


Figure 24. Multivalent carbohydrate-protein interaction.⁶⁷

The binding of receptors on the cell surface to the multivalent systems can trigger variety of biological processes. Such multivalent binding events can have

unique consequences that are exclusively different than those initiated by monovalent systems.^{70,71} Multivalent systems exhibit the specificity in protein-carbohydrate recognition processes.⁷² The superior binding affinities of multivalent systems arise from the steric stabilization and entropically enhanced binding.⁷³

There is growing interest on developing multivalent systems for studying carbohydrate-protein interactions. One of the first applications of multivalent inhibitors was focused on preventing binding of influenza virus to host cells.⁷⁴⁻⁷⁵ Hamilton et al.⁷⁶ have developed G-quadruplexes based multivalent systems to study the carbohydrate-protein interactions. Whitesides et al.⁷⁷ have developed sialic acid based liposomes as a polyvalent system for effective agglutination of RBCs by influenza virus.

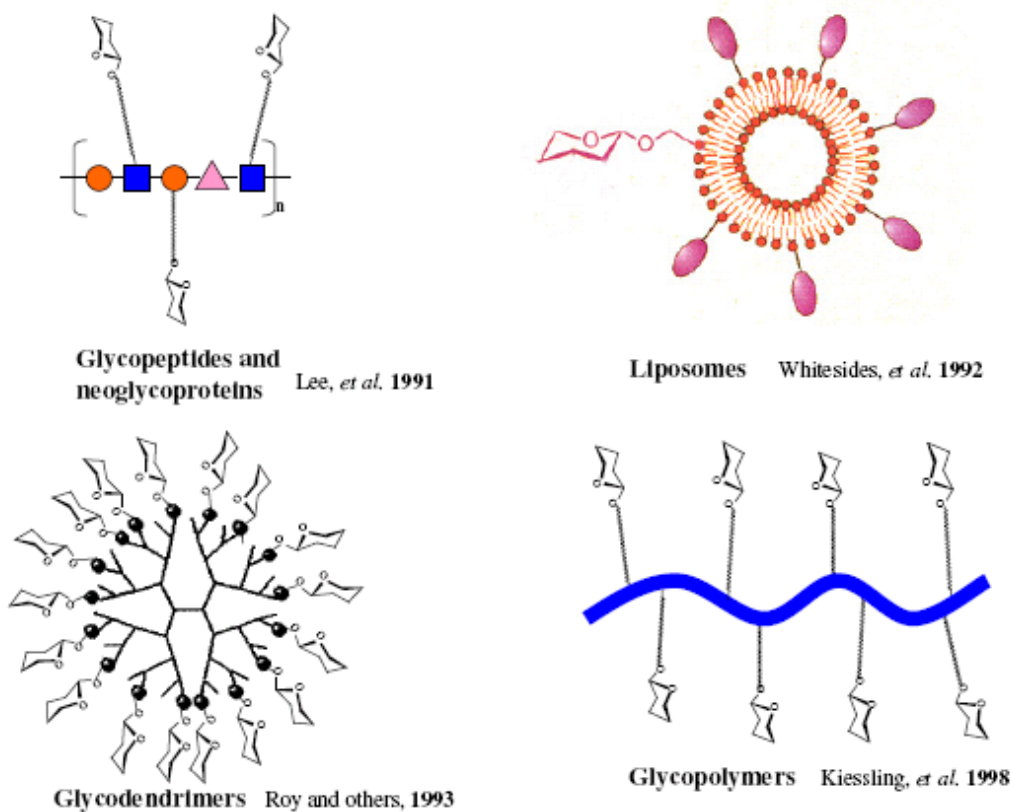


Figure 25. Multivalent systems reported to study carbohydrate-protein interaction

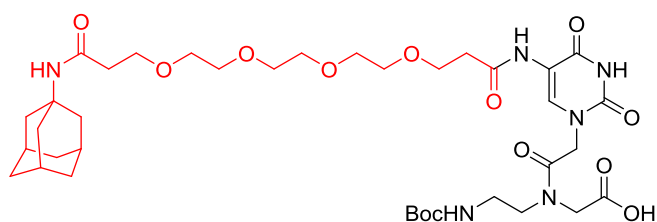
Multivalent systems can be generated from the self assembled structures. G-quadruplexes are the self assembled structures formed by the self association of guanine. Since PNAs form stable G-quadruplexeslike DNA, PNA based quadruplexes can be used to develop multivalent system to study the carbohydrate –protein

interactions. In this context, the present work involves the synthesis of adamantyl linked PNA quadruplexes to study the carbohydrate-protein interactions.

3B.2 Rationale and objective of present work

The main idea behind the present work is to develop PNA based multivalent system as PNA is stable to nucleases.¹³ The objective behind the present work is,

1) Synthesis of the adamantyl tetraethylene glycol conjugated PNA monomer ($U^{\#}$).



2) Incorporation of modified PNA monomer into PNA hexamer.

3) Use of the G-quadruplexes for host-guest system as adamantane is a good guest for cyclodextrin to study carbohydrate-protein interactions.

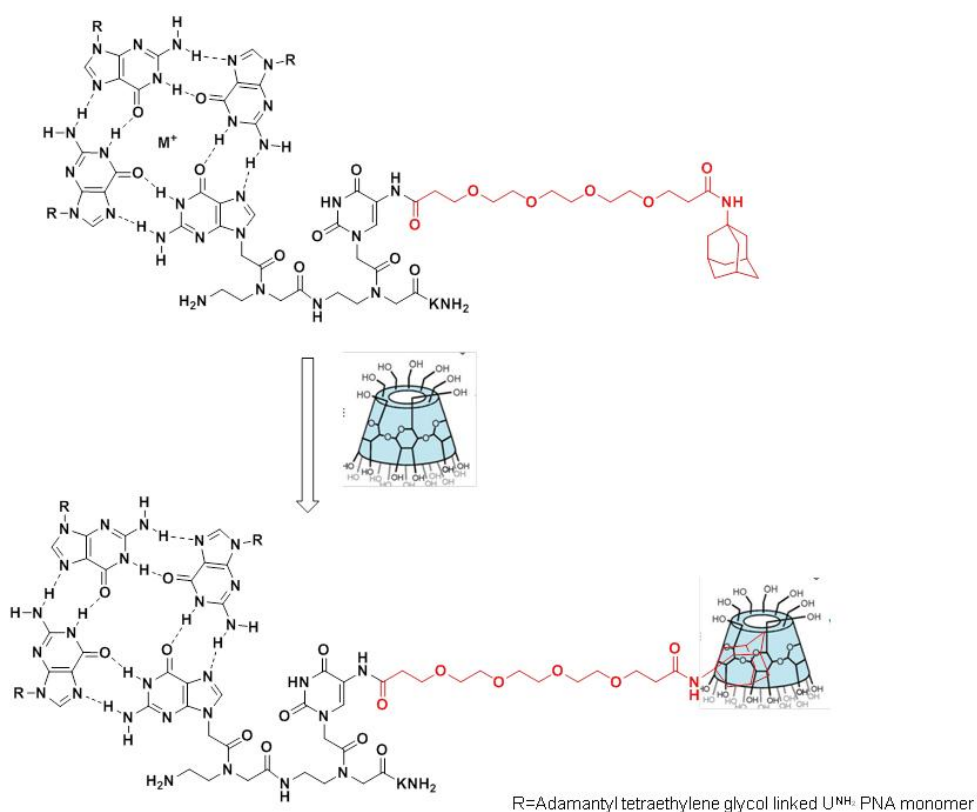


Figure 26. Rationale of the present work.

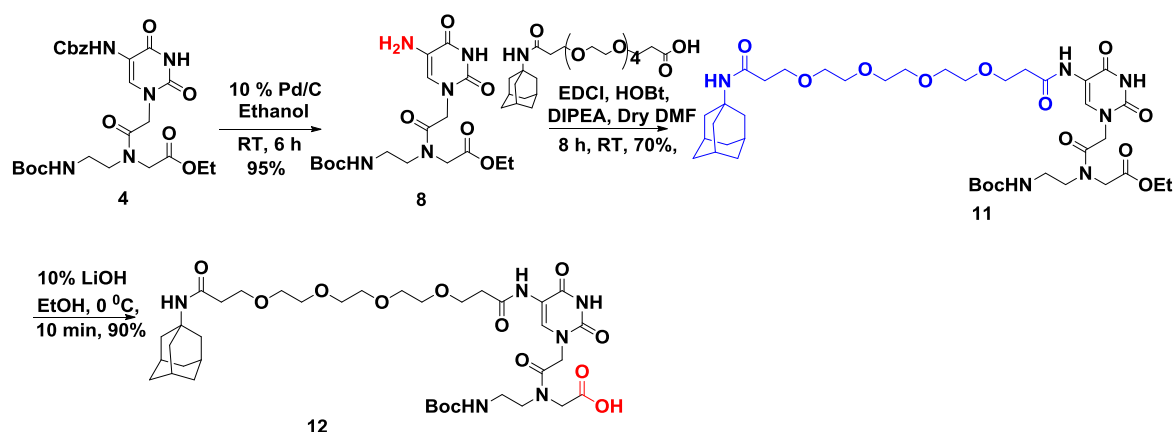
3B.3 Results and discussion

This section discusses the synthesis of desired monomer followed by its incorporation into PNA sequence by solid phase peptide synthesis and biophysical studies of tetraplex formation.

3B.3.1 Synthesis of adamantyl tetraethylene glycol-U-aeg-PNA monomer (U[#])

Compound **4** on hydrogenation with 10% Pd/C yielded the compound **8**, which was subsequently coupled with adamantyl tetraethylene glycol acid by using EDCI, HOBt and DIPEA in DMF to obtain compound **11**. This compound upon hydrolysis with 10% aq. LiOH gave the desired aeg-PNA-adamantyl tetraethylene glycol-U-acid monomer **12** (U[#]).

Scheme 1:



3B.3.2 Synthesis and characterization of PNA oligomers

The *N*-Boc protected monomer was incorporated into PNA oligomers through established solid phase peptide synthesis protocol as per described in Chapter 1. The synthesized oligomers were purified by RP-HPLC and characterized by MALDI-TOF mass spectroscopy (Table 4).

Table 4: MALDI-TOF of PNA hexamers.

S. No.	PNA sequence	Mol. formula	Calcd mass	Obsvd mass
1	H-TGGGGT _{Lys} NH ₂	C ₇₂ H ₉₇ N ₃₉ O ₂₁	1842.7643	1842.9417
2	H-U [#] GGGGT _{Lys} NH ₂	C ₉₃ H ₁₃₀ N ₄₁ O ₂₇	2253.006	2253.4951

3B.4 UV-Vis spectroscopy

The UV absorbance spectra of synthesized oligomers were recorded in 10 mM phosphate buffer and 100 mM NaCl at 10 °C. Both the oligomers exhibited two bands in the region 250-270 nm. The intense band at 253 nm and less intense peak at 270 nm suggested the self association bringing the strands together to form self-assembled structure. The UV spectrum of control DNA TG4T in 10 mM potassium phosphate buffer and 100 mM KCl showed overlapping of two peaks in this region.⁷⁸

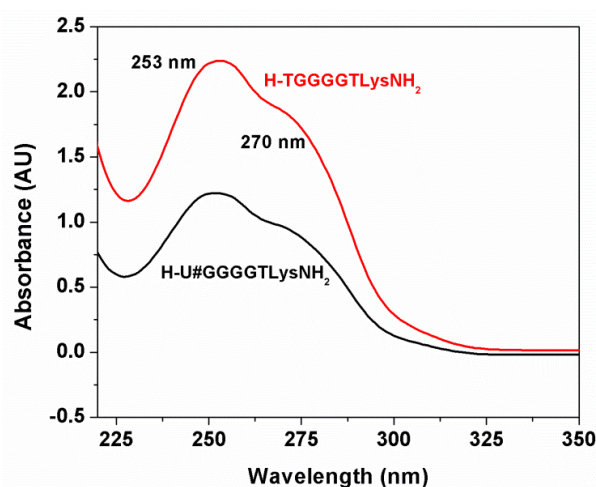


Figure 27. UV-Vis spectra of PNA oligomers.

3B.5 CD spectroscopic measurements

The CD spectroscopic measurements of synthesized PNA oligomers were recorded in the presence and absence of 100 mM NaCl. It was observed that both PNAs showed characteristic type I CD pattern of quadruplex formation in the presence of sodium chloride.

The PNA hexamer (H-TGGGGTLysCONH₂) without NaCl didn't show any significant CD pattern. Similarly modified PNA oligomer (H-U#GGGGTLysCONH₂) also didn't show a characteristic CD signature in the absence of NaCl. Upon addition of 100 mM NaCl, the stabilization of self assembled structure observed. It was found that both oligomers exhibited one positive band at 258 nm and one negative band at 236 nm along with the less intense band around 295 nm suggesting the formation of quadruplex structure (Figure 28).

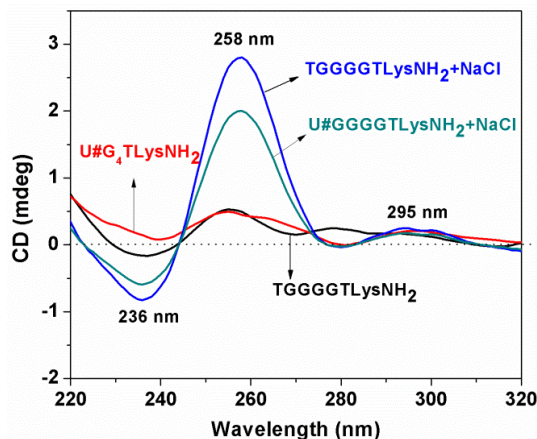


Figure 28. CD profile of PNA oligomers.

3B.6 Study of host-guest interaction by CD spectroscopy

The host-guest interaction was studied by CD spectroscopy. β -cyclodextrin was added in different equivalents to examine the effect of β -cyclodextrin on the tetraplex structure and hence to study the host-guest interaction. It was observed that upon addition of β -cyclodextrin reversed the CD pattern of tetraplex. The reversal of the positive band at 236 nm and negative band at 258 nm suggested that the β -cyclodextrin changes the orientation of tetraplex. The steric clash upon host-guest complexation with tetraplex might be responsible for reversing the CD pattern. The CD spectroscopic measurement of control PNA without adamantane linker ($TG_4TlysNH_2$) was recorded upon addition of β -cyclodextrin, which showed no effect of β -cyclodextrin on the tetraplex structure of G-rich PNA. It suggested that β -cyclodextrin interacts with adamantane linked PNA changing the orientation of tetraplex structure

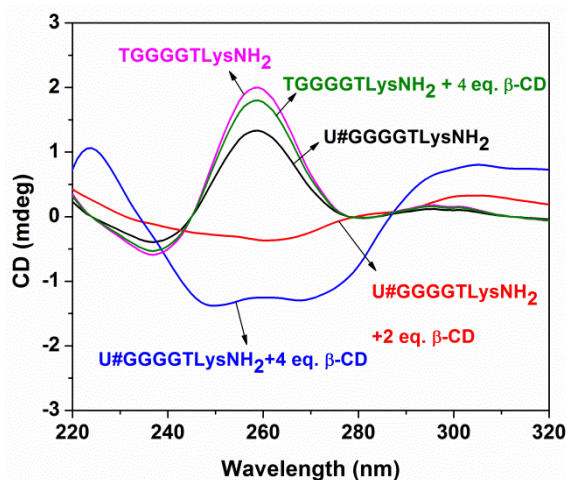


Figure 29. CD profiles of control and modified PNA oligomer after the addition of β -cyclodextrin

The host-guest complexation of adamantyl tetraethylene glycol conjugated PNA quadruplex need to be studied more by different techniques.

3B.7 Summary

To summarize this section deals with the synthesis of adamantyl tetraethylene glycol conjugated PNA monomer and its incorporation into PNA hexamers by using solid phase peptide synthesis protocol. The tetraplex formation of modified sequence was examined by CD spectroscopy. The interaction of adamantyl conjugated tetraplex with β -cyclodextrin was examined by CD spectroscopy and found that host-guest interaction leads to change the orientation of tetraplex. This PNA tetraplex based multivalent system can be used as a platform to study carbohydrate-protein interactions.

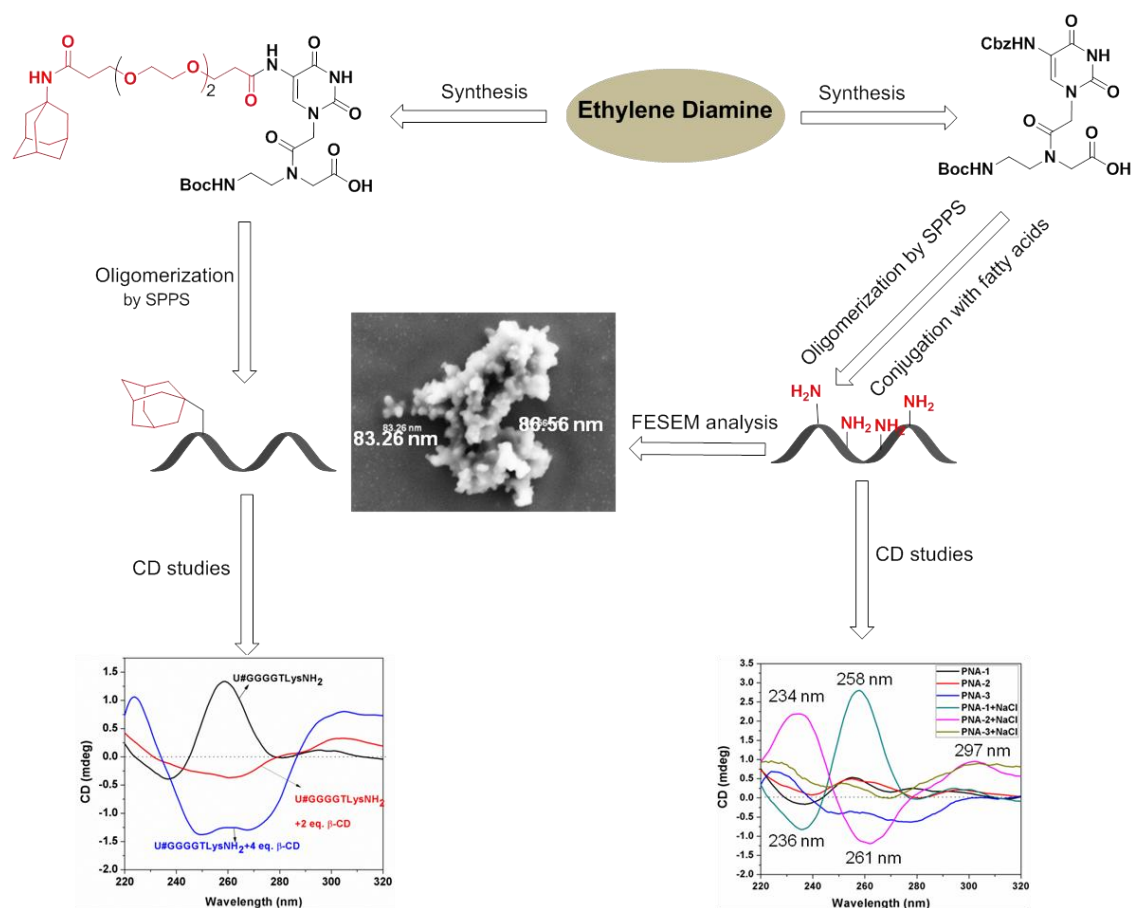


Figure 30. Summary chapter 3.

3.2 Experimental procedures

3.2.1 Synthesis, Cleavage and purification PNA oligomers

The modified and unmodified PNA monomers were incorporated into 6-mer PNA oligomers using standard solid phase protocol on L-lysine derivatized MBHA resin having loading value 0.35 mmol/g. All PNA oligomers were synthesized under microwave conditions (25 watts, 75 °C, for 5 min.) using the sintered glass column. The PNA monomers were coupled one after another to make a PNA sequence using HBTU, HOBT and DIPEA in DMF as coupling reagents.

After the synthesis, PNAs were cleaved from the resin using trifluoromethane sulfonic acid (TFMSA) and trifluoroacetic acid (TFA); After the cleavage reaction, the PNA was precipitated with cold diethyl ether and was isolated by centrifugation. The precipitate was dissolved in deionized water. The synthesized PNA oligomers were purified on Dionex ICS 3000 HPLC system using semipreparative BEH130 C18 (10 X 250 mm) column. Purification of PNA oligomers was performed with gradient elution method: A to 50% B in 20 min; 100% B in 30 min and B to 100% A in 35 min. A = CH₃CN:H₂O (5:95); B = CH₃CN:H₂O (50:50) having 1% TFA in each with a flow rate of 2 mL/min. All the HPLC profiles were monitored at 254 and 260 nm wavelength.

3.2.2 Circular dichroism

CD spectra were recorded on JASCO J-815 spectropolarimeter connected with a peltier. The calculated amounts of individual PNA oligomer and the complementary was dissolved in sodium phosphate buffer (10 mM) and NaCl (100 mM); pH 7. The samples were annealed by heating at 90 °C for 10 min. followed by slow cooling to room temperature for at least 12 h which were subsequently cooled at 4 °C for 48 to 72 h. CD measurements were recorded at 10 °C with accumulation of 15 scans from 350 to 190 nm using 2 mm cell, a resolution of 0.1 nm, band-width of 1 nm, sensitivity of 2 m deg, response of 2 sec and a scan speed of 50 nm/min.

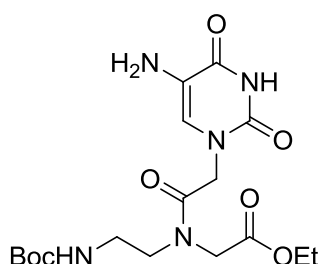
3.2.3 Sample preparation for FESEM

PNA oligomers with concentration of 40 µM and heated to 90 °C for 10 min and cooled to room temperature. 5 µL of each sample was placed on a silicon wrapper

and dried under high vacuum for 10-12 h which were subsequently subjected for FESEM imaging.

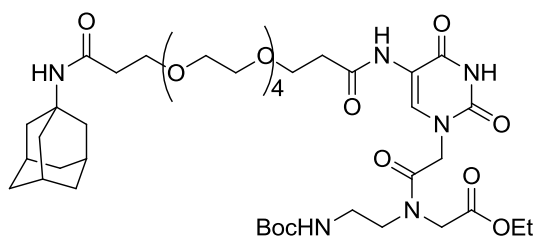
3.2.4 Procedures and spectral data

Ethyl-2-(2-(5-amino-2,4-dioxo-3,4-dihydropyrimidin-1(2H)-yl)-N-(2-((tert-butoxycarbonyl)amino)ethyl)acetamido)acetate



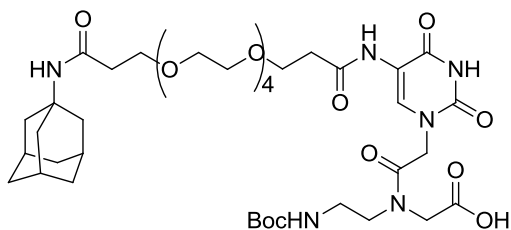
To the Compound **2** (3 g, 6 mmol) dissolved in ethanol, 10 % Pd/C was added under H₂ atmosphere and stirred at room temperature for 6 h. Completion of the reaction was monitored by TLC. After completion of reaction, the reaction mixture was filtered on celite-545 pad and filtrate was collected which on subsequently evaporated to obtain solid product. This compound was used for further reaction without any further purification.

Adamantan-1-yl-amino tetrarthylen glycol amido ethyl-2-(2-(5-amino-2,4-dioxo-3,4-dihydropyrimidin-1(2H)-yl)-N-(2-((tert-butoxycarbonyl)amino)ethyl)acetamido)acetate



Adamantane tetraethylene glycol acid compound was dissolved in dry DMF and stirred at 0 °C followed by subsequent addition of EDCI, HOBt and DIPEA and stirring was continued at same temperature for 5 min. To the resultant solution, compound **8** in dry DMF was added slowly with continuous stirring at same temperature for 5 min. After 5 min, reaction mixture was brought to room temperature and stirred for 12 h. Completion of the reaction was monitored by TLC. After completion of reaction, reaction mixture was diluted with water (40 mL) and extracted with ethyl acetate (3 x 75 mL). The combined organic layer was washed with saturated solution of NaHCO₃ (20 mL) and then again washed with water (3 x 40 mL) followed by washing with brine (25 mL). The collected organic layer was dried over anhydrous sodium sulfate, collected by filtration and concentrated on rota evaporator. The crude product was purified on column using silica gel in petroleum ether: ethyl acetate (1.5:3.5) (Yield 3.5 g, 75%).

Adamantan-1-yl-amino tetraethylene glycol amido ethyl-2-(2-(5-amino-2,4-dioxo-3,4-dihydropyrimidin-1(2H)-yl)-N-(2-((tert-butoxycarbonyl)amino)ethyl)acetamido)acetate



Compound **4** (1 g, 2 mmol) was dissolved in ethanol and stirred at 0 °C. To this, 10% aqueous LiOH (1.5 mL) was drop wise added at the same temperature for 10 min. The completion of reaction was monitored by TLC. After completion of reaction, solvent was removed on rotary evaporator. Ethyl acetate was added to the residue and it was acidified by addition of saturated aqueous solution of potassium bisulfate till the pH comes down to 3-4. Organic layer was collected and washed with brine solution. The organic layer was concentrated on rota evaporator to get solid product which was further dried on high vacuum and stored in vacuum dessicator (Yield 0.85 g, 90%).

3.3 References

1. (a) Shida, T.; Yokoyama, K.; Tamai, S.; Sekiguchi, J.; *Chem. Pharm. Bull.* **1991**, *39*, 2207-2211., (b) Xu, X.; Hamhouyia, F.; Thomas, S. D.; Burke, T. J.; Girvan, A. C.; McGregor, W. G.; Trent, J. O.; Miller, D. M.; Bates, P. J. *J. Biol. Chem.* **2001**, *276*, 43221-43230.
2. (a) Jin, R.; Breslauer, K. J.; Jones, R. A.; Gaffney, B. L. *Science*, 1990, *250*, 543-546; (b) Guschlbauer, W.; Chantot, J. F.; Thiele, D. *Biomol. Stru. Dyn.* **1990**, *8*, 491-511.
3. Gellert, M.; Lipsett, M. N.; Davies, D. R. *Proc. Natl. Acad. Sci. USA*, **1962**, *48*, 2013-2018.
4. (a) Balagurumoorthy, P.; Brahmachari, S. K.; Mohanty, D.; Bansal, M.; Sasisekharan, V. *Nucleic Acids Res.* **1992**, *20*, 4061-4067; (b) Mohanty, D.; Bansal, M. *Nucleic Acids Res.* **1993**, *21*, 1767-1774.
5. (a) Blackburn, E. H.; Szostak, J. W. *Annu. Rev. Biochem.* **1984**, *53*, 164-94; (b) Williamson, J. R. *Curr. Opin. Struct. Biol.* **1993**, *3*, 357-362.
6. Sen, D.; Gilbert, W. A. *Nature*, **1990**, *344*, 410-414.
7. Keniry, M. A.; *Biopolymers*, **2000**, *56*, 123-
8. Patel, D. J.; Phan, A. T.; Kuryavyyi, V. *Nucleic Acids Res.* **2007**, *35*, 7429-
9. Hardin, C. C.; Watson, T.; Corregan, M.; Bailey, C. *Biochemistry*, **1992**, *31*, 833-
10. Burge, S.; Watson, T.; Parkinson, G. N.; Hazel, P.; Todd, A. K.; Neidle, S. *Nucleic Acids Res.*, **2006**, *34*, 5402.
11. Phillips, K.; Dauter, Z.; Murchie, A. I. H.; Lilley, D. M.; Luisi, B. *J. Mol. Biol.* **1997**, *273*, 171-182.
12. Aboul-ela, F.; Murchie, A. I. H.; Norman, D. G.; Lilley, D. M. *J. Mol. Biol.* **1994**, *243*, 458-471.
13. Caceres, C.; Wright, G.; Gouyette, C.; Parkinson, G.; Subirana, J. A. *Nucleic Acids Res.* **2004**, *32*, 1097-1102.
14. Biffi, G.; Tannahill, D.; McCafferty, J.; Balasubramanian, S. *Nature Chem.* **2013**, *5*, 182-186.
15. Rodriguez, R.; Miller, K. M.; Forment, J. V.; Bradshaw, C. R.; Nikan, M.; Britton, S.; Oelschlaegel, T.; Xhemalce, B.; Balasubramanian, S.; Jackson, S. P. *Nature Chem. Biol.* **2012**, *8*, 301-310.
16. Bochman, M. L.; Paeschke, K.; Zakian, V. A. *Nature Rev. Genet.* **2012**, *13*, 770-780.
17. Maizels, N.; Gray, L. T. *PLoS Genet.* **2013**, *9*, e1003468.
18. Balasubramanian, S.; Hurley, L. H.; Neidle, S. T. *Nature Rev. Drug Discov.* **2011**, *10*, 261-275.
19. Simonsson, T. *Biol. Chem.* **2001**, *382*, 621-628.

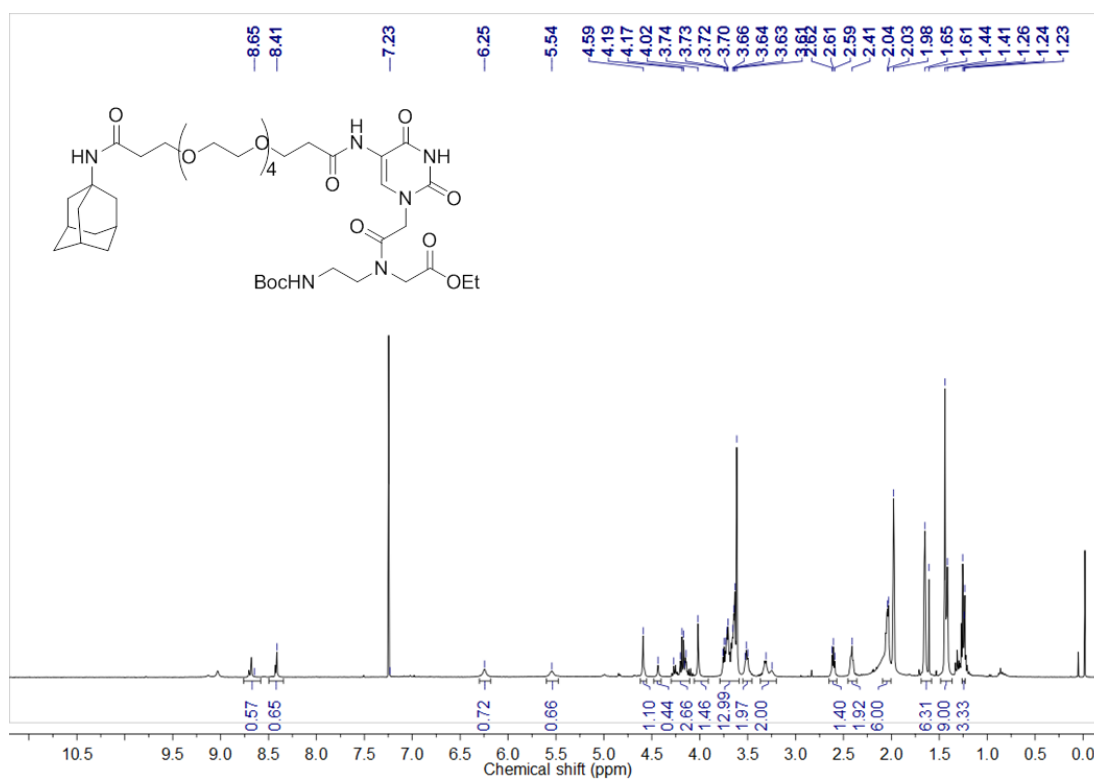
20. Kim, J.; Cheong, C.; Moore, P. B. *Nature*, **1991**, *351*, 331-332.
21. Christiansen, J.; Kofod, M.; Nielsen, F. C. *Nucleic Acids Res.* **1994**, *22*, 5709-5716.
22. Deng, J.; Xiong, Y.; Sundaralingam, M. *Proc. Natl. Acad. Sci. USA*, **2001**, *98*, 13665-13670.
23. Sacca, B.; Lacroix, L.; Mergny, J. L. *Nucleic Acids Res.* **2012**, *33*, 1182-1192.
24. Zhang, A. Y.; Bugaut, A.; Balasubramanian, S. *Biochemistry*, **2011**, *50*, 7251-7258.
25. Collie, G. W.; Haider, S. M.; Neidle, S.; Parkinson, G. N. *Nucleic Acids Res.* **2010**, *38*, 5569-5580.
26. Webba da Silva M. *Methods*, **2007**, *43*, 264-277.
27. Smith, F.W.; Schultze, P.; Feigon, J. *Structure*, **1995**, *3*, 997-1008.
28. Wang, Y.; Jin, R.; Gaffney, B.; Jones, R. A.; Breslauer, K. J. *Nucleic Acids Res.* **1991**, *19*, 4619-4622.
29. Wang, Y.; Patel, D. J. *Biochemistry*, **1992**, *31*, 8112-8119.
30. Wang, Y.; de los Santos, C.; Gao, X.; Greene, K.; Live, D.; Patel, D. J. *J. Mol. Biol.* **1991**, *222*, 819-932.
31. Mergny, J. L.; Phan, A. T.; Lacroix, L. *FEBS Lett.* **1998**, *435*, 74-78.
32. Rachwal, P. A.; Fox, K. R. *Methods*, **2007**, *43*, 291-301.
33. Paramasivan, S.; Rujan, I.; Bolton, P. H. *Methods*, **2007**, *43*, 324-331.
34. Kypr, J.; Kejnovska, I.; Renciuik, D.; Vorlickova, M. *Nucleic Acids Res.* **2009**, *37*, 1713-1725.
35. Liu, W.; Zhu, H.; Zheng, B.; Cheng, S.; Fu, Y.; Li, W.; Lau, T.C.; Liang, H. *Nucleic Acids Res.* **2012**, *40*, 4229-4236.
36. Padmanabhan, K.; Tulinsky, A.; *Acta Crystallogr.* **1996**, *52*, 272-282.
37. (a) Henderson, E.; Hardin, C. C.; Walk, S. K.; Tinoco, I.; Blackburn, E. H. *Cell*, **1987**, *51*, 899-908; (b) Macaya, R. F.; Schultz, P.; Smith, F. W.; Roe, J. A.; Feigon, J. *Proc. Natl. Acad. Sci. USA*, **1993**, *90*, 3745-3749.
38. Sundquist, W. I.; Klug, A. *Nature*, **1989**, *342*, 825-829.
39. Sen, D. and Gilbert, W. *Nature*, **1988**, *334*, 364-366.
40. Marathias, V. M.; Bolton, P. H. *Biochemistry*, **1999**, *38*, 4355-4364.
41. Kang, C.; Zhang, X.; Ratliff, R.; Moyzis, R.; Rich, A. *Nature* **1992**, *356*, 126-131.
42. Sen, D.; Gilbert, W. *Curr. Opin. Struct. Biol.* **1991**, *1*, 435-438.
43. Phan, A. T.; Mergny, J. L. *Nucleic Acids Res.* **2002**, *30*, 4618-4625.
44. Zhou, J.; Amrane, S.; Korkut, D. N.; Bourdoncle, A.; He H. Z.; Ma, D. L.; Mergny J. L. *Angew. Chem. Int. Ed.* **2013**, *52*, 7742-7746.

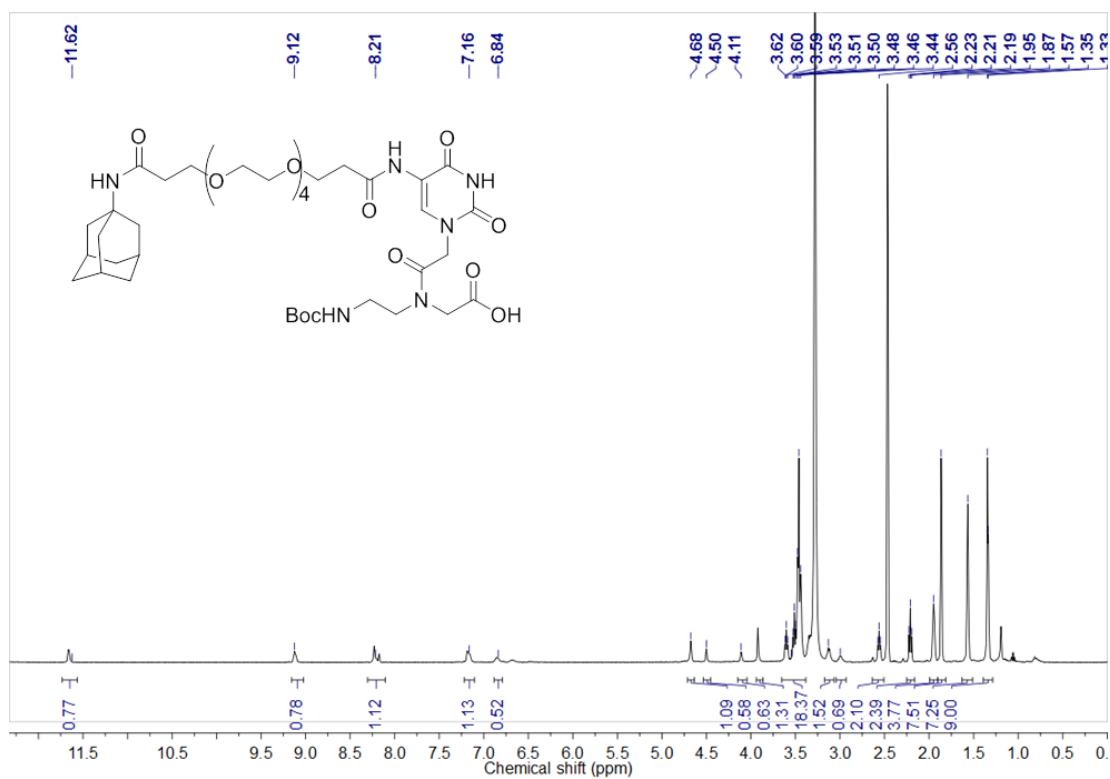
45. (a) Bogdarina, W.; Schroeder, E.; Taylor, I. A.; Kneale, G. G. *J. Mol. Biol.* **2000**, *301*, 575-584; (b) Gaffney, B. L.; Wang, C.; Jones, R. A. *J. Am. Chem. Soc.* **1992**, *114*, 4047-4050.
46. (a) White, L. K.; Wright, W. E.; Shay, J. W. *Trends Biotechnol.* **2001**, *19*, 114-120; (b) Bearss, D. J.; Hurley, L. H.; Von Hoff, D. D. *Oncogene*, **2000**, *19*, 6632-6641; (c) Mergny, J. L.; Mailliet, P.; Lavelle, F.; Riou, J. F.; Laoui, A.; Helene, C.; *Drug Des.* **1999**, *14*, 327-339; (d) Simonsson, T.; Pecinka, P.; Kubista, M. *Nucleic Acids Res.* **1998**, *26*, 1167-1172. (e) Kettani, A.; Kumar, R. A. Patel, D. J. *J. Mol. Biol.* **1995**, *254*, 638-656.
47. Dominick, P. K.; Jarstfer, M. B.; *J. Am. Chem. Soc.* **2004**, *126*, 5050-5051.
48. Randazzo, A.; Esposito, V.; Ohlenschlager, O.; Ramchandran, R.; Mayol, L. *Nucleic Acids Res.* **2004**, *32*, 3083-3092.
49. Nielsen, P. E.; Egholm, O.; Berg, R. H.; Buchardt, O. *Science*, **1991**, *254*, 1497-1500.
50. Egholm, M.; Buchardt, O.; Christensen, L.; Beherns, C.; Freir, S. M.; Driver, D. A.; Berg, R. H.; Kim, S. K.; Norden, B.; Nielsen, P. E. *Nature*, **1993**, *365*, 566-568.
51. Esposito, V.; Galeone, A.; Mayol, L.; Messere, A.; Piccialli, G.; Randazz, A. *Nucleosides, Nucleotides and Nucleic Acids*, **2003**, *22*, 1681-1684.
52. (a) Datta, B.; Schmitt, C.; Armitage, B. A. *J. Am. Chem. Soc.* **2003**, *125*, 4111-4118; (b) Armitage, B. A. *Drug Discov. Today*, **2003**, *8*, 222-228.
53. Esposito, V.; Randazzo, A.; Messere, A.; Galeone, A.; Patraccone, L.; Giancola, C.; Piccialli, G.; Mayol, L. *Eur. J. Org. Chem.* **2003**, 3364-3371.
54. Ghosh, Y. K. Balasubramanian, S. A. *J. Am. Chem. Soc.* **2004**, *126*, 5944-5945.
55. Sharma, N. K.; Ganesh, K. N. *Org. Biomol. Chem.* **2011**, *9*, 725-729.
56. Sharma, N. K.; Ganesh, K. N. *Chem. Commun.* **2005**, 4330-4332.
57. Esposito, V.; Pepe, A.; Filosa, R.; Mayol, L.; Virgilio, A.; Galeone A. *Org. Biomol. Chem.* **2016**, *14*, 2938-2943.
58. Lau, C.; Bitton, R.; Peled, H. B.; Schultz, D. G.; Cookson, D. J.; Grosser, S. T.; Schneider, J. W. *J. Phys. Chem. B*, **2006**, *110*, 9027-9033.
59. Xu, J.; Luo, S. Z.; Shi, W. F.; Liu, S. Y. *Langmuir*, **2006**, *22*, 989-997.
60. Ge, Z. S.; Hu, J. M.; Huang, F. H.; Liu, S. Y. *Angew. Chem., Int. Ed.* **2009**, *48*, 1798-1802.
61. Cui, H. G.; Webber, M. J.; Stupp, S. I. *Pept. Sci.* **2010**, *94*, 1-18.
62. Vernille, J. P.; Kovell, L. C.; Schneider, J. W. *Bioconjugate Chem.* **2004**, *15*, 1314-1321.
63. Liu, L. H.; Li, Z. Y.; Rong L.; Si, Y. Q.; Lei, Q.; Cheng H.; Zhou, X.; Zhuo, R. X.; Zhang, X. Z. *ACS macro lett.* **2014**, *3*, 467-471.

64. Berger, O.; Abramovich, L. A.; Sakin, M. L.; Grunwald, A.; Peer, Y. L.; Bachar, M.; Buzhansky, L.; Mossou, E.; Forsyth, V. T.; Schwartz, T.; Ebenstein, Y.; Frolow, F.; Shimon, L. J. W.; Patolsky, F.; Gazit, E. *Nature nanotechnology*, **2015**, *10*, 353-360.
65. Ellipilli, S.; Murthy, R. V.; Ganesh, K. N. *Chem commun.* **2016**, *52*, 521-524.
66. Lowe, J. B.; *Curr. Opin. Cell Biol.* **2003**, *15*, 531-538.
67. Karsson, K. A. *Adv. Exp. Med. Biol.* **2001**, *491*, 431-443.
68. Holgersson, J.; Gustafsson, A.; Breimer, M. E.; *Immunology and cell biol.* **2005**, *83*, 694-708.
69. Mammen M.; Choi S.; Whitesides G. *Angew. Chem. Int. Ed.* **1998**, *37*, 2754–2794.
70. Mammen, M.; Choi, S. K.; Whitesides, G. M. *Angew Chem. Int. Ed. Engl.* **1999**, *37*, 2255-2794.
71. Lee, Y. C.; Lee, R. T. *Acc. Chem. Res.* **1995**, *28*, 321-327.
72. Matrosovich, M. N.; Mochalova, L. S.; Marinina, V. P.; Byramova, N. E.; Bovin, N. V. *FEBS Lett*, **1990**, *272*, 209-212.
73. Gamian, A.; Chomik, M; Laferriere, C. A.; Roy, R. *Can J Microbiol* **1991**, *37*, 233-237.
74. Ochsenein, A. F.; Fehr, T.; Lutz, C.; *Science*, **1999**, *286*, 2156-2159.
75. Mergulies, D.; Hamilton, A. D. *Angew. Chem. Int. Ed.* **2009**, *48*, 1771–1774.
76. Spaltenstein, A.; Whitesides, G. M. *J Am Chem Soc*, **1991**, *113*, 686-687.
77. Blackburn, E. H.; Szostak, J. W. *Annu. Rev. Biochem.* **1984**, *53*, 164-94.

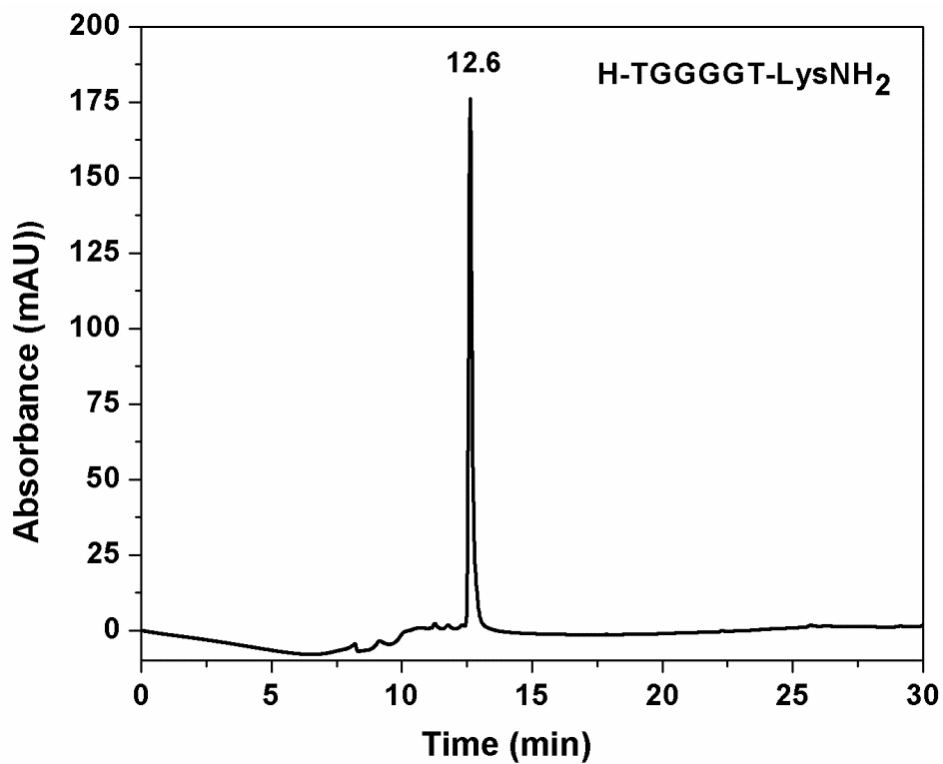
3.4 Appendix III: Characterization data of synthesized compounds/PNA

Sr. No.	Description of spectral characterization	Page No.
1	^1H NMR of compounds 11-12	188-189
2	HPLC spectra of PNAs 1-10	189-194
3	MALDI-TOF spectra of PNAs 1-10	194-199

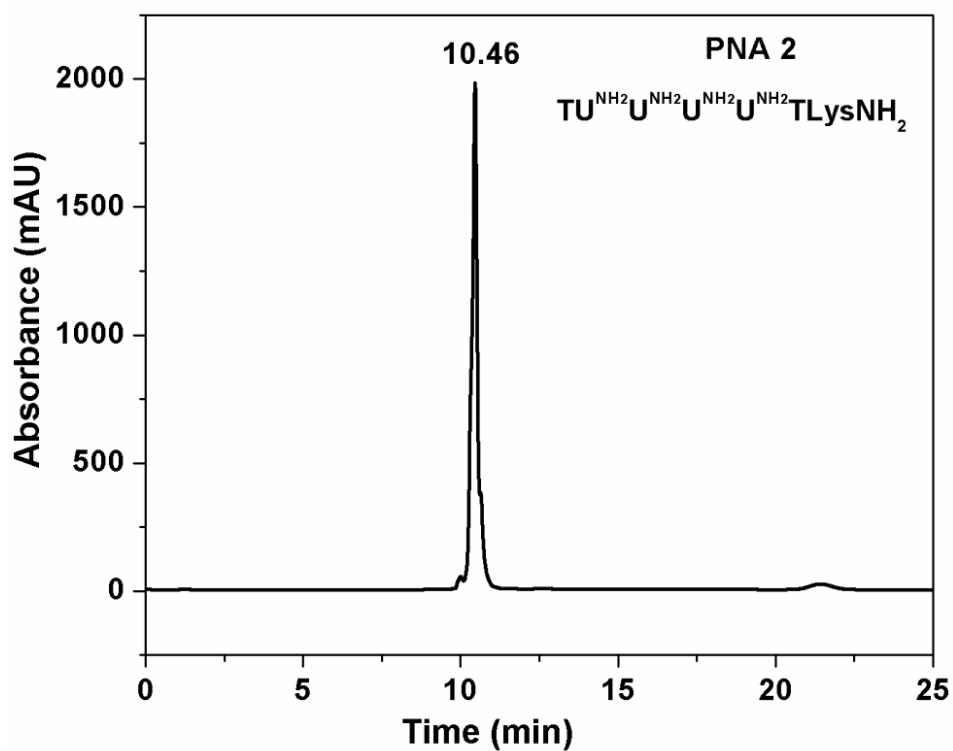
 ^1H NMR of compound **11**

^1H NMR of compound **12**

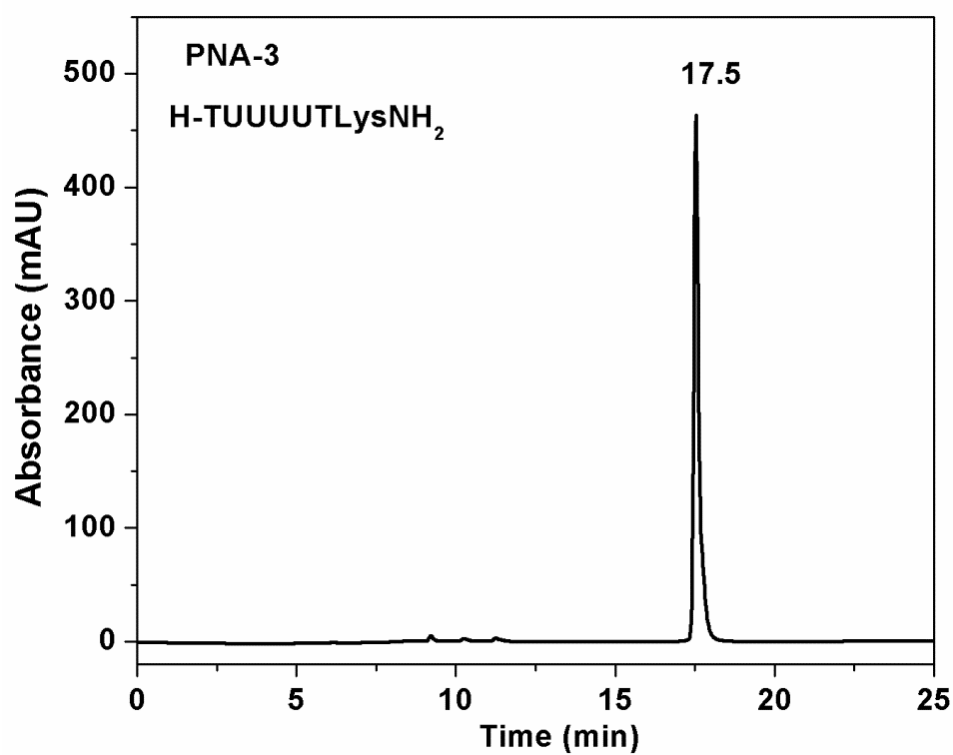
HPLC of PNA-1



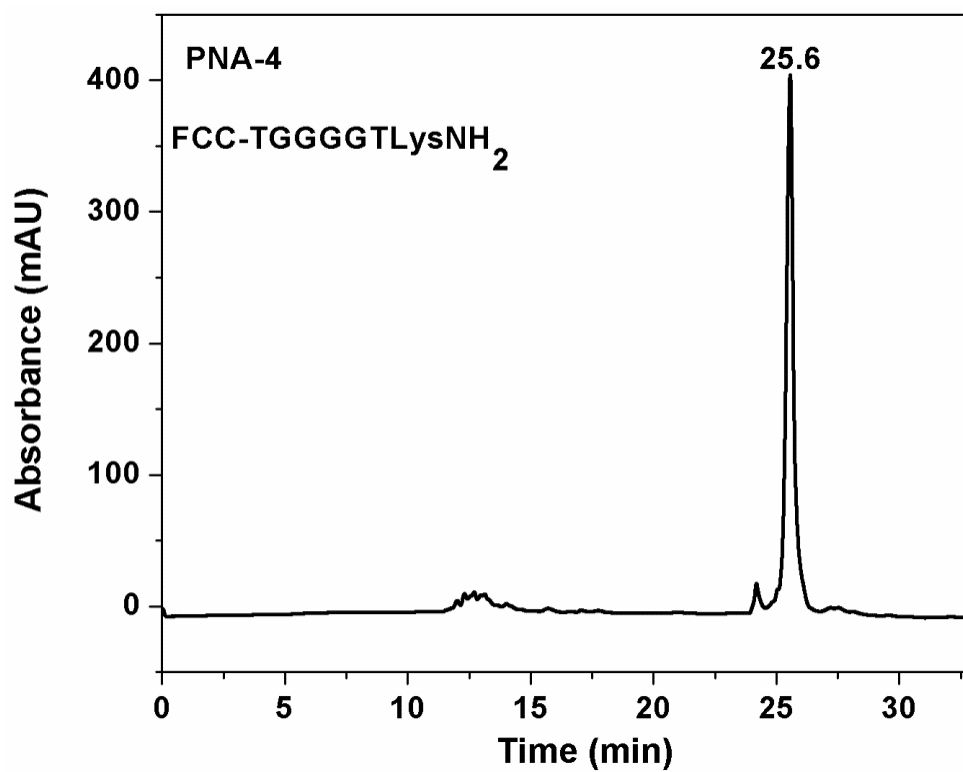
HPLC of PNA-2



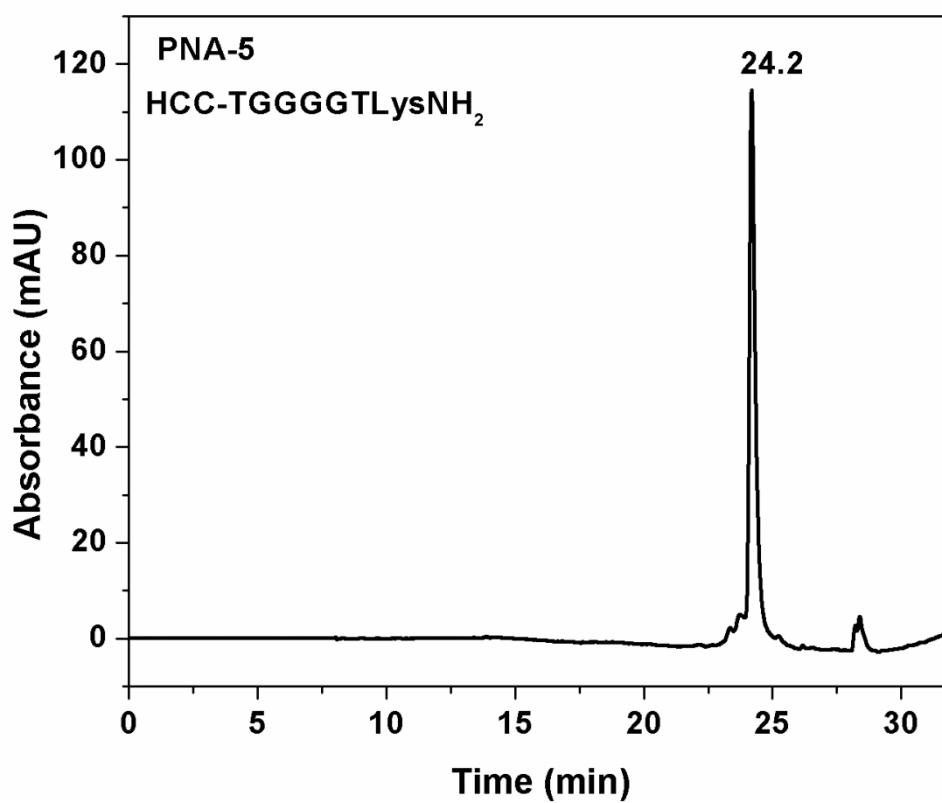
HPLC of PNA-3



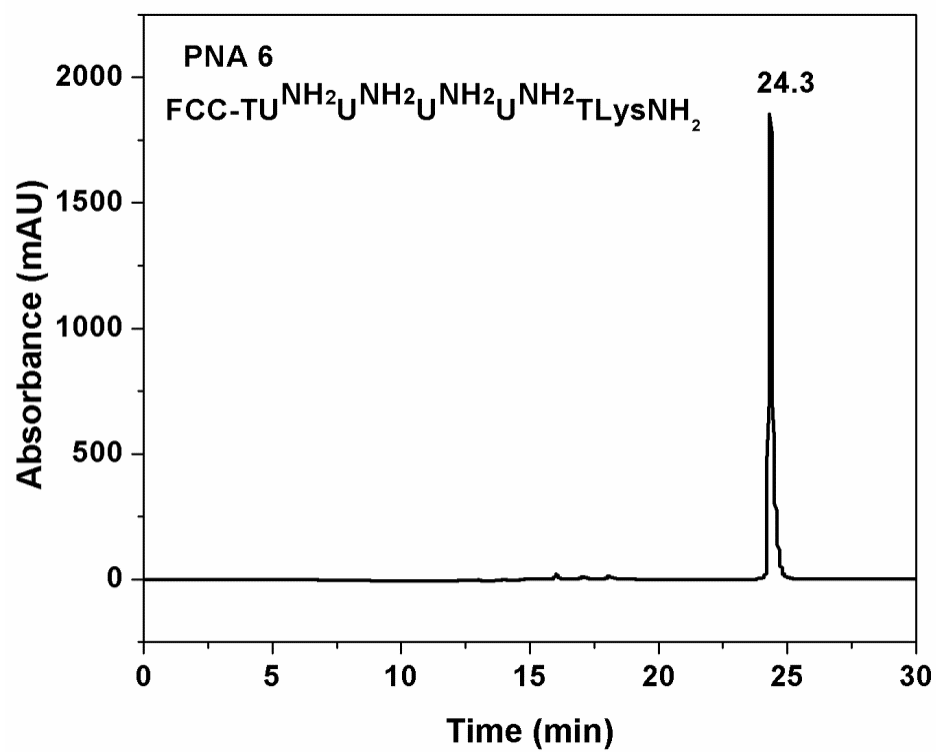
HPLC of PNA-4



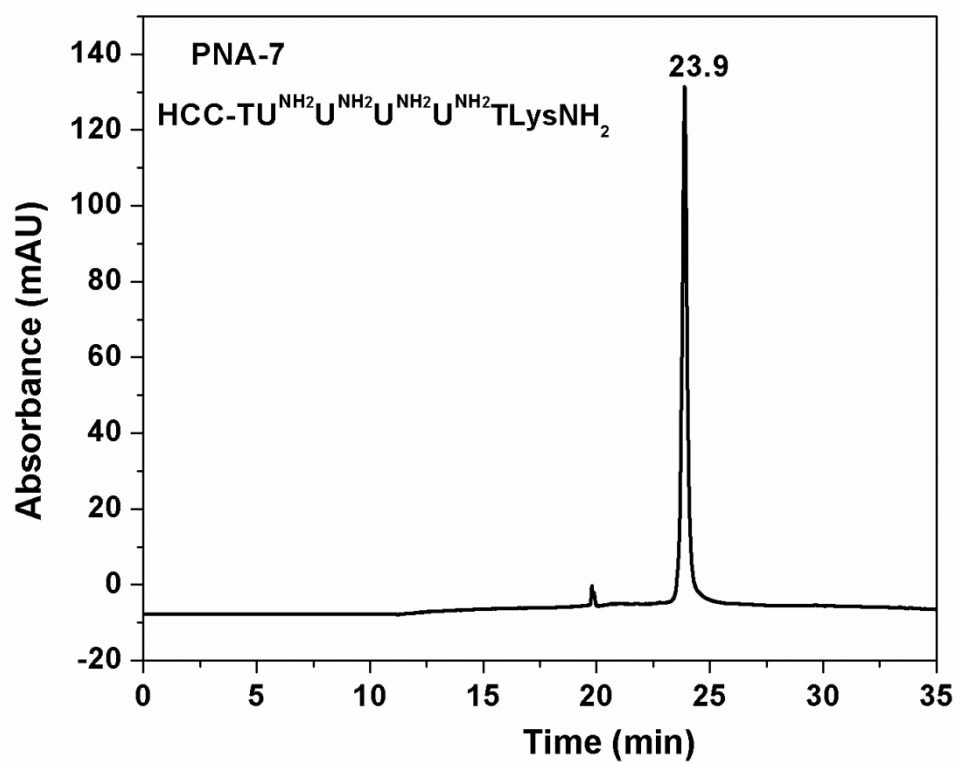
HPLC of PNA-5



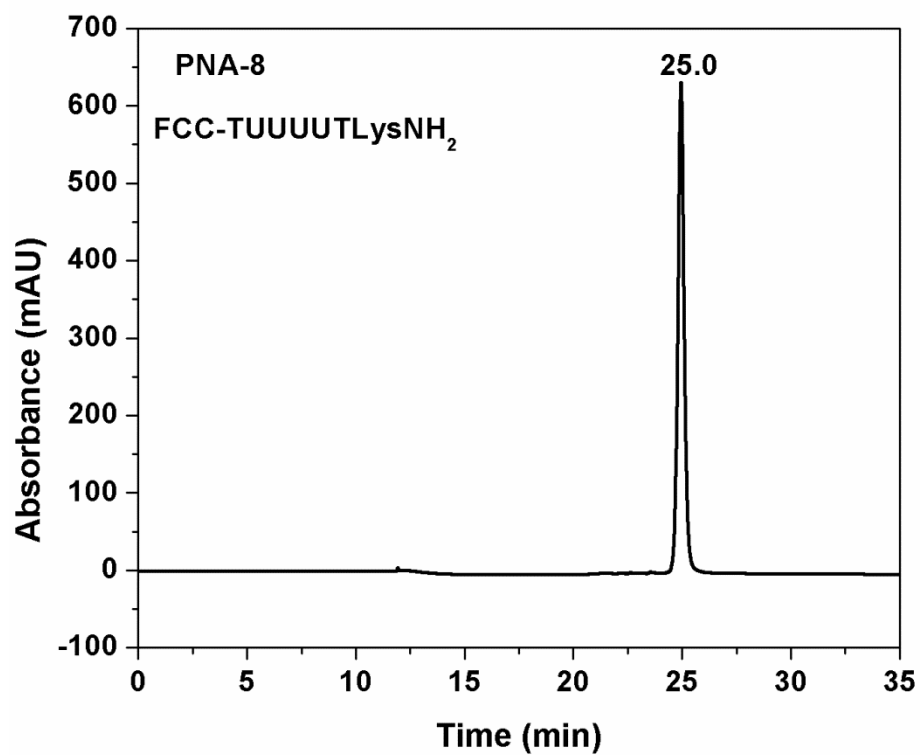
HPLC of PNA-6



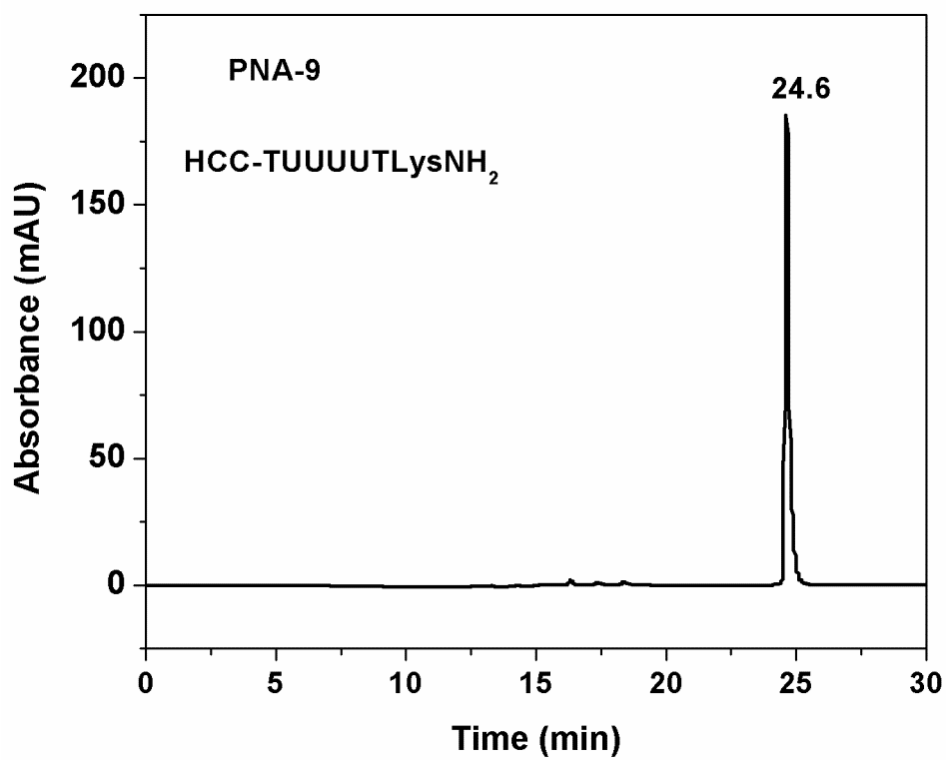
HPLC of PNA-7



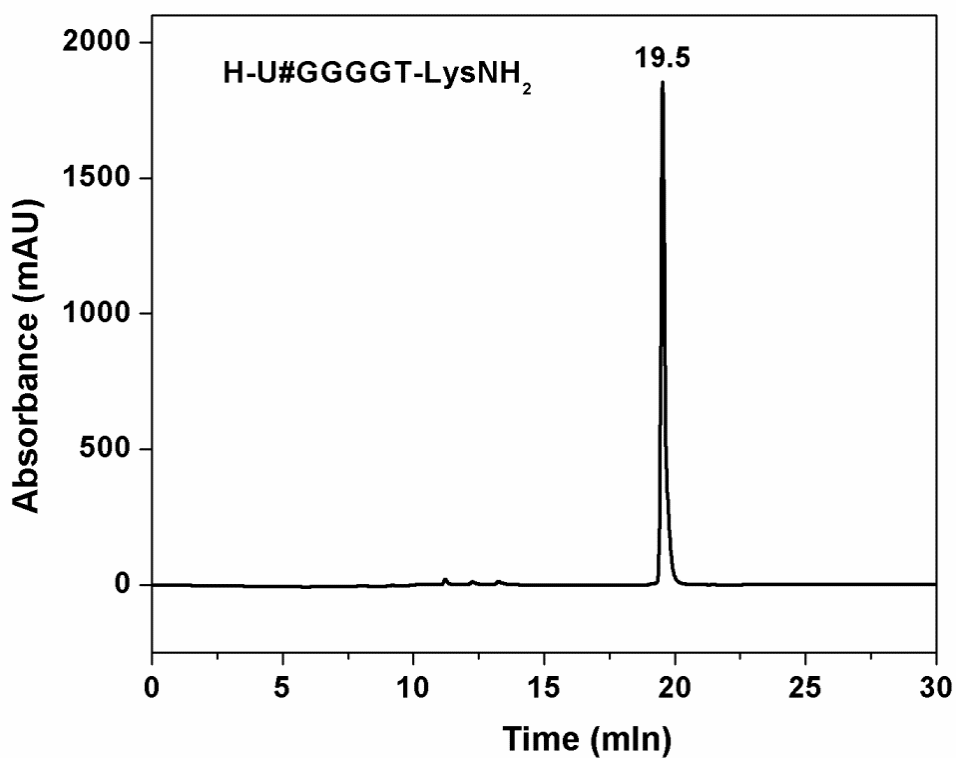
HPLC of PNA-8



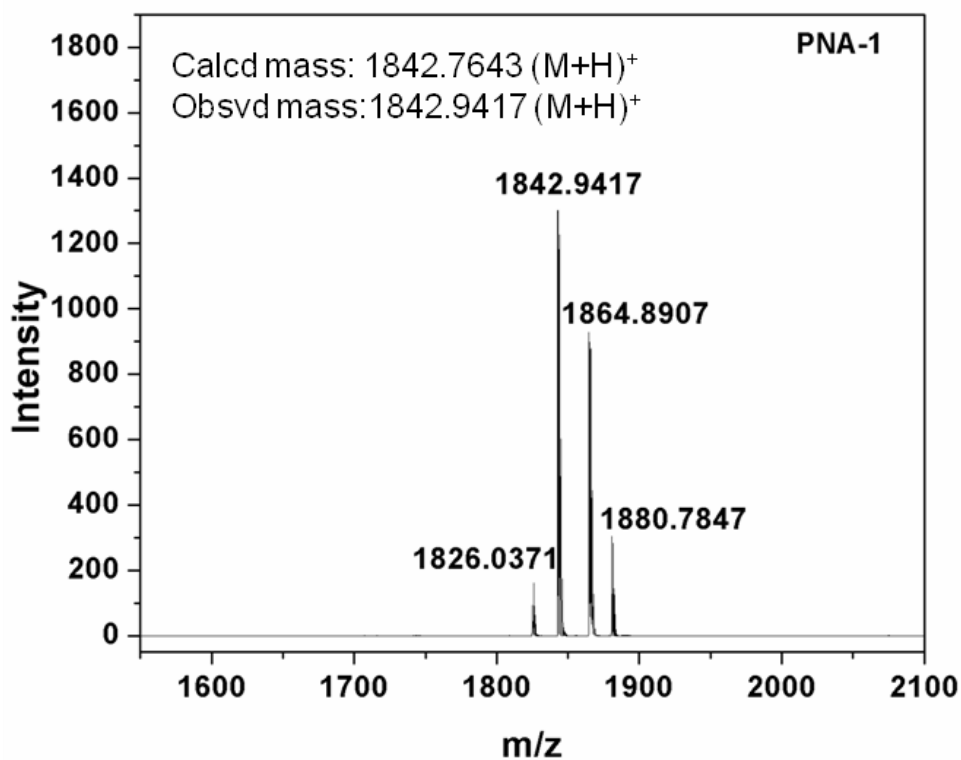
HPLC of PNA-9



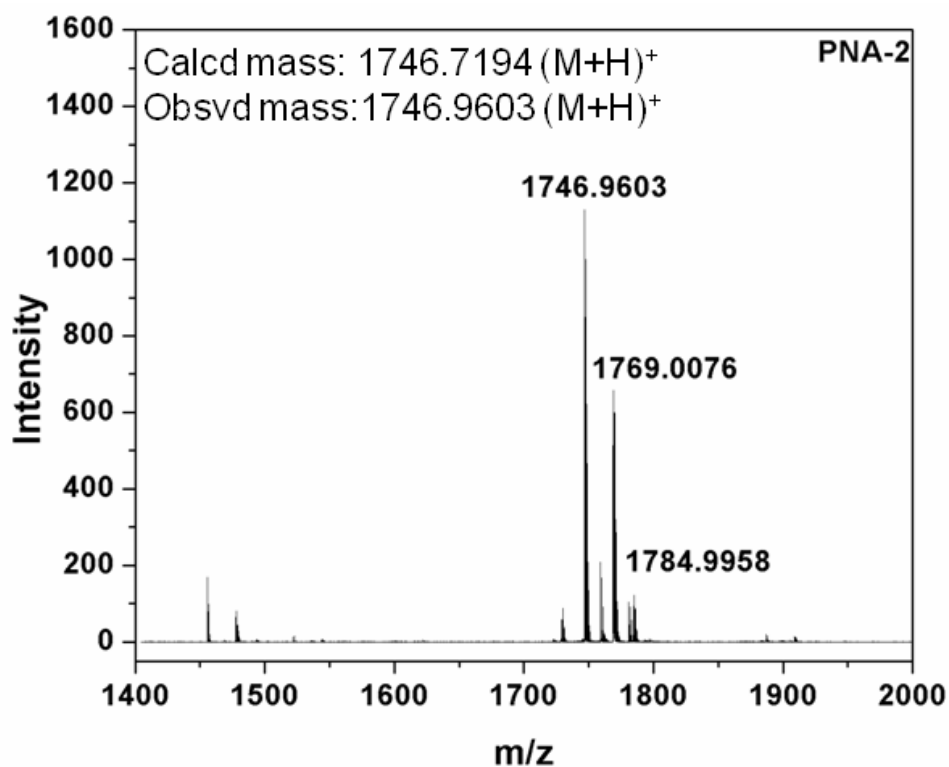
HPLC of PNA-10



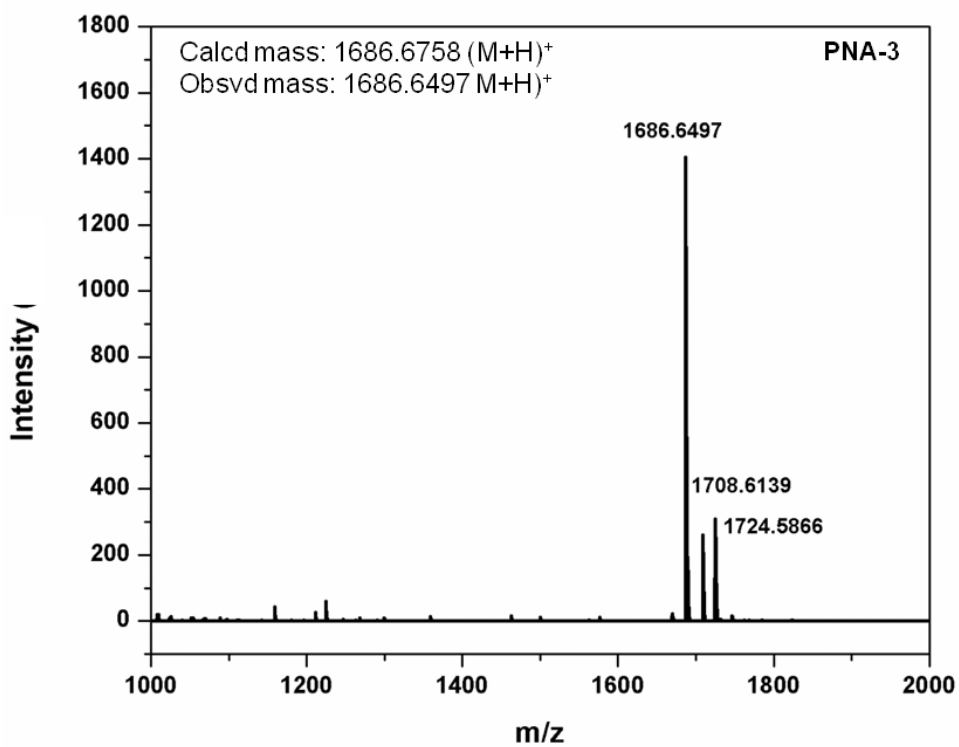
MALDI-TOF of PNA-1



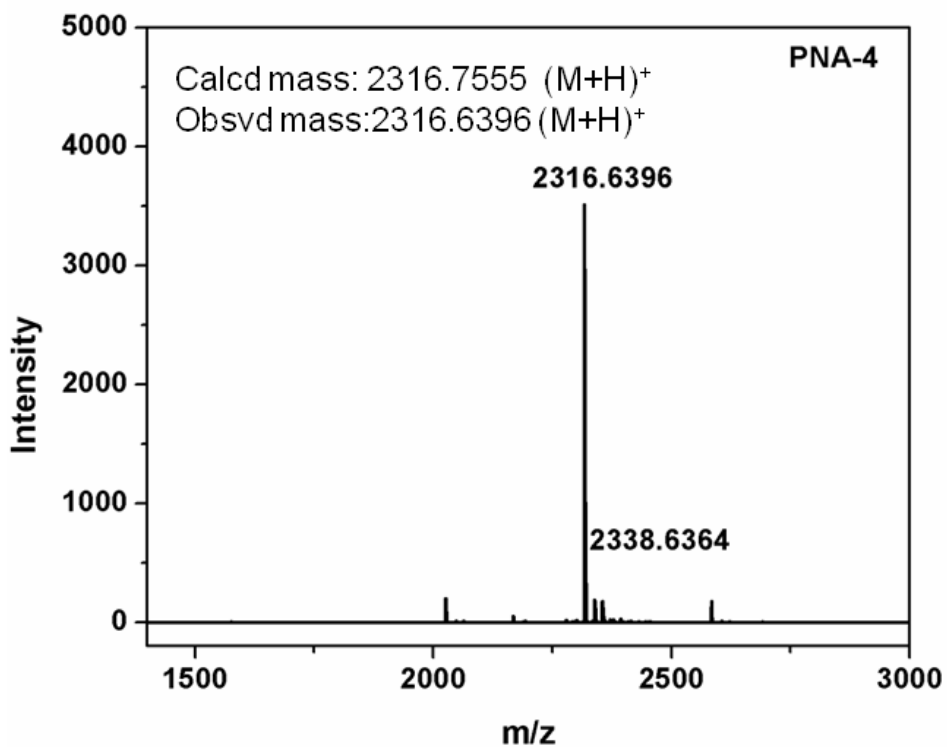
MALDI-TOF of PNA-2



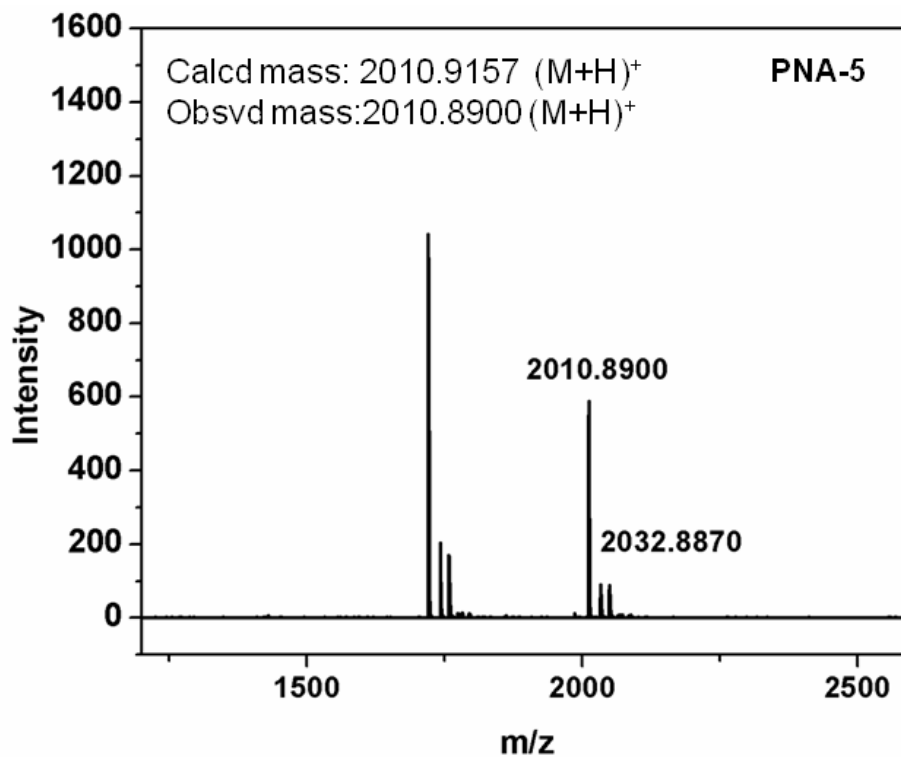
MALDI-TOF of PNA-3



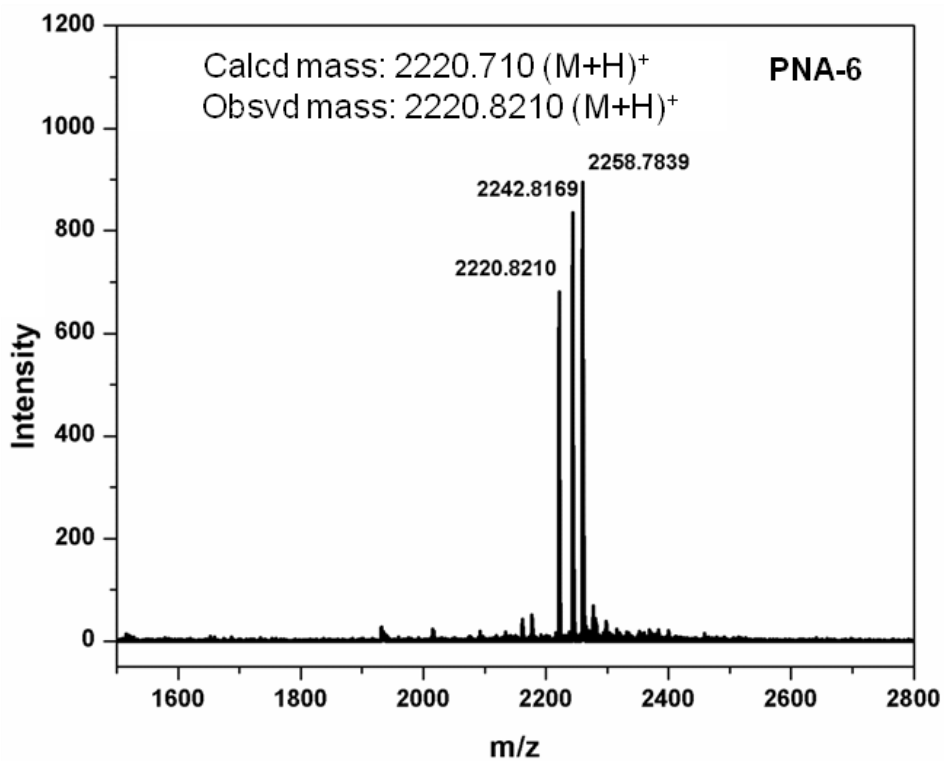
MALDI-TOF of PNA-4



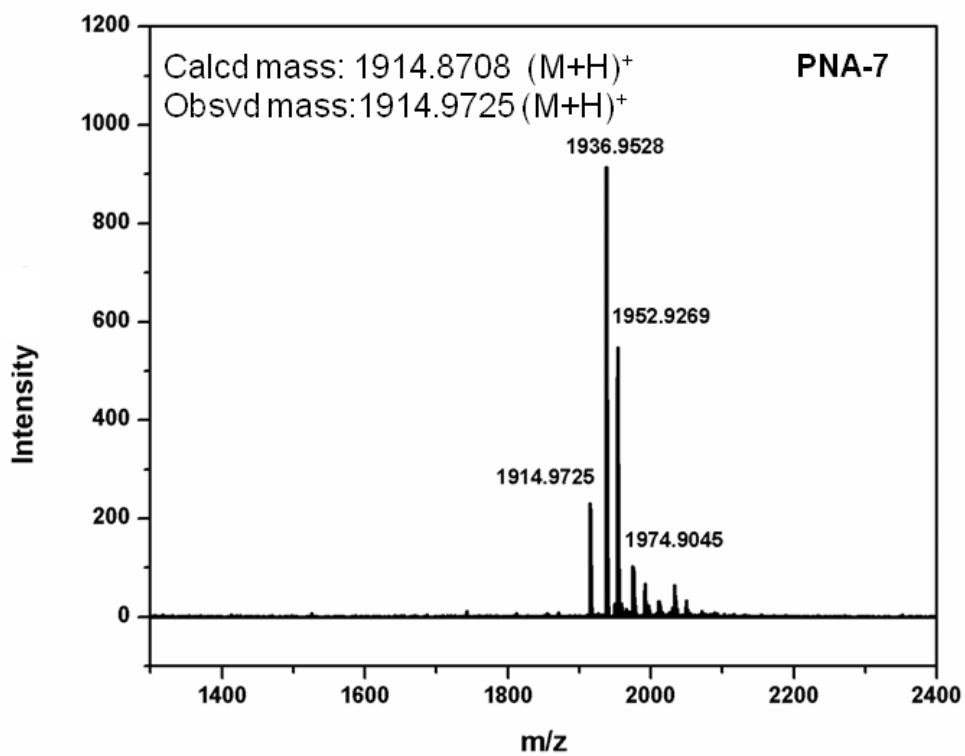
MALDI-TOF of PNA-5



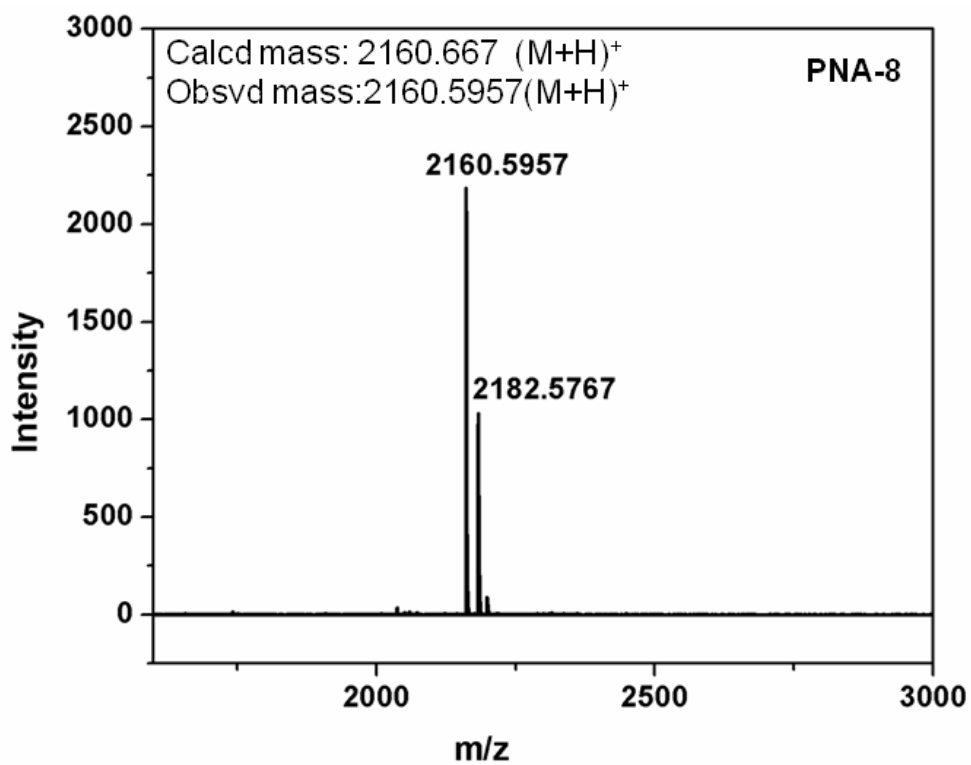
MALDI-TOF of PNA-6



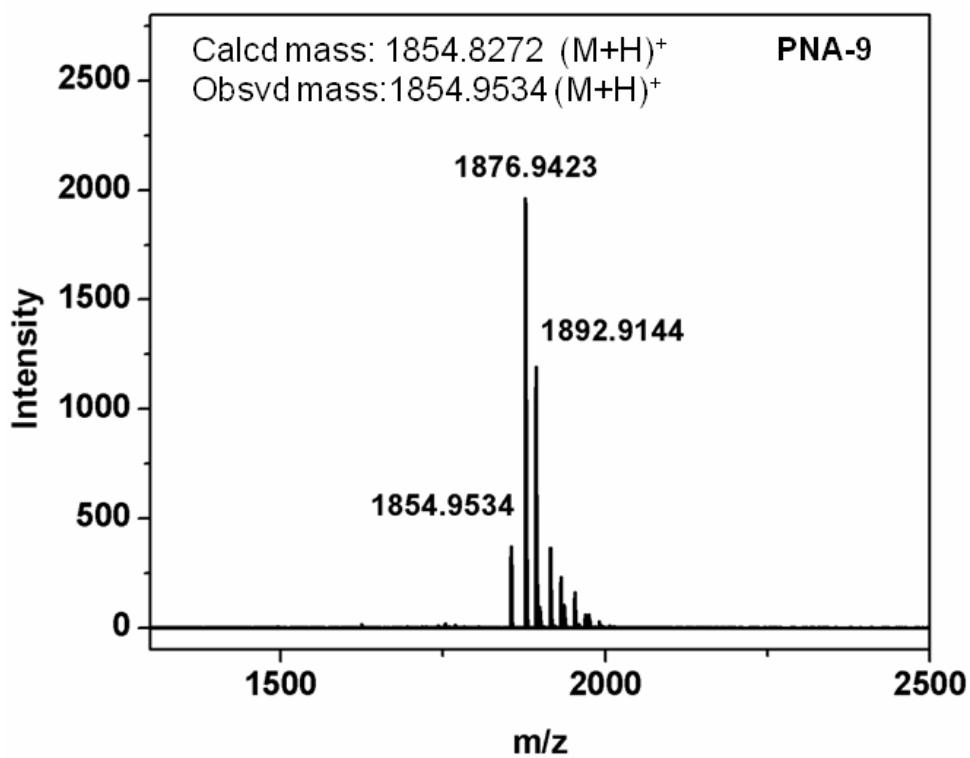
MALDI-TOF of PNA-7



MALDI-TOF of PNA-8



MALDI-TOF of PNA-9



MALDI-TOF of PNA-10

